

INCISED VALLEYS OF END-MEMBER FLUVIAL SYSTEMS IN THE GULF OF CADIZ SHELF: CONSTRAINING THE ROLE OF CONTROLLING FACTORS

Álvaro Carrión Torrente

Ph.D. Thesis

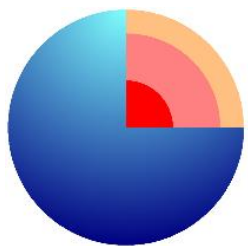
2023

Departamento de Geociencias Marinas
Instituto Andaluz de Ciencias de la Tierra (CSIC-UGR)
Departamento de Estratigrafía y Paleontología
Facultad de Ciencias (UGR)

Supervisors:

Francisco José Lobo Sánchez

Ángel Puga Bernabéu



Editor: Universidad de Granada. Tesis Doctorales
Autor: Álvaro Carrión Torrente
ISBN: 978-84-1195-243-9
URI: <https://hdl.handle.net/10481/90740>

*Agua, ¿Dónde vas?
Riyendo por el río
A las orillas del mar
Mar ¿A dónde vas?
Río arriba voy buscando
Fuente donde descansar*

Federico García Lorca

*Ten siempre a Itaca en tu mente.
Llegar allí es tu destino.
Mas no apresures nunca el viaje.
Mejor que dure muchos años
y atracar, viejo ya, en la isla,
enriquecido de cuanto ganaste en el camino
sin aguantar a que Itaca te enriquezca.*

Konstantino Kavafis

This PhD thesis has been carried out in the Department of Marine Geosciences, at the Instituto Andaluz de Ciencias de la Tierra and in the Department of Stratigraphy and Paleontology, at the University of Granada . Financial support was provided by a grant Formacion de Profesorado Universitario – FPU (FPU16/04730), from the Ministerio de Universidades de España. Additionall financial support was received by research projects PID2021-125489OB-I00, CGL2011-30302-C02-02 and PID2021-125489OB-I00, supported Spanish Ministries of Economy and Competitiveness and Science and Innovation. Seismic interpretations were made using IHS Kingdom™ software, thanks to the participation of the Instituto Andaluz de Ciencias de la Tierra in the IHS University Grant program.

AGRADECIMIENTOS

Allá por 2009 tomé una de las decisiones más importantes de mi vida, en el momento en el que decidí estudiar Geología. Han pasado los años y aún no sé muy bien cómo llegue hasta allí, pero sin duda sé que ha sido de las mejores decisiones que he tomado nunca, sobretodo por todas las personas importantes que ha traído a mi vida. Poco a poco, conforme avanzaba en mi carrera, empezaba a apasionarme más y más por esta ciencia. Yo quería investigar, explorar y buscar respuestas; me encantaba poder ver el mundo con otros ojos, o cómo alguien a quién le debo mucho en mi desarrollo como geólogo y a quién luego agradeceré en particular, ponerme las gafas de geólogo. Así, siguiendo adelante fue cómo llegué a empezar esta tesis doctoral. Durante el transcurso de estos años en los que me he adentrado en este mundo, noto que me he desarrollado no sólo cómo científico, sino especialmente como persona.

En lo personal ha sido un camino muy duro, especialmente a consecuencia de circunstancias externas a lo que debería de ser el desarrollo de cualquier tesis doctoral, y que no me apetece reflejar aquí, ya que, aunque no todo ha sido bueno, sí que hay muchas, pero muchas cosas que han merecido la pena y que me reafirman cada día en que tome una buena decisión en el momento de tirar por este camino. Terminar esta tesis doctoral me ha supuesto un reto, llevándome al límite mental algunas veces, y si he podido llegar hasta aquí es gracias a todas las personas que me han ayudado y apoyado de una u otra forma. Es por eso que quiero dedicar las siguientes líneas a agradecerles lo mucho que ha significado para mí, y aunque posiblemente me olvide de alguien y sea imposible reflejar toda mi gratitud en unas pocas palabras, quiero que sepan de alguna manera lo mucho que me han ayudado.

Quiero expresar mi profundo agradecimiento en primer lugar a mis directores de tesis, les debo un reconocimiento especial por su incansable guía y dedicación, ya que sin su apoyo no hubiese sido posible. Muchas gracias *Paco*, por tu gran ayuda, tus consejos, por estar ahí siempre que subía esas escaleras a preguntarte cualquier duda y mostrar tu disponibilidad, por ser un trabajador incansable y una gran persona. A *Ángel* a ti también muchas gracias, además de en lo que se refiere al apartado científico y de trabajo, que poco más te puedo decir, te doy las gracias ya que fue gracias a ti que empecé en este camino, cuando estaba perdido por los cerros de Sorbas midiendo turbiditas.

Así mismo agradezco a todos mis compañeros y amigos del Instituto Andaluz de Ciencias de la Tierra y de la Universidad de Granada, por ser una grata compañía e ir apoyándonos en lo que íbamos marchando del centro. Gracias a *Erwin, Jon, Sara, Rubén, Manu, Adrián, Marga, Raef, Mapi, Nono, Willy, Africa, Cristi, Marievi, Manolis, Claudia, Julia*, y tantos otros que han pasado por aquí o acaban de llegar. Sin olvidar también darle las gracias mi tutor, Julio, por no rendirse ante el abuso burocrático que supone esa labor; y a todo el personal de administración y secretaría tanto del IACT, cómo de la UGR que me han ayudado con los papeleos y sobretodo con los jaleos a nivel de permisos (*Ana, Carolina, Juani, Socorro, Alejandro, etc.*). Gracias a la gente de la UTEXAS y de la NSYSU, que

me acogió durante mis estancias. Y gracias al Departamento de Estratigrafía y Paleontología de la Universidad de Granada, por vuestras enseñanzas durante mi desarrollo científico desde que empecé cómo un estudiante de grado, y por darme la oportunidad en los últimos años de formar parte del equipo docente.

Quiero también dedicarle unas líneas a los que considero una de las cosas más valiosas que tengo, mis AMIGOS. Aunque necesitaría de muchas páginas, para agradecer y recordar a todos, con las que recordar los buenos momentos en los que hemos compartido risas, y también lágrimas intentaré ser lo más breve posible. A *Aniceto, Iván, César, Tatito, Kesada, Alexis, Linkin, Ekhi, Sandra, Antonio Mirón e Ismael*, vamos a los de toda la vida, os doy las gracias a vosotros y a la vida por teneros presentes después de tantos y tantos años. Tengo presentes a todas las personas que han estado a mi lado durante mi vida en Granada. A *Raquel, JD, Mada, Bob, Aguayo, Inés, Gersan*, que después de tantísimo tiempo también ahí seguís, llenando un cachito de mi corazón, y apoyándome, sacando risas y alegrías, muchas gracias, no sabéis lo que os quiero. A *Blanca y Ocho*, con los que he salido del túnel en innumerables veces, y que siempre me sacan una sonrisa. A *Claudia* (y Laura de noche), por dejar a los chiquillos que camelen, y ser fiestera y organizada. A *Aurora*, compañera almeriense de turbiditas, y por supuesto al resto de los geólogos y no tan geólogos que me han acompañado y que a día de hoy siguen estando allí, y aunque no nos veamos tanto siempre quedan los momentos (*Pepelu, Paloma, Serpa, Rocío, Juanan, Lidia, Guille, Leo, Sara, Michu, Cris, Sofi, Alicia, Carlos, Fran, Lucía, Carlos, Javi, Mario, Alba, etc.*, seguro que me dejo a alguien, pero ya sabéis quienes sois). A *Ceci* y a *Javi*, agradecerles también, os he dejado a parte para daros vuestro lugar, no sólo cómo amigos, sino cómo compañeros de despacho, de comidas y de vivencias. También quiero agradecer y tener otro rinconcito, aunque me repita para *Bob, Mada* y en especial *JD* (y también *Gea*), con los que doy las gracias de haber compartido tantos y tantos días.

Gracias a ti Lidia, por ser mi compañera durante el último año y medio, por quererme y aguantarme, y sobretodo por animarme e inspirarme con tu coraje para afrontar la vida. Me has enseñado a seguir adelante con las dificultades que nos trae la vida. Gran parte de haber llegado hasta aquí ha sido gracias a ti, esto también es tuyo. Te quiero!

Gracias de forma muy especial a mi extraordinaria familia. Esto es vuestro desde la portada, vuestro amor incondicional ha sido mi mayor fortaleza, les dedico un agradecimiento especial. A mis padres, José Antonio y Rosa Mari, soy lo que soy gracias a vosotros, no podría de estar más agradecido de teneros como padres, vuestro apoyo, paciencia y comprensión han sido el pilar sobre el cual he podido avanzar por este camino. A ti *Eva*, gracias por ser mi otra mitad, desde hace 29 años, no dejas de sorprenderme y cuidarme día a día. Te quiero hermana. También gracias a mis Abuelos, a María y Luis, y a Piedad y Domingo, a los cuatro, a los que están y a los que me miran desde otro lugar, esto también es para vosotros, os tengo presente cada día.

Y por supuesto gracias a mis demás familiares, a mi tío Juan que siempre ha sido uno más de mi núcleo duro, tenemos que descorchar un par de botellas, yo incito esta vez; a mi tío Luis que siempre me ha animado a hacer cosas desde bien chiquitito; gracias a Lola, Lucas y Alberto (qué también os considero familia); y gracias a todos los demás tías, primas y resto de familiares.

Por último, y no menos importante gracias a todas las personas que me ayudaron cuándo lo necesité, a los que hicieron posible con su granito de arena que pudiera regresar con los míos desde Taiwán.

ABSTRACT

Incised valleys are common stratigraphic features beneath modern coastal plains and continental shelves, whose incision and sedimentary fill might provide critical crucial insights into earth-surface processes, depositional histories, and their controlling factors. The formation and evolution of these valleys result from the dynamic interplay of various controlling elements, including changes in relative sea level, tectonics, sediment supply, hydrodynamic processes, pre-existing tectonic features, and antecedent geology. This study aims to enhance our understanding of the geological processes governing incised valley systems, emphasizing their significance across different temporal scales.

The northern margin of the Gulf of Cadiz provides an ideal setting to examine the interaction between sediment supply and sea-level changes. Characterized by a hierarchical stratigraphic architecture, this region reflects the complex influence of late Quaternary glacio-eustatic changes and tectonic forces. The Gulf of Cadiz features locally high fluvial supplies within a moderately energetic oceanographic regime, presenting an intermediate environment between low-energy delta-forming and high-energy ravinement-forming settings.

A network of cross-shelf paleovalleys off the Gilão-Almargem Estuary, situated in the eastern Algarve shelf, has been studied to discern the driving controls shaping ancient fluvial systems. The investigation focuses on primary glacio-eustatic controls, such as antecedent geology, low fluvial supply, and changing hydrodynamic regimes, along with secondary controls on valley genesis and evolution. Antecedent geology strongly influences valley formation, limiting the development of wide incised valleys and determining landward incision near a well-defined break of slope. The postglacial infilling is predominantly estuarine, suggesting a dendritic system with barriers interrupted by tidal inlets and channels in a mixed estuarine environment with low fluvial supply.

On the Guadiana Shelf, the study of two N-S incised valleys systems separated by a few kilometres, revealing a compound nature with up to five repeated incision phases, suggesting a major glacio-eustatic origin likely linked to 100 ka sea-level cycles. Significant differences in internal architecture and morphology between both valleys suggests varying sediment supply conditions and hydrodynamic controls, emphasizing the role of variable fluvial supplies and antecedent morphology in influencing the distribution of valley infill facies.

The postglacial sea-level rise after the Last Glacial Maximum provided ideal conditions to study the transgressive sedimentary response to sudden shelf flooding driven by different rates of sea-level rise. Analysis of four postglacial transgressive units linked to the mouth of the Guadiana River reveals a complex deltaic evolution in response to

varying rates of sea-level rise and climatic changes. Delta progradation and preservation episodes were observed during periods of high sediment flow associated with significant climatic events.

The investigated incised valleys and transgressive deposits exhibit complex stratigraphic architectures influenced by glacio-eustatic cycles, underlying geology, and sediment supply dynamics, resulting in distinct morphologies, infilling patterns, and responses to postglacial transgression. The stratigraphic architecture of postglacial transgressive units off the Guadiana River mouth reveals significant variability in driving factors, highlighting the intricate interplay between sea-level rise, sediment fluxes, and climatic conditions. This research significantly contributes to understanding geological and sedimentary processes in the Gulf of Cadiz, with direct applications in the oil and gas industry and insights into biogeographic and paleoclimate processes.

RESUMEN

Los valles encajados constituyen rasgos estratigráficos comunes en las plataformas continentales, cuya incisión y relleno sedimentario pueden proporcionar mucha información sobre los procesos de la superficie terrestre, su historia deposicional y sus factores de control. La formación y evolución de estos valles resultan de la interacción dinámica de varios agentes de control, incluyendo cambios en el nivel relativo del mar, tectónica, aporte de sedimentos, procesos hidrodinámicos, características tectónicas preexistentes y la influencia de la geología previa. Este estudio tiene como objetivo mejorar nuestra comprensión de los procesos geológicos que rigen los sistemas de valles encajados, enfatizando su importancia en diversas escalas temporales, y en relación a los cambios globales.

El margen norte del Golfo de Cádiz proporciona un entorno ideal para examinar la interacción entre el aporte de sedimentos y los cambios en el nivel del mar. Esta área está caracterizada por reflejar la compleja influencia de los cambios glacio-eustáticos del Cuaternario y las fuerzas tectónicas, en una arquitectura estratigráfica bastante jerárquizada. El Golfo de Cádiz presenta aporte fluviales locales bastante elevados dentro de un régimen oceanográfico moderadamente energético, representando una situación intermedia entre ambientes de formación de deltas de baja energía y ambientes de formación de retrabajamiento de alta energía.

Una red dendrítica de valles encajados en la plataforma interna frente al estuario de de los ríos Gilão y Almargem, situada en la plataforma este del Algarve, ha sido estudiada para discernir los controles que dieron forma a antiguos sistemas fluviales. La investigación se centra en los controles glacio-eustáticos primarios, como la geología previa, el bajo aporte fluvial y los agentes hidrodinámicos, junto con controles secundarios sobre la génesis y evolución del valle. La geología previa influye fuertemente en la formación del valle, limitando el desarrollo de los valles encajados y confinando la incisión hacia el interior de la plataforma, cerca de una bien definida ruptura de pendiente. El relleno postglacial es predominantemente estuarino, sugiriendo un sistema dendrítico, con numerosas barreras interrumpidas por canales de marea o surcos en un sistema estuarino mixto.

En la plataforma del Guadiana, se estudiaron dos sistemas de valles encajados N-S separados por pocos kilómetros entre sí, revelando una naturaleza compuesta con hasta cinco fases de incisión repetida, sugiriendo un origen glacio-eustático del nivel del mar de 100 ka. Las diferencias significativas en la compleja arquitectura y en morfología entre ambos valles sugieren condiciones variables en el aporte de sedimentos sedimentario y la hidrodinámica durante su desarrollo, destacando el papel de los aportes y de la morfología previa en influir en la distribución de las facies de relleno del valle.

El aumento del nivel del mar postglacial después del Último Máximo Glacial proporcionó condiciones ideales para estudiar la respuesta sedimentaria transgresiva a la repentina inundación de la plataforma impulsada por diferentes tasas de aumento del nivel del mar. El análisis de cuatro unidades transgresivas postglaciales (UTP) vinculadas a la desembocadura del río Guadiana revela una evolución deltaica compleja en respuesta a variaciones en las tasas de aumento del nivel del mar y cambios climáticos. Se observaron episodios de progradación y preservación del delta durante periodos de alto flujo sedimentario asociados con eventos climáticos significativos.

Los valles encajados investigados y los depósitos transgresivos exhiben arquitecturas estratigráficas complejas influenciadas por ciclos glacio-eustáticos, la geología previa y las dinámicas de aporte sedimentario, dando lugar a morfologías distintas, patrones de relleno y respuestas a la transgresión postglacial. La arquitectura estratigráfica de las unidades transgresivas postglaciales frente a la desembocadura del río Guadiana revela una variabilidad significativa en los factores de control, destacando la intrincada interacción entre el aumento del nivel del mar, los flujos de sedimentos y las condiciones climáticas. Esta investigación contribuye significativamente a la comprensión de los procesos geológicos y sedimentarios en el Golfo de Cádiz, con aplicaciones directas en la industria del petróleo y el gas, así como en la comprensión de procesos biogeográficos y paleoclimáticos

Summary

In this doctoral thesis, a high-resolution seismic stratigraphic interpretation and sedimentological analysis were conducted on data from the northern Gulf of Cadiz continental shelf (SW Iberian Peninsula). It aims to comprehensively characterize incised valleys and associated deposits, highlighting their scientific, social, and industrial implications. Focusing on the northern margin of the Gulf of Cadiz, the research aims to enhance understanding of the geosphere's response to climate and eustatic changes, particularly in the formation of incised valleys. The study provides insights into sedimentary system responses across temporal scales and contributes to understanding the role of fluvial systems in continental margin development. The research also explores implications for the transfer of biological species and human settlement patterns on the shelf. With direct applications in the petroleum industry, the findings aid in assessing reservoir rocks' geometry, spatial distribution, and temporal variations in analogous systems.

The study area, characterized by locally high fluvial supplies and moderate oceanographic energy, provides an intermediate environment between delta-forming and ravinement-forming settings. Two major rivers, Guadiana and Guadalquivir, contribute significant sediment flux, driving outward margin growth. However, incised valleys in this region remain limitedly recognized and interpreted. Recent mapping identified N-S valleys off the Guadiana River, related to the Last Glacial Maximum and reoccupied by older incised valleys. The Algarve coast west of the Guadiana River exhibits abundant incised valleys, suggesting significant hydrological changes.

First, in Chapter 4, a network of cross-shelf paleovalleys has been recognized over the paleo-inner shelf off the Gilão-Almargem Estuary, a small fluvial drainage system that presently receives minor sediment supply in the eastern Algarve shelf, northern margin of the Gulf of Cadiz (SW Iberian Peninsula). This system is composed of several incised valley features which exhibit a remarkable similar internal architecture, and his study aims at determining the driving controls that triggered substantially different paleohydrological conditions and sedimentary dynamics of ancient fluvial systems in this margin, focusing on evidences of secondary controls on valley genesis and evolution, superimposed to primary glacio-eustatic control such as antecedent geology, low fluvial supply and changing hydrodynamic regimes.

Then, in Chapter 5, the architecture and late Quaternary development of two N-S paleovalleys on the Guadiana River shelf, located eastward (Guadiana main valley and Guadiana eastern valley), were studied. The plan-view morphology and the postglacial infilling patterns vary between both paleovalleys. It study allow to reconstruct paleoenvironmental conditions during the last major phase of valley incision through a geomorphological analysis, and to reveal distinct responses of paleovalley infilling following the Last Glacial Maximum.

Additionally, in Chapter 6, four backstepping seismic postglacial transgressive units (PTUs; 4 to 1 from oldest to youngest) that are linked to the retreating mouth of the Guadiana River were interpreted. Together, these seismic units display a wedge-shape geometry, are located over the inner to middle shelf, and overlie a regional unconformity formed during the Last Glacial Maximum. Each PTU can be divided into several sub-units with distinctive seismic facies that have a similar stratigraphic organization. Each PTU contains lower sub-units that are composed of low-angle tangential oblique clinoforms. The clinoforms are locally topped by a channelized sub-unit. The distal and/or lateral parts of the clinoforms are occasionally buried by sheet-like semitransparent subunits. The uppermost sub-units are present over the proximal and central parts of each seismic unit and are also sheet-like. PTUs can also be subdivided and described sedimentologically. Fine-grained sands with intercalated silty layers dominate the lower part of each PTU (lower clinoform sub-units). The upper part of each PTU (upper sheet-like sub-units) is characterised by reworked facies, composed of highly fragmented bioclasts within a mixture of silt and coarse to medium sand. Finally, mud deposits occur as a sediment drape over the PTUs.

The inner-shelf paleovalley system studied in chapter 4 is associated with the Last Subaerial Discontinuity (LSD) and exhibits two major incisions (IP 1 and IP 2), and was interpreted as a simple incised-valley model developed during the last glacial cycle. The common organization of paleovalleys here reveals the frequent occurrence of coarse-grained sediment bodies like estuarine bars, estuary-mouth sand plough and coastal barriers, and a second phase of incision interpreted as tidal inlets/channels. Finally, the result presented in Chapter 4, remarks that the formation of the eastern Algarve paleovalleys was strongly determined by background geology, where the occurrence of a flat, lithified paleo-inner shelf bounded seaward by a break of slope conditioned the formation of small-sized incised valleys. Subsequently, the infilling of the valleys took place under a context of high rates of sea-level rise and limited fluvial, where hydrodynamic factors, particularly tidal and wave influences, play a crucial role in sediment reworking and preservation of the system.

The two major studied incised valleys in chapter 5 are considered compound valleys with a complex history of repeated avulsion and periodic reoccupation of the fluvial system during consecutive glacio-eustatic cycles. The valleys are believed to be younger than the Middle Pleistocene Discontinuity (MPD), which is estimated to be around 0.7-0.9 million years old. The study also remarks that the antecedent geology and the hydrodynamic regime also plays a significative role in the genesis of the Guadiana shelf incised valleys. Firstly, it is interpreted that the plan-view morphology of the paleovalleys was influenced more by the underlying geology and the contrast between an indurated inner shelf and a more erodible middle to outer shelf than by shelf gradients (as was the case of the Algarve valleys). Differences in cross-sectional shapes between both valleys where V-shape (GMV) and U-shape (GEV), are likely attributed to underlying structure, lithology, and hydrodynamics, possibly indicating distinct sediment transport and

deposition dynamics. Additionally, the study reveals that not only are there remarkable differences between these valleys and the undersupplied Algarve valleys, but there are also differences in infilling patterns between the main and eastern valley. Thus, the post-LGM record of the Guadiana main valley reveals three major upward evolutionary phases: (1) fluvio-deltaic (characterized by fluvial channel deposits or bayhead delta deposits); (2) estuarine (with mud and sand alternations suggesting a central estuarine basin fill), and (3) shallow-water environments (representing shallow-water deltas studied in chapter 6, formed during the last postglacial sea-level rise), and (3) by an open-marine sedimentation that could be ascribed to the recent most HST. The Guadiana eastern valley's infilling exhibits a simpler stratigraphic pattern compared to the main valley, featuring a transgressive dominance, with estuarine and shoreface-shelf depositional systems. This study suggests that differences in infilling patterns between the main and eastern valleys are partially driven by variation in sediment supply conditions, where the main valley is associated with strong fluvial supply, while the eastern valley exhibits transgressive sediments indicative of small sediment input.

The results presented in Chapter 6, also remarks the significant importance of sea-level changes as a control for the formation of the studied PTUs, concretely, its formation is framed within the 14-9 ka interval, suggesting that changes in rates of sea-level rise played significant role. Thus, the older PTUs (4 and 3) seem to be related to periods of reduced sea-level rise, such as the terminal part of MWP-1A and the Younger Dryas event. Meanwhile, the younger PTUs (2 and 1) are related with the MWP-1B, a period of high rate of sea-level rise during the deglaciation. The Guadiana shelf PTUs exhibits a diverse internal stratigraphic organization compared to many other postglacial transgressive deltaic systems. In that sense, the genesis of PTUs 2 and 1 (that comprises the shallow-water deltas linked to the Guadiana main valley) is attributed primarily to the overall climatic conditions established in SW Iberia after the Younger Dryas that triggered significant changes in sediment supply in the river basin. Those phases of enhanced sediment supply probably resulted from increased rainfall runoff during humid periods and scarce land vegetation cover. Finally, the results presented in Chapter 6 also constrain the significant role of all these controlling factors. The rich stratigraphic architecture of the four postglacial transgressive units (PTUs) reveals the occurrence of several major phases of development, indicating a high variability in the driving factors. The stratigraphic pattern of these PTUs likely resulted from the combination of relatively significant sediment fluxes, mentioned above, an active oceanographic regime with wave and/or tidal reworking in the nearshore and along-shelf redistribution by currents.

INDEX:

Abstract	I
<i>Resumen</i>	III
Summary	VII
Index	XI
List of acronyms	1
1. Introduction	5
1.1. Incised valleys	5
1.1.1 Historical background.	5
1.1.2 Incised valleys and sequence stratigraphy	7
1.1.2.1 Fundamentals of sequence stratigraphy	7
1.1.2.2 Incised valleys in a sequence stratigraphy framework	11
1.1.2.3. Transgressive deposition in continental shelves	15
1.1.2.4 Simple versus complex incised valleys	17
1.1.2.5 Incised valleys shape	18
1.2. Controlling Factors	18
1.2.1 Sea-level variations	19
1.2.1.1. Late Quaternary cycles	20
1.2.1.2 Higher frequency cycles during the Last Glacial Cycle	20
1.2.2 Tectonics, sediment supply, hydrodynamic regime, and antecedent geology	23
1.2.2.1 Tectonic influence	23
1.2.2.2 Sediment supply and hydrodynamic regime	25
1.2.2.3 Antecedent geology	27
1.3. Hypotheses and aims	29
2. Regional setting	35
2.1. Geological setting	35
2.2. Coastal geology and sediment sources	37
2.2.1. Eastern Algarve coast	38
2.2.2. Huelva Coast	39
2.3. Oceanographic setting	40
2.4. Physiography	41
2.5. Surficial sediment distribution	43
2.6. Margin stratigraphy	46
3. Methods	53
3.1. Geophysical methods	54
3.1.1. Seismic data	54
3.1.1.1 TOPAS sub-bottom acoustic profiles	56
3.1.1.2 Parasound acoustic profiles	57
3.1.1.3 Sparker single-channel seismic profiles	58
3.1.1.4 Geopulse seismic profiles	59
3.1.2. Seismic Interpretation	60
	XI

3.2. Sedimentological methods	61
3.2.1. Sedimentological data	61
3.2.2. Sedimentological interpretations	64
3.2.3 Age data	64
3.3. Geomorphological methods	66
3.4. Chronostratigraphic framework	68
4. Incised valleys on the Algarve Shelf	71
4.1 Results	73
4.1.1 Seismic stratigraphy of the inner-shelf paleovalley system	73
4.1.2 Sedimentary facies and core descriptions	80
4.1.2.1 Sedimentary facies	80
4.1.2.2 Sediment core GeoB19508	81
4.2 Discussion	83
4.2.1 Regional chronostratigraphic framework	83
4.2.2 Interpretation of stratigraphic architectures of incised valleys	85
4.2.3 Driving factors of the paleo-inner-shelf incised valley system	87
4.2.3.1 Postglacial sea-level changes	88
4.2.3.2 Low sediment supplies	88
4.2.3.3 Role of antecedent geology	89
4.2.3.4 Hydrodynamic regime	90
5. Incised paleovalley systems on the Guadiana Shelf	95
5.1. Results	96
5.1.1 Incised paleovalleys on the Guadiana shelf: Seismic Stratigraphy and major regional seismic surfaces	96
5.1.1.1 Incision phases in the Guadiana Main Valley	98
5.1.1.2 Incision phases in the Guadiana Eastern Valley	102
5.1.2 Morphology of incised valleys related to the last shelf-wide unconformity (mws)	104
5.1.1.1 Guadiana Main Valley	105
5.1.1.2 Guadiana Eastern Valley	105
5.1.3. The sedimentary infilling of the last incision phase.	108
5.1.3.1 Seismic stratigraphy of the infilling	108
5.1.3.2 Sedimentary facies and core descriptions	118
5.2 Discussion	120
5.2.1 Long-term development of incised valleys: Routes for shelf-margin growth	120
5.2.2 Valley morphology during the last sea-level lowstand: Some genetic constraints	124
5.2.3 Variable patterns of postglacial infilling	125
5.2.3.1. Tripartite infilling of the main valley	126
5.2.3.2. Transgressive dominance in the eastern valley	128
5.2.3.3. Variability of valley environments: hydrodynamics versus sediment supply conditions	131
5.2.3.4. Considerations about along-valley stratigraphic arrangement in the main valley	132

6. Episodic deltaic development off the Guadiana River mouth during the postglacial transgression	135
6.1. Results	137
6.1.1. Seismic Stratigraphy	137
6.1.1.1 Postglacial Seismic Units (PTUs): Internal Architecture and Seismic Facies	137
6.1.1.2 Spatial Distribution	143
6.1.2. Sedimentological Analysis	145
6.1.2.1 Types of Sediment Facies	145
6.1.2.2 Core description	146
6.1.2.3 Age Dates	149
6.2 Discussion	152
6.2.1 Development of the Transgressive Stratigraphic Architecture	152
6.2.1.1 Depositional Environments and Processes	152
6.2.1.2 Implications for Transgressive Development	155
6.2.2 Chronological Framework of the Postglacial Transgression: Implications for Driving Processes	158
6.2.2.1 The Importance of Sea-Level Change Trends	158
6.2.2.2 The Role of Sediment Fluxes in the River Basin	158
7. Conclusions / Conclusiones	165
References	175
APPENDIX: Figures and tables	213

List of acronyms

AIW	Atlantic Inflow Water
ASM	Accelerator Mass Spectrometry
B-A	Bølling–Allerød Warm Period
BSFR	Basal Surface of Forced Regression
CC	Correlative Conformity
CCC	Coastal Counter Current
CNA	<i>Centro Nacional de Aceleradores</i>
ENACW	Eastern North Atlantic Central Water
FSST	Falling Stage Systems Tract
GC	Gravity-Corer
GCC	Gulf of Cádiz Current
GEV	Guadiana Eastern Valley
GIS	Geographic Information System
GMV	Guadiana Main Valley
H1	Heinrich Event 1
HR	High-Resolution
HST	Highstand Systems Tract
IACT	<i>Instituto Andaluz de Ciencias de la Tierra</i>
IGME	<i>Instituto Geológico y Minero de España</i>
IP	Incision Phase
IV	Incised Valley
ka	Kiloannum
LGM	Last Glacial Maximum
LQD	Late Quaternary Discontinuity
LSD	Last Subaerial Discontinuity
LST	Lowstand Systems Tract
Ma	Million Years
mbpsl /mbsl	Meters Below Present Sea Level / Meters Below Sea Level
mbsf	Meters Below Seafloor
MFS	Maximum Flooding Surface
MIS	Marine Isotopic Stages
ML	Mediterranean Lower Branch
MOW	Mediterranean Outflow Water
MPD	Mid-Pleistocene Discontinuity

List of acronyms

MRS	Maximum Regressive Surface
MSCL	Multi-Sensor Core Logger
MU	Mediterranean Upper Branch
MWP	Meltwater Pulse
mws	Margin Wide Surface
NASW	North Atlantic Superficial Water
PTU	Postglacial Transgressive Units
RFBIS	Ria Formosa Barrier Island System
RS	Ravinement Surface
RSME	Regressive Surface of Marine Erosion
RV	Research Vessel
SU	Suaerial Unconformity
SWIM	South West Iberian Margin
TOPAS	Topographic Parametric Sonar
TS	Transgressive Surface
TSE	Transgressive Surface Of Erosion
TST	Transgressive Systems Tract
UGR	University of Granada
VC	Vibro-Corer
XRF	X-Ray Fluorescence
YD	Younger Dryas

CHAPTER

1

CHAPTER 1:

Introduction

1.1. Incised valleys

Incised valleys are common stratigraphic features beneath modern coastal plains and continental shelves (Blum and Törnqvist, 2000; Holbrook et al., 2006; Blum et al., 2013). Incised valleys were initially characterized based on three main criteria (Van Wagoner et al., 1990): 1) significant erosional relief with truncation of older strata; 2) juxtaposition of fluvial or estuarine strata on marine deposits; and 3) demarcation of a significant basinward shift in facies, with subaerial exposure on interfluves (see also Zaitlin et al., 1994; Boyd et al., 2006). Later, the geological definition of a valley was challenged; the presence of a valley was not considered a fundamental criterion, as the occurrence of landward sediment transport and transgression (Dalrymple, 2006). Other studies (e.g., Blum and Törnqvist, 2000; Blum et al., 2013) used terms such as “valley” or “paleovalley system” because modern analogs of incised valleys are commonly buried beneath Holocene delta plains or submerged on the shelves and no longer have morphological expression. Throughout this doctoral thesis, I will use the terms ‘incised valleys’ and “paleovalley systems” interchangeably.

The incision and the sedimentary fill of valleys systems might provide critical information about earth-surface processes, related depositional histories, and their controls (Posamentier and Vail, 1988; Dalrymple et al., 1994; Zaitlin et al., 1994; Boyd et al., 2006; Blum et al., 2013; Wang et al., 2019, 2020). The interest in the study of these systems has varied considerably over the years.

1.1.1 Historical background

The first steps in the study of incised valleys preceded the development of radiometric dating techniques, when geologists were very interested in terrestrial valley formation and believed that the observed rates of incision could be used to estimate the age of the Earth (Lyell, 1853; Dana, 1880). These early investigations likely contributed to the historical consideration of erosional unconformities as significant geological features, with a specific focus on their recognition and classification throughout the first half of the twentieth century. Nevertheless, relatively little attention was paid to incised valleys or their sedimentary infillings during the following years (1940s to 1970s). Most of these early studies of incised valley systems primarily focused on regional geological mapping, or were driven by economic interests, as many examples of these stratigraphic features were identified as hydrocarbon reservoirs. As a result, pioneering studies concentrated on the study of the three-dimensional (3D) geometry of sedimentary bodies rather than on their depositional environment (Dalrymple et al., 1994).

From the mid-1960s to the early 1980s, sedimentological research changed its focus from stratigraphic studies to the development of 'static' facies models (Walker, 1992), which emphasized the role of autocyclic processes and ignored the influence of relative sea-level changes. However, with the publication of sequence stratigraphy concepts (e.g., Payton, 1977; Mitchum, 1985; Wilgus et al., 1988), the research on incised-valley systems gained a new focus. In that sense, Mitchum (1977) redefined the concept of incised valleys within the context of sequence stratigraphy, and the interpretation of valley incision as the result of relative sea-level falls became more prevalent. Under that initial interpretation, paleovalley systems were mainly characterized by incision and complete sediment by-pass, whereas subsequent deposition within valleys took place preferentially during sea-level lowstands and sea-level rise conditions.

During the 1980s, technological advances enabled the application of sequence stratigraphy principles to higher-resolution datasets. As the number of documented incised-valley deposits increased, a significant variability in facies and stratigraphic complexity was revealed. This led to a huge improvement in the identification of stratigraphically significant surfaces allowing for a better determination of sequence boundaries, which constitutes the basis for sequence stratigraphic analysis (e.g., Van Wagoner et al., 1988, 1990; Zaitlin et al., 1994). The rapid acceptance of sequence stratigraphy as the preferred method for stratigraphic analysis and hydrocarbon exploration fostered the recognition of incised valley deposits during the decade of the 1990s. These models of valley formation highlighted the complex nature of many incised-valley deposits as a result of cut-and-fill processes over several sea-level cycles. Therefore, valley evolution was considered to be driven largely by a combination of different patterns of sea-level change and downstream forcing mechanisms, such as shelf gradient and morphology (Wellner and Batek, 2003). These efforts led to a significant increase in the knowledge of the stratigraphic organization of estuarine facies within many incised valley systems, and provided important insights into the preservation potential of estuarine facies in transgressive settings (Nelson and Bray, 1970; Kraft et al., 1973; Belknap and Kraft, 1985; Kraft et al., 1987). Ultimately, the first integrated facies models for these systems were proposed, based on the distinction between wave- and tide-dominated estuaries (Dalrymple et al., 1994; Zaitlin et al., 1994).

During the 2000s, research focus on incised valleys benefited from the development and improvement of exploration techniques such as seabed imagery and 3D seismic geomorphology, as well as the application of quantitative approaches and numerical modelling (Boyd et al., 2006; Dalrymple et al., 2006). These advances resulted in refinements of the facies model through the classification of not fluvially-dominated estuaries and the assignment and abundance of system tracts within incised valleys. Specifically, more studies improved the knowledge of tide-dominated estuaries (Tessier, 2012). A critical view of initial founding schemes involved the reassessment of the importance of carbonate facies, climatic processes, and the slope of exposed surfaces in the formation of incised valleys (Boyd et al., 2006).

In addition, studies in incised valley systems have prompted a redefinition and/or reconsideration of conventional sequence stratigraphy concepts originally linked with incised valleys. In this sense, the chronostratigraphic significance of incised valleys as sequence boundaries has been questioned. Fluvial sediment deposition may be common during relative sea-level falls, instead of complete sediment bypass. Consequently, incised valleys may separate above and below strata of similar age and can be considered as facies boundaries represented by onlap-to-downlap surfaces underlying regressive shelf to shelf-margin deltaic and shoreface strata (Blum et al., 2013). Besides, paleovalley systems have been increasingly integrated in broader source-to-sink approaches, with shifting boundaries that correspond to changes in sediment routing and storage, ultimately controlling the connection between hinterland sediment supply and shelf-margin to basin floor final deposition.

Most recent investigations on these systems have focused on understanding the controlling factors beyond the dominant influence of rates and magnitude of relative sea-level change and, in general, of downstream forcing mechanisms (Chaumillon et al., 2008, 2010; Chaumillon and Weber, 2011; Mattheus and Rodriguez, 2011; Wang et al., 2019, 2020; Klotsko et al., 2021; De Falco et al., 2022; Mat Yusoff et al., 2023). Thus, significant variability in the stratigraphic architectures of incised valleys may be attributed primarily to upstream mechanisms and features such as basin physiography, catchment area, or river size (Mattheus and Rodriguez, 2011). Other factors, such as continental margin type, isostatic adjustments, and shoreline hydrodynamics, may also play a role in controlling the dimensions and distribution of incised valleys (Wang et al., 2019, 2020).

1.1.2 Incised valleys and sequence stratigraphy

1.1.2.1 Fundamentals of sequence stratigraphy

As it was previously mentioned, much of the modern significance of research on incised valleys derives from their association with sequence-stratigraphic concepts (e.g., Posamentier and Vail, 1988; Van Wagoner et al., 1988, 1991; Van Wagoner, 1990), as their formation was promoted as a sedimentary response to sequential phase changes. Sequence stratigraphy emerged as a formalized methodology in the late 20th century, building upon earlier concepts related to sedimentary cyclicity and stratigraphic architecture concepts (e.g., Payton, 1977; Mitchum, 1985; Wilgus et al., 1988). Initially developed for petroleum exploration, it has evolved into a versatile tool applicable to a wide range of geological studies, from outcrop analyses to seismic interpretations.

Sequence stratigraphy initially aimed to understand and interpret the vertical and lateral relationships of sedimentary rocks in the context of sea-level changes and related depositional processes. Latter scientific assumptions led to significant rethinking and the realization that multiple controls can interplay at overlapping timescales to generate stratigraphic cyclicity (e.g., Posamentier and Allen, 1999; Catuneanu, 2006; Miall, 2010). It is now understood that stratigraphic cyclicity often reflects the importance of local

controls on accommodation and sedimentation (Catuneanu, 2017, 2019). This scientific approach provides a framework for recognizing, correlating, and predicting the distribution of sedimentary successions, ultimately contributing to a comprehensive understanding of Earth's dynamic geological history.

The absence of formal standardization during the development of sequence stratigraphy, along with the significant variability in sedimentary successions, resulted in the proliferation of unnecessary complexity and sometimes conflicting terminologies that caused confusion within the scientific community. To address this problem, Catuneanu et al. (2009) initiated an international effort to standardize the sequence stratigraphy method. The former pertains to the objective features of stratigraphic sequences, such as the observation of stratal stacking patterns and changes thereof, whereas the latter refers to the nomenclature of stratigraphic surfaces and systems tracts, and the selection of sequence boundaries. The International Subcommission on Stratigraphic Classification recommended the adoption of a standard workflow based on model-independent principles free of any model-oriented personal preference to describe the cyclicity in sedimentary successions (Catuneanu et al., 2011). The sequence stratigraphic methodology provides a genetic, process-based analytical approach to stratigraphic interpretation that necessarily involves conceptual depositional models (Catuneanu et al., 2011).

The sequence stratigraphy model integrates multiple types of data, such as geophysical, sedimentological, petrographic, biostratigraphic, and geochemical data, to enhance the detailed and reliable interpretation of sequences. The definition of "sequence" has undergone refinement due to the gradual increase in stratigraphic resolution, and the latest definition describes it as "a cycle of change in accommodation or sediment supply defined by the recurrence of the same types of sequence stratigraphic surfaces through geologic time" (Catuneanu et al., 2009, 2010, 2011; Catuneanu, 2019). Sequences can be applied at different hierarchical levels, ranging from second-order to fourth-order or lower rank sequences, depending on the scale of observation, and the controls on their development are diverse, ranging from allogenic (eustatic, tectonic, and climatic) to autogenic processes (sediment supply). All sequences are bounded by sequence stratigraphic surfaces and can be subdivided into component systems of corresponding hierarchical rank. Hence, the identification and understanding of these sequence stratigraphic surfaces (Fig. 1.1; Table 1.1) are essential for comprehending the organization of sedimentary successions. These surfaces play a crucial role in serving as boundaries between sequences and delineating stratigraphic units that represent distinct phases of sedimentary response to sea-level changes (Catuneanu et al., 2009, 2010, 2011; Zecchin and Catuneanu, 2013).

Once these surfaces are identified, it is possible to subdivide stratigraphic sequences into systems tracts (genetic units *sensu* Catuneanu et al., 2009) that are linked to specific shoreline trajectories. Systems tracts, as defined by Brown and Fisher (1977) and further developed by Catuneanu (2019), refer to a stratal unit characterized by a stratigraphic

stacking pattern and its bounding surfaces, forming the subdivision of a sequence. These tracts play a pivotal role in categorizing sequences based on different shoreline trajectories, encompassing transgression, normal regression (lowstand or highstand), and forced regression. The types of systems tracts include: Transgressive Systems Tract (TST), Normal Regressive Systems Tract, including Highstand (HST) and Lowstand (LST), and Falling-Stage Systems Tract (FSST) (Fig. 1.1):

1) Transgressive Systems Tract (TST). Transgressive deposits display diagnostic retrogradational stacking patterns, bounded by the Maximum Regressive Surface–MRS and/or Ravinement Surface–RS at the base and the Maximum Flooding Surface–MFS at the top (Fig. 1.1). The TST retrogradational architecture results from rates of accommodation creation that outpace those of sediment supply at the shoreline, typically accompanied by a deepening-upward trend in shallow-marine settings (Posamentier and Allen, 1999; Catuneanu, 2002, 2006). The thickness of transgressive deposits relative to that of the entire sequence may vary considerably due to factors such as accommodation to supply ratio, the shape of sea-level curve, local physiography, and sediment input.

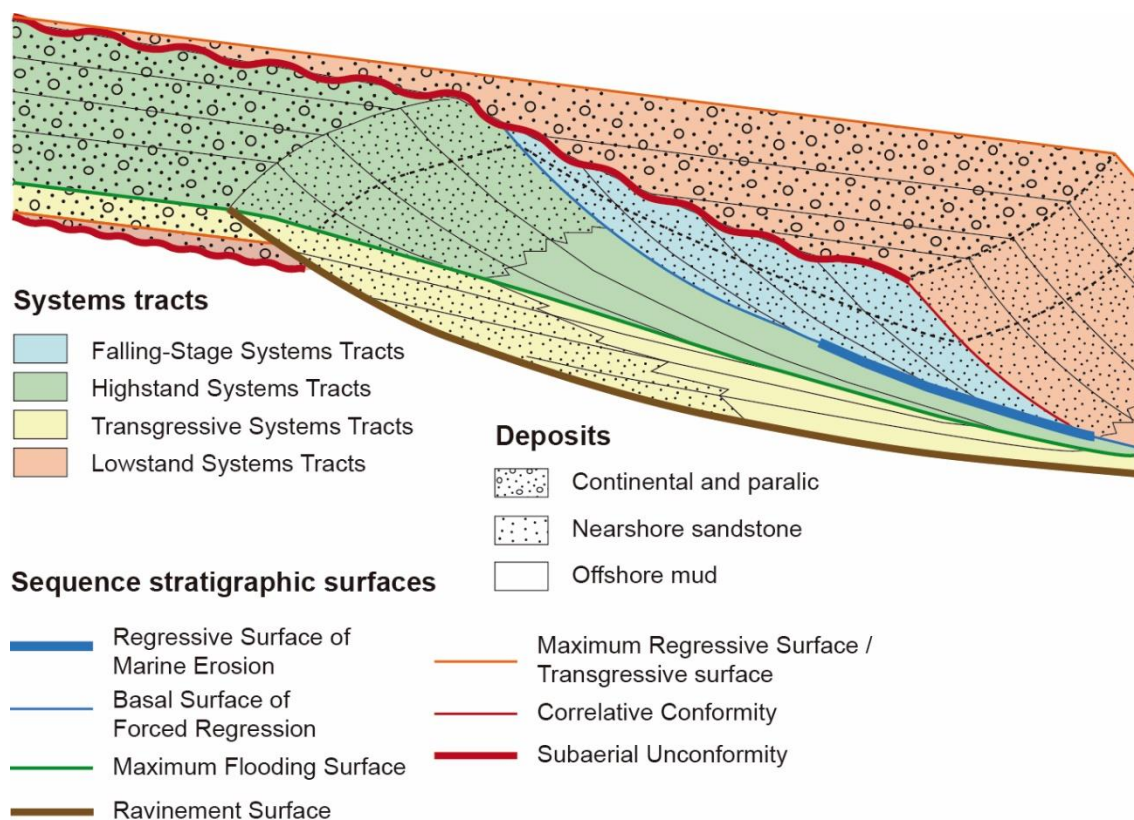


Figure 1.1: Sequence stratigraphic surfaces and systems tract beds developed during a full cycle of relative sea-level change in a clastic shelf/ramp setting. Continental to offshore deposits are considered (Adapted from Zecchin and Catuneanu, 2013).

2) Normal Regressive Systems Tract (Lowstand and Highstand). Normal regressive deposits display a combination of progradational and aggradational depositional trends (Fig. 1.1). Positioned between forced regressive (below) and transgressive (above) strata,

or between two FSST units, the LST is bounded by the Subaerial Unconformity–SU and the Correlative Conformity–CC at the base and the MRS and/or RS at the top (Fig. 1.1). The HST is bounded by the MFS at the base and the SU with the Basal Surface of Forced Regression–BSFR (or with the MRS in case that Falling-stage Systems Tract was absent), and/or the Regressive Surface of Marine Erosion–RSME at the top (Fig. 1.1). Normal regressions are driven by sediment supply, leading to shallowing-upward bathymetric trends near the shoreline but potentially offset in deeper basin areas. Normal regressive deposits are typically composed of clinofolds and include continental, deltaic, shoreface/shelf, shelf margin, and deeper marine sediments (Posamentier and Allen, 1999; Catuneanu, 2006, 2019a; Zecchin and Catuneanu, 2013).

Table 1.1: Sequence stratigraphic surfaces identified in high-resolution sequence stratigraphic studies (Catuneanu, 2006, 2019a; Zecchin and Catuneanu, 2013).

Surface	Definition
Subaerial Unconformity and Correlative Conformity (SU and CC; Sloss et al., 1949)	SU forms under subaerial conditions, associated with erosion, non-deposition, or pedogenesis, indicating temporal hiatus. CC represents the paleo-seafloor at the end of forced regression. It develops during relative sea-level fall and may continue during lowstand regression or transgression. It can also be triggered by climatic and tectonic factors
Maximum Regressive Surface (MRS; Helland-Hansen and Martinsen, 1996)	Also known as the ‘transgressive surface’ (TS; Posamentier and Vail, 1988). MRS/TS separates regressive deposits below from transgressive deposits above, marked by a shift from progradational to retrogradational stacking patterns.
Ravinement Surface (RS)	It is an erosional surface cut during transgression by waves (WRS; Swift, 1968) in shallow-marine settings or by tidal currents (TRS; Allen and Posamentier, 1993) in estuarine settings. The RS is relatively flat but can show high relief or irregularities in post-glacial transgressed shelves. Now is named as transgressive surface of erosion (TSE; Nummedal and Swift, 1987)
Maximum Flooding Surface (MFS; Posamentier et al., 1988; Van Wagoner et al., 1988)	MFS marks the seafloor at maximum shoreline transgression, indicating the change between transgressive and normal regressive trajectories
Basal Surface of Forced Regression (BSFR; Hunt and Tucker, 1992)	BSFR coincides with the seafloor at the onset of forced regression, marking the base of all marine forced regressive deposits. It results of increased sediment supply during relative sea-level fall.
Regressive Surface of Marine Erosion (RSME; Plint, 1988)	RSME is a diachronous surface formed by wave erosion in the lower shoreface during relative sea-level fall, marking the base of forced-regressive shorefaces. This surface may not form in front of river-dominated deltas with steep seafloor gradients.

3) Falling-Stage Systems Tract (FSST). Forced regressive deposits display diagnostic progradational and downstepping stacking patterns. They are bounded by the BSFR, the

RSME and the SU at the base and by the SU with its Correlative Conformity–CC at the top, potentially truncated by younger RSs (Fig. 1.1). The FSST occurs during relative sea-level falls, forcing shoreline regression irrespective of sediment supply (Catuneanu, 2002, 2006; Zecchin and Catuneanu, 2013).

Independent to scale of observation, stratigraphic cycles define sequences, which consist of systems tracts and component depositional systems, reflecting the interplay of local and global controls on accommodation and sedimentation (Catuneanu, 2019). This interplay may result in a great variability in the stacking pattern of systems tracts that needs to be accounted for in sequence stratigraphic analyses (Catuneanu et al., 2011).

1.1.2.2 Incised valleys in a sequence stratigraphic framework

The formation and development of valley systems and their associated deposits occur during two main sequential phases: 1) incision of valley systems during episodes of relative sea-level fall that cause rivers to incise their bed in an attempt to reach a new lowered equilibrium profile and may continue during lowstand (LST; Summerfield, 1985; Blum and Törnqvist, 2000; Holbrook et al., 2006; Blum et al., 2013); and 2) deposition within valleys, in response to relative sea-level lowstand and sea-level rise, when the resulting valleys were subsequently inundated, infilled and reworked by fluvial, coastal and marine processes (Posamentier and Vail, 1988; Posamentier and Allen, 1999; Dalrymple and Zaitlin, 1994; Zaitlin et al., 1994; Blum et al., 2013).

Incised valleys record a complex history of infilling (Fig. 1.2; Posamentier and Vail, 1988; Thomas and Anderson, 1994; Zaitlin et al., 1994; Rodriguez et al., 2005; Simms et al., 2007; Blum et al., 2013). Conceptual stratigraphic models for sedimentary infilling in wave-dominated and tide-dominated settings have been proposed (Dalrymple et al., 1992; Boyd, 2010; Dalrymple, 2010). In wave-dominated estuaries, wave energy plays a pivotal role in sediment transport and deposition, and sandy facies are prevalent, characterizing a typical tripartite facies distribution (Dalrymple et al., 1992; Boyd, 2010) that consists of sandy barrier beaches and tidal-inlet complexes at the mouth, transitioning inland to central-basin muds and sandy bayhead delta deposits (Fig. 1.2G to 1.2J). In contrast, in tide-dominated estuaries, the tidal forces generate complex patterns of sedimentation, resulting in the development of tidal sandbars grading into mudflats and salt marshes further up-estuary (Fig. 1.2A to 1.2C). Mud and silt facies are dominant in the upper reaches of tide-dominated estuaries, where fine-grained sediments settle down due to reduced energy levels. In the ideal case of a tide-dominated estuary, the facies distribution consists of longitudinal tidal bars at the mouth, followed landward by sandy tidal channel-and-bar complexes (Tessier, 2012).

The two end-member models are not drastically different as both illustrate a single transgressive-regressive infilling cycle, with landward and then seaward shift of facies and sedimentary bodies.

a) Typically, the lower part of the incised valley infilling comprises coarse-grained fluvial deposits such as point bars or channel lags that are bounded at their base by fluvial erosion surfaces (e.g., Horozal et al., 2021). These deposits accumulated at their bases during falling-stage and/or lowstand conditions (FSST and/or LST; Blum and Price, 1998; Strong and Paola, 2008; Martin et al., 2011; Blum et al., 2013).

b) Estuarine and marine deposits subsequently fill the valleys from lowstand to the following early transgressive conditions, when fluvial gradients are reduced by slowly rising sea levels promoting accumulation (Blum and Törnqvist, 2000; Holbrook et al., 2006; Blum et al., 2013; Wang et al., 2019). As transgression progresses, the valley margins and fill may be reworked by coastal and marine processes, resulting in estuarine depositional systems separated by different ravinements, such as bay, tidal, and shoreface ravinements, or ebb-flood diastems (Foyle and Oertel, 1997; Liu et al., 2017). The bay flooding surface or bay ravinement is formed by the initial flooding of the fluvial system (Nummedal and Swift, 1987). It separates underlying fluvial deposits from overlying estuarine deposits and marks the first major paralic-marine flooding event in an evolving paleovalley-fill succession (Foyle and Oertel, 1997; Nordfjord et al., 2006). Tidal ravinement is caused by the erosion of tidal currents in coastal inlets or channels due to the landward and lateral migration of the estuary-mouth during a continuous transgression (Zaitlin et al., 1994; Nordfjord et al., 2006). While this tidal ravinement forms in or near the mouth of the drowning incised valley, a bayhead channel diastem is produced locally in the landward part of the estuary-mouth complex by the seaward progradation of a bayhead delta (e.g., Ashley and Sheridan 1994). Similar to tidal ravinements but with less relief, estuarine ebb-flood channel diastems are produced over relatively small areas within the bay mouth and are not associated with the estuarine main ebb-flood channels (Foyle and Oertel, 1997). Finally, the shoreface or wave ravinement surfaces truncate all underlying estuarine deposits and result from the landward retreat of the shoreface during transgression (Swift, 1968; Roy, 1994). The wave and current erosion must remove both flood tidal-delta deposits and possibly some central-basin facies to create this ravinement surface (Ashley and Sheridan, 1994). All these transgressive surfaces are diachronous and may amalgamate within a preserved sequence boundary associated with the transgression (McHugh et al., 2004).

c) Valley infillings are capped by shoreface to open shelf depositional systems and facies composing the succeeding highstand system tract, characterized by an aggradational to progradational stacking pattern (HST; Posamentier et al., 1988, Allen and Posamentier, 1993; Boyd et al., 2006; Horozal et al., 2021). Sub-environments developed during the HST of valley fills include different facies such as tide- and wave-dominated deltaic facies (Fig. 1.2A, and 1.2B), tidal flat and marsh muds (Fig. 1.2C), open marine muds (Fig. 1.2D, and 1.2E), and sandy sheet deposits (Fig. 1.2I, and 1.2J).

The architecture of individual valleys shows a large variability, although the preservation of the complete spectrum of depositional systems from lowstand to highstand is rare during successive cycles of valley infilling. Stratigraphic variability is

particularly high in recent infillings postdating the Last Glacial Maximum (Fig. 1.2). A tripartite occurrence of facies (fluvial to estuarine to coastal shelf) is recognized in some valley fills in response to the alternance of hydrodynamic and sedimentary conditions (Fig. 1.2; Aquino da Silva et al., 2016; Liu et al., 2017; Graves et al., 2021). However, many valleys seem to contain simple infillings, either mud-rich with dominance of vertical aggradation (Long et al., 2021) or sand-rich progradational sandy units (Fig. 1.2D; Chaumillon et al., 2008). These simple infillings are characterized by the dominance of a particular system tract (i.e., lowstand versus transgressive deposition; Fig. 1.2E, and 1.2H).

Some valleys are characterized by thick fluvial channel deposits exhibiting both lateral accretion and vertical aggradation, due to the preservation of different fluvial facies such as channel lags or laterally accreted bar complexes (1.2F; Wellner and Bartek, 2003; Meckel and Mulcahy, 2016; Ronchi et al., 2018). Specifically, the dominance of lateral channel migrations is typical of meandering rivers (Wetzel et al., 2021). Most of these infillings are composed of LSTs, where estuarine-related deposits are limited (Wellner and Bartek, 2003). In these valleys, accumulation rates were strongly reduced after fluvial systems were flooded and stepped back (Tjallingii et al., 2010). The preferential dominance of lowstand deposits within incised valleys is characteristic of large fluvial systems where drastic modifications of sediment supply are conditioned by climatic changes.

Other types of valley systems are characterized by successions of estuarine sediments truncated by transgressive ravinements. These valleys contain a wide variety of depositional systems (Maselli and Trincardi, 2013), including bay-head deltas, central basin facies, and estuary-mouth deposits (Fig. 1.2G, 1.2I, and 1.2J). These valleys are completely filled by TSTs and are usually connected to small rivers with low sediment inputs (Qiu et al., 2019; Long et al., 2021). In these transgressive-dominated valleys, the recognition of the transgressive architecture along the valley is rarely achieved, not even the connection of these valley fills with genetically related shallow-water transgressive deposits. In some cases, even nearby incised valleys exhibit different stratigraphic architectures due to different interactions between fluvial-to-estuarine and littoral transport processes (Chaumillon and Weber, 2006).

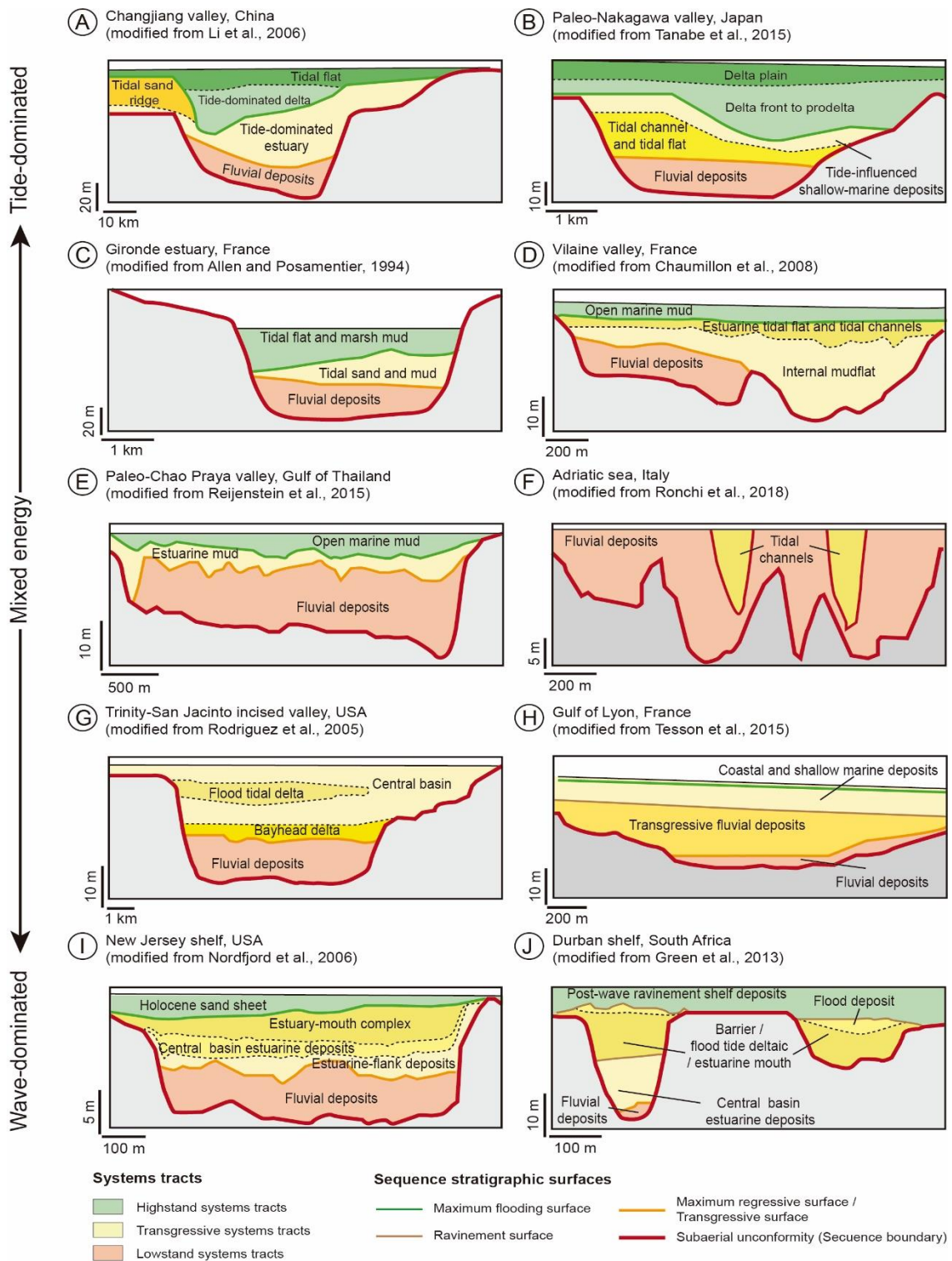


Figure 1.2: Stratigraphic architectures of worldwide incised-valley fills, illustrating the seismostratigraphic variability (bounding surfaces and system tracts) between them. The examples are grouped by the hydrodynamic regimes from wave- to tide-dominated. A) Changjiang valley, China (Li et al., 2006); B) Paleo-Nakagawa valley, Japan (Tanabe et al., 2015); C) Gironde estuary, France (Allen and Posamentier, 1994) D) Vilaine valley, France (Chaumillon et al., 2008); E) Paleo-Chao Praya valley, Gulf of Thailand (Reijenstein et al., 2015); F) Adriatic Sea, Italy (Ronchi et al., 2018); G) Trinity-San Jacinto incised valley, USA (Rodriguez et al., 2005) H) Gulf of Lyon, France (Tesson et al., 2015); I) New Jersey shelf, USA (Nordfjord et al., 2006); J) Durban shelf, South Africa (Green et al., 2013).

1.1.2.3. Transgressive deposition in continental shelves

Transgressive deposits exhibit a great variability on continental shelves, where their development may or may not be related to incised valleys. Several models of transgressive development have been proposed: 1) in-place drowning; 2) erosional shoreface retreat; and 3) transgressive submergence. In-place drowning involves the formation of coastal deposits followed by rapid flooding. The result of rapid flooding is the preservation of original deposits, and the amount of reworking is limited (Sanders and Kumar, 1975; Rampino and Sanders, 1980). This process is typical of low-gradient shelves during intervals of accelerated relative sea-level rise (Cattaneo and Steel, 2003). Erosional shoreface retreat describes widespread erosion as the shoreface moves landward, with a continuous, slow sea-level rise. In these cases, the preservation of coastal deposits is low, and the transgressive record consists mainly of reworked deposits (Fisher, 1961; Bruun, 1962; Swift, 1968, 1975, 1976; Kraft, 1971). Transgressive submergence defines an intermediate situation with a lower phase of coastal deposition and an upper phase of marine reworking. This takes place during periods of high rates of relative sea-level rise and is common for low-gradient continental shelves with limited local sand sources in a high-energy, storm-dominated environment (Penland et al., 1988).

The greatest abundance, distribution, and thickness of postglacial transgressive deposits (Fig. 1.3) occur on deposition-dominated continental shelves, such as the Gulf of Lions (Fig. 1.3A; Gensous and Tesson, 2003) or the Adriatic Sea (Fig. 1.3B; Maselli et al., 2011) in the Mediterranean Sea. Deposition-dominated shelves are characterized by high rates of sediment supply provided by large rivers, such as the Rhône (Labaune et al., 2008) or the Po rivers (Trincardi et al., 1996). These conditions are combined with gentle topography, which results in reduced reworking and favors sedimentary preservation (Belknap and Kraft, 1985).

Lower transgressive development occurs in settings characterized by decreased sediment supplies and/or higher-energy oceanographic regimes. For example, stretches of the Californian shelves contain a reduced amount of transgressive depositional bodies compared to the Mediterranean cases, possibly because of lower sediment inputs (Fig. 1.3C; Klotsko et al., 2015). In the East China Sea, the postglacial transgressive architecture is strongly influenced by the tide-dominated hydrodynamic regime, leading to the development of tidal sand ridges (Fig. 1.3D; Li et al., 2014). On the Durban shelf, eastern South Africa, the increased role of currents and waves may lead to the preferential development of barrier and backbarrier deposits due to increased sediment redistribution (Fig. 1.3E; Pretorius et al., 2016, 2019).

In erosion-dominated shelves such as the continental shelf offshore New Jersey (Fig. 1.3F; Nordfjord et al., 2009), transgressive ravinement plays a major role in forming recognizable surfaces. Due to the continuous dominance of erosional processes, even during relative deep-water conditions, transgressive strata exhibit a low preservation potential (Goff et al., 2005; Nordfjord et al., 2009).

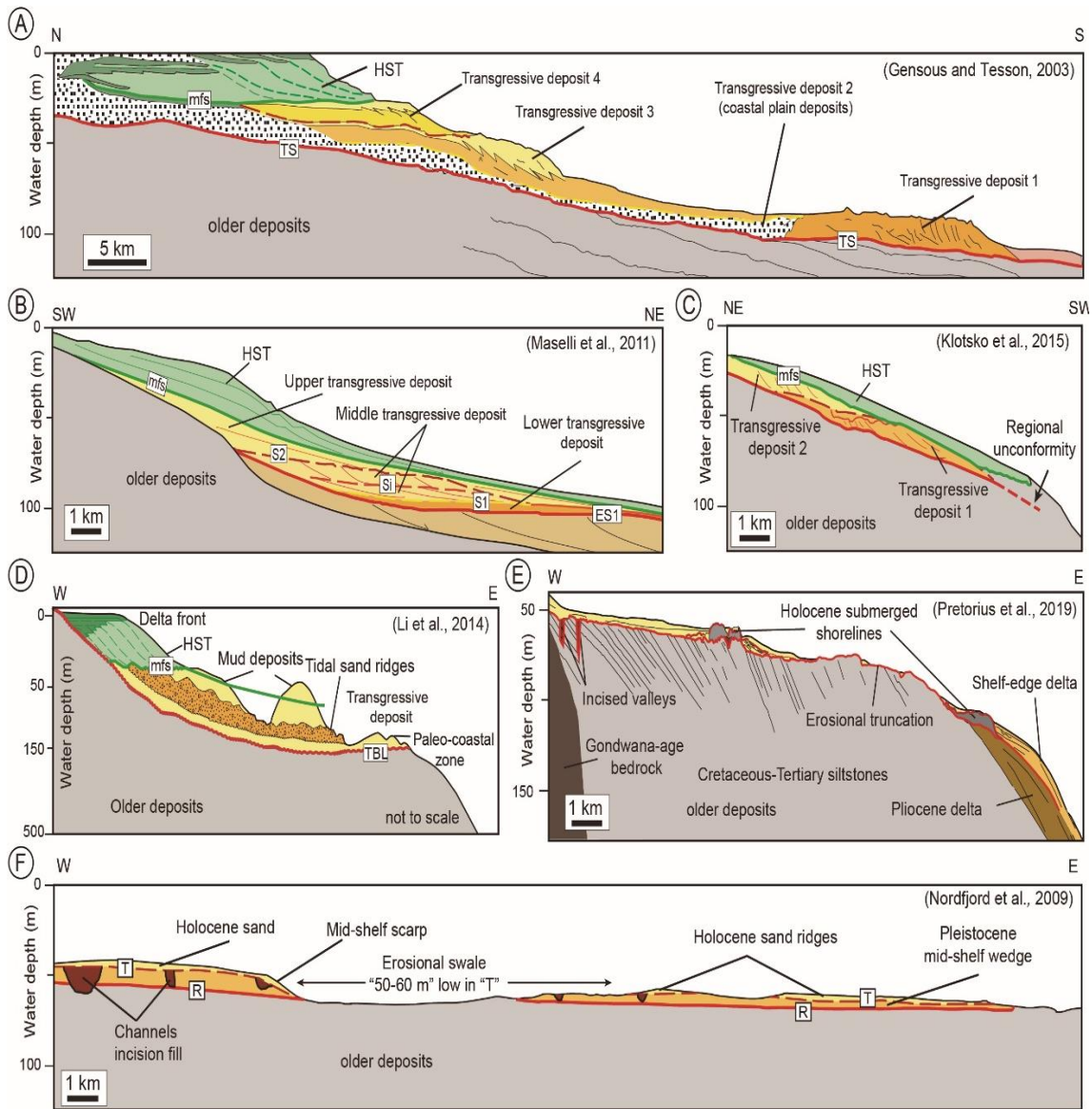


Figure 1.3: Examples of stratigraphic organization of postglacial transgressive deposits. The relative position of each example is based on the prevailing sedimentation/erosion ratio in each setting (up and left, where sedimentation is higher than erosion). A) Gulf of Lions, characterized by high rates of sediment supply (adapted from Gensous and Tesson, 2003). B) Central Adriatic margin, also characterized by high rates of sediment supply. ES1, regional unconformity; S1 and S2, regional surfaces, each recording a specific interval of sea-level rise; Si, internal surface of erosion (adapted from Maselli et al., 2011). C) Offshore San Onofre, California characterized by a reduced amount of transgressive depositional bodies, possibly because of lower sediment inputs (adapted from Klotsko et al., 2015). D) East China Sea, where the transgressive architecture is strongly influenced by the hydrodynamic regime. TBL, transgressive boundary layer (adapted from Li et al., 2014). E) Durban shelf, eastern South Africa, characterized by the preferential development of barrier and backbarrier deposits (adapted from Pretorius et al., 2019). F) Continental shelf off New Jersey, characterized by a major role of transgressive ravinement. "R" horizon, a composite product of erosion, forms the base of three seismically recognized sedimentary deposits of latest Pleistocene-Holocene age older than the LGM. "T" horizon, the transgressive ravinement associated with Holocene sea-level rise (adapted from Nordfjord et al., 2009). Highstand systems tracts (HST) are represented in green, and transgressive deposits are represented in yellow-orange. The different transgressive units are designated differently according to their sequential order in each location. mfs, maximum-flooding surface; TS, transgressive surface.

1.1.2.4 Simple versus complex incised valleys

There is a significant and intricate variability in incised valleys and their deposits. Attending to this, incised-valley systems can be categorized into two main classes, depending on the presence or absence of multiple internal, high-frequency sequence boundaries (Boyd et al., 2006):

1) Simple paleovalley systems; these are related with a single phase of sea-level fall and the corresponding depositional sequence (e.g., Allen and Posamentier, 1991, 1994; Li et al., 2002; Gutierrez et al., 2003; Weber et al., 2004a, b). Most of these simple paleovalleys are small sized, such as fluvial tributary channels or barrier inlet throats. Tributary channels tend to be backfilled with muds. In barrier inlets, the migration of the tidal inlet results in the creation of a tidal cut ravinement under the barrier (Ashley and Sheridan, 1994).

2) Compound paleovalley systems, formed during multiple superimposed cycles of incision and deposition (e.g., Thomas and Anderson, 1994; Foyle and Oertel, 1997; Proust et al., 2001; Tesson et al., 2005). Most intermediate-sized and large drowned valleys can be considered compound systems, where the preservation potential increases with valley size. Large valleys are typically characterized by alternating sandy and muddy deposits and by the imprint of diverse estuarine to marine erosional surfaces (Ashley and Sheridan, 1994). There are two main types of stratigraphic organization of compound incised valleys and/or shelf paleochannels:

a) The occurrence of superimposed simple valleys associated with different generations of vertically stacked stratigraphic horizons. These incisions tend to be located in different places in distinct stratigraphic horizons, and reoccupation processes are limited (Burger et al., 2001). This leads to the reset of drainage patterns during successive incision phases (Matthews et al., 2020). These incised horizons are usually interpreted as widespread fluvial erosion surfaces generated in response to periods of shelf exposure associated with relative sea-level falls and subsequent lowstands (e.g., Foyle and Oertel, 1997; Burger et al., 2001; Darmadi et al., 2007; Weschenfelder et al., 2014; Brothers et al., 2020).

b) The occurrence of amalgamated complex valleys, which may exhibit lateral shifting of thalweg axis (i.e., multilateral paleochannels) or vertical superposition of thalwegs axis (i.e., multistorey paleochannels). These amalgamated valleys tend to have larger dimensions than individual simple valleys and are considered the result of autogenic processes, such as channel avulsion leading to channel abandonment or reoccupation leading to renewed incision (Long et al., 2021). These processes are supposed to be particularly effective during sea-level lowstands (Horozal et al., 2021). In those settings where amalgamated valleys occur, their connection with regionally extensive subaerial surfaces may not be straightforward. However, in cases where a complete picture of the

entire shelf environment was provided, these incision surfaces could be correlated seaward with the boundaries of forced regressive lowstand wedges (Labaune et al., 2010).

The occurrence of simple versus amalgamated valleys may be attributed to a combination of factors, such as the fingerprint of background geology (e.g., Labaune et al., 2010), and the occurrence of lithological changes between previously incised valleys and lateral interfluves (Matthews et al., 2020).

1.1.2.5 Incised valleys shape

The morphology of incised valleys is variable according to multiple factors, such as duration of sea-level falls, changing climatic conditions, drainage basin characteristics, underlying structure and lithology, and river-to-shelf gradients (Horozal et al., 2021; Klotsko et al., 2021). Different cross-sectional geometries can provide information about the nature of dominant hydrodynamic processes (i.e., fluvial versus tidal) and their influence on sediment transport and deposition (Nordfjord et al., 2006). Besides, valley shapes can be also used to estimate paleo-discharges (Nordfjord et al., 2005; Bae et al., 2018).

Plan-view geometries may exhibit a full gradation ranging from low to high sinuosity (Bae et al., 2018; Tan et al., 2020) that is determined to some extent by gradients, which ultimately lead to changes in dominant sediment composition (coarse- versus fine-grained) (Alqahtani et al., 2017). Comparison of plan-view channel patterns with paleo-discharges can reveal the degree of maturity of the valley systems (Nordfjord et al., 2005).

In several settings and at different timescales, the relief, plan-view pattern, and extent of incised valleys and associated interfluves change with time. These temporal changes have also been related with a multiplicity of controlling factors. Specifically, climatically driven changes may affect fluvial discharge and sediment supply from the adjacent drainage basins, ultimately leading to changes in hydraulic energy (Darmadi et al., 2007; Alqahtani et al., 2017; Dubey et al., 2019; Tan et al., 2020). Other influences on temporally variable valley morphology may include the alteration of different-magnitude sea-level changes (Xu et al., 2022) or changing hydrodynamic conditions (Labaune et al., 2010).

In contrast to the temporal variability, the spatial variability of incised valleys through the Quaternary has been seldom addressed, as its detection relies on the existence of more extensive and dense datasets. These lateral changes in paleochannel density and/or thickness have been related to regional structural trends and variability of dominant coastal processes (Long et al., 2021).

1.2. Controlling Factors

The development of incised valley systems is considered to be a consequence of changes over time of boundary conditions in fluvial systems (Blum et al., 2013). These boundary conditions can be classified into two main classes: upstream (i.e., water supply,

volume, rate and size distribution of sediment inputs, distribution of uplift or subsidence along the system) and downstream (i.e., sea-level changes, hydrodynamics, and shelf physiography). These changes in the boundary conditions result from the interplay between allogenic and autogenic processes. Allogenic refers to externally imposed changes (i.e., tectonic activity and/or climate change), whereas autogenic refers to internally generated fluctuations (i.e., sediment supply, hydrodynamic variables, and antecedent topography).

The relative importance of allogenic versus autogenic forcing is the subject of much interest (e.g., Blum et al., 2013; Wang et al., 2019, 2020). Allocyclic processes such as the rate and magnitude of relative sea-level variations are the primary drivers of the development and stratigraphic organization of incised valleys (Dalrymple et al., 1994; Chaumillon et al., 2010; Wang et al., 2020). However, other controlling factors such as variations in sediment supply, hydrodynamic processes, pre-existing tectonic features, or the nature of antecedent geology also play an important role during the formation and evolution of these systems (Zaitlin et al., 1994; Dalrymple, 2006; Chaumillon et al., 2010).

1.2.1 Sea-level variations

Changes in relative sea level have been assumed to be the primary controlling mechanism for the development of incised valleys, driven by allocyclic processes such as tectonic activity and climate change. In passive margins and over time scales of 10^6 yr or less, it is difficult to envision tectonic signals, and sea-level changes are mostly driven by climatic changes (Blum et al., 2013).

In the context of sequence stratigraphy, the stratigraphic cyclicity observed at different scales can be described as hierarchical sequences, in which the stacking pattern of a higher order is composed of an organized amalgamation of lower-ranked sequences (Catuneanu, 2006). Depositional sequences recording Milankovitch cyclicity are considered high-frequency sequences and fall within the 4th and 5th order of the sequence stratigraphy hierarchical classification. These sequences typically cover time intervals of 100-200 and 10-40 ka, respectively (Mitchum and Van Wagoner, 1991; Vail et al., 2002).

During the Plio-Quaternary, global changes in ice volume and sea level have followed different rhythms (~400, 100, 41, 23, and 19 ka) predicted by the Milankovitch theory of orbital forcing (Hays et al., 1976). Such changes in global sea level have deeply influenced global environments and sedimentary processes. Along the Plio-Quaternary, significant changes in climatic cyclicity and dynamics of glacial-interglacial cycles took place, including a crucial transition in the frequency and amplitude of climatic cycles (Fig. 1.4A; Berends et al., 2021). During the early part of the record (~2.7 to 3.6 Ma BP; Fig. 1.4A), average oscillations were relatively small in amplitude, in coincidence with globally warm conditions and no major ice sheets in the Northern Hemisphere (Lambek et al., 2002). At ~2.7 Ma ago, the oscillations increased in amplitude and the mean value also increased;

glacial-interglacial climatic cycles changed to an approximate periodicity of ~40 ka, aligning with orbital variations related to axial obliquity. These dominant Early Pleistocene 5th-order cycles occurred between 2.6 and 1.2 Myr and persisted until the Mid-Pleistocene Transition (MPT; ~0.9 Ma), when the Pleistocene glacial cycles changed from 41 to ~100 kyr periodicity.

1.2.1.1. Late Quaternary cycles

At ~0.9 Ma the dominant oscillations changed to a 100 ka periodicity (Fig. 1.4A, and 1.4B; Lambeck et al., 2002; Berends et al., 2021). These high-frequency, high-amplitude sea-level oscillations driven by glacio-eustasy during the late Quaternary constituted an exceptional pattern for the development of incised valleys and associated deposits. Although the temporal spans involved in repeated shelf valley development are highly variable and the number of incised surfaces is variable from place to place, the frequency of incisions has been mostly related to the dominant imprint of glacial-interglacial cycles, which exhibit a dominant 100 ka periodicity with amplitudes of about 100 m during the Late Quaternary (Fig. 1.4A, and 1.4B; Foyle and Oertel, 1997; Labaune et al., 2010; Brothers et al., 2020); more specifically, continuous valley incision has been documented for the last 500 ka (Burger et al., 2001). During these cycles, most valleys were incised during episodes of relative sea-level fall and infilled during subsequent rises (e.g., Lambeck and Chappell, 2001; Grant et al., 2012).

1.2.1.2. Higher frequency cycles during the Last Glacial Cycle

The imprint of higher-frequency sea-level cycles (i.e., temporal spans shorter than 100 ka or 40 ka cycles) on valley development has been proposed in a number of settings, where individual surfaces have been linked to intra-Late Pleistocene sea-level changes (e.g., Long et al., 2021; Xu et al., 2022). Even in some recent examples, multiple generations of fluvial channels have been framed within short temporal spans (i.e., 5 ka) during Marine Isotopic Stage (MIS) 3, in response to multiple base level cycles (Liu et al., 2023). Incised valleys systems formed during the last glacial cycle show significant variability worldwide, as this cycle provides an unusual record of their development (Figs. 1.2, and 1.3; e.g., Lambeck and Chappell, 2001; Grant et al., 2012).

The most recent phase of valley incision and infilling is the best studied, in connection with the Last Glacial Maximum (LGM) lowstand and subsequent postglacial sea-level rise. The LGM is globally dated from 26 to 19 ka (Clark et al., 2009). The rise in global mean sea level began at ~ 20 ka when the sea level was located at ~ 120 m below the present level (Fig. 1.4C; e.g., Fairbanks, 1989; Bard et al., 1990, 1996; Lambeck et al., 2002; Siddall et al., 2003; Peltier and Fairbanks, 2006). This sea-level rise was non-uniform, with different phases related to major climate events identified (Fig. 1.4C; e.g., Bard et al., 1990, 1996, 2010; Stanley, 1995; Stanford et al., 2011; Lambeck et al., 2014; Peltier et al., 2015; Harrison et al., 2019).

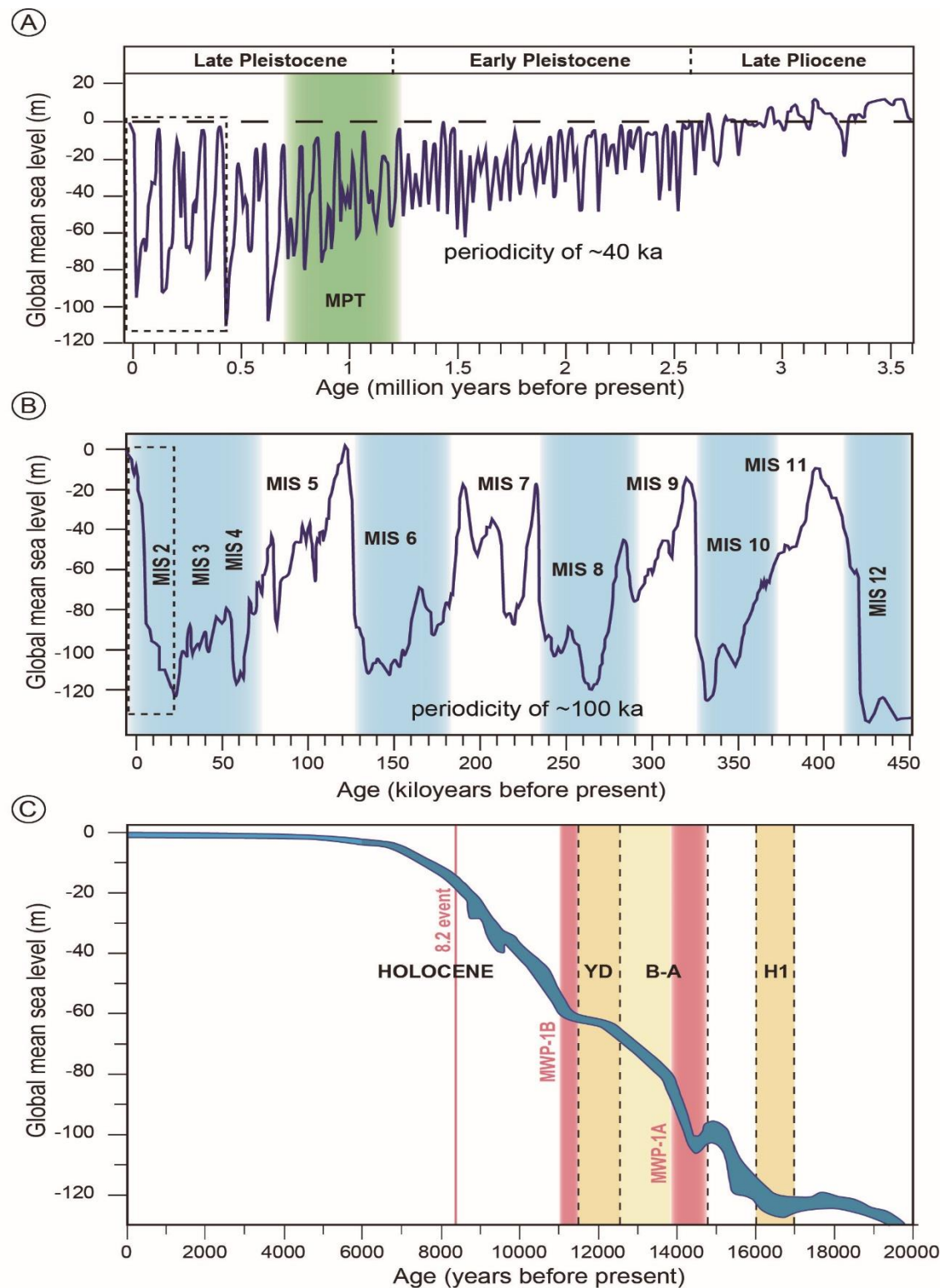


Figure 1.4: A) Schematic global mean sea level curve from the last 3.5 Ma (modified from Berends et al., 2021). The position of the Mid-Pleistocene Transition (MPT) is indicated. B) Schematic late Quaternary sea-level curve showing 100 ka glacio-eustatic cycles from the last 450 ka (Modified from Grant et al., 2014, and Mestdagh et al., 2019). Marine Isotopic Stages (MISs) 2-11 are highlighted. C) The pattern of postglacial sea-level rise, with indication of major climatic events such as: Heinrich Event 1 (H1), the Bølling-Allerød warm period (B-A), and the Younger Dryas (YD) cold period. Timing of Melt-Water Pulses (MWPs) 1A and 1B and the 8.2 ka cooling event (in red) are also indicated. Sea-level curve is modified from Lambeck et al. (2014).

An initial phase of ~ 10-15 m sea-level rise occurred between ~ 21-20 and 18 ka (Fig. 1.4C; Harrison et al., 2019), followed by a short period of near-constant sea level from ~ 18-16.5 ka, which corresponds with the occurrence of Heinrich Event 1 (H1) (Fig. 1.4C; Carlson and Clark, 2012; Lambeck et al., 2014). Subsequently, the major phase of deglaciation occurred from ~ 16.5-8.2 ka, with an average rate of sea-level rise of 12 m/ka (Lambeck et al., 2014). In this interval, several phases driven by the occurrence of meltwater pulses (MWP) have been identified (e.g., Fairbanks, 1989; Stanford et al., 2011; Lambeck et al., 2014). MWPs were global events involving the rapid introduction of meltwater into the ocean from ice-proximal environments as ice sheets decayed (Carlson and Clark, 2012; Harrison et al., 2019).

The major phase of deglaciation (16.5-8.2 ka) was initiated by a ~ 25 m rise from ~ 16.5-15 ka (Fig. 1.4B; Stanford et al., 2011), which was followed by a nearly constant period of sea-level stability lasting ~ 500-600 yrs. A period of high rate of sea-level rise (MWP-1A) began at ~ 14.5 ka, coinciding with the onset of the Bølling–Allerød (B-A) warm period (Fig. 1.4B; Bard et al., 1990; Carlson and Clark, 2012). The MWP-1A was characterized by an initial ~ 20 m sea-level rise at rates up to ~ 40 mm/y over ~ 500-600 yrs followed by another 20 m sea-level rise during 14-12.5 ka (Bard et al., 1996; Lambeck et al., 2014). MWP-1A was followed by an interval from ~ 12.5-11.5 ka of significantly reduced rates of sea-level rise, coeval to the Younger Dryas (YD) stadial in the Northern Hemisphere (Fig. 1.4B; Bard et al., 2010). The final interval of this major phase of deglaciation (~ 11.5-8.8 ka) was driven by MWP-1B (Bard et al., 2010), marked by a rapid 500-years long sea-level rise at a rate of ~ 16.5 mm/y (Fig. 1.4B; Harrison et al., 2019). Other periods of accelerated sea-level rise (MWPs-1C and 1D) postdating MWP-1B and separated by periods of slow sea-level rise have been described in sea-level curves with a well-defined stepped pattern (e.g., Liu et al., 2004). However, the sea-level imprint of these more recent MWPs is not recorded in well-known global sea-level curves (Fig. 1.4B; e.g., Lambeck et al., 2014). The early Holocene was characterized by a nearly uniform global rise with an average rate of ~ 15 m/ka; this phase was marked by a cooling event at 8.2 ka (Fig. 1.4B; Stanford et al., 2011; Carlson and Clark, 2012). Finally, a reduced rate of sea-level rise after 8.2 ka has been reported in a number of settings (e.g., Fairbanks, 1989; Lambeck et al., 2014).

In summary, sea-level fluctuations resulting from allocyclic processes (mainly governed by glacio-eustasy) are considered the primary control mechanism for the development of incised valley systems and their associated deposits during the Quaternary. However, the significant diversity in shape and infill of these valleys indicates that other controlling factors have also played a crucial role in their morpho-stratigraphic development.

1.2.2 Tectonics, sediment supply, hydrodynamic regime, and antecedent geology

Considerable variability exists in both the stratigraphic architecture and the spatial distribution of incised valleys. If sea level were the only factor responsible for the genesis of incised valleys, it would be expected that valleys in close proximity would have a similar architecture due to the fact that they have experienced similar sea-level changes. Nevertheless, many studies demonstrate that despite these similarities, their shape, sediment infill, and internal organization are surprisingly different (Chaumillon and Weber, 2011). Hence, setting aside the unquestionable influence of sea-level changes, the formation, geometry, dimensions and architecture of incised valleys are believed to be influenced by the interplay of tectonics, sedimentary characteristics, and climatic controls (Wellner and Batek, 2003). These other factors include variations in upstream and downstream forcing mechanisms, such as river and sediment discharges (Mattheus and Rodriguez, 2011; Wang et al., 2019, 2020), river and shelf gradients, pre-existing tectonic features, and the morphology and nature of antecedent geology, which may offer different resistance to erosion, eventually dictating hydrodynamic processes and sediment supply (Zaitlin et al., 1994; Dalrymple, 2006; Chaumillon et al., 2010).

The distinct influences of those controlling factors are variable depending on the scale of the valley systems. Concerning their stratigraphic expression, their complexity increases with valley size, from small to large drowned valleys (Ashley and Sheridan, 1994). Thus, small valleys tend to be composed of simple sequences, and their architecture is more influenced by the effects of background geology on marine processes (Chaumillon and Weber, 2006; Chaumillon et al., 2008; Menier et al., 2010; Klotsko et al., 2021; De Falco et al., 2022) rather than by the characteristics of catchment areas (Maselli and Trincardi, 2013). In that sense, shelf gradients and antecedent morphology have interacted with variable rates of sea-level rise, modulating the variation of accommodation (Wellner and Batek, 2003) and the hydrodynamic regimes, which ultimately influenced the nature and distribution of depositional systems. As valley size increases, physiographic controls become less important, and climatic and hydrodynamic variations usually lead to significant modifications of sediment supply and sources (Chaumillon et al., 2008; Cartelle et al., 2022). In such larger valleys, the thickness of fluvial and estuarine deposits increases (Wang et al., 2020), and compound incised valleys may be preserved (Zaitlin et al., 1994), reflecting the influence of superimposed sea-level cycles (Dalrymple et al., 1994).

1.2.2.1 Tectonic influence

Tectonics is a first-order factor that controls patterns of uplift and subsidence, which results in changes in relative sea level and accommodation. These processes ultimately affect the drainage evolution and the steering of river systems into depositional basins (Miall, 1996; Blum et al., 2013; Wang et al., 2019). Recent studies suggest that the type of continental margin can likely predict the internal fills and geometry of incised valleys

because of the effects of the tectonic setting on basin physiography (Fig. 1.5; Wang et al., 2019, 2020). Hence, the tectonic setting of continental margins appears to control the geometry of incised-valley fills, probably through its effects on relative sea-level change, characteristics of basin physiography, climate, water discharge, rates and modes of sediment supply, and nature of sediment load (Wang et al., 2019, 2020; Mat Yusoff et al., 2023).

Tectonics can significantly influence fluvial incision through a first-order control on basin physiography (tectonically active margins versus passive margins). Active margins are commonly characterized by narrow, high-gradient shelves, which favor deep fluvial incision (Schumm and Brackenridge, 1987; Leckie, 1994). In contrast, passive margins are characterized by wider, low-gradient shelves that result in shallower incisions, in part because such margins are generally associated with larger drainage-basin areas (Blum et al., 2013). Besides, larger rivers are typically associated with passive margins (Syvitski and Milliman, 2007), and therefore usually associated with higher rates of sediment supply, which control shoreline progradation rates, and with larger maximum bankfull depths, which translate to thicker channel belts, bars, and channel fills (Gibling, 2006; Syvitski and Milliman, 2007; Blum et al., 2013).

The resulting incised-valley fills developed along active margins are shown to be thicker and wider, on average, than those along passive margins. Contrary to expectations based on river size, active margins host incised-valley fills with a higher proportion of fluvial deposits and a lower proportion of central-basin estuarine deposits compared to passive margins. This discrepancy is attributed to variations in sediment load; river systems along passive margins are generally larger and transport high suspended-sediment loads, fostering estuarine deposits (Fig. 1.5A; e.g., Portela et al., 2013; Carlin et al., 2015). Active margin settings (Fig. 1.5B) undergoing rapid uplift are typically associated with high relief, which favors orographic precipitation (Joeckel, 1999; Ruddiman, 2013), and controls water discharge, which subsequently leads to larger runoffs per basin area (Milliman and Syvitski, 1992). In addition, tectonically active systems are generally associated with smaller catchment areas, and storms can affect the entire drainage basin, leading to floods that propagate through the entire channel network (Fig. 1.5; Sømme et al., 2009). These factors promote a tendency for more rapid equilibrium profile attainment, enhancing the lateral migration of fluvial channel belts, valley widening, and deeper incision (Fig. 1.5B).

Additionally, in certain distal settings, incised valleys depths of tens of meters and without a clear connection with inland drainages have been documented (Reynaud et al., 1999; Lericolais et al., 2003; Paquet et al., 2010). The explanation for the formation of these incised valleys resulted in a combined effect of glacio-eustatic cycles and tectonic processes, such as tilting or local tectonic uplift (Reynaud et al., 1999; Burger et al., 2001).

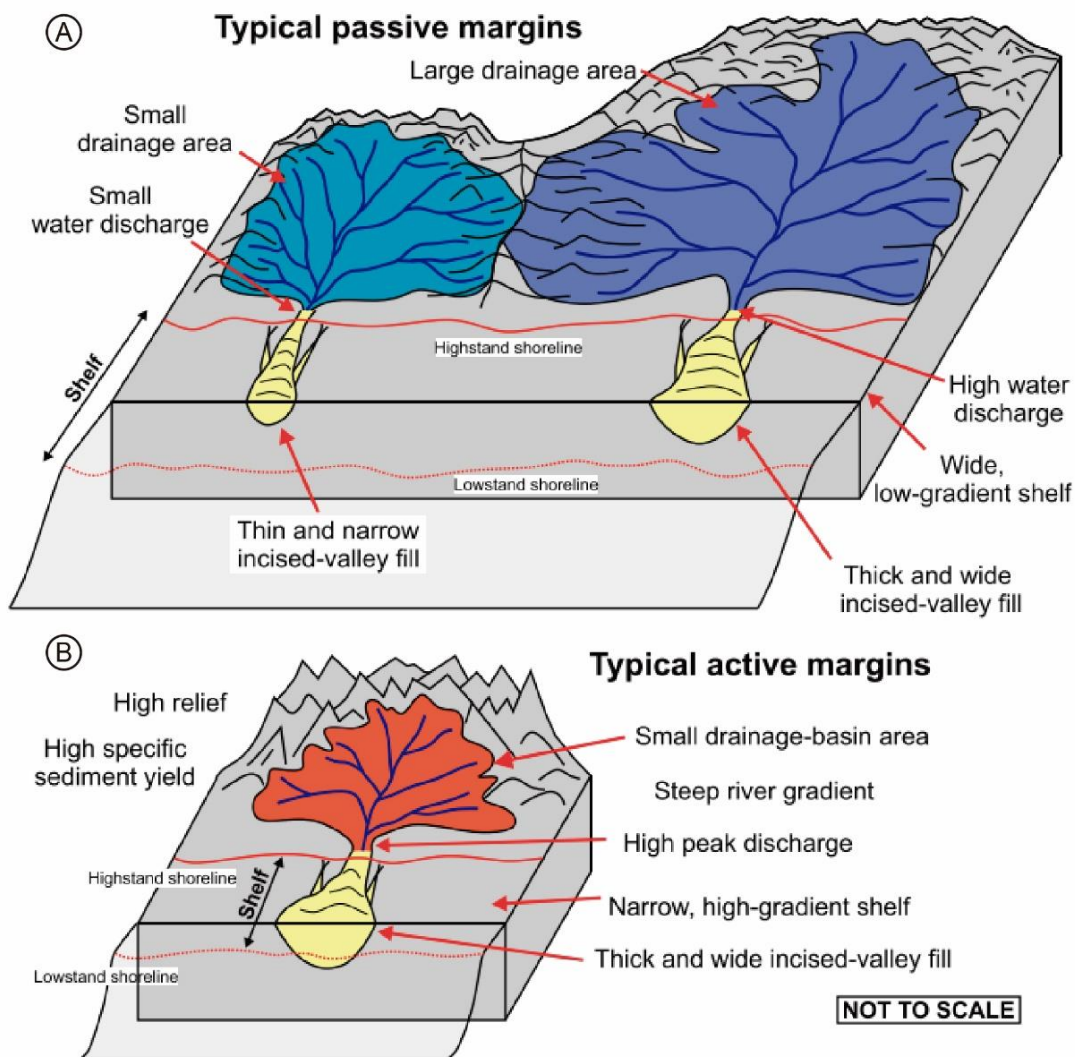


Figure 1.5: Schematic diagrams of different incised-valley-fill dimensions corresponding to passive margins (A) and active margins (B). Along passive margins (A), the scale of incised-valley fills associated with large and small drainage-basin areas is compared (taken from Wang et al., 2019).

1.2.2.2 Sediment supply and hydrodynamic regime

The nature of valley infilling is mostly determined by the rates of sediment supply and the potential of hydrodynamics (i.e., waves and tidal currents) to rework the sediments (Dalrymple et al., 1994; Chaumillon et al., 2010; Tessier, 2012). The balance between hydrodynamics and sediment supply exerts a major control on the preservation of systems tracts (Boyd et al., 2006) and on the formation of distinctive surfaces within incised-valley infillings, such as ravinement surfaces (Zaitlin et al., 1994; Tessier, 2012).

Sediment supply is controlled by upstream factors such as drainage basin size and climate, which are correlated with the shape and size of incised valleys (Wang et al., 2019). Drainage-basin area emerges as a primary factor, as it could be indicative of water discharge and sediment yield, particularly in passive continental margins. Vegetation

cover in catchment areas, especially in tropical or subtropical regions, influences evapotranspiration, runoff characteristics, and sediment supply. This, in turn, affects rates of fluvial incision and lateral migration, contributing to variations in valley-fill thickness, width, and cross-sectional area (Wang et al., 2019). Climate, through its influence on temperature, precipitation, vegetation, and permafrost, also affects water discharge, sediment supply, and bank stability, contributing to variations in valley-fill dimensions (Mattheus et al., 2007; Mattheus and Rodriguez, 2011; Blum et al., 2013). The proportion of fluvial and estuarine facies in these systems appears to be influenced by the rate of sediment supply (Dalrymple et al., 1994).

In areas with low fluvial inputs, where catchment areas and river sizes are small, hydrodynamics is a key mechanism for the development and preservation of incised valley systems. Hydrodynamic conditions at the shoreline significantly influence sedimentary processes (Tessier, 2012). Specifically, tidal ravinement surfaces may constitute the most important stratigraphic features locally developing tidal inlets (Ronchi et al., 2018), extending through the estuarine phase of incised valleys (Tessier, 2012).

The relationship between present-day hydrodynamic conditions and the width of incised valleys is complex. The bay-ravinement, or estuarine shoreline erosion, which is controlled by the imposing energy regime of waves and tides, can lead to the widening of incised valleys (Mattheus and Rodriguez, 2011). Nevertheless, other studies (Wang et al., 2020) do not consistently support this notion, as there is no clear correlation between incised-valley-fill width and mean wave height at modern shorelines.

The geometry of flooded incised valleys has also been recognized as a factor controlling the internal fills of incised valleys through its control on hydrodynamic conditions (Dalrymple et al., 1992; Chaumillon et al., 2010; Nordfjord et al., 2006). Funnel-shaped valleys enhance tidal wave amplification, favoring tide-dominated conditions (Dalrymple et al., 1992; Chaumillon et al., 2010; Tessier et al., 2012). Nordfjord et al., (2006) argued that narrower and deeper valleys should promote the development of tide-dominated environments, whereas wider valleys might be, comparatively, more dominated by wave processes. Nevertheless, recent observations of positive correlation between incised-valley-fill width and the proportion of tide-dominated elements contradict this idea and may reflect how these two variables co-vary in response to a common control exerted by the present hydrodynamic regime (mean tidal range) at the shoreline (Wang et al., 2020). These observations support the idea that wider valleys with gentler gradients, associated with larger rivers, have larger tidal prisms and stronger tidal currents.

1.2.2.3 Antecedent geology

The antecedent geology and basin physiography are considered second-order controlling factors, as they influence hydrodynamics and sediment supply in incised valleys (Chaumillon et al., 2010). The control of background geology on the development and preservation of incised valley systems seems to be mainly related with the morphology of the basin. Therefore, shelf-break depth, shelf width, and shelf gradient are key factors that play an important role in shaping incised-valley dimensions and in the genesis and preservation of its deposits (Wang et al., 2019, 2020). Additionally, other factors related to the control of antecedent geology on incised valleys are the presence or absence of pre-existing tectonic features, the preservation of barrier islands, which could protect the systems from marine and coastal erosion, and the nature of antecedent geology, which may offer different resistance to erosion.

a) Antecedent coastal and shelf physiography.

The type of coastal physiography and size of the sea into which a valley discharges exert a direct influence on hydrodynamic conditions. For example, enclosed or semi-enclosed seas are generally characterized by more restricted fetch, lower wave heights, and lower tidal ranges. Wave energy at the shoreline depends largely on deep-water wave energy, the water depth of the basin, and the frictional attenuation that occurs on the shelf (Reading and Collinson, 1996). The relationship between mean wave height and shelf-break depth and the proportion of wave-dominated elements and average shelf gradient suggest that shallower shelves are subject to lower wave energy (Wang et al., 2020).

Antecedent shelf physiography also plays a key role in modulating the influence of sea-level changes. Previous conceptual models suggest that the shelf becomes fully exposed when relative sea-level falls exceed in magnitude the depth of the shelf break, driving the formation of incised valleys cutting through the shelf (Talling, 1998; Posamentier, 2001; Törnqvist et al., 2006). Consequently, fluvial systems on shallower shelves are expected to undergo a greater vertical river-profile adjustment, resulting in greater valley incision. However, recent studies do not fully support this view, documenting shelves with breaks deeper than 120 m that tend to contain larger incised-valley fills (Wang et al., 2019). This could be explained by the fact that the studied shelves with shelf breaks deeper than 120 m are primarily linked to larger drainage-basin areas compared to those with shallower shelf breaks. Subsequently, they tend to have steeper shelf gradients on average, which results in larger differences between the shelf gradient and the fluvial equilibrium profile. Therefore, they tend to drive deeper fluvial incision for a given relative sea-level fall (Schumm and Brackenridge, 1987; Leckie, 1994; Wang et al., 2019).

b) Shelf width.

The relation between shelf width and valley dimensions suggests a co-variation due to a common control exerted by the size of drainage areas, where large fluvial basins are generally associated with wider shelves through the control on sediment input and shelf progradation (Burgess et al., 2008; Blum et al., 2013).

c) Shelf gradient.

Changes in shelf gradient play a role in the initiation and/or enhancement of fluvial incision on the shelf (Klotsko et al., 2021). Steeper shelves could lead to a more significant difference between the shelf gradient and the fluvial equilibrium profile. Consequently, a relative sea-level fall is likely to result in deeper fluvial incision, which increases accommodation and enhances preservation of estuarine bay/lagoon deposits within incised valleys (Posamentier and Allen, 1999; Wang et al., 2019). Therefore, shelf gradients may indirectly control the development and preservation of the geometry of estuarine bay/lagoon deposits within cross-shelf incised valleys through its effects on the dimensions and the resultant accommodation space (Wang et al., 2020).

Furthermore, most cross-shelf valleys become less distinctive towards the middle to outer shelf, as backwater effects evolve during relative sea-level falls (Blum et al., 2013). Consequently, valley incision tapers at variable distances from landward coastlines at maximum water depths of 70-80 m (Lericolais et al., 2001; Maselli and Trincardi, 2013).

Antecedent shelf gradient is also shown to play a role in controlling the establishment and preservation of barrier-complex deposits within shelf incised valleys (Storms et al., 2008; Pretorius et al., 2016; Green et al., 2018). As the effects of erosion at the shoreline across high-gradient shelves are much greater than across low-gradient shelves during ensuing transgressive ravinement, severe reworking or breakdown of barrier systems is a likely process (Cattaneo and Steel, 2003).

d) Substratum composition.

The nature of the underlying substratum could also control the development of incised valleys, implying that valleys that are hosted in unconsolidated sedimentary covers are expected to be deeper than bedrock valleys at any time before equilibrium is reached. In addition, the decreased erodibility of bedrock valley walls should result in narrower valleys. Nevertheless, in some cases, certain studied valleys may not align with these expectations since larger fluvial systems are more likely to scour to the depths of lithified strata (Wang et al., 2019).

Antecedent geology may also consist of indurated paleo-barriers, ancient counterparts of barriers related with the transgressive evolution of the system, which could directly influence the basinward continuity of incised valleys. Shelves mainly covered by lithified, indurated deposits would preclude the development of wide fluvial

valleys. Seaward of these indurated paleo-shelves, finer-grained sediments would be more susceptible to widespread erosion, and the traces of the valleys would be more easily removed (De Falco et al., 2022).

1.3. Hypotheses and aims

The justification and significance of this doctoral thesis stem from its potential scientific, social, and industrial applications arising from the comprehensive characterization of incised valleys and their associated deposits. The primary goal of this PhD thesis is to enhance the understanding of the geosphere's response to climate and eustatic global changes that primarily control the formation and development of incised valley systems within the northern margin of the Gulf of Cadiz. Furthermore, the study of incised valleys and their associated deposits provides insights into the response of these sedimentary systems to global changes across diverse temporal scales. It also contributes to delineating the varying roles played by fluvial systems in the development of continental margins. The study of drainage network evolution on the shelf carries implications for comprehending the transfer of biological species between adjacent basins and for determining settlements and preferred migration routes during early stages of human occupation on the shelf. The research findings derived from the thesis hold direct applications in the petroleum industry by aiding in the understanding and assessment of the geometry, spatial distribution, and temporal variations of facies that make up reservoir rocks in analogous systems.

The northern margin of the Gulf of Cadiz is an ideal location to evaluate the interplay between sediment supply and sea-level change. It is characterized by a hierarchical stratigraphic architecture and presents a unique geological setting shaped by late Quaternary glacio-eustatic changes and tectonic influences. Here, several orders of sequences have been established during the Plio-Quaternary. A change of the dominant cyclicity after the Middle Pleistocene at 900 ka led to the preferential development of shelf-margin wedges under the influence of 100 ka cycles (Somoza et al., 1997; Hernández-Molina et al., 2000b, 2002; Lobo et al., 2005). Additionally, the post-LGM sea-level rise provides exceptional conditions for studying the sedimentary response to sudden shelf flooding caused by the alternation of periods with different rates of sea-level rise.

The study area is characterized by locally high fluvial supplies combined with an oceanographic regime of moderate energy, representing a situation intermediate between low-energy delta-forming environments and high-energy ravinement-forming environments. The main sediment inputs come from two major rivers (Guadiana and Guadalquivir), whose continuous sediment flux has driven the outward margin growth at least during the late Quaternary (Hernández-Molina et al., 2000b; Lobo et al., 2005; Mestdagh et al., 2019). The recognition and interpretation of incised valleys in the

previously reported stratigraphic framework of the northern margin of the Gulf of Cadiz remains limited. Recent studies mapped two main N-S valleys in the inner shelf off the Guadiana River, which were initially related to the LGM and reoccupied other older incised valleys. In addition, previous studies described a succession of backstepping deposits attributed to the post-LGM transgressive interval, which seems to be associated with these incised valleys (Lobo et al., 2001; González et al., 2004). These deposits are partially covered by a suite of highstand depositional systems formed during the last 6.5 ka (Lobo et al., 2004b; Hanebuth et al., 2021). West of the Guadiana River, the Algarve coast in southern Portugal is dominated by an extensive barrier-lagoon system (i.e., the Ria Formosa system) with reduced fluvial supply, where abundant incised valley features are identified, likely suggesting the existence of significant hydrological changes during the recent past.

Bearing in mind these preliminary observations, the general goals of this PhD thesis are:

1) To integrate the formation of incised valleys linked to different significance fluvial sources in relation to late Quaternary glacio-eustatic changes and to provide a sequence stratigraphic framework.

2) To determine the influence of variable sediment supplies in the generation of incised valley stratigraphic architectures.

3) To reveal the role played by antecedent topography and hydrodynamic regimes.

These overarching objectives will be addressed throughout the following chapters of this doctoral thesis through the execution of a series of specific objectives.

First, Chapter 4 of this PhD thesis aims at characterizing a network of cross-shelf paleovalleys in the eastern Algarve inner shelf off the Gilão-Almargem Estuary, a small fluvial drainage system that presently receives minor sediment supply in order:

1) To frame the paleovalleys in the chronostratigraphic scenario available for the northern Gulf of Cadiz shelf.

2) To determine the driving factors which may have enabled the formation and/or eventual preservation of incised valleys in a presently undersupplied shelf.

3) To constrain the relative influence of these controlling factors that triggered substantially different paleohydrological conditions and sedimentary dynamics of ancient fluvial systems in this margin, focusing mainly on evidences of secondary controls on valley genesis and evolution, such as antecedent geology, low fluvial supply, and changing hydrodynamic regimes.

Then, Chapter 5 focuses on the study of the long-term evolution of two main N-S valleys in the inner shelf off the Guadiana River, characterized by locally high fluvial supplies, and their links with the progressive shelf growth. The specific objectives of this study are:

1) To document the architecture of the main paleovalleys recognized on the shelf of the Guadiana River and to establish genetic links with the late Quaternary development of the continental shelf.

2) To reconstruct paleoenvironmental conditions during the last major phase of valley incision through a geomorphological analysis.

3) To reveal distinct responses of paleovalley infilling following the Last Glacial Maximum.

Finally, Chapter 6 aims to study in detail a succession of backstepping deposits attributed to the post-LGM transgressive interval, which seems to be related with the N-S incised valleys studied in previous Chapter 5. The specific objectives of that study are:

1) To understand the variability and succession of sedimentary processes and systems during each shelf flooding episode under the light of existing models for transgressive development (i.e., in-place drowning, transgressive submergence, or erosional shoreface retreat).

2) To explain the differential development of postglacial deposits in response to different rates of sea-level rise, postglacial climatic variability, and sediment fluxes.

CHAPTER

2

CHAPTER 2:

Regional setting

The study area is located on the northern Gulf of Cadiz continental margin, southwestern Iberian Peninsula (Fig. 2.1). This area comprises three well-defined physiographic domains: the continental shelf, the continental slope, and the abyssal plain (Fig. 2.1B; Hernández-Molina et al., 2006; Mestdagh et al., 2019). This PhD thesis focuses on two main areas of the shelf: 1) the eastern Algarve continental shelf (Portugal), offshore the Gilão-Almargem Estuary (Chapter 4); and 2) the Huelva continental shelf off the Guadiana River mouth, where both incised valleys (Chapter 5) and related transgressive deposits (Chapter 6) were studied.

2.1. Geological setting

The geological evolution of the Gulf of Cadiz, particularly in the late Cenozoic era, is primarily influenced by the convergence of the Eurasian (Iberia sub-plate) and African (Nubia sub-plate) plates since the mid-Oligocene (Dewey et al., 1989; Srivastava et al., 1990; Rosenbaum et al., 2002). The Azores-Gibraltar fracture zone serves as the boundary between these plates in the Atlantic Ocean. Dextral strike-slip faults, known as South West Iberian Margin (SWIM) faults, traverse the Gulf of Cadiz, accommodating the present-day oblique WNW-ESE convergence (e.g., Terrinha et al., 2009; Zitellini et al., 2009; Bartolomé et al., 2012). The region also experienced the westward migration of the Gibraltar arc, leading to NE-SW-striking thrust faults and the formation of an accretionary wedge during the Late Miocene (Maldonado et al., 1999; Gutscher et al., 2002). As a consequence, several major morpho-tectonic domains are recognized in the northern margin of the Gulf of Cadiz (Maldonado et al., 1999):

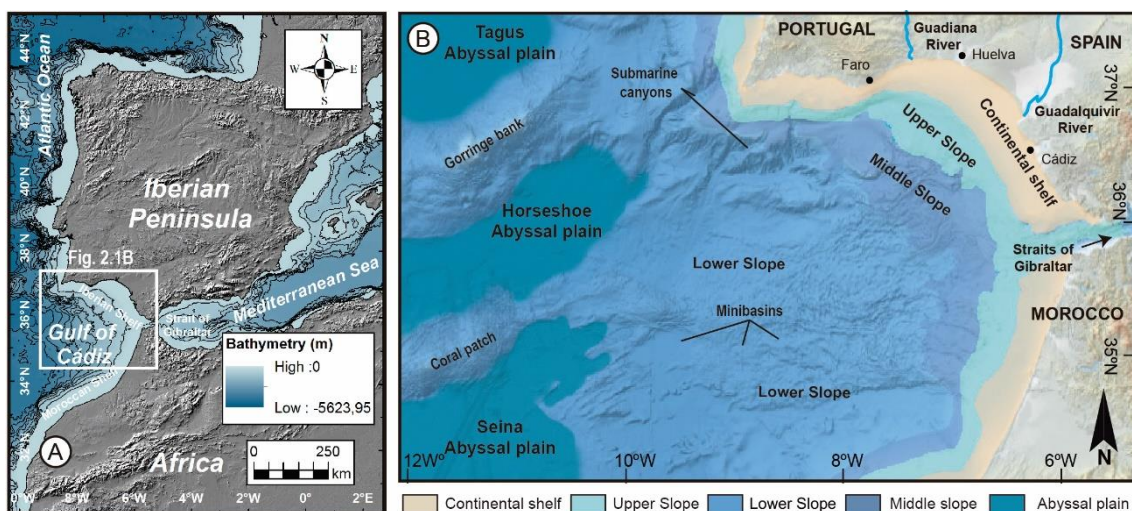


Figure 2.1: A) Geographical location of the Gulf of Cádiz within the general context of the NE Atlantic Ocean. B) Physiographic domains along the Gulf of Cádiz.

a) The western prolongation of the Betic Chain in the Gulf of Cadiz includes the Campo de Gibraltar Flysch and the accretionary wedge (Gràcia et al., 2003; Medialdea et al., 2004). Outcrops of fault-bounded blocks of flysch and Subbetic units occur in the southeastern shelf of the northern Gulf of Cadiz margin (Maldonado et al., 1999). The accretionary wedge is also known as the Allochthonous or Olistostrome Unit. It is a seismically chaotic body composed of gravitational deposits such as debrites and olistostromes, and salt and shale nappes affected by extensional collapses (Torelli et al., 1997; Medialdea et al., 2004).

b) The Neogene Guadalquivir foreland basin formed on top of NNW-moving olistostromes forming imbricate Miocene wedges, and mostly filled with Middle to Late Miocene depositional sequences (Fernández et al., 1998). Both the Allochthonous Unit and the Sudiberic paleomargin formed a relatively unstable base for Neogene sedimentary basins (Hernández-Molina et al., 2016).

c) The Algarve Basin extends from inshore, where a Paleozoic basement of the Hercynian massif of Iberia and a flysch sequence of slates and greywackes crop out, to offshore where the basin fill is composed of Mesozoic and Cenozoic sedimentary rocks (Terrinha, 1998; Maldonado et al., 1999).

The following major evolutionary phases have been recognized in the Gulf of Cadiz (Fig. 2.2; Maldonado and Nelson, 1999):

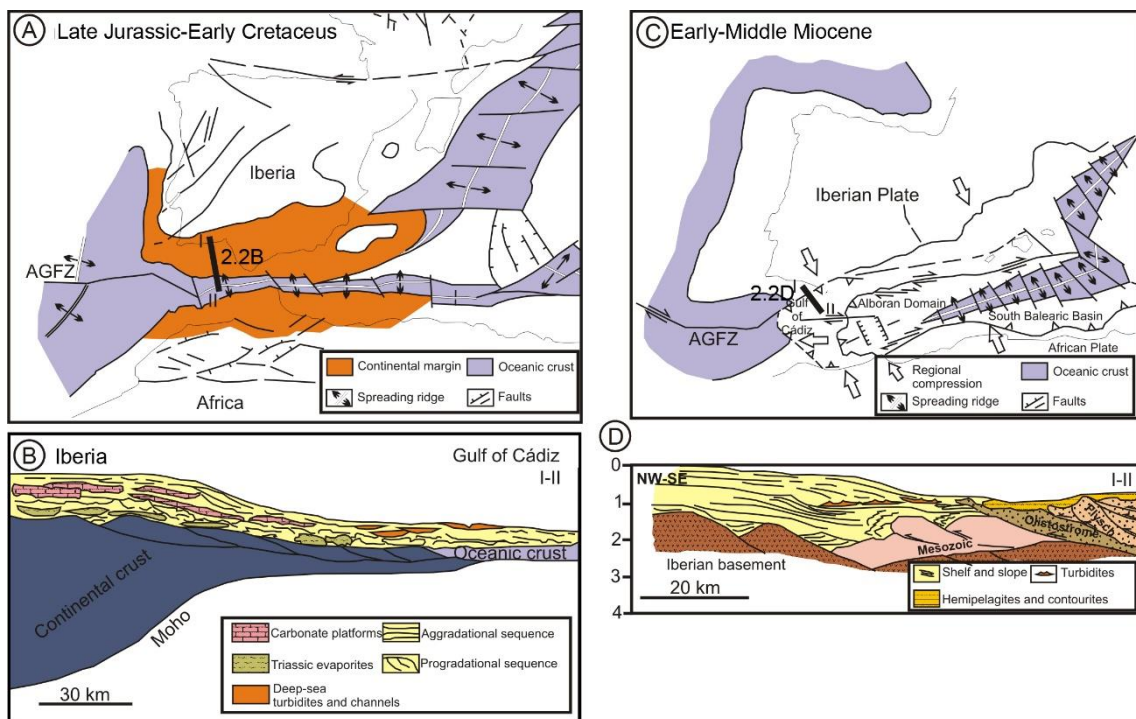


Figure 2.2: Long-term geological evolution of the Gulf of Cádiz: A) geological setting during the Late Jurassic and Early Cretaceous; B) interpretative cross-section during the Late Jurassic and Early Cretaceous; C) geological setting during the Early-Middle Miocene; and D) interpretative cross-section during the Early-Middle Miocene. Adapted from Maldonado and Nelson (1999).

An oblique passive margin was developed in the Mesozoic and continued until the early Tertiary (Fig. 2.2A and 2.2B); this margin was characterized by half-graben extensional structures and marine carbonate platforms (Maldonado et al., 1999). A Lutetian to Oligocene halokinetic phase resulted from the reactivation of N-S to NW-SE Hercynian basement structures and thin-skinned contraction of a thick evaporitic unit of Late Triassic to Early Jurassic (Hettangian) age (Lopes et al., 2006; Matias et al., 2011; Ramos et al., 2017).

The margin evolved from the Oligocene towards the Early Miocene to a terrigenous regime under active transcurrent tectonics (Fig. 2.2C and 2.2D). Closely juxtaposed regions of compression and extension were formed near the Iberian-African plate boundary due to the relative motions between both tectonic plates, the orientation and geometry of preexisting basement tectonic structures, and the development of the Alpine orogeny involving the westward migration of the Gibraltar Arc (Maldonado and Nelson, 1999; Lopes et al., 2006; Ramos et al., 2016, 2020). A Late Miocene paroxysmal phase of Iberia-Africa convergence led to the emplacement of the Allochthonous Unit (Torelli et al., 1997) and was accompanied by a second halokinetic phase originated from the Hettangian salt in the Algarve margin (Lopes et al., 2006; Matias et al., 2011). This phase was terminated by a period of accelerated tectonic subsidence (Maldonado et al., 1999).

During the Pliocene-Quaternary, faults and folds underwent several reactivations under a transpressive regime (Rodero et al., 1999; Zitellini et al., 2009). The early Pliocene witnessed the instauration of a terrigenous drift regime which led to the deposition of thick progradational-to-aggradational depositional sequences (Maldonado and Nelson, 1999), under conditions of enhanced subsidence due to the development of extensional collapses in the Allochthonous Unit (Medialdea et al., 2004). The Late Pliocene-Quaternary was dominated by glacio-eustatic sequences mainly composed of regressive and lowstand deposits (Hernández-Molina et al., 2002), accompanied by substantial decreases of subsidence rates (Maldonado and Nelson, 1999). 100 ka sequences have been formed after the Mid Pleistocene Transition (MPT) in response to a significant increase in sea-level amplitudes (Maldonado and Nelson, 1999; Hernández-Molina et al., 2002; Mestdagh et al., 2019). Late Quaternary deposits are affected by different sets of faults with diverse trends (ranging from N-S to NW-SE) in the Betic and Algarve margins (Vázquez et al., 2010; Mestdagh et al., 2019; Luján et al., 2020), in relation with the reactivation of basement faults and underlying diapiric structures.

2.2. Coastal geology and sediment sources

This margin is mainly fed by two major rivers (Guadiana and Guadalquivir) (Fig. 2.3), which drain most of the southern half of the Iberian Peninsula (Lobo et al., 2018); their continued sediment flux has driven the outward margin growth at least during the late Quaternary (Hernández-Molina et al., 2000b; Lobo et al., 2005a; Mestdagh et al., 2019).

For this study, two different stretches have been considered: the eastern Algarve coast and the Huelva coast.

2.2.1. Eastern Algarve coast

The eastern Algarve coastline is located on the passive continental margin of the Gulf of Cadiz, between the Ria Formosa Barrier Island System (RFBIS) to the west and the Guadiana River estuarine system to the east (Fig. 2.3). The RFBIS is composed of five barrier islands and two peninsulas that enclose a coastal lagoon (Figs. 2.3, and 2.4A), which covers an area of $8.4 \times 10^7 \text{ m}^2$ with an average water depth of 2 m (Andrade, 1990). The islands and peninsulas are separated by six tidal inlets that protect the lagoon from the direct impact of marine waves (Fig. 2.4A). The barrier islands are actively changing due to tidal inlet dynamics (Vila-Concejo et al., 2006; Pacheco et al., 2010; Ferreira et al., 2016) and longshore drift (Ciavola et al., 1997; Garcia et al., 2002), characterizing a highly dynamic system. The Holocene evolution of the RFBIS implies three main steps (Pilkey et al., 1989; Sousa et al., 2014; 2019): 1) marine flooding of paleovalleys in the Early Holocene; 2) development of a proto-barrier during the Early-Middle Holocene; and 3) full development of the barrier and enclosing of the coastal lagoon from the Middle Holocene to the present.

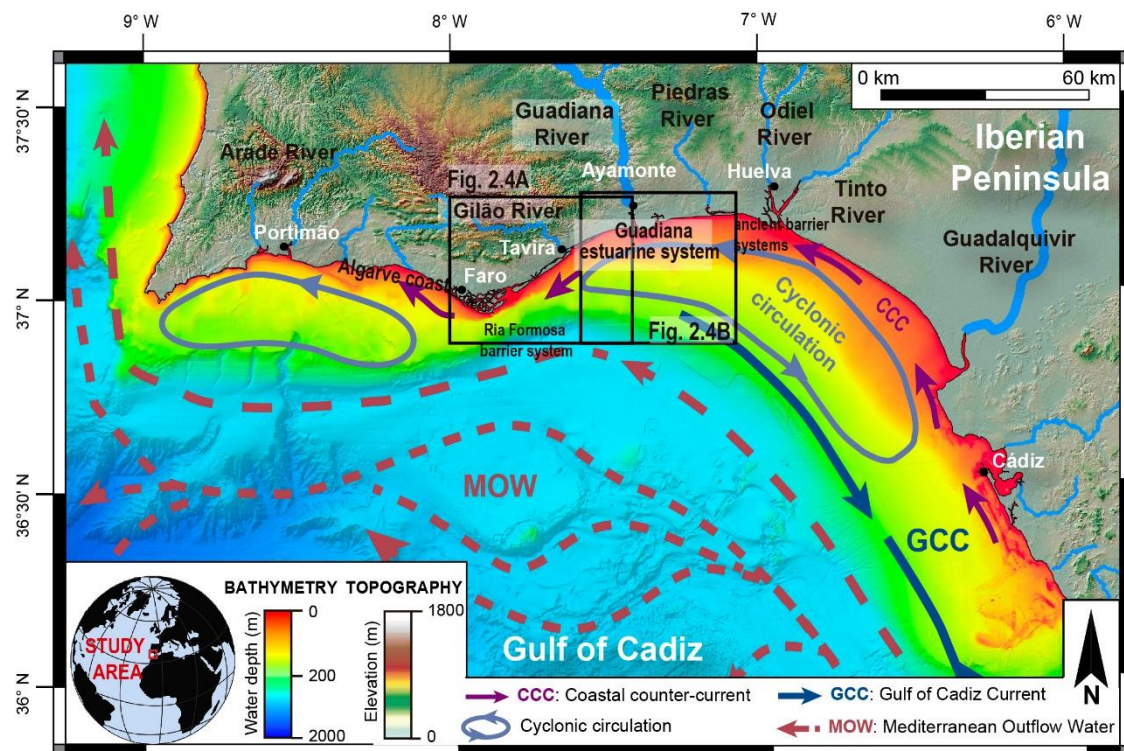


Figure 2.3: Location of the study area on the northern Gulf of Cadiz. Topo-bathymetric map showing the main rivers and pathways of the main water masses and currents. Topography from Spanish National Geographic Institute, 2015 (MTN50 raster). Bathymetry from EMODnet Bathymetry Consortium, 2020. The position of Figure 2.4 is indicated here.

The eastern Algarve coast is composed of low-lying sandy beaches with some small estuaries. This shelf sector receives at present minor fluvial or marine sediment supplies. The average precipitation in this region for the last 75 years has been 530 mm yr^{-1} and is concentrated between October and April. Small rivers such as the Gilão and Almargem with a total catchment of ca. 290 km^2 drain Mesozoic carbonatic and Miocene siliciclastic substrates. The Gilão-Almargem Estuary is located off Tavira, protected by Tavira and Cabanas barriers, which are separated by the Tavira inlet (Fig. 2.4A). The inner part of the estuary contains an almost continuous record of sediment accumulation in a tidal flat/salt marsh environment. However, the outer barriers are the result of more discontinuous processes (Boski et al., 2008). Indeed, the present barrier was formed in the sixteenth century (Veiga-Pires et al., 2000). Until then, the Gilão-Almargem estuary was open to the ocean (Rocha et al., 2004).

2.2.2. Huelva coast

Two main sources provide sediments to the Guadiana Shelf: the Guadiana River and littoral drift (González et al., 2004). The Guadiana River represents the boundary between the Algarve coast (west of the river) and the Huelva coast (east of the river) (Fig. 2.3). Water discharge of the Guadiana is characterized by large intra-annual variability, with maximum levels during winter and extremely low levels in summer. Mean annual discharges also show considerable variability ($80\text{--}140 \text{ m}^3 \text{ s}^{-1}$) (Palanques et al., 1995; Morales, 1997). The average annual suspended load of the Guadiana River between 1946 and 1990 was $57.90 \times 10^4 \text{ m}^3 \text{ yr}^{-1}$, and the average annual bed load for the same period was $43.96 \times 10^4 \text{ m}^3 \text{ yr}^{-1}$ (Morales, 1997). The estuary of the Guadiana River is narrow and rock-bounded, showing a meandering pattern controlled by fault systems (Morales and Garel, 2019). Sediment transport within the estuary is dominated by faster ebb currents enhanced by increasing river flows (Lobo et al., 2004a; Garel et al., 2009). Distally, a wave-dominated delta is formed by sandy barriers separated by marshes and tidal channels (Morales et al., 1994; Morales, 1997; González et al., 2001). Two major deltaic protuberances indicate the existence of a historical delta (located to the east of the present-day estuary) and a developing modern delta (Morales and Garel, 2019).

The coast between the Guadiana and Guadalquivir rivers is fed by the Piedras and Tinto-Odiel rivers (Fig. 2.3), with low mean annual discharges (between 1 and $10 \text{ m}^3 \text{ s}^{-1}$) (Borrego et al., 1995; Palanques et al., 1995). All these fluvial systems are protected seaward by ancient barrier systems where coastal spit progradation is driven by beach ridge formation after storm activity (Rodríguez-Ramírez et al., 2003). These coastal barriers are interrupted by three estuarine mouths and by two tidal inlets (Morales et al., 2019). The spit located at the mouth of the Piedras River is constructed over older ebb-tidal delta facies (Morales et al., 2001), whereas the Tinto-Odiel Estuary is completely filled due to the interaction of waves and tides (Pendón et al., 1998); as a consequence, a deltaic deposit is actively prograding (Carro et al., 2019). Southeast of the Tinto-Odiel

Estuary, the coast is characterized by a long beach attached to a Pleistocene paleo-cliff (Morales et al., 2019). The Guadalquivir River is the southeast boundary of the Huelva coast, where it provides the highest mean water discharge ($164 \text{ m}^3 \text{ s}^{-1}$) to the Gulf of Cadiz (Palanques et al., 1995).

Littoral drift carries sediments from the Algarve coast towards the eastern part of the Gulf of Cadiz. This results in a net eastward annual littoral drift between 10×10^4 and $30 \times 10^4 \text{ m}^3$ of mostly sandy sediments. Most of these sediments remain within the inner shelf, except for the coarser fraction, which is trapped in the Guadiana estuarine system (González et al., 2001, 2004).

2.3. Oceanographic setting

The tidal regime is mesotidal (mean tidal range of 2.20 m) and semidiurnal along most of the northern part of the Gulf of Cadiz. The wave energy is moderate, with dominant waves approaching mainly from the W and SW (71% of occurrences), associated mainly with moderate-energy Atlantic swells. These have an average wave height of about 1 m and generate a longshore current towards the east (Del Río et al., 2012). Storm events are frequent in fall and winter, generating significant wave heights of 4-7 m (Del Río et al., 2012; Plomaritis et al., 2015). Southwestern storms are more energetic and frequent than southeastern storms (Costa et al., 2001). Measurements of the depth of closure, i.e., the depth below which limited sediment transport due to wave action is expected to occur (Nicholls et al., 1998), on the Algarve coast provide disturbance depths up to 10 m during high-energy periods (Dolbeth et al., 2007). In other sectors of the Gulf of Cadiz, the influence of high-energy events extends to the 15-30 m water depth interval, as inferred by bedform occurrence (Gutiérrez-Mas et al., 2009).

The oceanographic regime in the Gulf of Cadiz was established after the opening of the Strait of Gibraltar in the Late Miocene (e.g., Duggen et al., 2003; Roveri et al., 2014). The strait has acted as an oceanic gateway through which the exchange of Atlantic and Mediterranean water masses has taken place (Fig. 2.3).

Shelf currents are mainly directed alongshore, and the circulation is generally continuous along the coast (De Oliveira Júnior et al., 2022). Inner-shelf waters (< 60 m water depth) are strongly affected by coastal and atmospheric processes and are periodically affected by poleward flows (Bellanco and Sánchez-Leal, 2016). In winter, those poleward flows extend over the entire margin, and are mainly wind-driven. In summer, the poleward flows usually consist of coastal counter-currents (CCCs) (Fig. 2.3; Garel et al., 2016; De Oliveira Júnior et al., 2022). CCCs are associated with a cyclonic circulation between the RFBIS and the Guadalquivir River (Fig. 2.3) (García-Lafuente et al., 2006), and their development seems to be related with regional alongshore pressure gradients after relaxation of upwelling-favorable winds (Garel et al., 2016; De Oliveira Júnior et al., 2022). The influence of those CCCs has been recorded on the inner shelf of

the eastern Algarve Shelf, where the time-averaged along-shelf sediment transport is SW-directed (Bosnic et al., 2017).

The present-day surface circulation is dominated by the southeastward movement of a branch of the Portuguese-Canary eastern boundary current that moves toward the Strait of Gibraltar into the Mediterranean Sea, in agreement with an anticyclonic circulation (Criado-Aldeanueva et al., 2009). This current is designed as the Gulf of Cadiz Current (GCC) or Atlantic Inflow Water (AIW) and sweeps the middle to outer shelf between 100 and 250 m water depths, transporting Eastern North Atlantic Central Waters (Fig. 2.3; Bellanco and Sánchez-Leal, 2016). This large-scale surface circulation is wind-driven, as the background circulation results from the dominance of north-westerlies, and can be episodically reversed during strong easterlies (Criado-Aldeanueva et al., 2009; De Oliveira Júnior et al., 2022).

Off the GCC, slope water depths are mainly influenced by the dense Mediterranean Outflow Water (MOW), which moves westward to compensate the exit of Atlantic water masses through the Strait of Gibraltar (Price et al., 1993). The MOW is transported along two main branches, the Mediterranean Upper branch and the Mediterranean Lower branch, and has experienced variations in circulation intensity influenced by climatic and sea-level changes (Fig. 2.3; Ambar et al., 1999; Borenäs et al., 2002; Hernández-Molina et al., 2016).

2.4. Physiography

The northern Gulf of Cadiz continental margin comprises three well-defined physiographic domains: continental shelf, continental slope (upper, middle, and lower), and abyssal plain (Fig. 2.1B; Hernández-Molina et al., 2006). A brief characterization of these domains is provided here, although the focus of this study is the continental shelf.

The northern shelf of the Gulf of Cadiz is crescent-shaped and relatively flat ($<0.3^\circ$), with the largest width in the central part off the Guadalquivir River (~ 30 km) and narrowing towards the Strait of Gibraltar to the E and Portuguese margin to the W (Fig. 2.4). The shelf break is located at maximum water depths of 130-150 m (Fig. 2.4; Hernández-Molina et al., 2006). Three sectors are distinguished (Lobo et al., 2014): the Algarve Shelf, the Huelva Shelf, and the western Cadiz Shelf. Considering the focus of this study on incised valleys and associated deposits, I will describe the eastern Algarve Shelf and the Huelva Shelf, where those deposits have been identified.

The eastern Algarve Shelf is the seaward prolongation of the Mesozoic Algarve Basin (Fig. 2.4A). It shows a narrow and steep morphology, with an average gradient of 0.5° and maximum values of 1.5° (Roque et al., 2010). Shelf width increases from 5 km in the southwestern area off the city of Faro, to 25 km off the Guadiana River mouth (Fig. 2.4A; Lobo et al., 2001; Hernández-Molina et al., 2006). The shelf break occurs between 110 and 150 m water depths (Fig. 2.4; Baldy, 1977; Vanney and Mougénot, 1981). The shelf off the RFBIS exhibits a proximal well-developed Infralittoral Prograding Wedge laterally

continuous for more than 10 km (Hernández-Molina et al., 2000a). The eastern Algarve Shelf is covered by several muddy depocenters that show elongated patterns (Lobo et al., 2004b); there are, however, some non-depositional areas where several wave-cut terraces have been preserved (Roque et al., 2010).

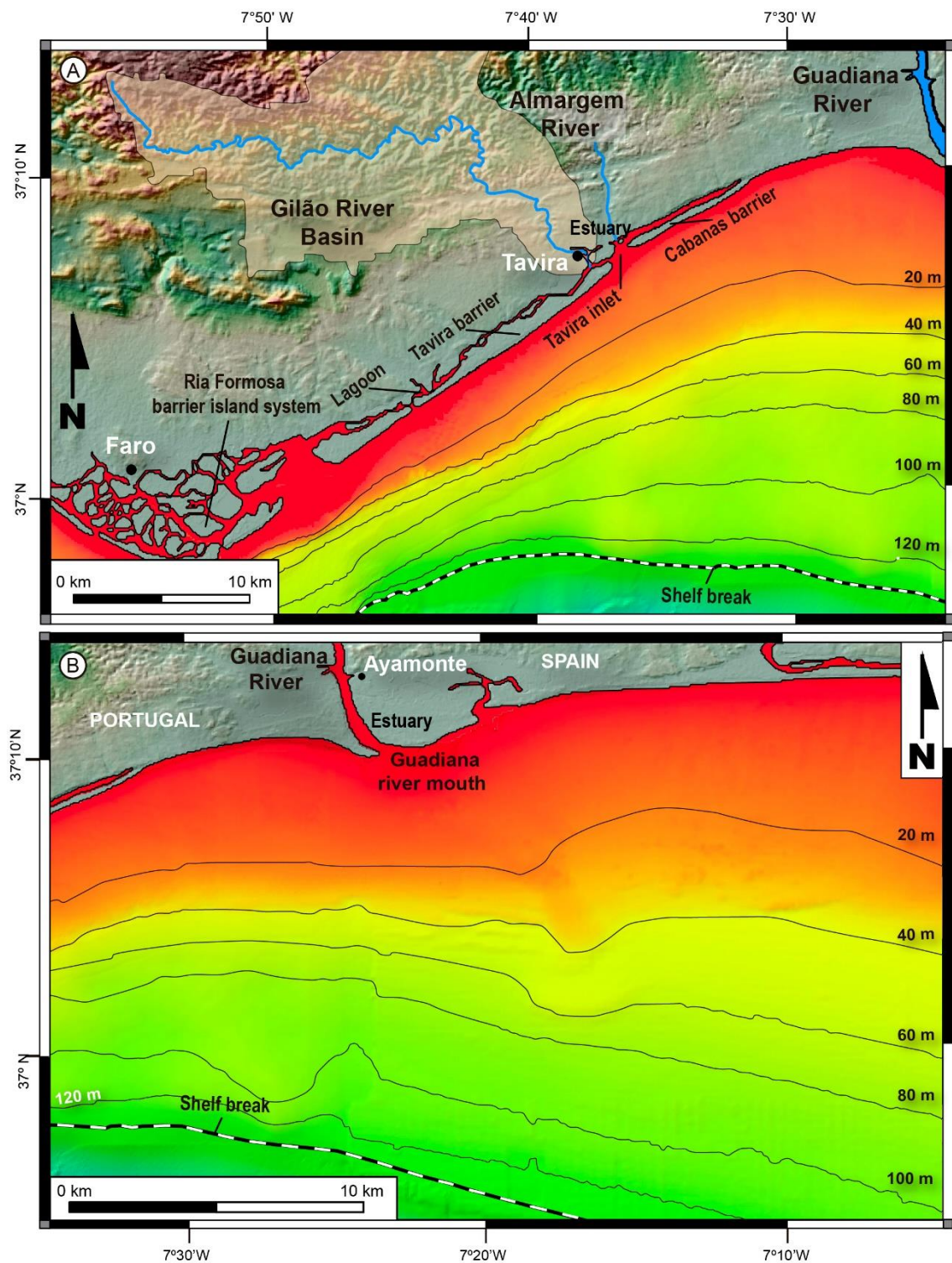


Figure 2.4: A) Bathymetric map showing the study area (Chapter 4) on the eastern Algarve Shelf (Portugal), offshore the Gilão-Almargem Estuary, in the northern Gulf of Cadiz. Bathymetry from EMODnet Bathymetry Consortium, 2020. B) Bathymetric map showing the study area (Chapters 5 and 6) off the Guadiana River mouth in the northern Gulf of Cadiz. Bathymetry from EMODnet Bathymetry Consortium, 2020.

The Huelva Shelf has a relatively flat morphology, with an average gradient of 0.32° off the Guadiana River decreasing towards the SE (Fig. 2.4B). Shelf width increases from 20-25 km at the mouth of the Guadiana River to more than 30 km to the SE (Lobo et al., 2001; Hernández-Molina et al., 2006). The shelf break occurs at an average water depth of 130 m, with a maximum value of 150 m off the Guadiana River (Fig. 2.4B; Maldonado and Nelson, 1999; Nelson et al., 1999). From a morphological point of view, the shelf exhibits three domains: 1) inner shelf, covered by prodeltaic bodies off the main rivers (Fernández-Salas et al., 1999), and by erosional morphologies in interdeltic areas (Gutiérrez-Mas et al., 1996; Fernández-Salas et al., 1999); 2) middle shelf, where sandy wedges are recognized off the Guadiana River (Lobo et al., 2001; González et al., 2004), evolving laterally to a major muddy belt to the SE (Lobo et al., 2004b); and 3) outer shelf, mostly covered by an elongated wedge-shaped progradational body (Lobo et al., 2015).

The upper slope (130-400 m) has an average width of ~ 10 km and gradients between 1° and 3° (Hernández-Molina et al., 2006). It exhibits depositional features, erosive surfaces, neotectonic elements (related to diapirism and faults), gravitational elements (e.g., slumps), and fluid flow features (e.g., pockmarks) (e.g., Baraza et al., 1999; Rodero et al., 1999; Hernández-Molina et al., 2006; Mestdagh et al., 2020). Submarine canyons are only present in the Portuguese western part of the Gulf of Cadiz (Fig. 2.1B) (Hernández-Molina et al., 2003; Mulder et al., 2006).

The middle slope (400-1200 m) exhibits a gentler morphology (gradients $\sim 1^\circ$) and is up to 100 km wide (Fig. 2.4), and as such can be considered a slope "terrace" (Hernández-Molina et al., 2003; García et al., 2009). The main features here are related to MOW-influenced contourite deposition.

The lower slope (1200-4000 m) has a slope gradient between 2° and 4° , and a width varying from 50 km in the NW to more than 200 km in the SE. On a regional scale, it has a convex morphology, with a wavy to irregular physiography controlled by the underlying Allochthonous Unit (Madelain, 1970; Melières, 1974; Gardner and Kidd, 1983). The main morphological elements identified in this domain are small-scale depressions, including channel and ponded lows (intra-slope minibasins) and intervening irregular highs (Fig. 2.1B).

Three abyssal plains are identified in the outer Gulf of Cádiz region at water depths greater than 4300 m (Fig. 2.1B; Tagus, Seine, and Horseshoe abyssal plains), separated by submarine banks (or seamounts), which trend broadly ENE (Melières, 1974). The Seine and Horseshoe abyssal plains are separated by the Ampere and Coral Patch seamounts, while the Horseshoe and Tagus abyssal plains are separated by the Gorringer Bank and the Hirondelle Seamount (Melières, 1974; Lebreiro et al., 1997; Weaver et al., 2000).

2.5. Surficial sediment distribution

Three shelf domains can be distinguished according to the nature of surficial sediments (Figs. 2.5, and 2.6; Nelson et al., 1999; Lobo et al., 2000, 2018; Maldonado et al., 2003; González et al., 2004; Roque et al., 2010).

1) Inner shelf (< 30 m water depth): In the eastern Algarve Shelf (Fig. 2.6A), the inner shelf sediment distribution exhibits significant alongshore variability due to the major influence of coastal processes, such as littoral drift and storm currents (Bosnic et al., 2017). Most of the inner shelf is mainly composed of littoral quartz-bioclastic sands (Roque et al., 2010). However, the inner shelf close to the RFBIS receives a low amount of sand, as these sediments tend to be trapped in inlets located to the west (Rosa et al., 2013). In addition, the inner shelf next to the Guadiana River is also covered by muds (Roque et al., 2010).

In the Huelva shelf (Fig. 2.6B), the inner shelf is covered by sandy shoreface deposits and scattered rocky outcrops, which show a parallel-to-shoreline distribution (Fig. 2.6B; Rey and Medialdea, 1989; Fernández-Salas et al., 1999; Nelson et al., 1999). Sands are dominated by quartz grains, which compose up to 80% of the sand fraction (González and Dias, 2004). Additionally, small muddy patches occur off the river mouths (e.g., Lopez-Galindo et al., 1999; González et al., 2004).

2) Middle shelf (30-100 m water depths): The middle shelf domain (Figs. 2.5, and 2.6) is characterized by an extensive mud belt of Holocene age, originated from river mouth sources lately redistributed towards the SE by Atlantic inflow currents (Nelson et al., 1999). In the eastern Algarve Shelf (Fig. 2.6A), the distribution of these muds is patchier, and bioclastic sandy deposits are also found (Roque et al., 2010).

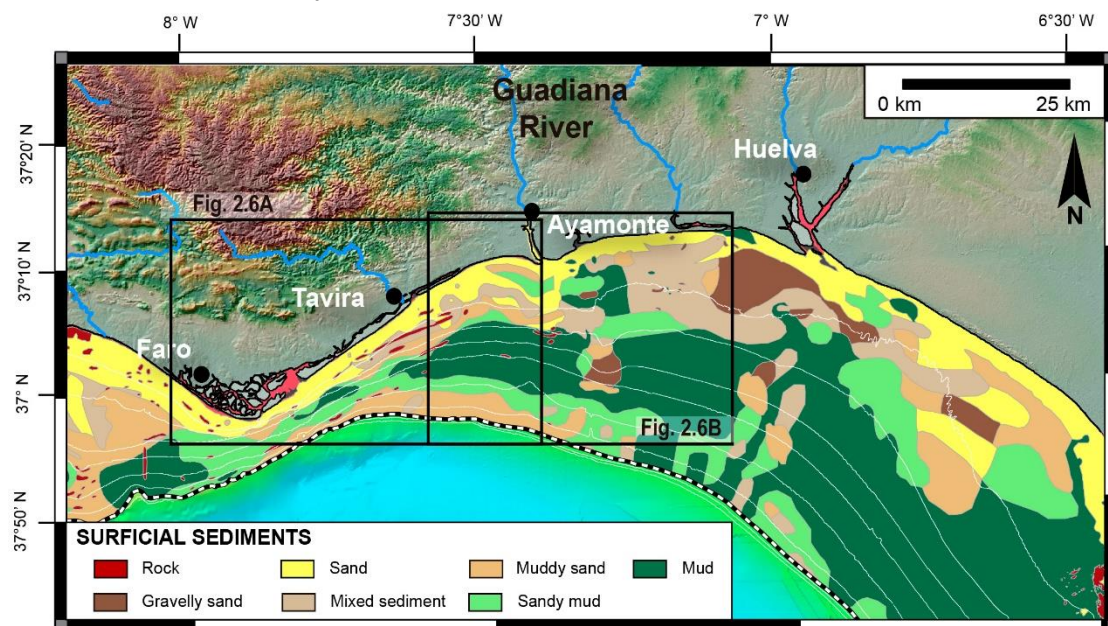


Figure 2.5: Map showing the surficial sediment distribution on the shelf in the study area (extracted from González et al., 2004). The position of Figure 2.6 is indicated here.

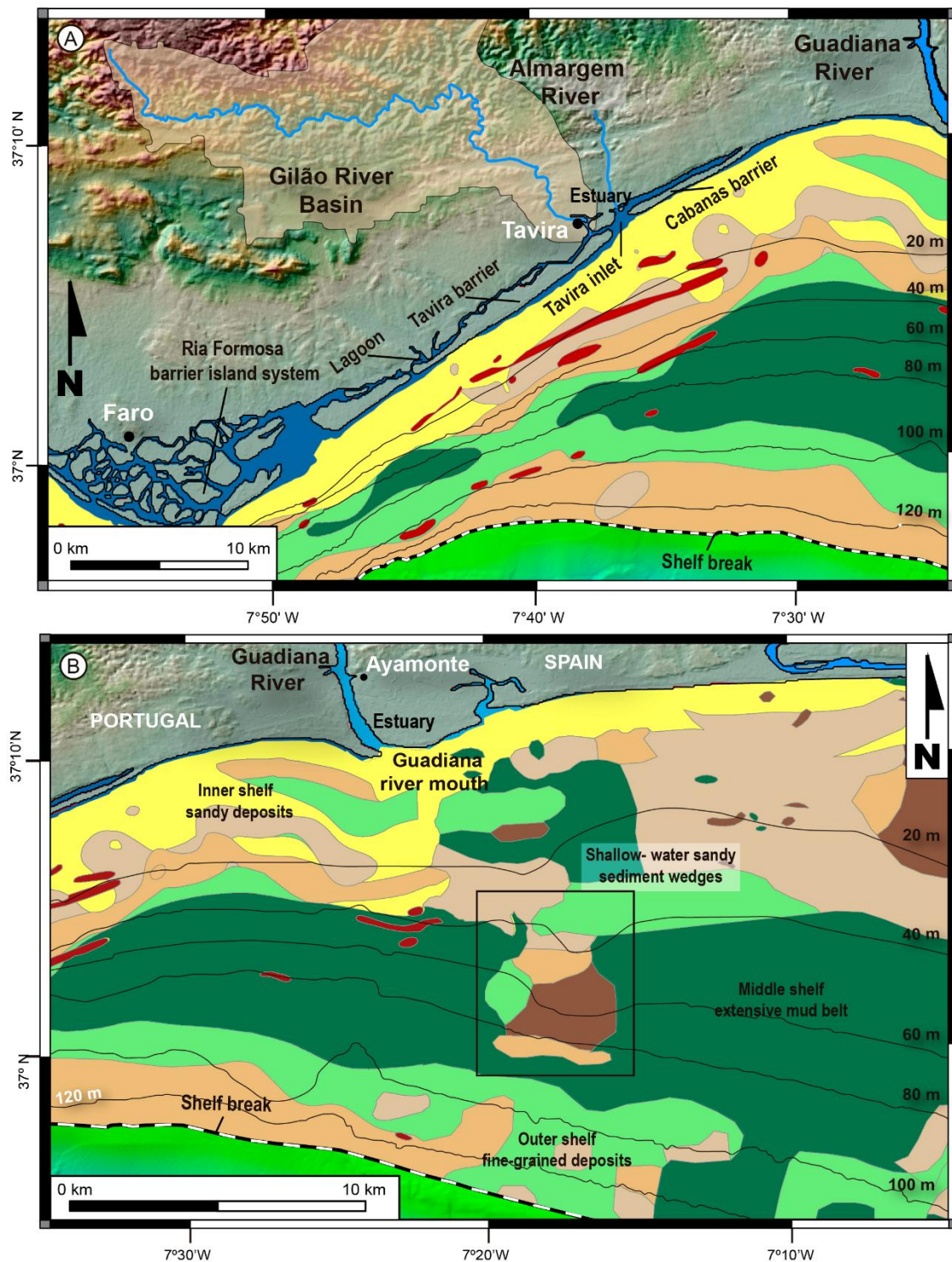


Figure 2.6: A) Map showing the sediment distribution on the shelf in the study area offshore of the Guadiana River mouth (extracted from González et al., 2004) and the Gilão River basin. B) Map showing the sediment distribution on the shelf in the study area off the Guadiana River mouth (extracted from González et al., 2004).

Off the Guadiana River (Fig. 2.6B), the muddy middle shelf is crosscut from north to south by a sandy zone composed of muddy-gravelly sands and muddy sands, which correspond with a succession of nearshore to shallow-water sediment wedges (Fig. 2.6B; Nelson et al., 1999; González et al., 2004).

(3) Outer shelf (> 100 m water depth): The outer shelf exhibits fine-grained deposits, such as sandy and silty clays, which are locally interrupted by coarser-grained patches of coarse sands, gravelly sands, and gravels (Fig. 2.5; Nelson et al., 1999; González et al., 2004), which compose a Late Pleistocene-Holocene sand sheet (Nelson et al., 1999).

2.6. Margin stratigraphy

The shelf stratigraphy of the northern shelf of the Gulf of Cadiz is influenced by Milankovitch-driven sea-level fluctuations cycles. Four major depositional sequences separated by widespread erosional unconformities on the shelf compose the Plio-Quaternary record in relation to 3rd order sea-level cycles. Most of these sequences are constituted by regressive deposits (Hernández-Molina et al., 2002). The late Quaternary stratigraphy comprises one major depositional sequence bounded at the base by the mid-Pleistocene Discontinuity (MPD) occurring around 0.7-0.9 Ma (Hernández-Molina et al., 2002, 2016; Lofi et al., 2016). This major sequence is also separated in other two by the late Quaternary Discontinuity (LQD, 0.3-0.6 Ma; Hernández-Molina et al., 2016). Both discontinuities are related to tectonic activity and uplift-induced erosion on the slope (Llave et al., 2007; Hernández-Molina et al., 2016).

After the Middle Pleistocene at 900 ka, development of sequences driven by 100 ka sea-level cycles took place in relation with the instauration of glacial-interglacial cycles which led to an abrupt increase in sea-level amplitudes (Hernández-Molina et al., 2002). Within these 100 ka sequences, diverse depositional systems were formed, comprising five units (U5 to U1; Fig. 2.7), ranging from littoral wedges and tidal flats on the inner to middle shelf, and shelf-margin deltas on the distal shelf, and hemipelagic lowstand wedges on the slope (Rodero et al., 1999). The main shelf growth was determined by a preferential development of shelf-margin wedges mostly interpreted as forced regressive to lowstand systems tracts (Fig. 2.7). The dominance of forced regressive deposits has been attributed to the asymmetric character of 100 ka sea-level changes, characterized by gentle, stepped sea-level falls and abrupt sea-level rises (Somoza et al., 1997; Hernández-Molina et al., 2000b, 2002; Lobo et al., 2005a). Additionally, several tectonic events have influenced the shelf-margin wedges during the late Quaternary (Rodero et al., 1999; Mestdagh et al., 2019), modulating the glacio-eustatic signal. Indeed, compressive periods separated by phases of tectonic stability have been deduced from the existence of variable stacking patterns of the shelf-margin wedges and by the occurrence of diapir-related faulting in the wedges (Rodero et al., 1999; Mestdagh et al., 2019); as a consequence, shelf-wide unconformities exhibit different significance and regional development. Finally, the distribution and internal architecture of the wedges have also been impacted by oceanographic processes, with strong dominance of along-shelf depocenter distribution (Mestdagh et al., 2019).

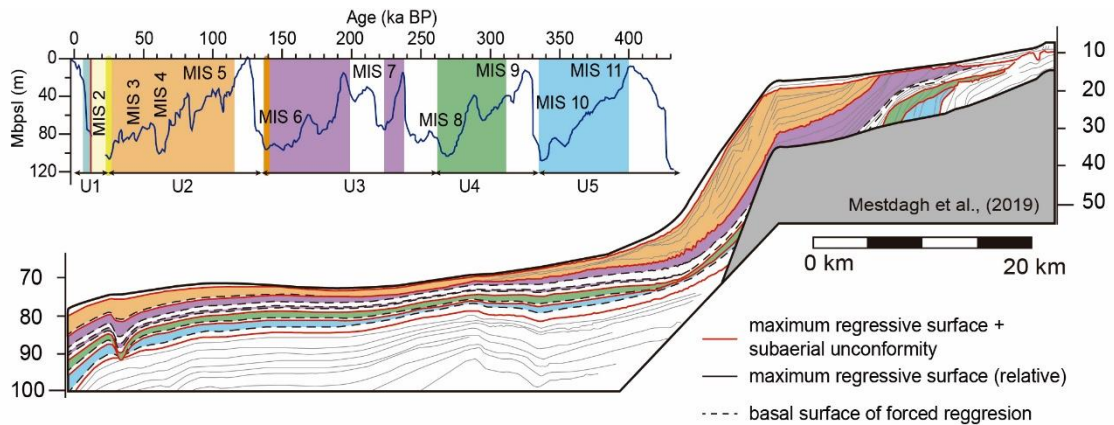


Figure 2.7: Late Quaternary sequences (U1-U5) and sequence stratigraphic surfaces on the northern Gulf of Cadiz continental margin, from the middle slope to the shelf. Taken from Mestdagh et al., (2019). MIS: Marine Isotopic Stage.

The depositional sequence that developed during the last glacial-interglacial cycle (i.e., the last 125 ka) has been studied in greater detail. This sequence is characterized by a thick shelf-margin wedge whose development was conditioned by multiple processes involving complex interactions between downslope and alongslope sedimentary processes. Downslope processes are dominant on the distal margin east of the Guadiana River, due to eastward dispersal of fluvially supplied sediments. In contrast, the distal margin of the eastern Algarve Shelf is mostly influenced by current-driven sedimentation. The resulting sediment wedge is further destabilized by diapirism and fluid flows (Mestdagh et al., 2020). On the shelf, the LGM is recorded by a shelf-wide subaerial unconformity, which exhibits a well-marked shelf partitioning. An indurated inner shelf is mainly covered by lithified coastal deposits where reoccupation of previously incised valleys is limited to two main N-S valleys in the inner shelf off the Guadiana River (Fig. 2.8; Chapter 5). A fine-grained outer shelf is composed of more easily erodible materials, resulting in the formation of an irregular and, in places, highly erosive unconformity (Lobo et al., 2018).

Postglacial and Holocene transgressive to highstand deposits overlying the LGM sequence boundary record short-term (millennial-scale) changes in the rate of sea-level rise, sediment supply, hydrodynamic regime, and shelf circulation patterns (Lobo et al., 2001, 2004b, 2005a; Hanebuth et al., 2021; Mendes et al., 2012, 2020).

The postglacial transgressive stratigraphy of the shelf is the main scope of this PhD thesis. In the nearby estuarine environments, rates of sediment accumulation changed drastically in response to variable rates of sea-level rise, and sediments were preferentially accumulated in tidal flat and salt marsh environments (Boski et al., 2008). Seaward, the infilling of inner incised valleys was initially characterized with variable internal configurations, ranging from aggradational to progradational, which were attributed to generic fluvial to estuarine deposits (Lobo et al., 1999). Additionally, a series of backstepping seismic units (named as Postglacial Transgressive Units-PTUs;

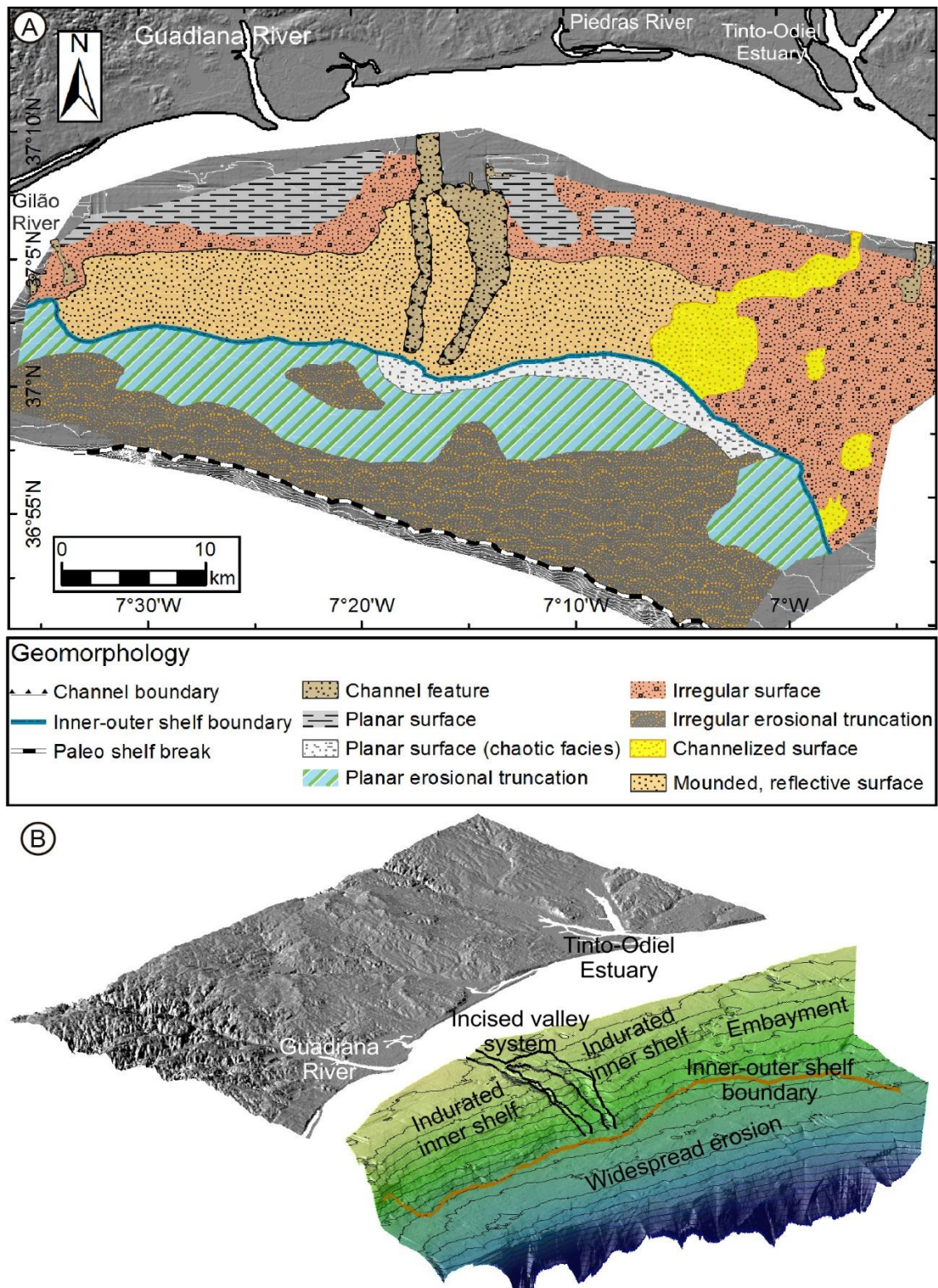


Figure 2.8: A) Geomorphological interpretation of the most recent subaerial unconformity surface, featuring two distinct domains (inner versus outer shelf) bounded by a clear physiographic boundary. Major valley incision seems to be constrained to the inner shelf landward of the boundary. B) 3D scheme of the last subaerial unconformity, highlighting the distinct geomorphological boundary between the inner and outer shelf. Most of the inner shelf exhibits an extensive physiographic high, interpreted as indurated facies resistant to erosion. More significant erosion occurred to the east, where an arc-shaped embayment was possibly developed. Most of the outer shelf shows a planar pattern, indicative of widespread transgressive ravinement. Taken from Lobo et al. (2018).

Lobo et al., 2001) are exposed off the Guadiana River in the middle shelf area (Chapter 6). PTUs occur seaward of the N-S paleochannels located on the inner-middle shelf up to 75 m water depth, eroding older Pleistocene units (Lobo et al., 2001, 2018; González et al., 2004). These PTUs overlie a regional unconformity formed during the LGM in the shelf sector between the Guadiana and Guadalquivir rivers (Lobo et al., 2001). The PTUs are dominated by a mixture of bioclasts, quartz, and other terrigenous components in varying proportions (González et al., 2004). The oldest unit (PTU 5) is located on the outer shelf and exhibits a rather widespread lateral distribution. In contrast, the younger units (PTUs 4 to 1), exhibit a more restricted distribution, being confined to a sandy transgressive bathymetric high on the middle shelf (Lobo et al., 2001; González et al., 2004).

These transgressive deposits are partially covered by a suite of highstand depositional systems formed during the last 6.5 ka (Lobo et al., 2004b; Hanebuth et al., 2021), as the maximum flooding of river valleys was registered at 7-6 ka (Val-Peón et al., 2021). The Holocene highstand systems tract (HST) is characterized by the formation of several muddy depocenters and a well-developed infralittoral prograding wedge along the northern margin of the Gulf of Cadiz (Maldonado and Nelson, 1999; Hernández-Molina et al., 2000).

In the eastern Algarve Shelf, the infralittoral prograding wedge off the RFBIS exhibits a progradational trend oblique to shoreline. Its development has been associated to seaward sediment transport driven by downwelling storm currents, favored by the normal incidence of storm waves and the steep shelf profile (Fig. 2.4; Hernández-Molina et al., 2000; Lobo et al., 2004b). Along the rest of the northern shelf between the RFBIS and the Guadalquivir River, highstand depositional systems mostly comprise muddy depocenters (Fig. 2.5; Lobo et al., 2004b; Hanebuth et al., 2021). Off the Guadiana Estuary mouth, poorly developed subaqueous deltaic and prodeltaic muddy facies are found, evolving seaward into a separate chain of local depocenters on the middle to outer shelf (2.6B; Fernández-Salas et al., 2003; Lobo et al., 2004b, 2005b; Mendes et al., 2012, 2020). The Tinto-Odiel muddy depocenter is located in the northeastern part of the gulf, with an extent of 35 km alongshore and up to 15 km in offshore direction (Lobo et al., 2004b). Finally, a major fine-grained deposit is sourced from the Guadalquivir River and has been described as a prodeltaic muddy depocenter (Fernández-Salas et al., 2003; Lobo et al., 2004b, 2005b). This Guadalquivir muddy depocenter extends over 50 km parallel to the coast and 30 km in seaward direction down to the 100-m isobath (Gutiérrez-Mas et al., 1996; López-Galindo et al., 1999; Nelson et al., 1999; Fernández-Salas et al., 2003; Lobo et al., 2004b; González et al., 2004, 2007). The internal structure of most of those deposits was found to be complex, including the repetition of two major progradational-aggradational motifs believed to be the result of minor sea-level oscillations coupled with changes in the magnitude and/or direction of storm events and with changes of sediment supply (Fernández-Salas et al., 2003; Lobo et al., 2005b). More recent studies document that fine-grained sediment accumulations have been subjected to significant

Chapter 2

changes in sedimentation rates due to regional climatic changes that significantly influenced the frequency of fluvial flooding events (Mendes et al., 2012, 2020). During the last two centuries, those climatic anomalies (i.e., Roman Warm Period, Medieval Climate Anomaly, and Little Ice Age) have interacted with increased anthropic activities in the river basins, such as mining and agricultural practices (Mendes et al., 2012, 2020; Hanebuth et al., 2018, 2021).

CHAPTER

3

CHAPTER 3:

Methods

The methodology followed during this PhD thesis stands by its multidisciplinary approach. Marine geology research requires the simultaneous acquisition and analysis of different geological and geophysical data for its successful interpretation. The methods integrated in this PhD thesis can be classified into three main categories (Fig. 3.1):

- 1) Geophysical methods.
- 2) Sedimentological methods.
- 3) Geomorphological methods.

The author of this PhD thesis has conducted joint seismic, sedimentological, and geomorphological interpretations of previously acquired and post-processed seismic and sedimentological data (Table 3.1). Such dataset was collected during different oceanographic surveys.

Table 3.1: Specific methodologies employed in each chapter of the PhD thesis. The boxes colored in yellow refer to the analysis and methodologies conducted by the PhD candidate, and the boxes colored in grey refer to the methods or analysis conducted by collaborators and coordinated or integrated by the PhD candidate.

Method			Algarve shelf IVs Chapter 4	Guadiana shelf IVs Chapter 5	Guadiana shelf PTUs Chapter 6
Geophysical methods	Seismic interpretation	Type of seismic profiles			
		Topas	X	X	X
		Parasound		X	
		Sparker	X	X	X
		Uniboom	X	X	X
Sedimentological methods	Macroscopic description and visual logging (CT-scans, HR images, and cores)		X	X	X
	Carbonate content analysis		X		
	Quantitative grain-size analysis		X		
	Physical properties analysis			X	X
	Geochemical analysis			X	
	Radiocarbon dating		X	X	X
Geomorphological methods	Interpolation of channel morphology			X	
	Bathymetric analysis		X	X	X

Acronyms: IV: Incised Valley; PTU: Postglacial Transgressive Unit; CT: Computed tomography; HR: High-resolution

① Geophysical methods

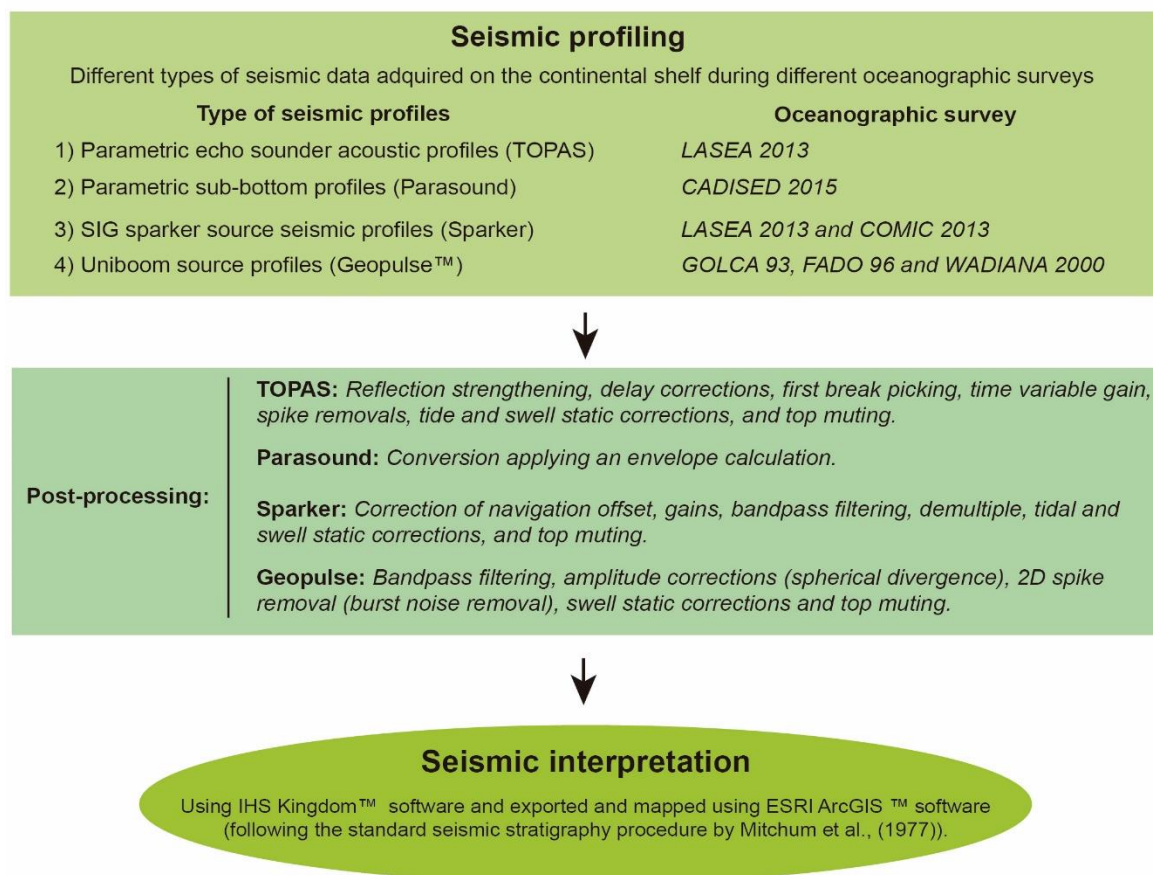


Figure 3.1: Outline of the methodology followed throughout the PhD thesis.

Detailed and extensive seismic interpretations and sediment core descriptions were carried out by the author of this PhD thesis at the *Instituto Andaluz de Ciencias de la Tierra*. Additionally, a carbonate content analysis (i.e., calcimetry) was performed at the *departamento de Estratigrafía y Paleontología*, University of Granada, and the interpolation of channel morphology, using the methodology developed by Goff and Nordfjord (2004), was performed at the University of Texas at Austin (USA) during a research stage that took place from March to May 2022.

All chapters of this PhD thesis have a distinctly multidisciplinary nature, combining geological, geophysical, and geomorphological methods. However, the use of techniques varies in each chapter (Table 3.1).

3.1. Geophysical methods

3.1.1. Seismic data

This PhD thesis is mainly based on the interpretation of different seismic reflection profiles acquired during different oceanographic surveys on the northern Gulf of Cadiz continental shelf (Figs. 3.1, and 3.2). Seismic reflection profiling is a fundamental method

② Sedimentological methods

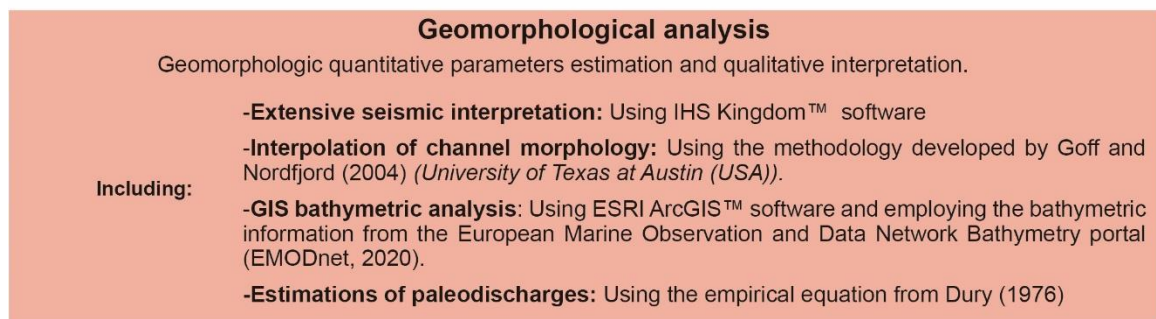
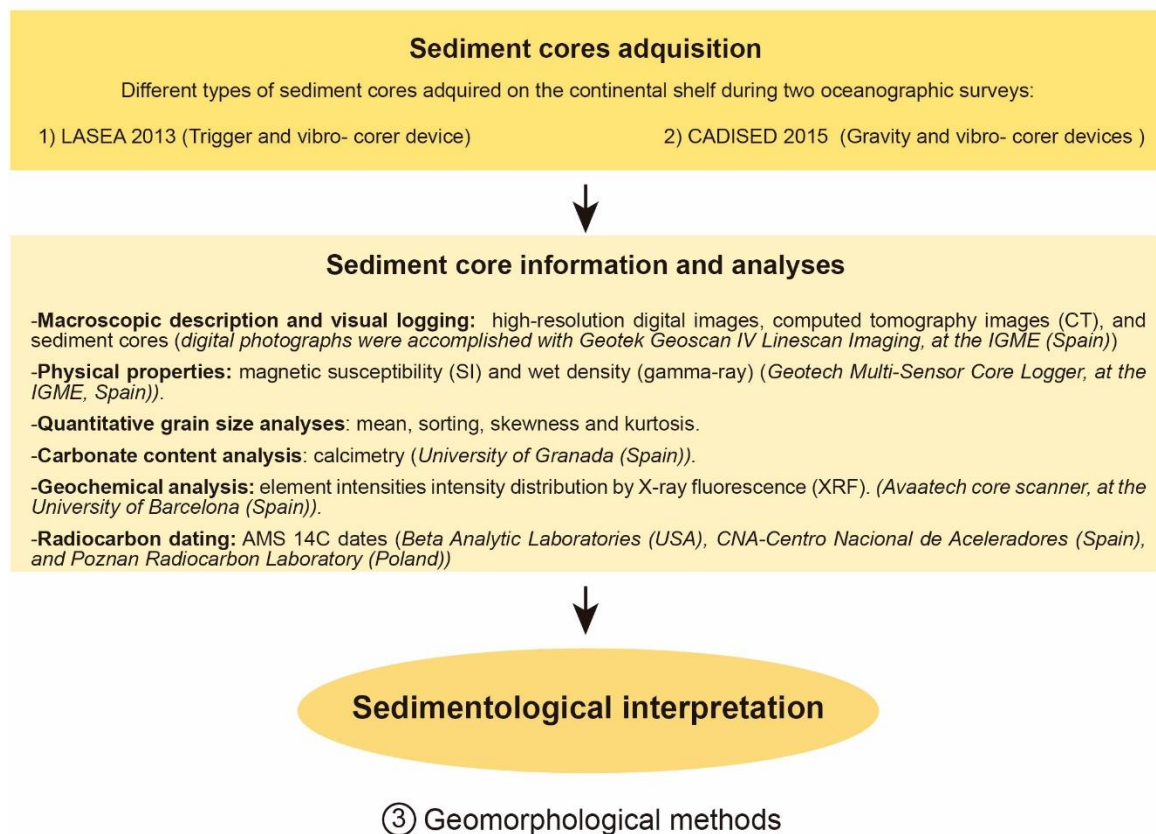


Figure 3.1: (Cont).

in marine geology, providing valuable insights into the subsurface structure and composition of the ocean floor. This technique involves the generation of acoustic waves, utilizing different types of acoustic sources, which travel through the water column and penetrate the seafloor and underlying sediment layers. As the acoustic waves encounter interfaces between different geological layers, they reflect back towards the sea surface. The reflected signals are then recorded by hydrophones and processed to create detailed images of the subsurface. The time taken for these reflections to return provides information about the depth and composition of subsurface structures. Finally, advanced processing techniques, including migration and stacking algorithms, are then applied to enhance the quality and resolution of the seismic images (Sheriff and Geldart, 1995; Kearey et al., 2013). The main types of data used for the seismic interpretation in this PhD thesis

are composed of high-resolution seismic reflection profiles, complemented with vintage seismic data (Fig. 3.2). The selection of source depends on the research objectives and desired depth of penetration.

3.1.1.1 TOPAS sub-bottom acoustic profiles

A grid of high-resolution Topographic Parametric Sonar sub-bottom acoustic data (TOPAS) comprises the main dataset used for seismic interpretation (Figs., 3.2 and 3.3). TOPAS is a parametric sonar system that operates based on the parametric array principle. It emits a primary frequency, and the interaction of sound waves in the water column generates a secondary frequency, known as the parametric frequency. This secondary frequency is used for imaging the sub-seafloor structure. TOPAS is particularly useful in shallow-water environments, where it can provide very high-resolution profiles, allowing for detailed identification of sub-bottom structures.

The TOPAS dataset is composed of 1,450 km of across- and along-shelf profiles acquired during the LASEA 2013 survey onboard *RV Ramón Margalef* from around 20 m water depth to around the shelf break (Fig. 3.3). TOPAS acquisition was achieved by a chirp (LFM) pulse form with transmitting frequencies of 1.5–5.5 kHz, a pulse length of 5 ms, and a power level of -2 dB. The sample rate was 30 kHz and the trace length was 200 ms. Post-processing included reflection strengthening, delay corrections, first break picking, time variable gain, spike removals, tide and swell static corrections, and top muting.

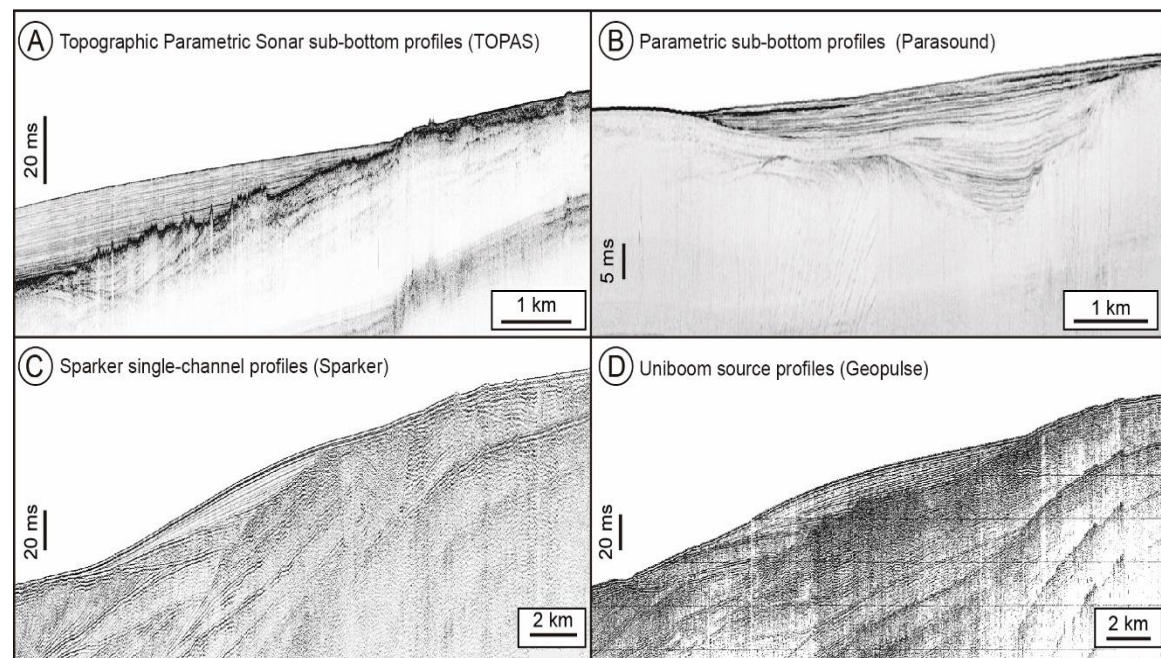


Figure 3.2: Different types of seismic data used in this PhD thesis: A) Topographic Parametric Sonar sub-bottom acoustic profiles; B) Parasound sub-bottom acoustic profiles; C) Sparker single-channel seismic profiles; and D) Uniboom source seismic profiles.

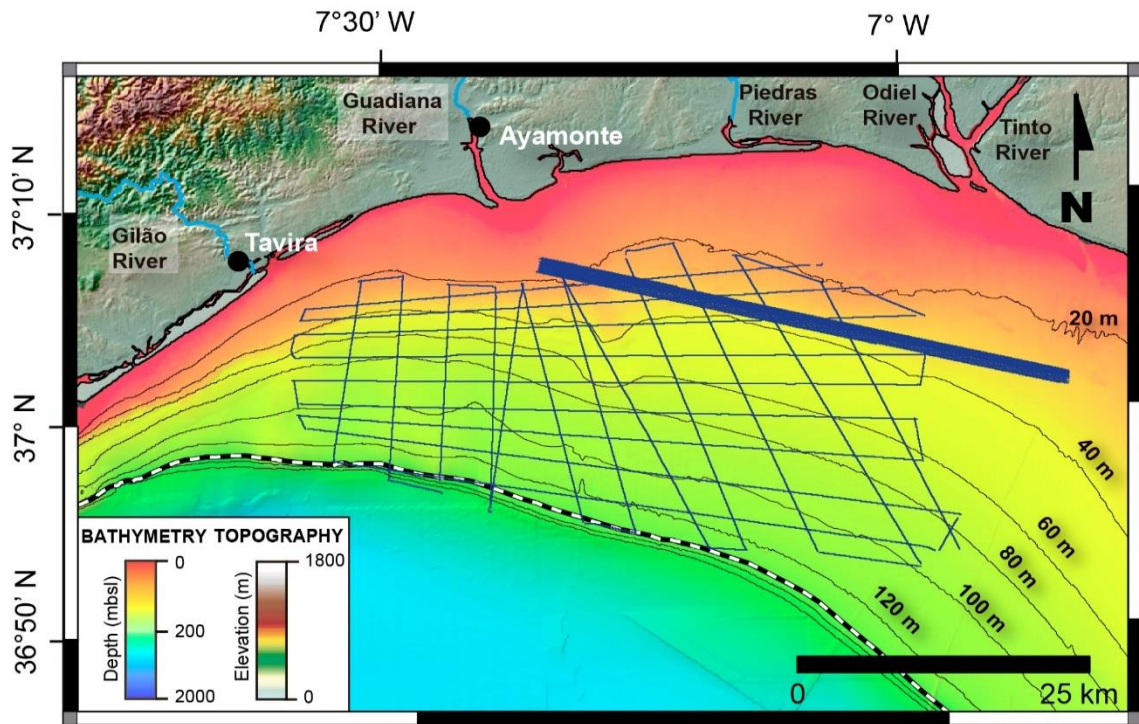


Figure 3.3: Location of high-resolution TOPAS seismic profiles on the shelf offshore the Guadiana River mouth (EMODnet Bathymetry Consortium, 2020).

3.1.1.2 Parasound acoustic profiles

Parametric sub-bottom high-resolution profiles were acquired during the CADISED 2015 oceanographic survey onboard *RV Poseidon* using a SES-2000 Standard (INNOMAR Technologie GmbH) sediment echo-sounder system (Fig. 3.2B). The Parasound profiler utilizes the parametric effect by simultaneously transmitting two slightly different primary frequencies at high sound pressures into the water column.

The interaction of these frequencies generates secondary frequencies confined to the central lobe of the transmitted beam pattern, such as the difference frequency of the transmitted primary waves. This results in an exceptionally narrow transmission beam, significantly enhancing lateral resolution and enabling the imaging of small-scale structures. This method stands out for its ability to provide good resolution for characterizing sediment layers and their properties, making it particularly suitable for capturing intricate details in marine geological studies.

The entire grid of parasound acoustic profiles has a total length of 1100 km (Fig. 3.4). Sediment echo-sounder standard acquisition was also achieved using a chirp (LFM) pulse form transmitting secondary frequencies of 4–15 kHz, a pulse width of 1.5 ms, a ping rate up to 50 Hz, and a power level of -3dB. The primary frequency is around 100 kHz and is used for seafloor depth detection. This device covers a depth range of 1–500 m and achieves a maximum bottom penetration of 50 m. However, the sediment penetration is strongly dependent on local sediment properties and reached a maximum penetration of

~20 m in the study area. The data were processed by applying an envelope calculation (Fig. 3.2B).

3.1.1.3 Sparker single-channel seismic profiles

Moderate to high-resolution seismic profiles acquired with a SIG sparker source were collected during the LASEA 2013 survey onboard *RV Ramón Margalef* and the COMIC 2013 survey onboard *RV Belgica* surveys (Fig. 3.2C). Sparker seismic profiling involves an underwater spark source that emits a high-energy spark, creating a shockwave that travels through the water and penetrates the seafloor. The reflected signals are recorded by a single-channel seismic system, producing seismic profiles. Sparker systems are versatile and widely used in marine geological surveys. They are effective in mapping subsurface structures, detecting sediment layering, and identifying geological features. Sparker profiles are valuable for understanding the stratigraphy of sedimentary sequences (Fig. 3.2C).

Sparker profiles were collected for approximately 700 km, generally following or paralleling the track of the TOPAS profiles (Fig. 3.5). Acquisition was made with a 300J seismic source, a 75 m long SIG single-channel streamer, and had a vertical resolution of about 1.5 m; the shot interval was 2 s, the sampling frequency was 10 kHz, and the trace length varied between 0.5 and 2 s. Post-processing included correction of navigation offset, gains, bandpass filtering, demultiple, tidal and swell static corrections, and top muting.

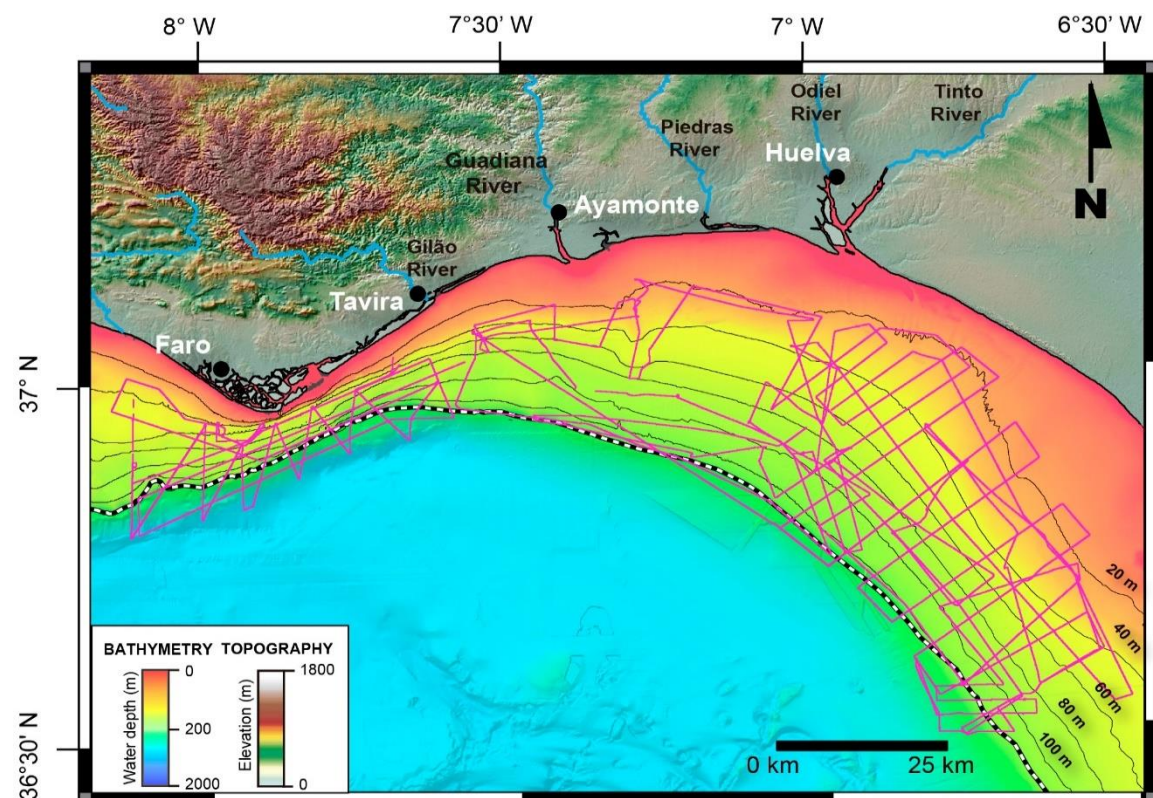


Figure 3.4: Location of the grid of Parasound seismic profiles on the shelf in the study area along the northern Gulf of Cádiz shelf (EMODnet Bathymetry Consortium, 2020).

3.1.1.4 Geopulse seismic profiles

These vintage seismic profiles were collected during GOLCA 93, FADO 96 and WADIANA 2000 surveys, which used a Uniboom source (Geopulse™; Fig. 3.2D). The Uniboom system, also known as Geopulse, employs **an acoustic source, which consist in a Boomer plate mounted on a catamaran**. Sub-Seabed structures are delineated using reflexions from a selectable single frequency multi-cycle high power signal, which is transmitted from an over-the-side, towed or hull mounted platform. The signal is processed in the compact deck unit. Uniboom systems are suitable for deeper water environments and are commonly used in offshore geological exploration. They provide deeper penetration into the subsurface, making them effective for studying geological features at greater depths and understanding the geologic history of the seafloor, but resolution may be slightly lower compared to shallower water methods (Fig. 3.2D).

Those profiles (Fig. 3.6) have a cumulative total length of more than 1,500 km. The approximate vertical resolution of the system is 1–1.5 m. Basic post-processing included bandpass filtering, amplitude corrections (spherical divergence), 2D spike removal (burst noise removal), swell static corrections, and top muting.

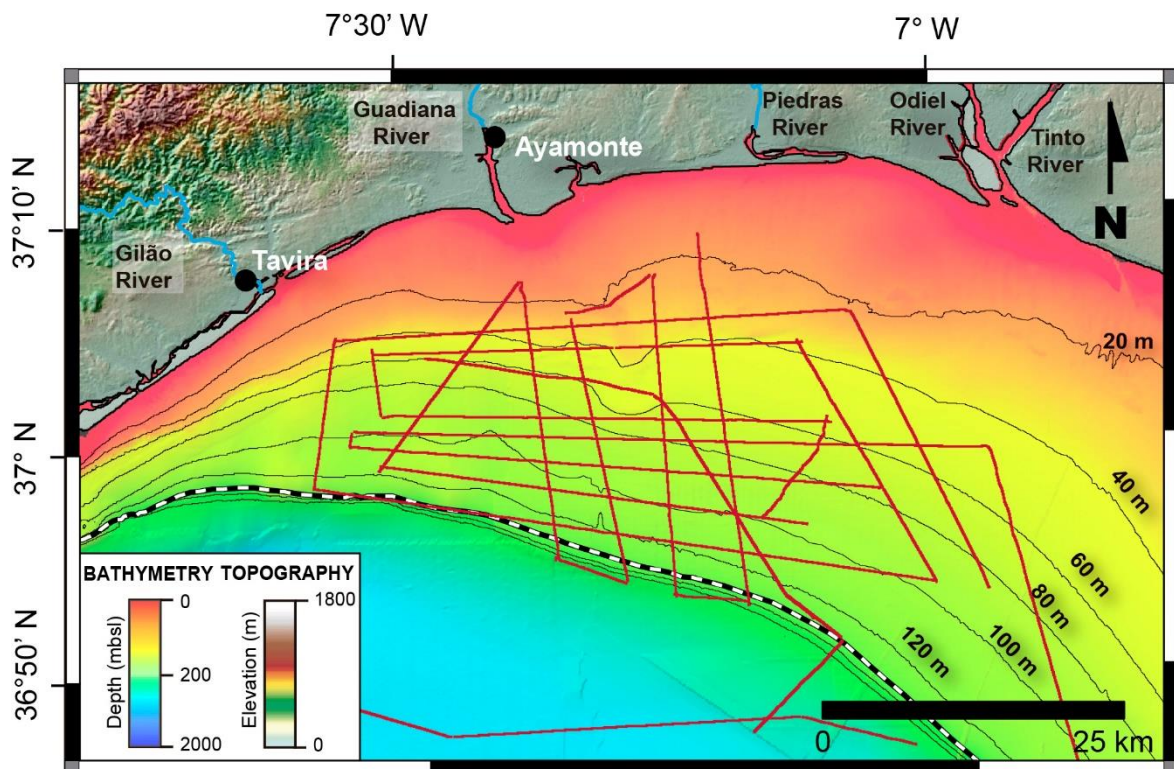


Figure 3.5: Location of the grid of high-resolution sparker seismic profiles on the shelf in the study area offshore of the Guadiana River mouth (EMODnet Bathymetry Consortium, 2020).

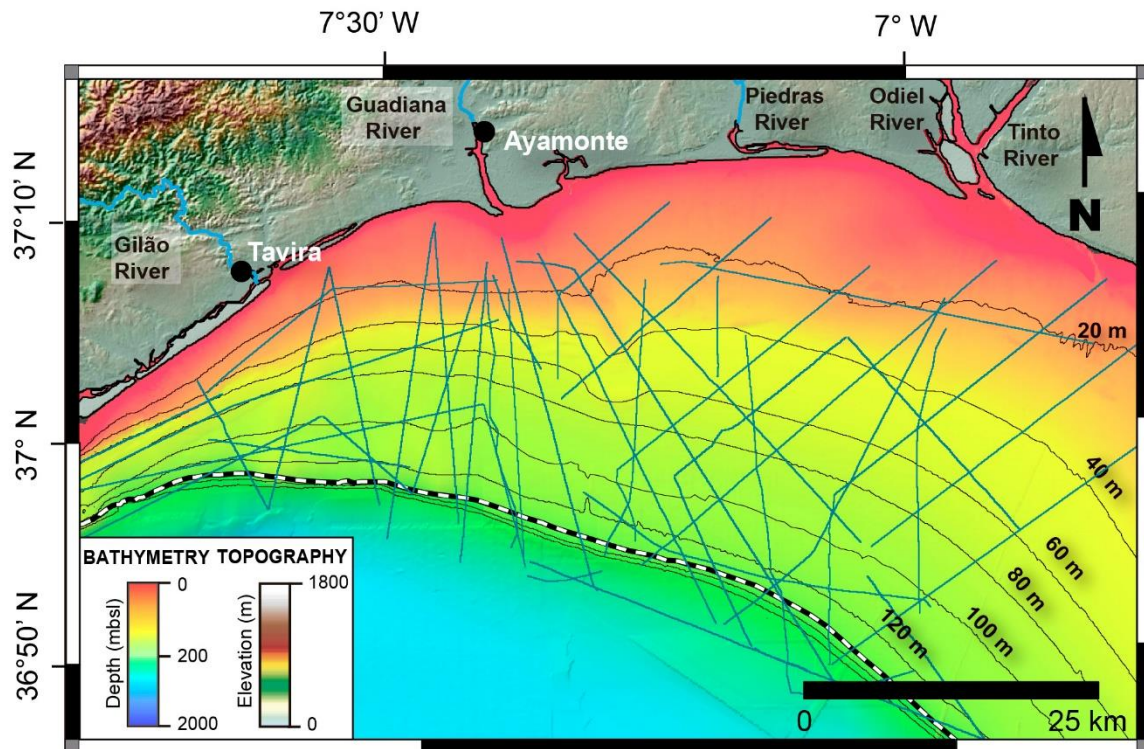


Figure 3.6: Location of the grid of vintage Uniboom seismic profiles on the shelf in the study area along the northern Gulf of Cádiz shelf (EMODnet Bathymetry Consortium, 2020).

3.1.2. Seismic interpretation

In this PhD thesis, seismic horizons and discontinuities were interpreted following a standard seismic stratigraphy procedure (Mitchum et al., 1977) and the high-resolution sequence stratigraphy method (Catuneanu et al., 2009, 2010, 2011; Zecchin and Catuneanu, 2013; Catuneanu, 2017, 2019a), which enabled the definition of seismic units using the commercially available software IHS Kingdom™. These data were subsequently exported and mapped using ArcGIS™ software.

The interpretation of incised valley systems (Chapters 4 and 5 of this PhD thesis) is based on current knowledge of incised valleys seismostratigraphic patterns, architectures, and bounding surfaces (e.g., Vail, 1987; Boyd et al., 2006; Catuneanu et al., 2011; Gomes et al., 2016; Aquino da Silva et al., 2016). The basal reflection associated with valley incision is considered the depositional sequence boundary generated during relative sea-level falls (Van Wagoner et al., 1988, 1990; Zaitlin et al., 1994). Transgressive surfaces (TS; Posamentier and Vail, 1988) are related to the flooding of the valleys and subsequent infilling (Vail, 1987; Catuneanu et al., 2011). Valley infillings exhibit a variable arrangement of seismic facies, with diverse sub-horizontal to laterally accreting deposits bounded by stratigraphic surfaces exhibiting variable degrees of erosion and/or non-deposition (e.g., Posamentier and Vail, 1988; Thomas and Anderson, 1994; Zaitlin et al., 1994; Rodriguez et al., 2005; Simms et al., 2006; Blum et al., 2013; Zecchin and Catuneanu, 2013; Tesson et al., 2015).

Transgressive deposits (Chapter 6) are disposed in a retrogradational stacking pattern characteristic of transgressive intervals (Catuneanu et al., 2009; Zecchin and Catuneanu, 2013; Catuneanu, 2019). I attempted an interpretation of transgressive stratigraphies and processes based on current knowledge of recent transgressive architectures and bounding surfaces (e.g., Trincardi et al., 1994; Saito, 1994). Specifically, the wave ravinement surface (WRS), a diachronous erosional surface cut during transgression by waves (WRS; Swift, 1968; Demarest and Kraft, 1987; Nummedal and Swift, 1987), is significant for the reconstitution of transgressive architectures in shallow-water shelf settings.

3.2. Sedimentological methods

3.2.1. Sedimentological data

The sedimentological dataset comprises sediment cores obtained during two oceanographic surveys: the LASEA 2013 onboard *RV Ramón Margalef* and the CADISED 2015 oceanographic survey onboard *RV Poseidon* (Fig. 3.7). The LASEA 2013 sediment cores were collected at forty-five sites on the shelf offshore the Guadiana River using vibrocorer, piston corer, and gravity corer devices, attaining maximum lengths of 5-6 m in specific locations (Figs. 3.7, and 3.8). The CADISED 2015 sediment cores were collected from forty sites along the northern Gulf of Cádiz continental shelf using vibrocorer, giant box corer, rumohr corer, and gravity corer devices with a maximum length of 6 m (Figs. 3.7, and 3.8). From this dataset, ten different sediment cores were selected for this PhD thesis (Table 3.2). Most of the following analyses were carried out on the LASEA sediment cores, which constitute the main dataset:

1) High-resolution digital images and computed tomography (CT) images were used for the basic sediment core analysis. Such analysis included descriptions of lithology, grain size, texture, sedimentary structures, and bioturbation.

Table 3.2: Summary table of studied sediment cores in this PhD thesis, including geographic location, length, and the water depths in which they were collected.

Unit	Core ID	Geographic Coordinates		Water depth (mbsl)	Core length (cm)
		Latitude (N)	Longitude (W)		
Algarve Reflective sheet-like unit	GeoB19508	37° 4.202	7° 32.910	51	491
	LA-12-VC	37° 6.345	7° 16.781	31	510
Guadiana main valley	LA-14-VC	37° 6.317	7° 16.734	31	530
	LA-44-VC	36° 59.115	7° 17.429	89	413.6
PTU 4	LA-25-VC	36° 58.386	7° 14.697	95	483.2
	LA-22-VC	37° 00.379	7° 15.926	77	444.3
PTU 3	LA-46-VC	37° 00.596	7° 17.899	67	399.7
	LA-48-VC	37° 01.560	7° 19.104	70.4	494.8
PTU2	LA-20-VC	37° 01.599	7° 16.721	52	70
	LA-18-VC	37° 03.226	7° 17.736	41	437.7

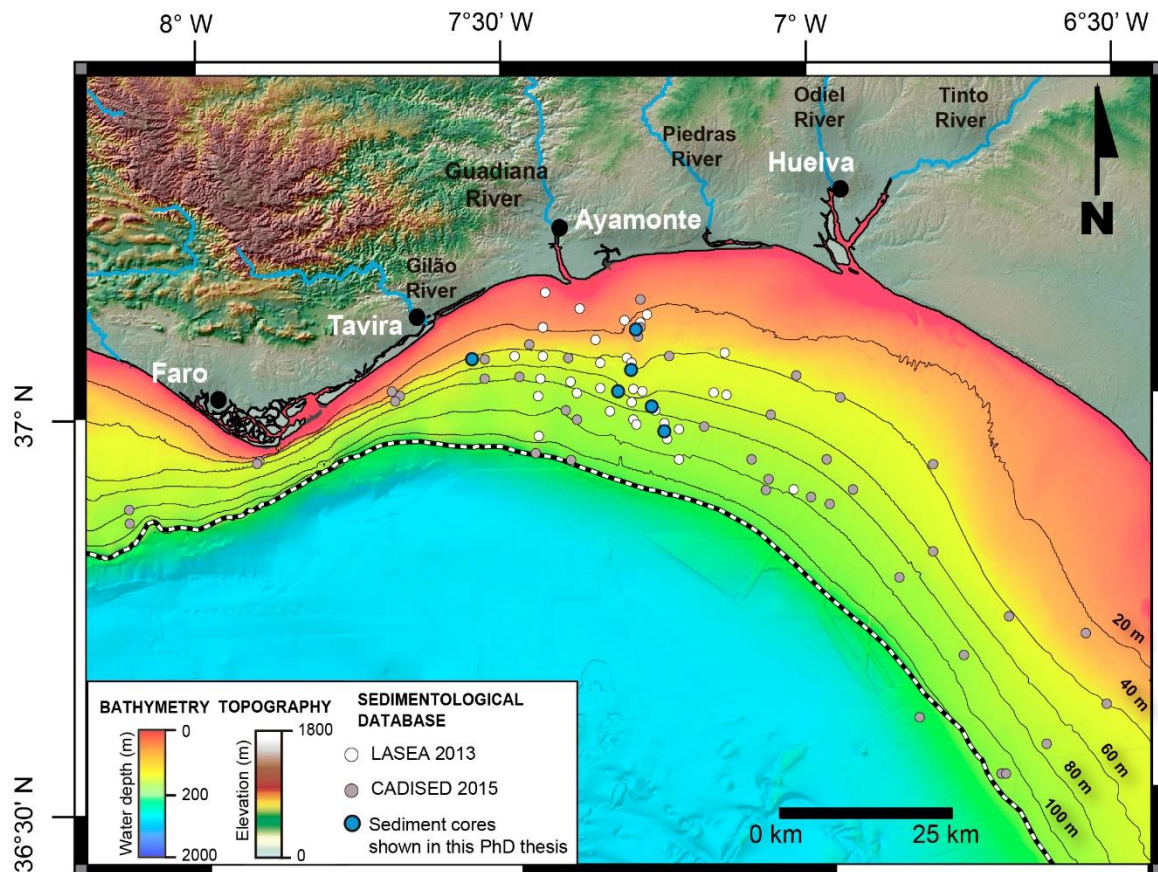


Figure 3.7: Location of sediment core stations on the shelf in the study area along the northern Gulf of Cádiz shelf (EMODnet Bathymetry Consortium, 2020). The position of sediment cores shown in this PhD thesis is also indicated.

2) Physical properties, including magnetic susceptibility (SI) and wet density (γ) in g cm^{-3} , were measured by continuous, non-destructive acquisition techniques using a Geotech Multi-Sensor Core Logger (MSCL) at a sampling interval of 1 cm at the Instituto Geológico y Minero de España (IGME). Sediment magnetic susceptibility (SI) measures a material's response to an applied magnetic field and reflects the abundance of magnetic minerals. In sediment cores, this property is often quantified using a magnetic susceptibility meter. High values suggest elevated concentrations of magnetic minerals, providing information about sediment sources, transport mechanisms, and climatic conditions (Maher and Thompson, 1995). The wet density, determined through gamma-ray attenuation, assesses sediment compaction and porosity variations. This method involves exposing sediment cores to gamma-ray sources and measuring attenuation as the rays pass through. Higher wet density values indicate more compacted and denser sediments, offering insights into compaction processes, sedimentation rates, and environmental conditions (Dadey et al., 1992; Kearey et al., 2013).

3) Geochemical logging of element intensity distribution by X-ray fluorescence (XRF) scanning was performed at the University of Barcelona (Spain) using an Avaatech XRF Core Scanner instrument. This method allows for non-destructive and semi-quantitative

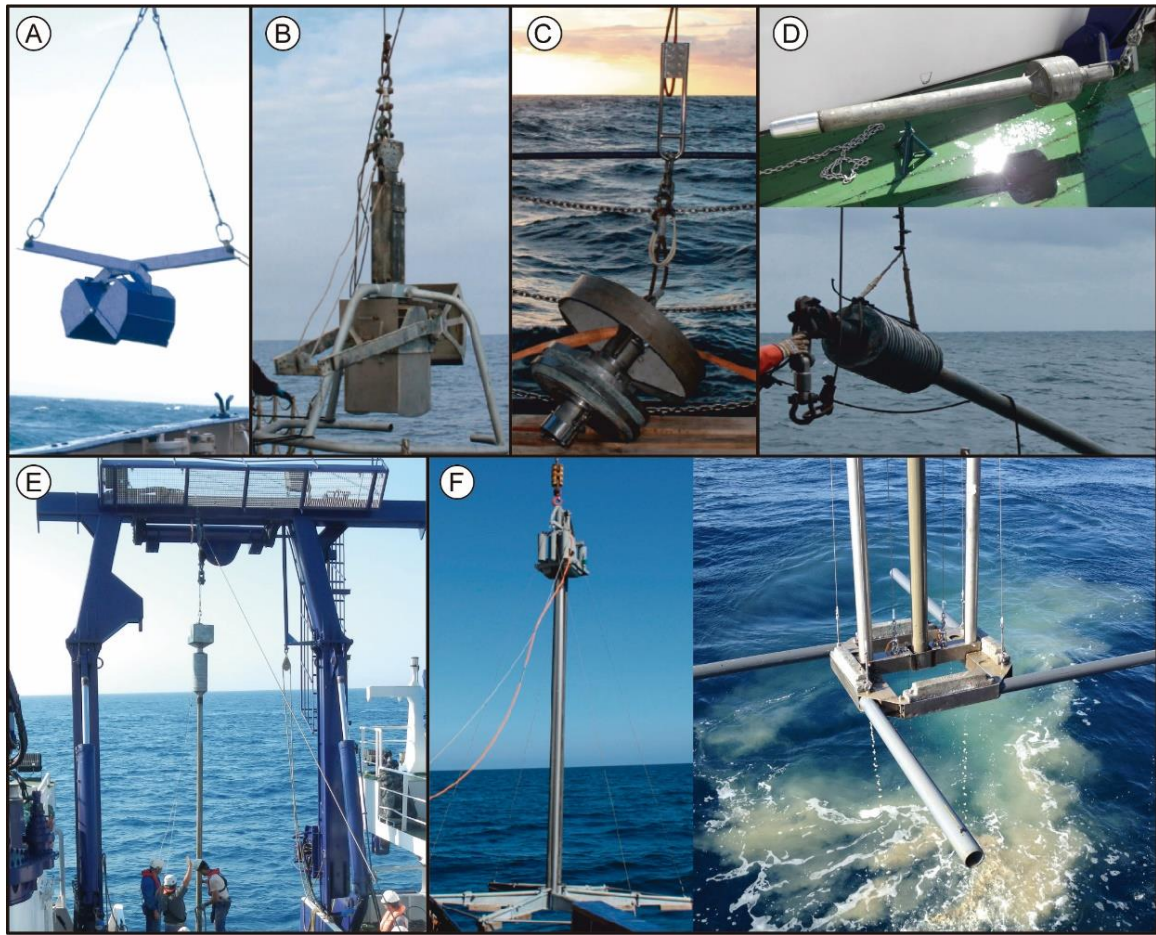


Figure 3.8: Sediment sampling devices deployed during LASEA 2013 AND CADISED 2015 oceanographic surveys: A) Grab Sampler; B) Giant Box Corer, C) Rumohr Corer; D) Gravity Corer, E) Piston Corer, F) Vibrocorer.

continuous measurement of the surface material to characterize the chemical element composition on continuous, split sediment core halves (Richter et al., 2006). The vertical step resolution was set at 1 cm intervals and the voltage ranged between 10 kV and 30 kV. Data were processed through the WinAxiBatch software. Element intensities were converted into ratios, and the natural logarithms of these ratios were used to normalize figure scales.

Additionally, other sedimentological analyses were carried out in sediment core GeoB19508, collected during the CADISED survey:

1) Grain size analyses were performed on sixteen samples collected along the sediment core GeoB19508 at intervals ranging from 20 to 35 cm. Statistical parameters, including mean, sorting, skewness, and kurtosis, were determined. Hydrogen peroxide was used to eliminate the organic matter. Fine and coarse fractions were wet separated using a 63 μm (4 phi) sieve. The grain size distribution of the fine fraction was analyzed with the pipette method and the coarse fraction was subdivided by dry sieving using a sieve rack. Both fractions were graded in phi intervals. Grain size parameters were obtained using the geometric method of moments and the textural classification after Folk (1954).

2) Carbonate content analysis (calcimetry) was carried out in two grain size classes (medium sand and gravel) along the sediment core GeoB19508. At least 2 g per sample were treated with 0.1 M HCl for carbonate dissolution. The samples were then left to stand for 24 hours before being centrifugated.

3.2.2. Sedimentological interpretations

Descriptions of lithology, grain size textures, sedimentary structures, bioturbation, and carbonate content analysis, in addition to the geophysical parameters and geochemical proxies, were used to obtain information about genetic sedimentary processes, to interpret lithological changes, and ultimately to define depositional systems.

In marine sediment cores, understanding physical properties is crucial for unraveling geological and environmental histories. These parameters are useful for identifying subtle lithological changes, reconstructing past environmental changes, and understanding sedimentary processes over geological timescales.

Geochemical data were used to detect compositional sediment variations that could be correlated with depositional environmental changes. The selected elements for this purpose were: iron (Fe), aluminum (Al), silicon (Si), and titanium (Ti). In the study area, the Guadiana River constitutes the main sediment source (Morales, 1997; Gonzalez et al., 2004, 2007) and Fe, Al, and Si are distributed homogeneously across the Guadiana River basin (Delgado et al., 2010). On the adjacent shelf, higher concentrations of most of these elements are associated with the fine fractions, and their concentrations generally decrease with distance from the sediment source (Gonzalez et al., 2007). The only exception to this general trend is Ti, which predominantly occurs in minerals commonly associated with sands and silts. Consequently, these elements were used as proxies for variations in terrigenous sediment supply, assumed to be mainly influenced by precipitation and run-off changes. Finally, calcium (Ca) is expected to be anticorrelated with the distribution of terrigenous elements as Ca mainly reflects the biogenic carbonate content in the sediments and therefore is used as an indicator of marine biogenic material (e.g., Rothwell and Croudace, 2015).

3.2.3 Age data

Fifteen Accelerator Mass Spectrometry (AMS) ¹⁴C dates were obtained from selected sediment cores (Table 3.3). Eight of these dates were obtained by using a mixture of benthic foraminiferal tests or different sizes of bivalve shells (Table 3.3), and were carried out by Poznan Radiocarbon Laboratory (Poland) using a 1.5 SDH-Pelletron Model "Compact Carbon AMS" serial number 003. Sample CNA3837 (Table 3.3), was duplicated at the CNA-Centro Nacional de Aceleradores (Seville, Spain), yielding similar ages. Two AMS ¹⁴C dates were obtained from mollusk shells without signs of transport or diagenetic alteration (Table 3.3), and were carried out at CNA-Centro Nacional de Aceleradores

Table 3.3: AMS radiocarbon data obtained on benthic foraminifera and shells in the studied sediment cores. Ages written in italics point out the anomalous results that provide ages older than expected.

Unit	Core ID	Core section	Depth in core (cm)	Laboratory (Country)	Sample code	Sample material	$\delta^{13}\text{C} \text{ ‰}$	pMC	Conventional Age ^{14}C BP	cal yr BP (68.3%-1s)	cal yr BP (95.4%-2s)	Median probability ^(a)	Relative area under probability distribution 1.000 ^(c)
Algarve Reflective sheet-like unit	GeoB19508	IV	274	CNA (Spain)	GeoB08-274	Mollusk shells	0.14 ± 1.5	31.57 ± 0.14	9261 ± 36	9968-9735	10100-9659	9880	1
	GeoB19508	IV	329	CNA (Spain)	GeoB19508-329	Mollusk shells	3.46 ± 1.5	30.51 ± 0.15	9535 ± 39	10310-10149	10427-10069	10248	1
GmvU1	LA-12VC	IV	400	Beta Analytic (USA)	LASEA12VCI97	Foraminifera	-2.05 ± 1.5	49.22 ± 0.21	5694 ± 35	5665-5934	5563-6103	5813	1
	LA-12VC	V	495	Beta Analytic (USA)	LASEA12VCI90	Foraminifera	-2.58 ± 1.5	43.46 ± 0.19	6695 ± 35	6737-7026	6611-7165	6888	1
GmvU2	LA-14VC	VI	528	Beta Analytic (USA)	LASEA14VCI92	Foraminifera	-1.6 ± 1.5	47.64 ± 0.18	8990 ± 40	9372 - 9665	9228-9864	9511	1
PTU1	LA-18-VC	II	292.3	Poznan (Poland)	Poz-78917	Shell alone	4.8 ± 1	34.21 ± 0.21	8620 ± 50	8985 - 9179	8885-9284	9080	1
PTU2	LA-20-VC	I	8.5	Poznan (Poland)	Poz-78920	Shells	3.3 ± 0.6	93.11 ± 0.32	575 ± 30	<i>post 1950</i> ^(b)	<i>post 1950</i> ^(b)		
		I	46	Poznan (Poland)	Poz-78921	Shell alone	-2.2 ± 0.7	29.69 ± 0.19	9760 ± 60	10409 - 10643	10273-10739	10521	1
	LA-48-VC	I	475.3	Poznan (Poland)	Poz-78703	Foraminifera	-5 ± 0.6	20.40 ± 0.18	12740 ± 70	14080 - 14410	13983-14653	14267	1 (68.3%) and 0.992 (95.4%)
PTU3	LA-46-VC	III	199.5	Poznan (Poland)	Poz-78916	Shells	-0.5 ± 0.7	27.7 ± 0.19	10310 ± 60	11180 - 11387	11097-11554	11291	1
		III	199.5	CNA (Spain)	CNA3837	Shells	-1.18 ± 1.5	27.26 ± 0.13	10441 ± 38	11347 - 11586	11255 - 11695	11469	1
	LA-22-VC	III	136.3	Poznan (Poland)	Poz-78922	Shells	0.7 ± 0.4	24.42 ± 0.18	11330 ± 60	12604 - 12747	12448-12830	12679	1
		I	428.9	Poznan (Poland)	Poz-78704	Foraminifera	-9.7 ± 0.6	6.73 ± 0.13	21670 ± 160	24817 - 25256	24591-25496	25039	1
PTU4	LA-44-VC	II	226.4	Poznan (Poland)	Poz-78923	Shell alone	-1.1 ± 0.5	17.04 ± 0.15	14210 ± 80	16202 - 16503	15967-16770	16355	1

(a) Online program Calib.8.2, which uses the marine20.14c calibration dataset recommended for marine samples limited to 603-50,788 14C year BP (Heaton et al., 2020; Stuiver et al., 2021)

(b) No valid radiocarbon age between 603 and 50779 yrs BP for this calibration curve

(c) Heaton et al., 2020.

(Sevilla, Spain). Finally, three AMS 14C dates on foraminifera tests (Table 3.3) were carried out at Beta Analytic Laboratories (USA). Age calibration was performed using the Calib 8.2 program (Stuiver et al., 2021), with the conventional radiocarbon ages and the Marine 20 calibration data set (Heaton et al., 2020). Local reservoir effect (ΔR) was not applied. The median of the probability distribution was used as a reliable estimation of the sample's calendar age (Telford et al., 2004). For years given with the notation BP (Before Present), the zero age is 1950 CE. Gregorian calendar years (BCE/CE) were considered for historic ages.

3.3. Geomorphological methods

A detailed geomorphological analysis was carried out in Chapter 5 of this PhD thesis. Such analysis integrates a seismic interpretation of the available sections together with the application of a methodology developed by Goff and Nordfjord (2004) for interpolating channel morphology. The fluvial channel morphology is interpolated using a coordinate transformation algorithm that converts geographic data points into a reference frame specified by distance along paths defined by the channel center and edge lines. These lines are generated through the user identification of the channel horizon interpreted from seismic data and displayed in plan view using the ArcGIS software. The completed interpolations for each channel were then transformed back into geographic coordinates. The methodology provides a straightforward means of estimating quantitative geomorphological parameters, such as cross-axis width, depth, and aspect ratio. This methodology was applied for the interpolation of two major valleys related with the most recent incision phases in the shelf off the Guadiana River, which were mapped using the available seismic database (Chapter 5), providing a complete visualization of the complex morphology of the fluvial systems (Fig. 3.9).

The following morphometric parameters were measured in the interpolation model and in a significant number of seismic sections: total (along the thalweg) and straight valley length, valley sinuosity, maximum and average valley width (maximum horizontal distance perpendicular to the valley thalweg), thalweg depth below the sea level and below the seafloor, valley incision and infill thickness (depth difference between the valley thalweg and the adjacent intervalleys; Fig. 3.10), valley gradient (average angle measured between two points along the valley thalweg relative to horizontal), gradient of the valley walls (average angle measured between the shallowest and deepest points along the valley wall relative to horizontal), number of thalwegs, thalweg symmetry coefficient (horizontal distance from the valley edge to the thalweg divided by the valley width), and north azimuth (Fig. 3.9).

Additionally, some morphometric parameters of paleo-channels can link channel morphology to paleo-hydrology, providing estimation of paleohydrological parameters.

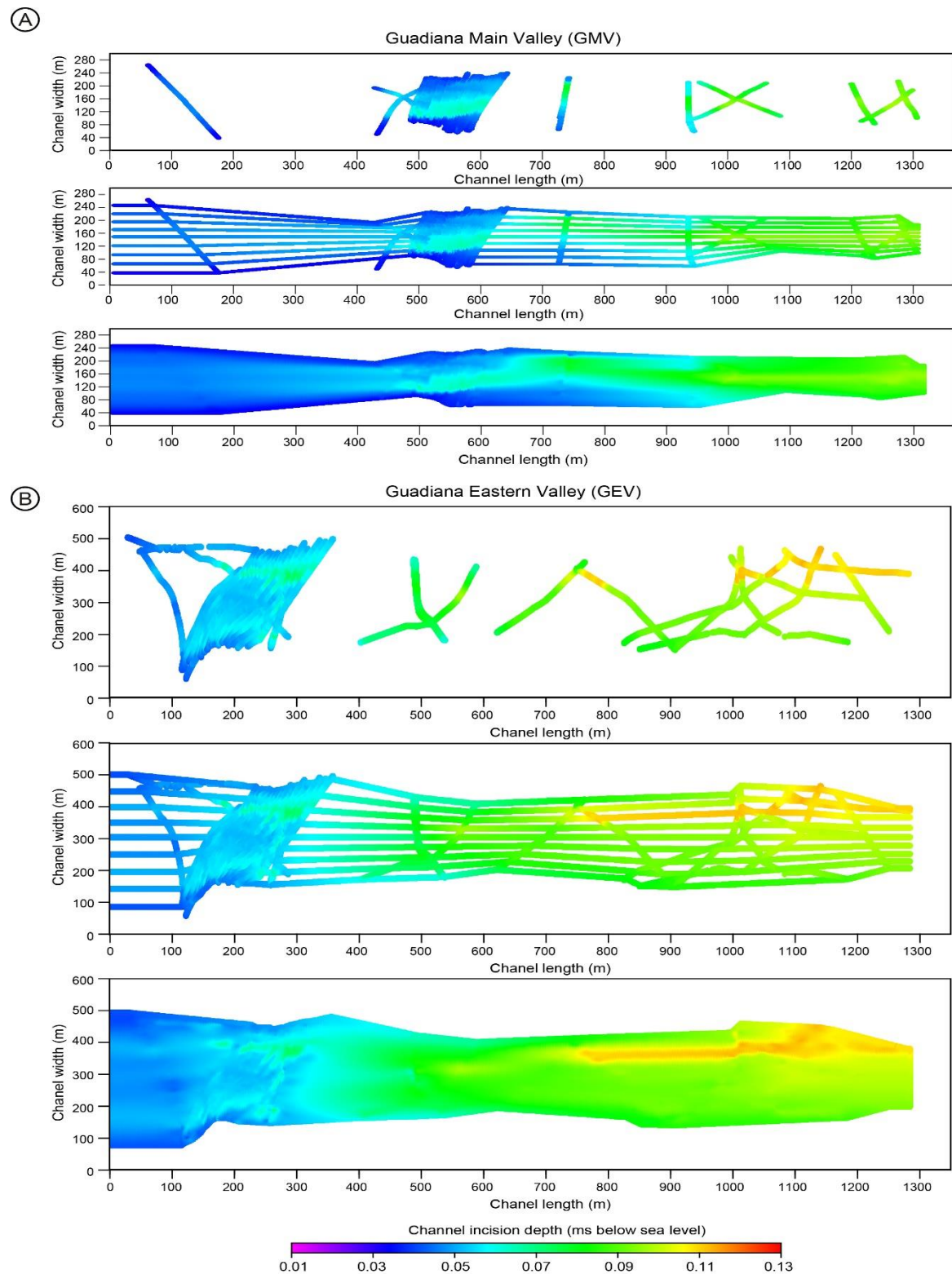


Figure 3.9: A: The Guadiana main Incised valley studied in Chapter 5: (up) Interpreted channel horizon data transformed into channel coordinate space. (center) Linear interpolation along three paths on each side interim to the edges and thalweg. (down) Completed interpolation in channel space using planar interpolation within an optimal triangulation of the values shown in (center). B: The Guadiana Eastern Incised valley studied in Chapter 5: (up) Interpreted channel horizon data transformed into channel coordinate space. (center) Linear interpolation along three paths on each side interim to the edges and thalweg. (down) Completed interpolation in channel space using planar interpolation within an optimal triangulation of the values shown in (center).

3.4. Chronostratigraphic framework

Age attribution of the different seismic horizons characterized in this PhD thesis has been framed by the most updated seismic stratigraphic framework proposed for the northern Gulf of Cadiz continental margin (Mestdagh et al., 2019). In that study, age attribution of seismic horizons was made through the correlation of the regional seismic grid with sites U1386 and U1387, drilled during Integrated Ocean Discovery Program (IODP) Expedition 339 (Hernández-Molina et al., 2016; Mestdagh et al., 2019; Luján et al., 2020). Two seismic profiles running along the IODP sites in the middle slope were connected to the seismic grid on the upper slope and the shelf, allowing to illustrate the lateral variability in the seismic stratigraphic architecture both downslope (shelf versus upper slope versus middle slope) and along-strike.

Afterwards, the major regional seismic surfaces were continued westward across the shelf around the Guadiana River by Luján et al. (2020), allowing to constrain the relative ages of the incised valleys by using these major regional seismic surfaces. The chronostratigraphic framework was completed by using radiocarbon ages extracted from sediment cores collected in different sites along the study area (Table 3.3).

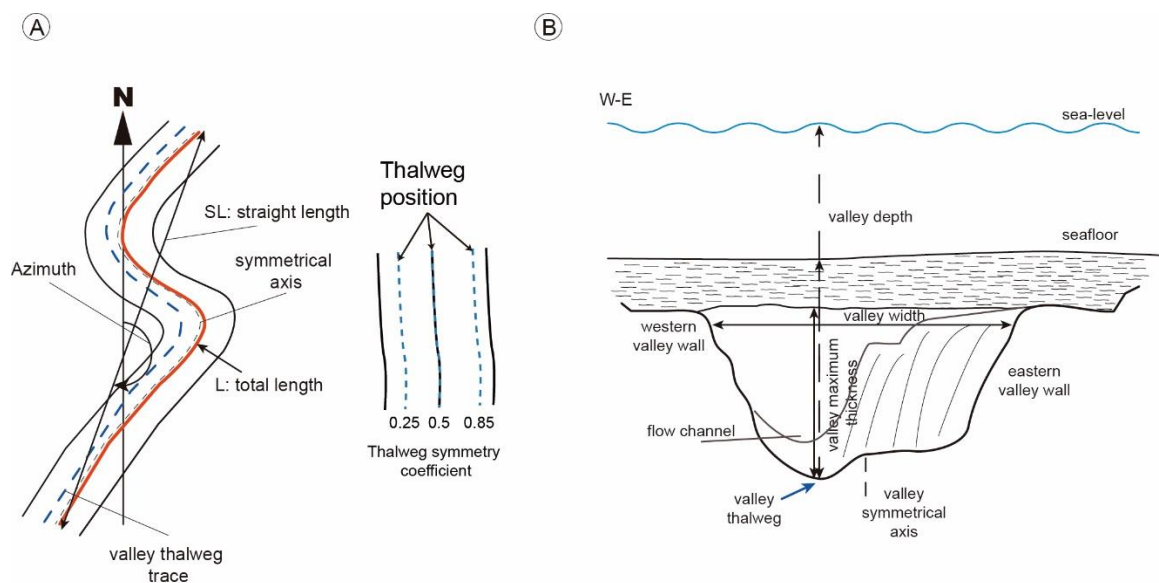


Figure 3.10: Sketches summarizing the main morphometric parameters measured in the two incised paleovalleys that comprise the main scope of Chapter 5 of this PhD thesis. A) Paleovalley in plan view. B) Cross-section of a paleovalley.

CHAPTER

4

CHAPTER 4

Incised valleys on the Algarve Shelf

The research work presented in the chapter is also a contribution to the paper:

Incised valleys on the Algarve inner shelf, northern Gulf of Cadiz margin: Stratigraphic architecture and controlling factors in a low fluvial supply setting.

Álvaro Carrión-Torrente^{1,2}, Francisco José Lobo¹, Ángel Puga-Bernabéu², María Luján³, Isabel Mendes⁴, Till J.J. Hanebuth⁵, Marga García⁶, María Isabel Reguera⁷, David Van Rooij⁸, Javier Cerrillo-Escoriza^{1,2}

¹ *Department of Marine Geosciences, Instituto Andaluz de Ciencias de la Tierra–IACT, Spanish Research Council–CSIC and University of Granada–UGR, Avenida de las Palmeras 4, 18100 Armilla, Granada, Spain.*

² *Departamento de Estratigrafía y Paleontología, University of Granada, Granada, Spain.*

³ *Department of Earth Sciences, University of Cadiz, Puerto Real, Spain.*

⁴ *Centre for Marine and Environmental Research–CIMA, Universidade do Algarve, Faro, Portugal.*

⁵ *Department of Coastal and Marine Systems Science, Coastal Carolina University, Conway, SC, USA.*

⁶ *Oceanographic Centre of Cadiz, Spanish Institute of Oceanography–IEO, CSIC, Ministry of Science and Innovation, Cadiz, Spain.*

⁷ *Instituto Geológico y Minero de España–Centro Nacional, Spanish Research Council–CSIC, Madrid, Spain.*

⁸ *Renard Centre of Marine Geology, Ghent University, Gent, Belgium.*

Published on:

Continental Shelf Research 266 (2023) 105095

<https://doi.org/10.1016/j.csr.2023.105095>

Received 17 February 2023; Received in revised form 7 July 2023; Accepted: 5 August 2023

Published: 6 August 2023

JCR (2022): 2.3 (Q2)

Abstract

A network of cross-shelf paleovalleys has been recognized over the paleo-inner shelf off the Gilão-Almargem Estuary, a small fluvial drainage system that presently receives minor sediment supply in the eastern Algarve Shelf, northern margin of the Gulf of Cadiz (SW Iberian Peninsula). This study is aimed at determining the driving controls that triggered substantially different paleohydrological conditions and sedimentary dynamics of ancient fluvial systems in this margin, focusing on evidences of secondary controls on valley genesis and evolution, superimposed to primary glacio-eustatic control such as antecedent geology, low fluvial supply and changing hydrodynamic regimes. The architecture and spatial distribution of these paleovalleys were interpreted based on a grid of seismic profiles with different resolutions. Likewise, a sediment core obtained in a distal position of the paleovalley system provided information about sedimentary processes during the most recent stage of valley infilling. The chronostratigraphic framework was constructed based on regional seismic horizons defined in previous studies and complemented with two AMS ¹⁴C dates obtained from bivalve shells.

The inner shelf paleovalley system is composed of several incised valley features which exhibit a remarkable similar internal architecture. These inner valley features exhibit two major incision phases (from oldest to youngest; IP 2 and IP 1) that are thought to constitute a simple paleovalley system formed during the last glacial cycle. The origins of the incision are considered to be different. The older one is related to fluvial incision during the sea-level fall leading into the Last Glacial Maximum, whereas the recent one is interpreted as the result of tidal scour during the postglacial transgression. Their corresponding infillings are interpreted, respectively, as estuarine bay-fill deposits and estuary-mouth sands. Overlying the paleovalley infilling, a distinctive reflective unit is in agreement with the generation of coastal barriers and related depositional systems.

The formation of the paleo-inner-shelf paleovalley system was strongly conditioned by antecedent geology, which strongly limited the generation of wide incised valleys and determined the amount of incision landward of a well-defined break of slope. Its postglacial infilling was mainly estuarine in nature, likely involving the development of a dendritic system, with numerous barriers interrupted by tidal inlets and channels in a mixed estuarine system with low fluvial supply.

Key points

- Inner-shelf valleys interpreted as a simple system formed during the last glacial cycle.
- The valleys infilling records the occurrence of wave- and tide- dominated processes.
- Incised valley formation was strongly determined by antecedent geology.
- The infilling took place under high rates of sea-level rise and low fluvial supply.
- The system comprised an estuarine system with multiple barriers and inlets.

4.1. Results

4.1.1. Seismic stratigraphy of the inner-shelf paleovalley system

Along the inner shelf off the Gilão-Almargem Estuary, a paleovalley system was identified between 10 and 40 m water depths (Fig. 4.1). The paleovalleys are carved in a well-marked unconformity, which has been correlated with a major regional seismic surface defined across the northern Gulf of Cadiz Shelf in previous studies (Luján et al., 2020; Mestdagh et al., 2019). The unconformity is characterized by low proximal gradients (0.29° - 0.4°) and a distal break of slope at about 30-40 m water depth that runs at around 6 to 7 km from the coastline (Fig. 4.2). In the intervalley areas of the inner shelf, the unconformity is eroding laterally extensive, highly reflective deposits, showing frequent erosional truncations (Fig. 4.3). Seaward of the break of slope, gradients of the unconformity increase to values of 0.79° to 1.07° .

The inner-shelf paleovalley system is composed of several incised features that could be identified along the available seismic sections (Figs. 4.3 to 4.8A). These valleys which constitute the inner-shelf system have small (width and incision depth), with maximum values, respectively, of 650 m and around 30 meters below the seafloor (mbsf; Figs. 4.3 to 4.7). Evidences of tectonic activity are not found in this area. The inner-shelf paleovalley system is composed of a main valley that can be followed along 8 km in a NW-SE trend

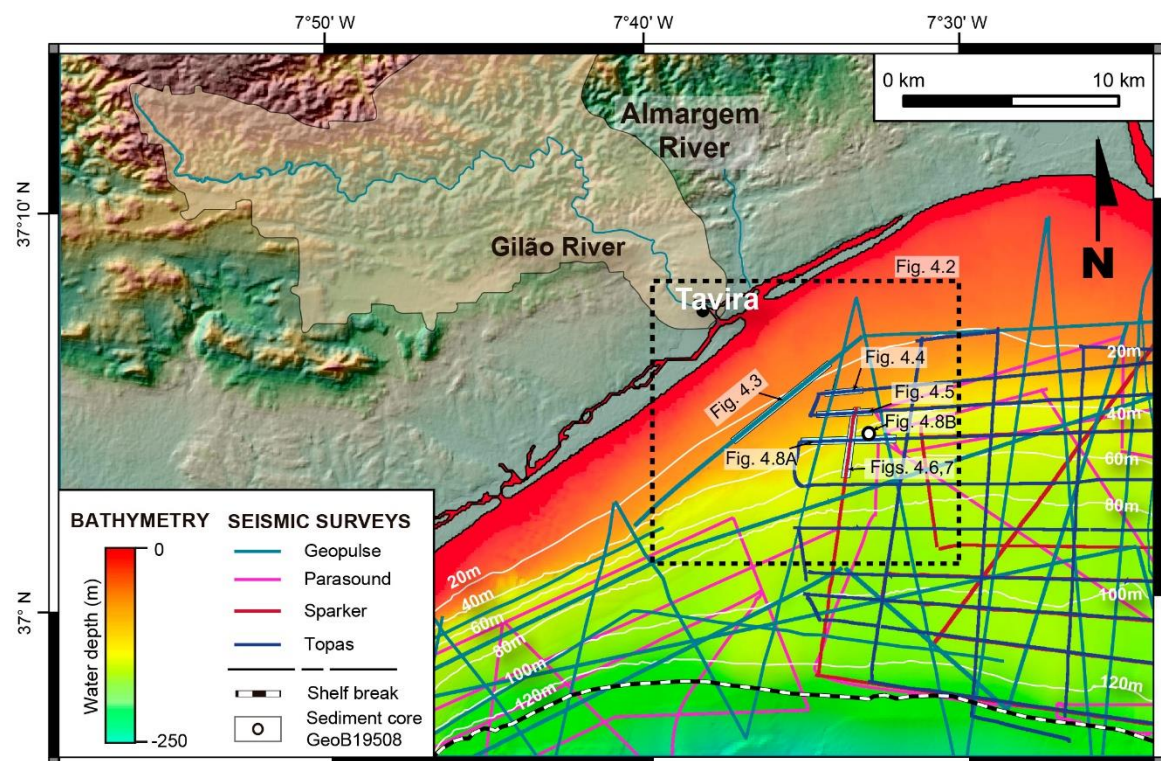


Figure 4.1: Location of the seismic database on the shelf in the study area offshore of the Gilão-Almargem Estuary (EMODnet Bathymetry Consortium, 2020). The location of Figure 4.2 is indicated in the inset rectangle, and the location of Figures 4.3 to 4.8 is highlighted.

from the present coastline, off the Gilão River mouth (Fig. 4.2). This main valley could be traced incising the shelf from depths of 20 to 30 mbsf. This valley has a mean width of 250 m and a mean maximum incision depth of 15 mbsf along the thalweg. Besides, smaller valleys (150-200 m of width) are located at both sides of the main valley. The continuity of these lateral valleys on the shelf was difficult to capture due to the sparse seismic coverage in this area.

Seaward of the break of slope that establishes the boundary of the inner shelf, other valley features are observed (Fig. 4.6). However, they occur at considerably higher depths (80 to 100 mbsf) than the inner shelf valleys, they are less abundant and exhibit blocky seismic facies with some hyperbola, which could indicate older ages. Because of those reasons, I suspect that these distal valleys may be not genetically linked with the inner shelf valleys, and therefore these features are beyond the scope of this study.

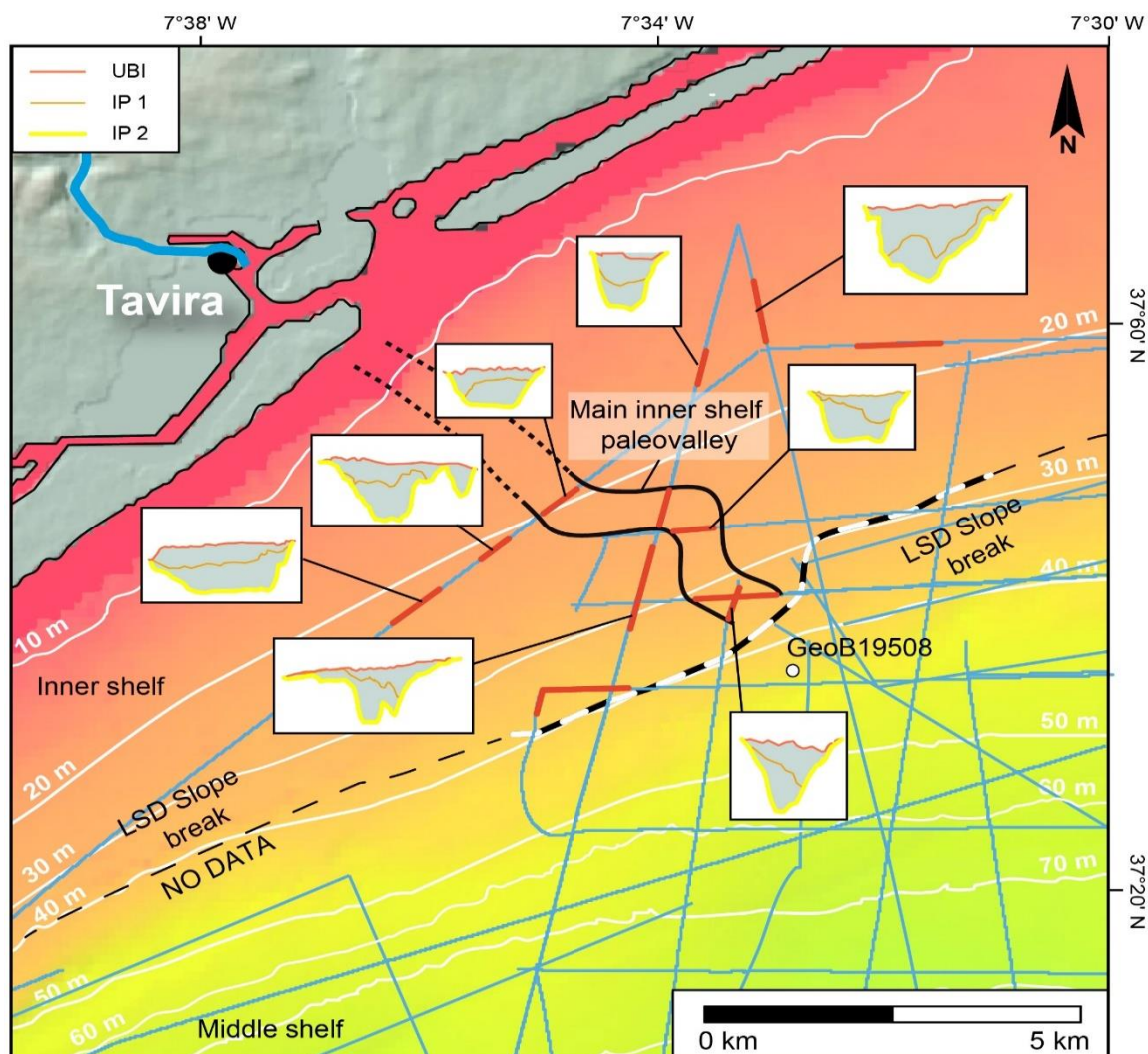


Figure 4.2: Spatial distribution and schematic cross-sections of the different incised valley features identified along the Algarve inner shelf off the Gilão-Almargem Estuary. The trace of the main fluvial valley, which can be considered the seaward extension of the Gilão River, is also represented. Background information consists of shelf bathymetry, the Last Subaereal Discontinuity (LSD) slope break line, and the position of sub-bottom seismic lines. UBI: Upper boundary of infilling; IPs 1 and 2: Incised phases 1 and 2.

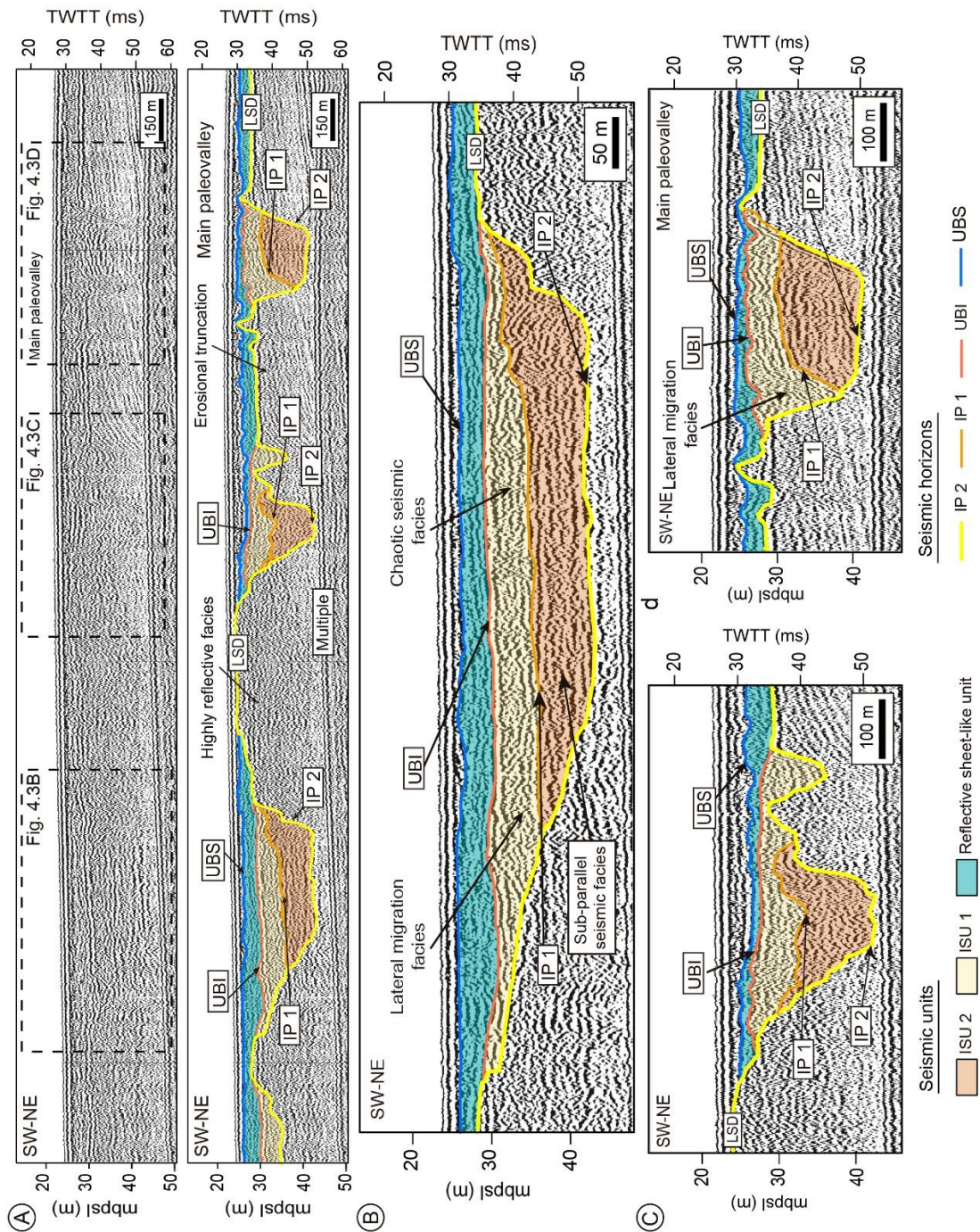


Figure 4.3: A) Coast-parallel (SSW-NNE-oriented) sub-bottom seismic Uniboom source (Geopulse™) profile focusing on the proximal inner-shelf paleovalley system (up) and its interpretation (below). B, C, D) Interpreted zoomed seismic windows of the different paleovalleys. Their location is indicated in Figure 4.3A. Here, the important characteristics observed are: the occurrence of highly reflective seismic facies in the intervalley areas with local identifications of well-marked erosional truncations; the distinctive seismic facies which compose the infilling of the paleovalleys, with sub-parallel facies infilling the older incision phase (ISU 2) and with chaotic facies with local occurrences of lateral migrations infilling the younger incision (ISU 1); the asymmetric shape of the younger phase IP 1, with thalwegs displaced laterally; and the thin, laterally extensive reflective unit covering the incisions. The color code and acronyms are indicated here, and the location of the seismic section is indicated in Figure 4.1. IPs 1 and 2: Incised phases 1 and 2; UBI: Upper boundary of infilling; UBS: Upper boundary of sheet-like unit.

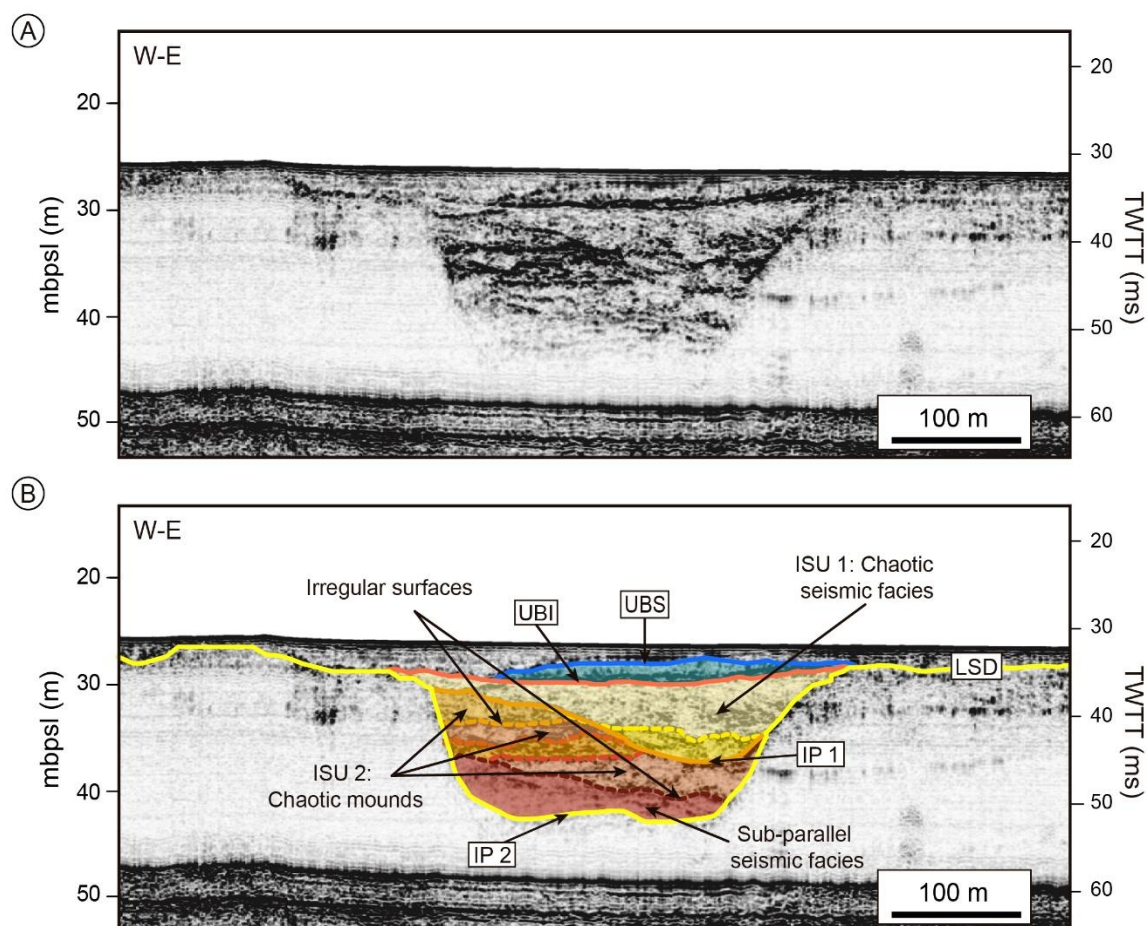
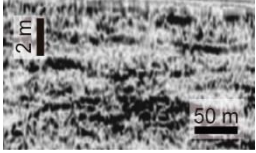
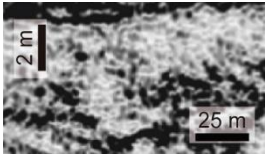
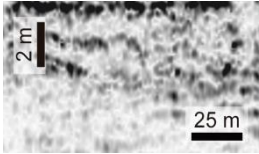


Figure 4.4: Along-shelf (W-E-oriented) sub-bottom acoustic profile showing the main inner-shelf paleovalley (A) and its interpretation (B) at around 30 m water depth. The infilling of the lower incision phase (ISU 2) is very complex, with the occurrence of erosional irregular surfaces and chaotic mounds intercalated within sub-parallel seismic facies. The younger incision phase is asymmetrical, with the thalwegs displaced eastward. The infilling of the younger incision phase exhibits a chaotic seismic configuration. The upper reflective unit is not laterally continuous at this location. The location of the seismic section is indicated in Figure 4.1 and the color code and acronyms are indicated in Figure 4.3.

The different inner-shelf incised valleys exhibit a similar stratigraphic architecture, where two incision phases (IPs 2 and 1) and their subsequent infillings (ISUs 2 and 1) could be characterized. The incised valleys and their infillings are buried by a reflective sheet-shaped seismic unit, which in turn is overlain by a rather transparent surficial seismic unit (Table 4.1; Figs. 4.3 to 4.7).

The oldest incision phase (IP 2) has incision depths that range from 15 mbsf in proximal areas (Fig. 4.3) until 32 mbsf in the more distal southeastward parts of the paleovalleys. It is characterized by an erosional high-amplitude seismic horizon which truncates the underlying reflective shelf seismic facies. Generally, these channels show nearly symmetrical U-shaped cross-sections characterized by a central thalweg (Figs. 4.3 to 4.7).

Table 4.1: Summary table of the seismic facies, including the seismic configurations, boundaries, interpretations and acronyms for each seismic unit characterized in the inner shelf paleovalley system identified in this chapter. IPs 1 and 2: Incised phases 1 and 2; UBI: Upper boundary of infilling; UBS: Upper boundary of sheet-like unit.

Seismic unit	Seismic image	Seismic configuration	Seismic Boundaries	Geometry	Interpretation
Reflective Sheet-like Unit		Amplitude: Low-very low Configuration: semitransparent with high amplitude reflections	Top: UBS Termination: Concordance/Toplap Bottom: UBI Termination: Downlap	Wedge	Paleobarrier
ISU 1		Amplitude: Low to medium Configuration: Massive/Chaotic	Top: UBI Termination: Toplap-Erosion Bottom: IP 1 Termination: Concordance / Downlap	Wedge / Channel-like	Estuarine-mouth massive sands // Tidal Inlet features
ISU 2		Amplitude: Low to medium Configuration: Sub-parallel	Top: IP 1 Termination: Toplap-Erosion Bottom: IP 2 Termination: Concordance / Downlap	Wedge / Channel-like	Estuarine infilling

The infilling of the oldest incision phase has a variable spectrum (ISU2; Table 4.1). It is generally characterized by a moderate to low continuity, sub-parallel seismic configuration (Figs. 4.3 to 4.7). However, a higher level of complexity is identified locally, where ISU 2 is constituted by several sub-units with mostly chaotic, highly reflective seismic configurations bounded by rather irregular horizons, intercalated between sub-parallel configurations (Fig. 4.4).

The younger incision phase (IP 1) of the inner paleovalley system is characterized by a high-amplitude seismic horizon that truncates the older phase (Figs. 4.3 to 4.7). This phase excavates the shelf from a range of incision depths of 10 mbsf in the proximal areas to around 22 mbsf basinward. During this phase, channels cross-sections display variable geometries that range from symmetric to asymmetric, characterizing both U-shaped and V-shaped cross-sections (Figs. 4.3, and 4.6), although asymmetric shapes, with laterally displace valley thalwegs are more common (Figs. 4.3, 4.4, 4.6 and 4.7).

The infilling of the younger incision phase (ISU 1) is characterized by chaotic, variable amplitude seismic configurations or by non-stratified, massive seismic facies (Figs. 4.3 to 4.7; Table 4.1); additionally, infilling facies which exhibit lateral migration with some weak tangential-oblique internal reflections are also identified (Fig. 4.3). The infilling has an average thickness of 9 m, reaching a maximum of 14 m in some valleys.

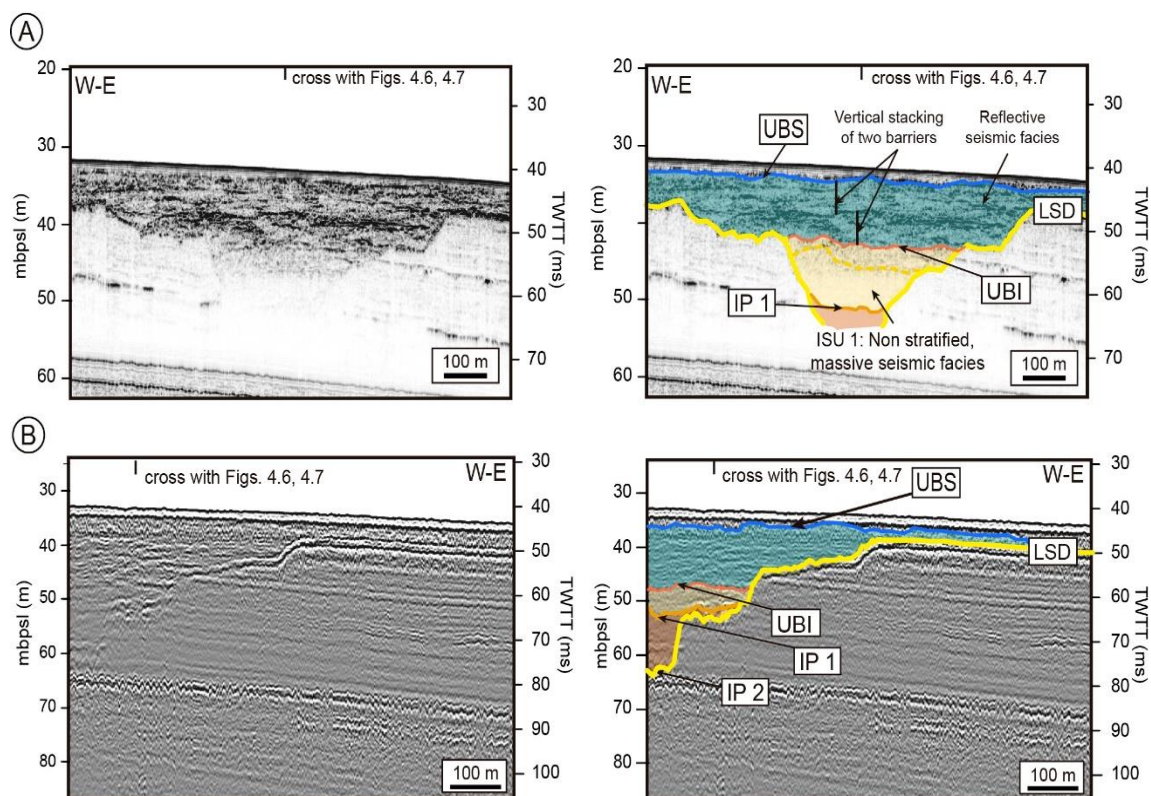


Figure 4.5: Along-shelf (W-E-oriented) sub-bottom seismic profiles focusing on the main inner-shelf paleovalley. A) TOPAS acoustic profile (left) and its interpretation (right). B) Sparker profile (left) and its interpretation (right). In the acoustic profile, the lack of penetration prevents the recognition of the oldest incision phase and its infilling. The reflective sheet-shaped unit that covers the paleovalley and its infilling is very thick (10 meters) at this location, where an internal high-amplitude reflection separates two sheet-like deposits. The color code and acronyms are indicated in Figure 4.3. The location of the seismic section is indicated in Figure 4.1. The crossings with Figures 4.6, and 4.7 are also indicated.

The two incision phases are bounded at the top by a high-amplitude, mostly flat surface which separates the infilling from the upper deposits (Upper boundary of infilling (UBI); Figs. 4.3 to 4.7).

The paleovalley system is buried along the inner shelf by a sheet-like reflective unit that locally exhibits internal reflections, usually sub-parallel but locally also landward dipping (Figs. 4.3 to 4.8) and its upper boundary it is marked by a mostly flat seismic horizon (UBS). The sheet-like reflective unit buries the paleovalleys and their infillings and extends laterally along intervalley areas beyond the confines of the previous depressions. In proximal areas (20-25 mbpsl), the unit is very thin (i.e., few meters thick), but it thickens in more distal locations, where it might reach 12 m in thickness in areas where the main paleovalley seems to be under filled by previous deposits (Fig. 4.6). There, at least two tabular deposits seem to be vertically stacked. In more distal locations, the thickness of the sheet-like reflective unit decreases again, to values of 5 m, where the reflective unit exhibit mounded features (Fig. 4.8A). The sheet-shaped reflective unit is covered by a rather transparent drape over most of the inner shelf, increasing the thickness to values of 8-10 m in distal locations (Figs. 4.6 to 4.8A).

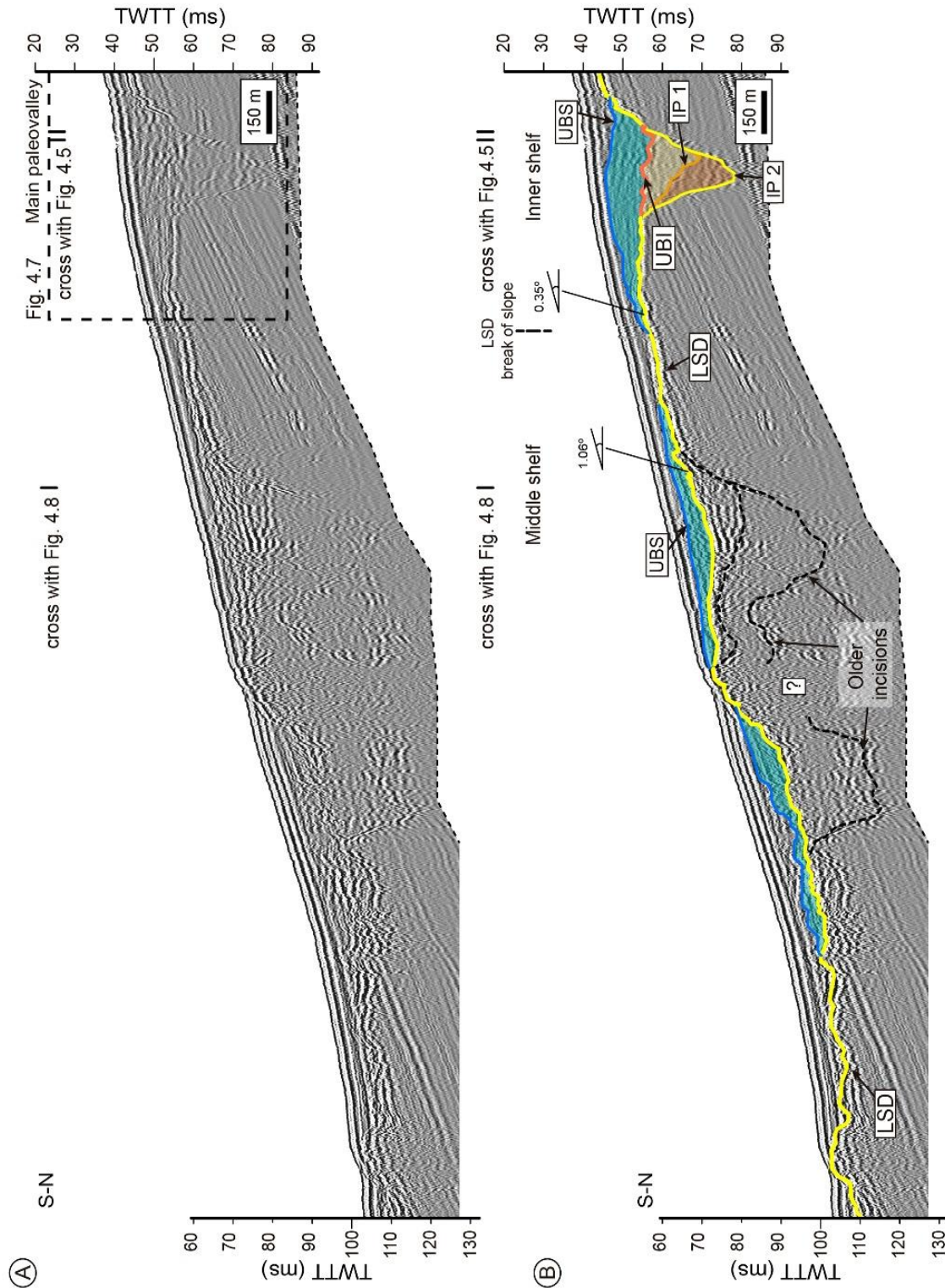


Figure 4.6: Downdip cross-shelf (S-N oriented) Sparker profile (A) and interpretation (B) showing the occurrence of valleys landward and seaward of the break of slope that establishes the seaward boundary of the paleo-inner shelf. Landward of the break of slope, the main inner shelf paleovalley is observed at an approximate depth of 40 to 80 ms (more details of this valley are provided in figure 4.7). Seaward of the break of slope, several valley features occur at water depths of 39 m. Here, the paleovalleys seem to be covered by blocky, highly reflective seismic facies, and the lateral flanks of the valleys are not easily identified. The location of the seismic section is indicated in Figure 4.1 and the color code and acronyms are indicated in Figure 4.3. The location of Figure 4.7 (inset rectangle), and the crossings with Figures 4.5, and 4.8 are also indicated.

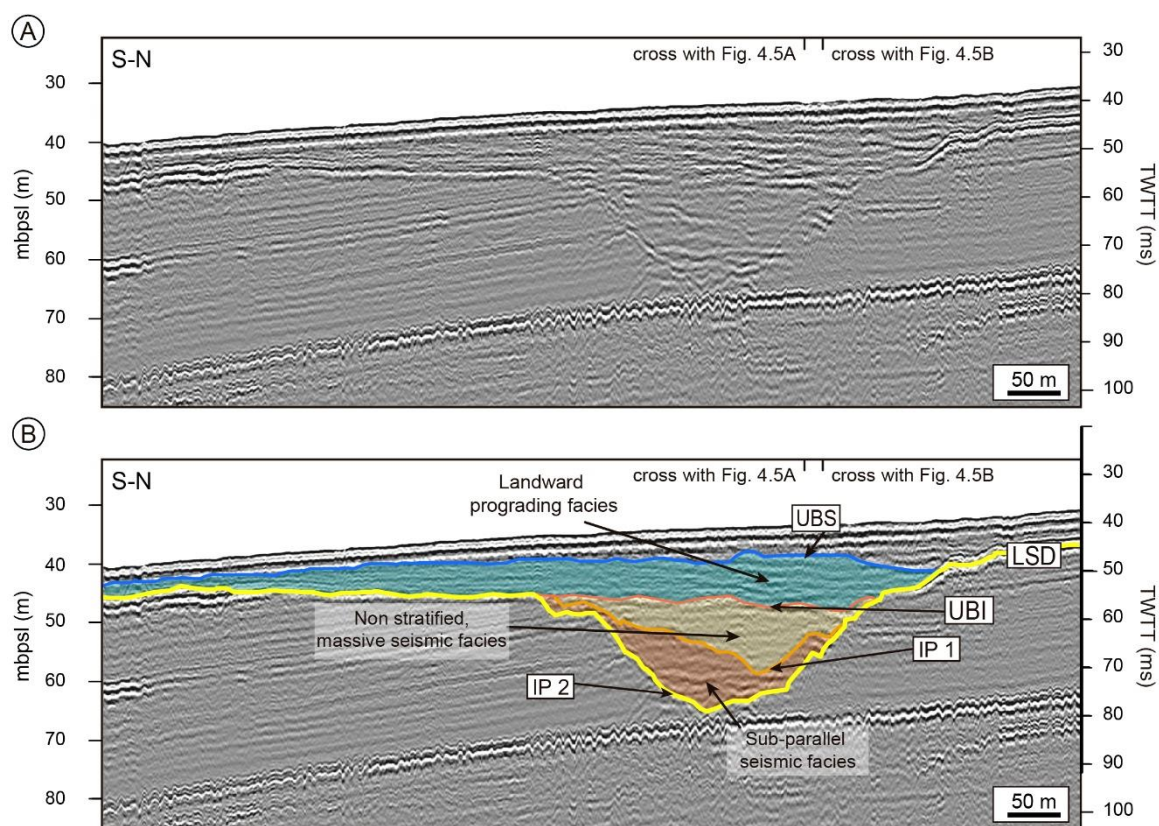


Figure 4.7: Downdip cross-shelf (S-N-oriented) Sparker profile showing the main inner-shelf paleovalley (A) and its interpretation (B). The paleovalley occurs landward of the break of slope, and is characterized by two phases of incision and infilling. The second incision phase is asymmetric and is mostly covered by non stratified seismic facies. The reflective unit covering the paleovalley and its infilling is relatively thick here (maximum thickness of 10 m) and exhibits some landward-directed prograding reflectors. The color code and acronyms are indicated in Figure 4.3. The location of the seismic section is indicated in Figures 4.1, and 4.6. The crossing with Figure 4.5 is also indicated.

4.1.1. Sedimentary facies and core descriptions

4.1.1.1 Sedimentary facies

The sedimentological analysis of the available sediment core obtained from the inner-shelf paleovalley system (Figs. 4.1, 4.2, and 4.8A), allow us to distinguish three main sedimentary facies types, which provide useful information about the sedimentary processes during the most recent stage of valley sediment infilling:

Facies Sc: Massive cemented sands. These facies are composed of well-sorted gravelly sands with abundant granule- to pebble-sized bioclasts, mainly bivalves and gastropods. This facies is generally homogenous and massive (Fig. 4.8B); in addition, strong to slight cementation is observed.

Facies G: Sandy gravels. This facies comprises granule- to pebble-sized gravels, mainly composed of highly fragmented bivalve shells and rounded rock grains, which are hosted

in a mixture of fine to coarse sands and silty sands. This facies is poorly sorted and structureless (Fig. 4.8B).

Facies Sm: Massive muddy sands. This facies is composed of well-sorted sands without sedimentary structures and with large amounts of bioclasts, mainly bivalves and gastropods. This facies is homogenous and massive (Fig. 4.8B), although silt nodules of varying sizes are scattered in the sands.

4.1.1.2 Sediment core GeoB19508

This sediment core is 491 cm long and is composed mainly of sands and gravels (Fig. 4.8). A correlation between the seismic data and the core projected position was made (Fig. 4.8A). Such correlation indicates that the core penetrates through the sheet-like reflective unit over the LSD surface between 50 and 60 mbpsl (Fig. 4.8A). Nevertheless, at the core location there is not any evidence of any incised feature, and the closer paleovalley is located 3.5 km westward (Fig. 4.8A).

From bottom to top, four intervals can be distinguished (Fig. 4.8B). The lower interval (491-436 cm deep; Fig. 4.8B) is characterized by widely cemented well-sorted sands (facies Sc) with some gravel-sized bioclasts (mollusk and gastropods). The second interval (436-345 cm deep) is dominated by homogenous medium to coarse sands with scarce pebbles (facies Sc). Along this interval, changes in sand cementation are observed: slightly cemented sands occur from 436 to 398 cm that are overlaid by strongly cemented sands from 398 to 381 cm. Then, slightly cemented sandstones occur from 381 to 360 cm. This latter cemented sand interval is interrupted by three mud layers (360-355 cm). Finally, the upper part of this second interval is characterized by highly cemented sands (355-345 cm). The third interval (345-262 cm deep) is dominated by sandy gravels, although grain sizes increase to around 315 cm and decrease in the upper part. The gravel is composed of pebble-sized clasts from a wide variety of lithologies with some shell fragments (facies G). Two AMS 14C dates were obtained in this interval (Table 3.3), providing age values that place the formation of these deposits between 9880 and 10248 cal yr BP (Fig. 4.8B). Finally, the upper part of the core (262-0 cm) is characterized by homogeneous fine to medium muddy sands (facies Sm) finning upward. This interval does not show any sedimentary structures and contains some silt nodules of variable size.

Mean grain size shows slight variations along the core ranging from 2.27 to -0.55 phi, with a mean value of 1.43 phi (Fig. 4.8B). These variations mostly occur in the third interval that has a mean value of -0.14 phi; the rest of the core shows values close to the mean grain size. Sorting values range from moderately well sorted in the top to poorly sorted in some intervals (Fig. 4.8B). Skewness and kurtosis show similar distributions along the entire core, characterized as coarse skewed and very leptokurtic; the main changes are found in the third interval (Fig. 4.8B), which shows a symmetrical skewness and a leptokurtic range.

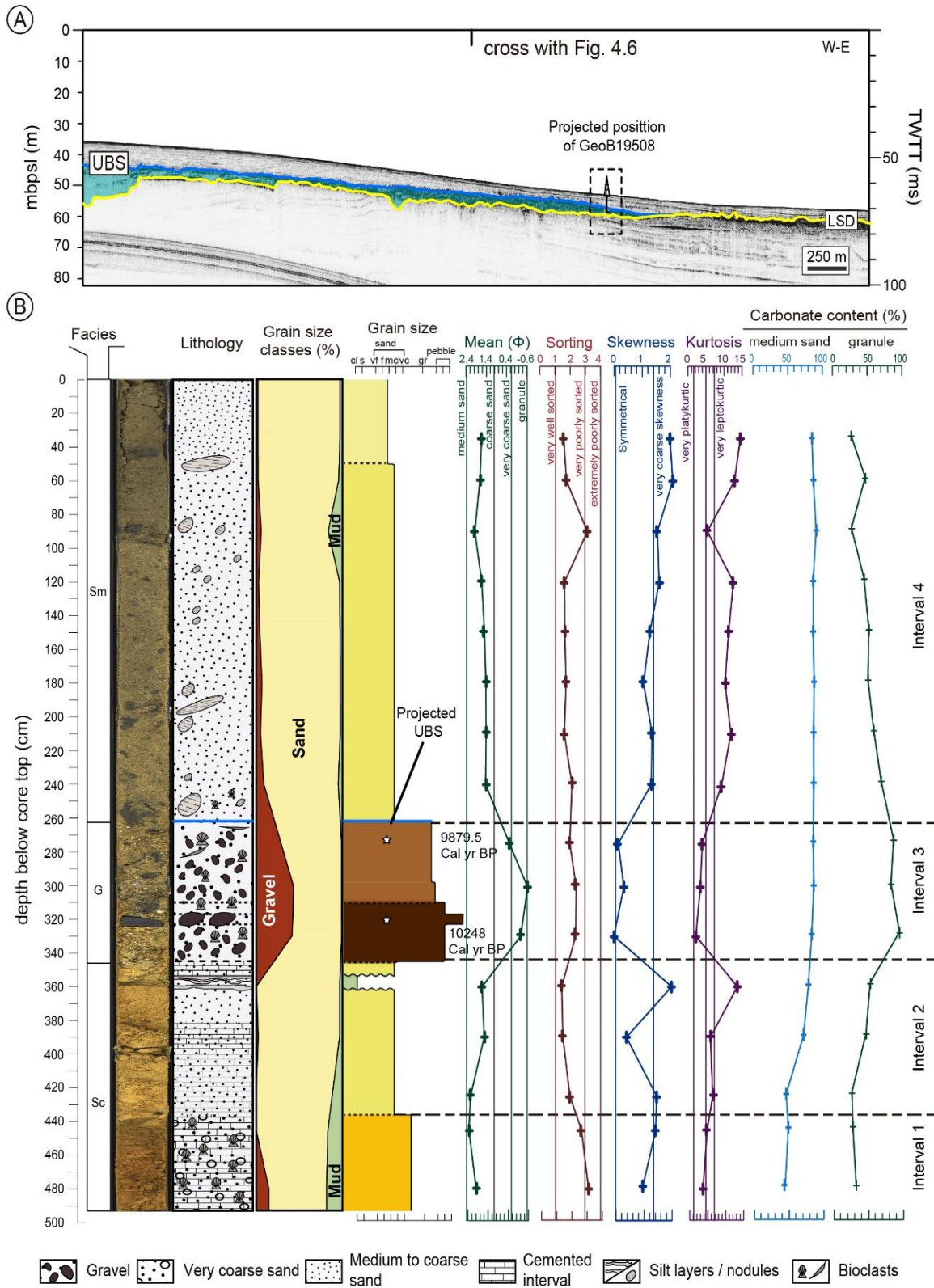


Figure 4.8: A) W-E-oriented sub-bottom acoustic profile including the projected position of the studied sediment core GeoB19508. The location of the seismic section is indicated in Figure 4.1. The crossing with Figure 4.6 is also indicated. B) Photography, facies distribution, lithological description, control age points, grain size statistical parameters (mean, sorting, skewness and kurtosis), and carbonate content of sediment core GeoB19508, characterizing the distal termination of an incised valley. The position of the sediment core is indicated in Figures 4.1, and 4.2.

Calcimetry analyzes reveal high and homogenous carbonate contents in the medium sand fraction, reaching up to 90% along most of the core (Fig. 4.8B). Meanwhile, the granule fraction shows a lower carbonate content along most of the core, ranging from 10% to 40%; the only exception to this trend occurs in the third core interval, where granule-sized grains have carbonate contents to 90% (Fig. 4.8B).

4.2. Discussion

4.2.1. Regional chronostratigraphic framework

Off the Guadiana River, major shelf erosional unconformities were correlated with the late Quaternary 100 ka glacio-eustatic cycles from 435 to 27 ka (Fig. 4.9A; Mestdagh et al., 2019). These surfaces were identified in the outer shelf; however, the lateral tracing of these shelf erosional surfaces revealed that they tend to merge landward and westward, generating protracted hiatuses that increase in magnitude in those directions (Luján et al., 2020) (Fig. 4.9A). Based on the study by Mestdagh et al., (2019), and on other previous studies conducted on the Algarve margin (Hernández-Molina et al., 2016; Luján et al., 2020, Duarte et al., 2022), the following major erosional surfaces have been recognized on the Algarve Shelf: LSD: Last Subaerial Discontinuity (0.02 Ma); LQD: Late Quaternary Discontinuity (0.3 Ma); and MPD: Mid Pleistocene Discontinuity (0.9 Ma).

The available chronostratigraphic information in the region derived from age-dated major regional seismic surfaces indicates the inner-shelf paleovalley system is genetically related to the LSD (20ka; Mestdagh et al., 2019; Luján et al., 2020), as this surface is the most regionally extensive and can be identified along the entire shelf. Considering the recognition of two main incisions in the different paleovalleys of the inner shelf, two major hypotheses can be proposed:

1) The paleovalley system is simple, related to a single phase of sea-level fall, and contains a single depositional sequence (Fig. 4.9B). Equivalent simple incised valleys have been documented elsewhere (*e.g.*, Allen and Posamentier, 1991, 1994; Li et al., 2002; Gutierrez et al., 2003; Weber et al., 2004a, b). If the inner shelf system is regarded as simple, the older incision phase IP 2 would be related to the prolonged sea-level fall that culminated in the LGM, whereas the whole valley fill would comprise a single depositional sequence deposited after the LGM (Fig. 4.9B).

2) The paleovalley system is a compound feature, which corresponds to multiple, superimposed cycles of incision and deposition (e.g., Thomas and Anderson, 1994; Foyle and Oertel, 1997; Proust et al., 2001; Tesson et al., 2005). The interpretation of inner shelf system as compound paleovalleys is based in the assumption that incision phases IP 1 and 2 would be related to two different sea-level falls culminating in two different lowstands (e.g., MIS 2 and MIS 6; Fig. 4.9C).

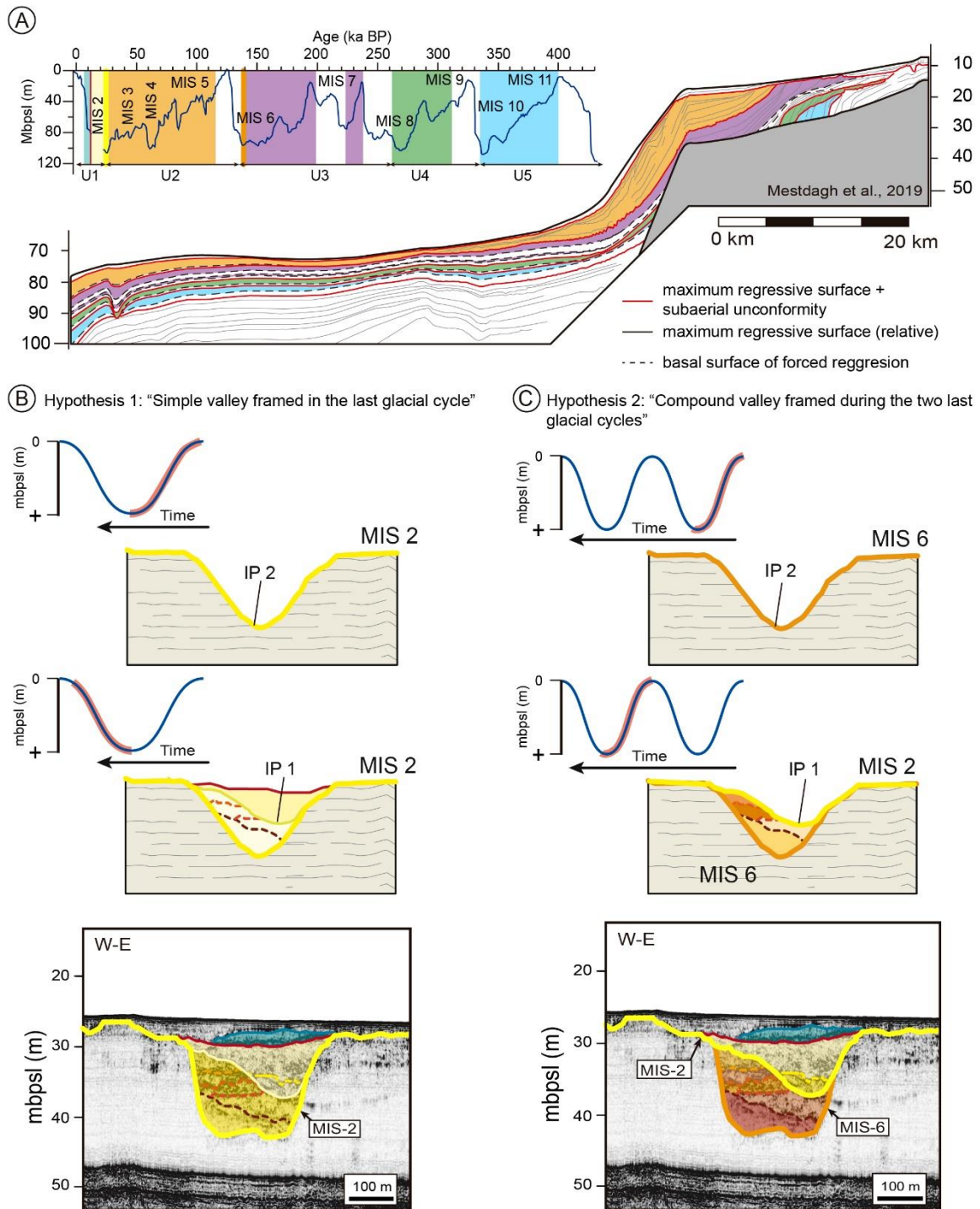


Figure 4.9: Synthetic seismic and sequence stratigraphic interpretation for the northern Gulf of Cadiz. A) Late Quaternary sequences and sequence stratigraphic surfaces on the northern Gulf of Cadiz continental margin, from the middle slope to shelf (taken from Mestdagh et al., 2019), and the last 430 ka BP sea-level curve. Marine Isotopic Stages (MIS) 2 to 11 are highlighted. Colors are according to the proposed hypothesis in this work: post-channel fill deposits: blue; MIS 2-LGM: yellow; MIS 6: orange. B) Schematic model and cross section showing the proposed model for a simple valley framed in the last glacial cycle. C) Schematic model and cross section showing the proposed model for a compound valley framed during the two last glacial cycles.

The distinction between simple and compound valleys is not straightforward in some cases, and many valleys that were initially interpreted as simple were later reinterpreted as compounds, such as the cases of the Ria of Vigo, Spain (Martínez-Carreño and García-Gil, 2017), or the Mobile Bay, USA (Greene et al., 2007). Nevertheless, considering the available data, the hypotheses of a simple incised-valley model for the inner-shelf system is supported, due to: 1) small incised valley systems tend to form simple architectures and repeated incisions are not favored (Ashley and Sheridan, 1994); in such small valleys, the subaerial exposure and subsequent erosion of the shelf during the LGM would impede the preservation of previous incised features; as analog examples, many incised valleys from the Bay of Biscay, with dimensions comparable to the valleys under scrutiny, are regarded as simple features (e.g., Allen et al., 1970; Allen and Truilhe, 1988; Allen and Posamentier, 1992; Chaumillon et al., 2008); also, small Mediterranean valleys are also interpreted as simple features (Ronchi et al., 2018; De Falco et al., 2015, 2022), and; 2) the occurrence of two distinct types of seismic facies within the sedimentary infilling of those inner valleys (Figs. 4.2 to 4.7, 4.9B, and 4.9C) is more compatible with a continuous, simple infilling scenario; (c) the second incision phase is distinctively different from the first one, being less pronounced and strongly asymmetrical in many sections, which is not in agreement with its interpretation as a renewed phase of fluvial erosion.

Assuming the interpretation of a simple valley system, the subsequent infill should have a postglacial age. Considering the proximal location of the paleovalleys, and the fact that the sheet-like reflective unit has been dated between 9880 and 10248 cal yr BP in a distal position off the termination of the paleovalleys, inferring that at least the second phase of valley infilling and overlying deposits should be Holocene in age, whereas the older estuarine infilling could be pre-Holocene.

4.2.2. Interpretation of stratigraphic architectures of incised valleys

Most of the paleovalleys identified in the study area exhibit a similar stratigraphic organization, suggesting the common repetition of similar depositional and erosional systems in the different paleovalleys. As explained above, the basal surface of the paleovalleys (IP 2) is interpreted as a fluvial incision associated to a widespread erosional surface, documenting the seaward prolongation of fluvial systems such as the Gilão and Almargem rivers during periods of shelf exposure associated with sea-level lowstands.

Equivalent Late Pleistocene fluvial incisions have been documented in numerous inner shelf settings adjacent to minor fluvial networks (e.g., Green, 2009; Green et al., 2013; Ronchi et al., 2018; De Falco et al., 2022).

The lower units (ISU 2) are characterized by a lack of chaotic facies at the base of the infilling and the dominance of low-to-medium amplitude sub-parallel seismic configurations (Figs. 4.3, and 4.4). Similar seismic facies have been interpreted in numerous incised valleys of the Bay of Biscay and the Celtic Sea as estuarine mud and sand alternations mainly composing bay-fill deposits (Reynaud et al., 1999; Weber et al., 2004a;

Chaumillon et al., 2008), constituting aggradational phases during periods of sea-level rise (Lericolais et al., 2003). Accordingly, it is interpreted that the lower unit's facies in the study area may indicate low-energy environments dominated by fine-grained deposits (Fig. 4.10), pointing to the establishment of estuarine sedimentation during rising sea-level conditions (Figs. 4.3, and 4.4). In the main inner-shelf paleovalley, lower sub-parallel facies, ISU 2, are replaced upward by chaotic facies with very irregular boundaries (Figs. 4.3, and 4.4). Equivalent erosional, channelized surfaces have been interpreted in the paleo-Etel River as tidal ravinements (Estournès et al., 2012); similarly, it is interpreted the chaotic facies as tidal estuarine bars modified by tidal ravinement surfaces (Fig. 4.10). Strong tidal ravinement could also have limited or erased lowstand deposition (Féniès and Lericolais, 2005).

The asymmetric character and lower dimensions of the second phase of incision (IP 1) in many of the incised valleys (Figs. 4.3 to 4.7) is commonly related in the literature with the development of tidal inlets (Ashley and Sheridan, 1994; Dalrymple, 2006; Mattheus and Rodriguez, 2011) or as tidal-related features such as tidal channels (Tessier, 2012) or tidal scours (Graves et al., 2021). The upper unit shows chaotic seismic fabrics with some lateral migration facies (Figs. 4.3, and 4.4). The chaotic facies would indicate a change in the depositional environment, as they are typically related with higher-energy environments dominated by coarser sedimentation. Similar infillings could indicate laterally migrating tidal inlet fill deposits (Lericolais et al., 2001) which could be constituted by flood tidal delta deposition (Reynaud et al., 1999). Accordingly, it is interpreted the transition from moderate amplitude and continuity reflections to chaotic facies as the result of a change in the sedimentary environment during ensuing transgressive conditions, with deposition of estuarine-mouth massive sands, as documented in other paleovalley systems (Fig. 4.10; Weber et al., 2004a; Proust et al., 2010; Estournès et al., 2012; Green et al., 2013).

The sheet-like reflective unit may consist of different depositional systems. In the distal termination of the paleovalleys, the occurrence of mounded morphologies at the top of the unit (Fig. 4.8A) and the strong reflectivity are indicative of submerged coarse-grained paleobarriers, likely extending orthogonal to the trace of the paleovalleys (Fig. 4.10). Equivalent deposits interpreted as distal barrier-island deposits have been documented during the postglacial evolution of several incised valleys (e.g., Maselli and Trincardi, 2013; Ronchi et al., 2018; De Falco et al., 2022). Sedimentological information supports that interpretation, as the sediment core penetrates the sheet-like reflective unit. The occurrence of cemented intervals (facies Sc) in the lower part of the sediment core (intervals 1 and 2; Fig. 4.8B) would indicate subaerial sediment exposure. The next interval (interval 3; Fig. 4.8B) dominated by sandy gravels (facies G) would indicate an increase in environmental energy, possibly related with the formation of the barrier. In more proximal locations, landward-directed progradations locally observed within the reflective unit could be related to depositional systems related to the paleobarriers, such as tidal deltas (e.g., Estournès et al., 2012). Besides, locally the reflective unit exhibits a vertical stacking

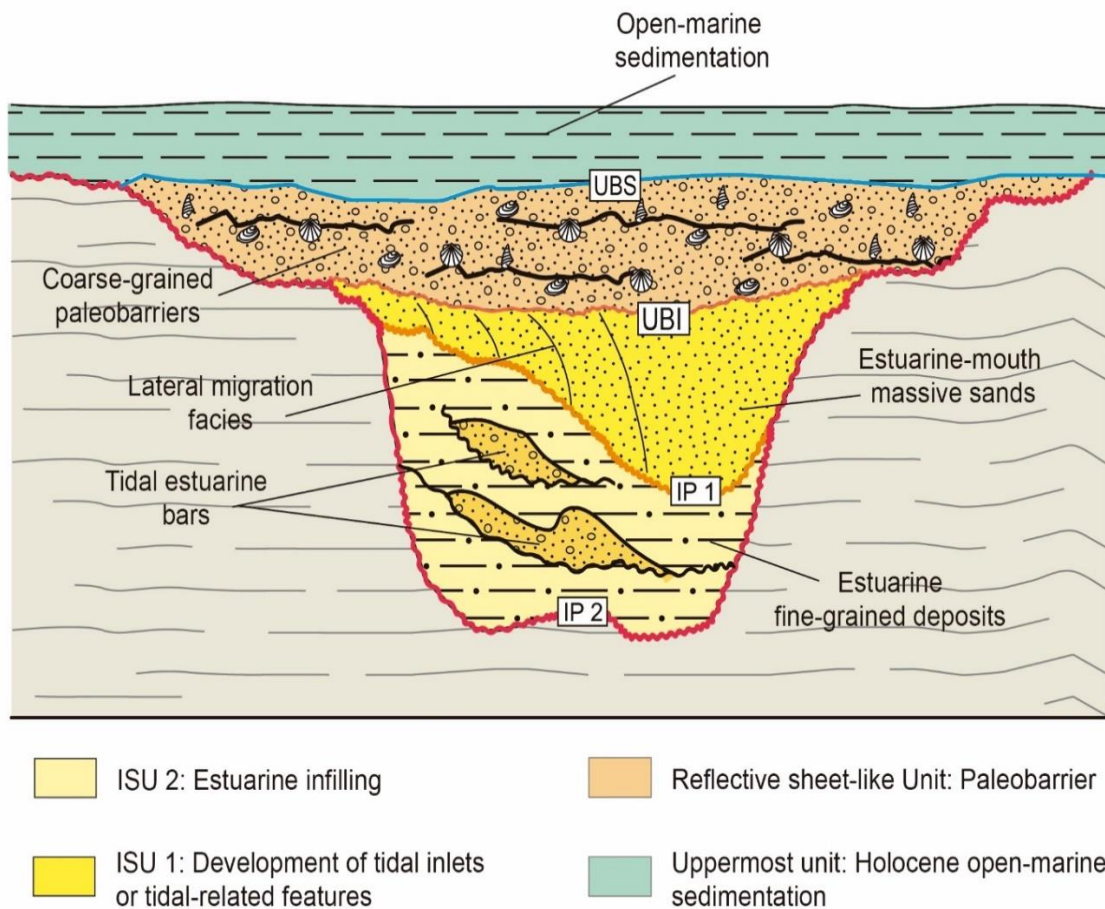


Figure 4.10: Idealized stratigraphic model for the incised valleys recognized on the inner shelf of the study area, relating the seismic surfaces and units with their geological interpretation.

of tabular deposits, suggesting the landward translation of the system and the generation of a shallower barrier. As those upper deposits are not confined to the valleys, but they extend beyond the banks, their boundaries should be interpreted as wave ravinement surfaces, as documented in some inner-shelf incised valleys in the Bay of Biscay (Chaumillon et al., 2008; Estournès et al., 2012). The uppermost transparent drape observed over the entire study area is interpreted as shelfal, open-marine sedimentation, developed during the Holocene highstand, as documented previously on the Gulf of Cadiz shelf (Fig. 4.10; Lobo et al., 2004b; Hanebuth et al., 2021).

4.2.3. Driving factors of the paleo-inner-shelf incised valley system

Assuming the above-mentioned preferred genetic scenario for the inner-shelf incised valley system (i.e., simple valley system hypothesis), its subsequent evolution was conditioned by the postglacial sea-level rise; therefore, it is interpreted that most of the infilling is transgressive in origin. In addition, driving factors such as amount and nature of sediment supply, geological heritage and changing oceanographic regimes should also be

considered, as evidenced in other incised valleys (Ashley and Sheridan, 1994; Nordfjord et al., 2005, 2006; Liu et al., 2010; Thanh et al., 2018; Qiu et al., 2019).

4.2.3.1 Postglacial sea-level changes

The role of rapid postglacial sea-level changes is difficult to evaluate in the studied starved valleys, due to the poor development of transgressive parasequences. In higher supplied incised valleys, postglacial deposits typically exhibit a backstepping pattern. This is the case of the nearby shelf off the Guadalquivir River, where several postglacial transgressive parasequences have been documented (Carrión-Torrente et al., 2022); their development has been related to periods of reduced sea-level rise between the final phase of meltwater pulse 1A and the Younger Dryas (13.8-11.2 ka), and to periods of high rates of sea-level rise triggered by meltwater pulse 1B during 11.5-8.8 ka.

In other incised valley infillings, coastal barriers have also been formed under different conditions of sea-level rise, either during rapid flooding usually in connection with meltwater pulses (Maselli and Trincardi, 2013; De Falco et al., 2022) or during temporary decelerations of the sea-level rise (Ronchi et al., 2018). In the study area, the ages obtained for the distal barrier unit (i.e., around 10 ka) place its formation during a phase of sustained high rates of sea-level rise (i.e., 130-150 cm/century at around 9.5 ka) after meltwater pulse 1B (Stanford et al., 2011). Landward of the distal barrier, the distribution of the reflective sheet-like unit extending laterally beyond the confines of the paleovalleys is compatible with a more recent generation of barriers, in fact with limited thickness. Barrier genetic environmental conditions would involve a very rapid transgressive inundation of the paleovalleys, conditioned by the fast sea-level rise after meltwater pulse 1B and the low gradients of the paleo-inner shelf. These conditions, together with scarce fluvial supplies, would account for the limited development of the barriers.

4.2.3.2 Low sediment supplies

As the relative amounts of fluvial versus estuarine facies seem to be controlled by the rate of sediment supply (Dalrymple et al., 1994b), inferring that the lack of representation of fluvial deposits in the inner paleovalleys is a result of low sediment supply related to the low dimensions of the associated fluvial catchments. The relatively low dimensions of the inner valleys also suggest that this system is scaled with the size of the drainage basin; this inference suggests the influence of upstream controls such as water discharge (Mattheus and Rodriguez, 2011; Wang et al., 2019). The dominance of postglacial transgressive deposition in most of the infilling of the inner channels is also compatible with general observations in incised valleys, which argue that lowstand deposition is not favored in small incised valleys (Wang et al., 2020).

The stratigraphic complexity and deposit thickness of the inner paleovalleys in the study area contrast with the paleo-Guadiana incised valley, as explained above; there,

coetaneous transgressive intervals appear well-developed showing a set of backstepping parasequences (Lobo et al., 2001, 2005b; Carrion-Torrente et al., 2022).

4.2.3.3 Role of antecedent geology

The absence of related tectonic features together with the minor size of the incisions suggests that the development of paleovalley incisions characterized along the inner shelf off the Gilão-Almargem Estuary was also controlled by antecedent morphology and lithology, which are considered second-order controlling factors, as they influence hydrodynamics and sediment supply in incised valleys (Chaumillon et al., 2010). Our limited data indicate that the identified valleys are narrow and display short cross-shelf extension (Fig. 4.2; 6-7 km off the present shoreline), indicating limited distal incision; in addition, the trace of the main fluvial valley, which can be considered the seaward extension of the Gilão River as it occurs exactly offshore of the present-day tidal inlet, also disappear in short distances.

Two factors involving antecedent geology and topography may explain the observed distribution of inner-shelf paleovalleys. The first one is the nature of the underlying substratum on the paleo-inner shelf, characterized by widespread highly reflective facies, which are suggestive of a coarse-grained sediment composition. This facies could likely represent indurated paleo-barriers, ancient counterparts of the barriers related with the transgressive evolution of the system. This interpretation agrees with reported evidence provided close to the study area, where the distal termination of the main paleovalley of the Guadiana River is also dictated by the occurrence of a coarse-grained inner shelf comprising lithified coastal deposits (Lobo et al., 2018). Therefore, it is invoked for the existence of a similar inner-outer shelf distinction along the study area; the paleo-inner shelf would be mainly covered by lithified, indurating deposits, precluding the development of wide fluvial valleys. Seaward of the indurated paleo-inner shelf, finer-grained sediments would be more susceptible to widespread erosion, and the traces of the valleys would be more easily removed. Such control of background geology on the postglacial development of inner incised valley system would be equivalent to the constraints reported in other inner valleys. For example, the course of the Tirso Incised Valley along the Western Sardinia shelf was limited by a barrier system formed at ~9 ka (De Falco et al., 2022).

Another significant topographic feature observed in the study area is a well-marked break of slope on the paleo-inner shelf, delimiting a distal area with higher steepness ($> 1^\circ$). The formation of the break of slope could be tentatively related to tectonic pulses reported in the northern shelf of the Gulf of Cadiz during the late Quaternary and involving tectonic uplift and enhanced margin progradation (Mestdagh et al., 2019). It has been reported that changes in shelf gradients play a role on initiation and/or enhancement of fluvial incision on the shelf (Klotsko et al., 2021). As most of the incised paleovalleys are limited to the landward, gentler paleo-inner shelf, it is proposed that the break of slope conditioned the

development of the paleovalleys, as they could have been initiated or the incision enhanced when sea level dropped below the feature.

4.2.3.4 Hydrodynamic regime

In incised valleys, the sedimentation depends on the balance between sediment availability and the potential of hydrodynamics (i.e., waves, tidal currents) to rework the sediments (Tessier, 2012). As was previously discussed, the potential fluvial inputs for this area are low, attending to the small dimension of the catchment area and the low river sizes. In this context, it is needed to point out the importance of hydrodynamic as a key mechanism for the development and preservation of this system. As described in other sediment starved margins, such as in the northern and eastern Bay of Biscay, the development of incised valleys system during transgression is driven by two successive processes of sediment reworking: 1) tidal ravinement, when the valley became an estuary, and; 2) wave ravinement, when the estuary was drowned (Chaumillon et al., 2008).

The paleogeographic configuration established in the study area during the postglacial transgression could be analogous to the present-day coastal pattern in the Ria Formosa Barrier Island System, characterized by a system of barriers interrupted by tidal inlets, and enclosing landward a system of tidal channels (e.g., Andrade, 1990; Pacheco et al., 2010) (Fig. 4.11). It is proposed that wave influence led the generation of barrier systems under an active littoral drift, similarly to the present-day where the net component of sediment transport is directed eastward (e.g., Morales, 1997; Gonzalez et al., 2001). Landward of the barrier, the observed patterns indicate enhanced tidal currents characteristic of small valleys, where the migration of the tidal inlet results in the creation of a tidal ravinement (Ashley and Sheridan, 1994). The recognition of paleotidal inlets/channels in several channels would agree with a major reoccupation of previous incised valleys by tidal channels (Fig. 4.11). Despite of low sediment inputs, the occurrence of sands within the valleys implies the activity of hydrodynamic processes such as tidal currents that have been effective transporting coarse-grained sediments and have led to a valley fill dominated by tidal related deposits (Fig. 4.11), such as estuarine tidal bars observed in the older phase of valley infilling, estuarine-mouth sand plough in the younger phase of valley infilling, and local tidal deltas/tidal mouth deposits associated to the barriers. Equivalent tidal deposits have been reported in other valley infillings (Féniès and Lericolais, 2005; Chaumillon et al., 2008). Those observations would indicate that the postglacial evolution of the inner system seems to have been influenced by both tidal- and wave-dominated processes, as at least local tidal influence extends landward of the tidal inlets (Tessier, 2012). Therefore, this system can be considered as mixed sensu Dalrymple et al., (1992) and Chaumillon et al., (2010).

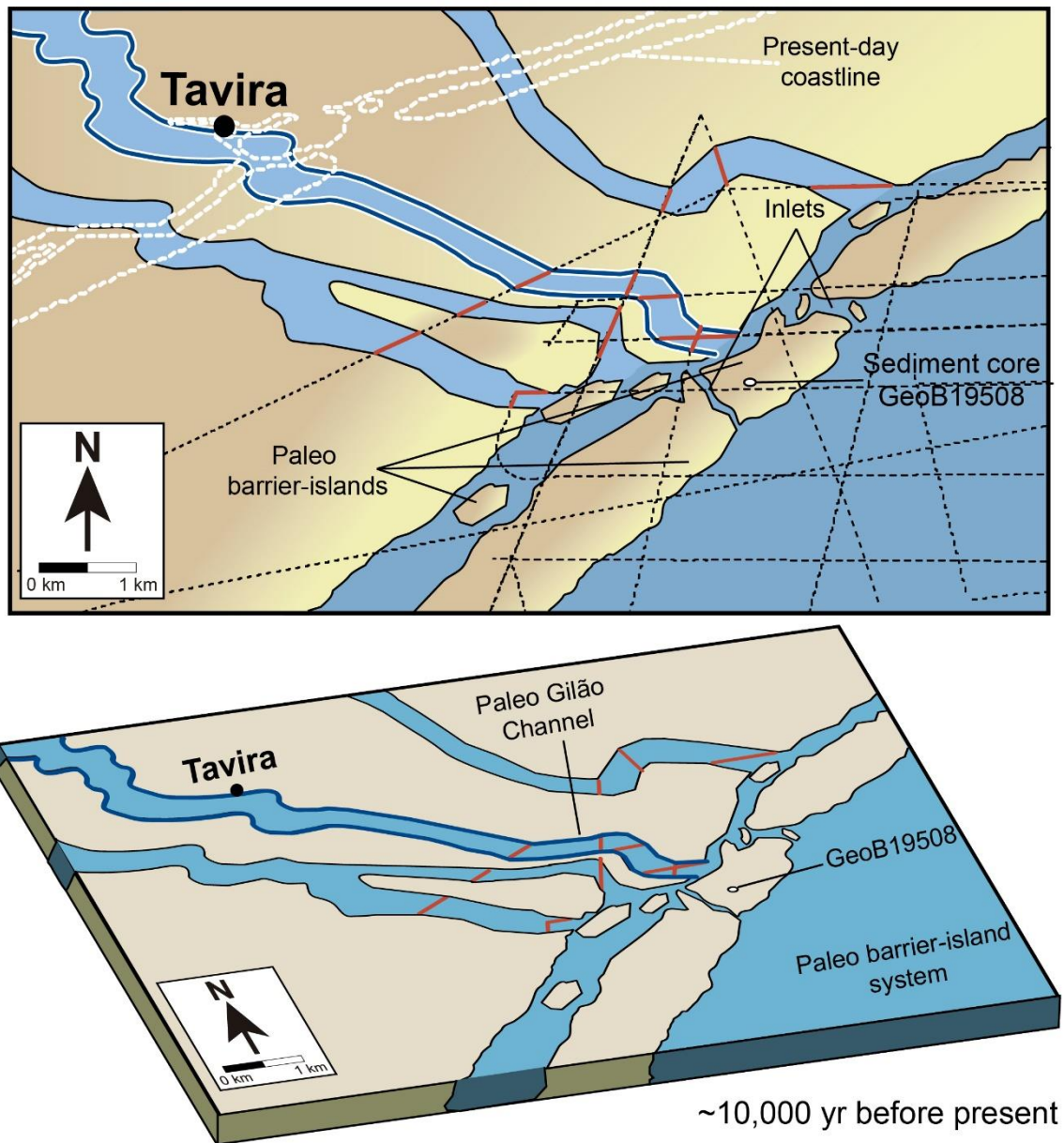


Figure 4.11: Proposed paleogeographic reconstruction of the study area at ~10 ka BP where multiple sandy islands are interrupted by numerous tidal inlets in several channels showing a coastal pattern, which is similar to that of the present-day Ria Formosa Barrier Island System. The position of seismic lines and the studied sediment core are indicated and the red lines correspond with the width of IP 1 along the different incised valleys.

CHAPTER

5

CHAPTER 5:

Incised valleys on the Guadiana Shelf

Abstract

This study investigates the architecture and late Quaternary development of the main paleovalleys on the Guadiana River Shelf, designed as Guadiana main valley and Guadiana eastern valley, employing a multidisciplinary approach that integrates a detailed seismic interpretation with sedimentary and geomorphological analyses.

The stratigraphic architecture of the studied paleovalleys reveals a compound nature with up to five repeated incision phases. The correlation of such incisions with the basinward development of shelf-margin sediment wedges is suggestive of a major glacio-eustatic origin likely linked to 100 ka sea-level cycles during the last 500 ka. The two studied paleovalleys exhibit different patterns of incision and seismic facies, indicative of distinct phases of fluvial incision and subsequent development of depositional environments.

The plan-view morphology of the paleovalleys is primarily influenced by underlying geology and the contrast between an indurated inner shelf and a more erodible middle to outer shelf, with distinct cross-sectional shapes attributed to underlying structure, lithology, and hydrodynamics.

Postglacial infilling patterns also vary between the main and eastern paleovalleys. The main valley exhibits a tripartite infilling comprising fluvio-deltaic, estuarine, and shallow-water facies, with a presumed dominance of fluvial deposition. In contrast, the eastern valley is characterized by estuarine and shoreface-shelf depositional systems mostly attributed to transgressive conditions. These differences suggest varying sediment supply conditions and hydrodynamic controls. The main valley's stratigraphic arrangement along its length correlates with the offshore transgressive stratigraphy, emphasizing the role of laterally variable fluvial supplies and antecedent morphology in influencing the distribution of valley infill facies.

Key points

- Compound nature of studied paleovalleys with up to five repeated incision phases suggests a major glacio-eustatic origin.
- Plan-view morphology influenced by underlying geology, indurated inner shelf, and contrasting inner to outer shelf dynamics.
- Tripartite infilling of the main valley includes fluvio-deltaic, estuarine, and shallow-water environments.
- The eastern valley demonstrates transgressive dominance with estuarine and shoreface-shelf depositional systems.
- Antecedent morphology plays a crucial role in the along-valley stratigraphic arrangement, influencing estuarine facies distribution.

5.1. Results

5.1.1. Incised paleovalleys on the Guadiana Shelf: Seismic Stratigraphy and major regional seismic surfaces

The seismic stratigraphic architecture of the northern margin of the Gulf of Cadiz off the Guadiana River is characterized by two key stratigraphic features: 1) major shelf erosional unconformities directly correlated with the late Quaternary stratigraphic framework proposed for the northern Gulf of Cadiz continental margin; and 2) the Guadiana Shelf incised valleys system (GSIVs) located along the inner to middle shelf, which constitutes the main objective of this work (Figs. 5.2 to 5.4).

Along the study area, five major shelf erosional unconformities could be identified that correspond with the margin-wide scale (mws) surfaces defined by Mestdagh et al. (2019) (Figs. 5.2 to 5.4), named from older to younger: mws 5; mws 4; mws 3; mws 2; and mws 1. This last surface can be identified over the entire shelf and is equivalent to the Last Subaerial Discontinuity (LSD; ~0.02 Ma; Lobo et al., 2018). Additionally, a sixth major seismic surface attributed to the Mid Pleistocene Discontinuity (MPD; 0.9 Ma; Hernández-Molina et al., 2002, 2016; Lofi et al., 2016) can be identified in some sectors along the middle-outer shelf below these five margin-wide surfaces (Figs. 5.2 to 5.4).

These surfaces are best identified in the distal margin, where they exhibit shelf-to-slope profiles with well-defined shelf breaks. Landward of the shelf breaks, these surfaces are defined by well-marked erosional truncations that tend to merge landward and westward, generating protracted hiatuses that increase in magnitude in those directions (Luján et al., 2020). For this study, the trace of these surfaces landward through the Guadiana Shelf was continued, focusing on the stratigraphic relationships between them and the GSIVs.

The densely spaced, high-resolution seismic grid (Fig. 5.1) enabled the identification of a network of cross-shelf paleovalleys between 20 and 90 m water depths. These paleovalley systems are composed of several incised features that could be identified along the available seismic sections (Figs. 5.2 to 5.4). The different Guadiana Shelf-incised valleys (GSIVs) are carved by high-amplitude erosional seismic horizons that truncate the underlying reflective shelf seismic facies and exhibit a variable stratigraphic architecture. The mapping effort has focused on the two major paleovalleys carved during the last incision phase, which could be followed along ~14 km in a N-S trend from the present coastline off the Guadiana River mouth (Fig. 5.1B). A first valley is identified in a central position on the shelf (Fig. 5.1B). This central valley can be considered the seaward extension of the Guadiana paleo-river, labeled as the Guadiana Main Valley (GMV; Fig. 5.1B). A second valley is located eastward at less than 2 km and was designed as the Guadiana Eastern Valley (GEV; Fig. 5.1B).

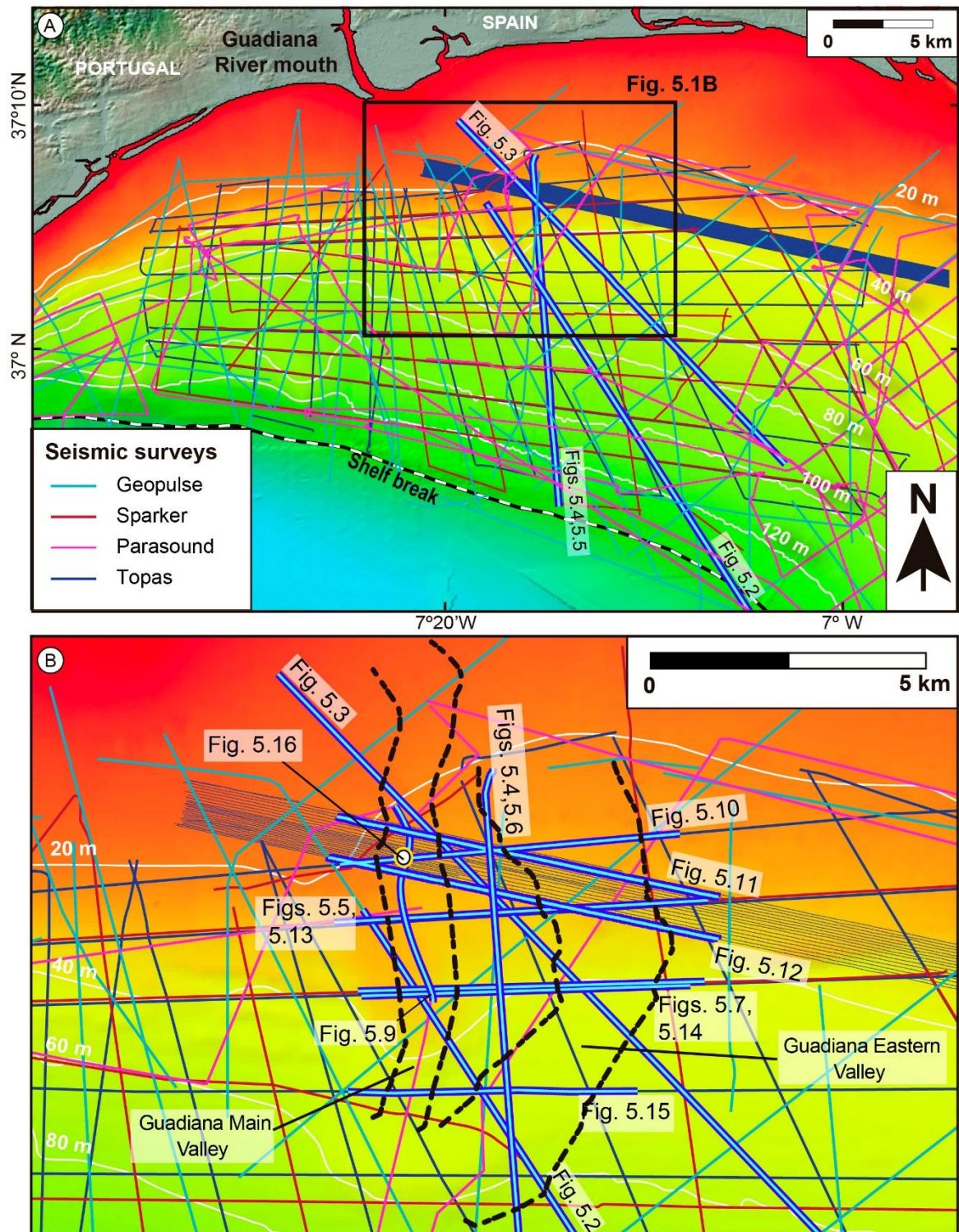


Figure 5.1: A) Bathymetric map of the study area including the location of the shelf seismic database (EMODnet Bathymetry Consortium, 2020). The location of Figure 5.1B is indicated in the inset rectangle, and the location of Figures 5.2 to 5.5 is highlighted. The shelf break and 20-meter bathymetric contours are included. B) Zoom window of the map shown in (A), highlighting the location of Figures 5.2 to 5.16.

The number of incision phases ranges from four to five, labeled from older to younger as Guadiana Shelf Incision Phases (GSIPs) 5 to 1. Their subsequent infillings could also be characterized (Figs. 5.2 to 5.6). Generally, these incision phases are superimposed and

truncate the lower ones. The older incision phases are only locally observed due to the erosional nature of such features and the frequent occurrence of multiple signals, which prevent a clear imaging of these lowermost incisions. In turn, the youngest incision phase (GSIP 1) could be identified along the Guadiana Shelf and seems to be genetically related with the most recent shelf-wide unconformity mws 1.

5.1.1.1 Incision phases in the Guadiana Main Valley

Four superimposed incision phases are identified in the GMV along the available seismic sections, labeled from older to younger as Guadiana main valley Incision Phases (GmvIPs) 4 to 1 (Figs. 5.2, 5.3, and 5.5).

The older incision phase GmvIP 4 is poorly imaged, as it could only be identified in a few seismic sections, where it excavates the present-day inner shelf at water depths of ~30 m below the present sea level (mbpsl; Fig. 5.5). It is bounded at the bottom by a moderate-amplitude seismic horizon that truncates the shelf and excavates the shelf with maximum incision depths of 50 mbsf (Figs. 5.3, and 5.5). GmvIP 4 is truncated by two younger incision phases (GmvIPs 3 and 2; Fig. 5.5). GmvIP4 shows a maximum width of ~900 m in W-E sections and is eroded westward by GmvIP 3 (Fig. 5.5). The infilling of this phase is up to 20 m thick (Fig. 5.5), and it is characterized by a very low-amplitude seismic configuration with some weak subparallel reflections.

Incision phase GmvIP 3 could be identified truncating the previous incision phase (GmvIP 4) in the present-day inner shelf at water depths of ~30 mbpsl (Figs. 5.3, and 5.5). It is bounded at the bottom by a moderate-amplitude seismic horizon that truncates the shelf and excavates the shelf with maximum incision depths that reach 50 mbsf (Figs. 5.3, and 5.5). GmvIP3 is truncated by younger incision phases GmvIP 2 and 1. This phase shows a maximum width of 550 m in W-E sections (Fig. 5.5) and displays a rather symmetric geometry characterized by V-shaped cross sections (Fig. 5.5). The infilling of this phase is up to 25 m thick (Fig. 5.5), and it is characterized by a very low-amplitude seismic configuration with some weak subparallel reflections.

Incision phase GmvIP2 is identified at shallower depths (~25 mbpsl) by a high-amplitude seismic horizon truncating the previous GmvIP3 and the underlying shelf deposits (Figs. 5.2, 5.3, and 5.5). At the top, GmvIP 2 is generally truncated by the next incision phase (GmvIP 1) and is locally cut by mws1 (Figs. 5.3, and 5.5). This phase has maximum incision depths of 35 mbsf and shows a maximum width of 700 m in W-E sections (Fig. 5.5). Channel cross sections display variable geometries that range from symmetric to asymmetric V-shaped, with a lateral shifting of the thalweg axis with respect to the previous incisions (Figs. 5.2, 5.3, and 5.5). The infilling of this phase raises up to a maximum thickness of 25 m, generally characterized by low- to medium-amplitude subparallel seismic configurations that laterally may display tangential-oblique dipping reflections with toplap and downlap terminations (Figs. 5.2, 5.3, and 5.5).

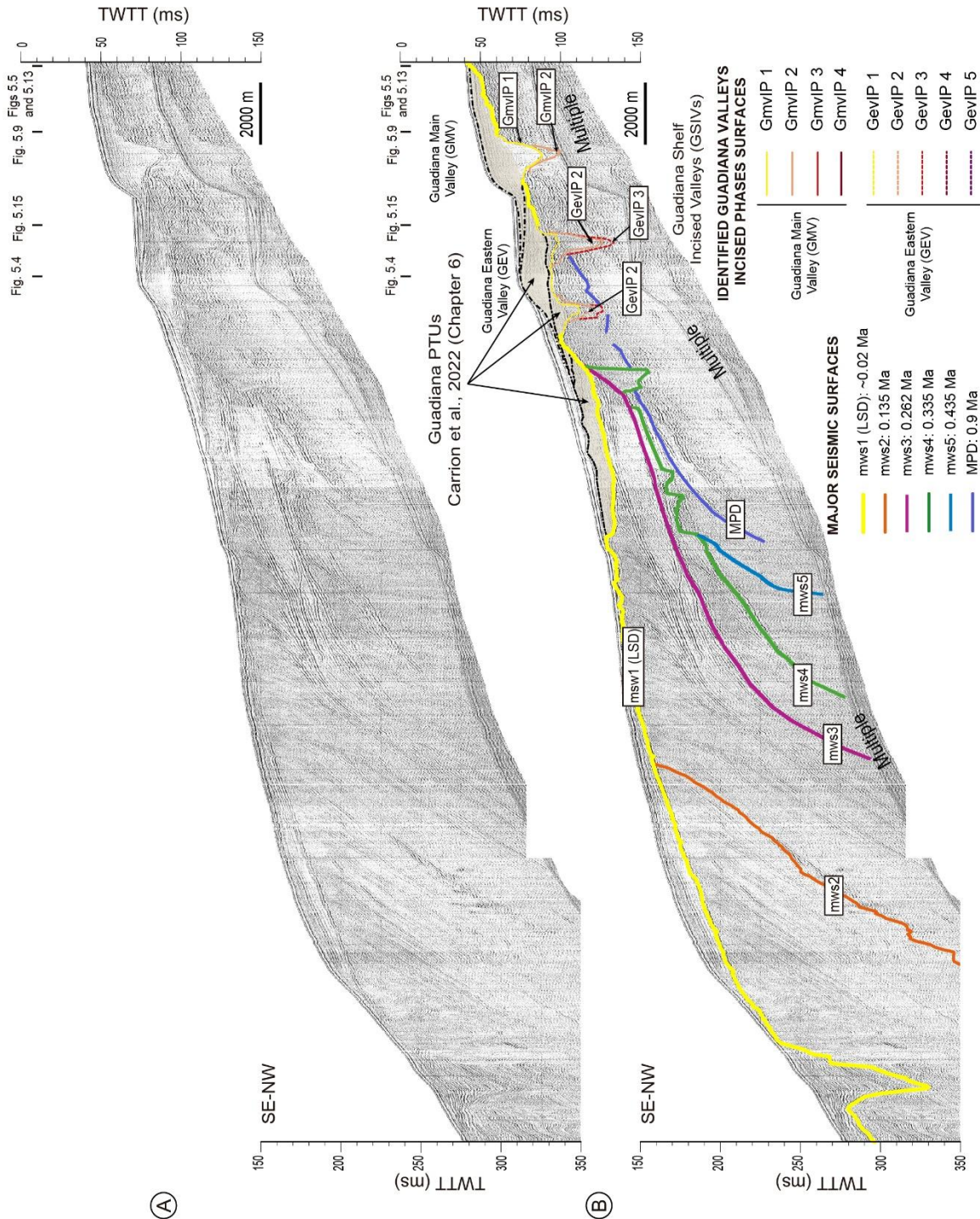


Figure 5.2: Downdip cross-shelf (SE-NW-oriented) sub-bottom seismic Uniboom source (Geopulse™) profile (A) and interpretation (B) showing the occurrence of two incised valley systems landward below the postglacial transgressive units (PTUs), studied in Chapter 6, and the margin-wide scale (mws) surfaces defined by Mestdagh et al. (2019) seaward. The color code and acronyms are indicated here, and the location of the seismic section is indicated in Figure 5.1. The crossings with Figures 5.4, 5.5, 5.9, 5.13, and 5.15 are indicated. The age of the major seismic horizons is also shown. GMV: Guadiana main valley; GEV: Guadiana eastern valley; IPs: Incised phases; mws 1 to 5: margin-wide surfaces; LSD: Last Subaerial Discontinuity; MPD: Mid-Pleistocene Disconformity.

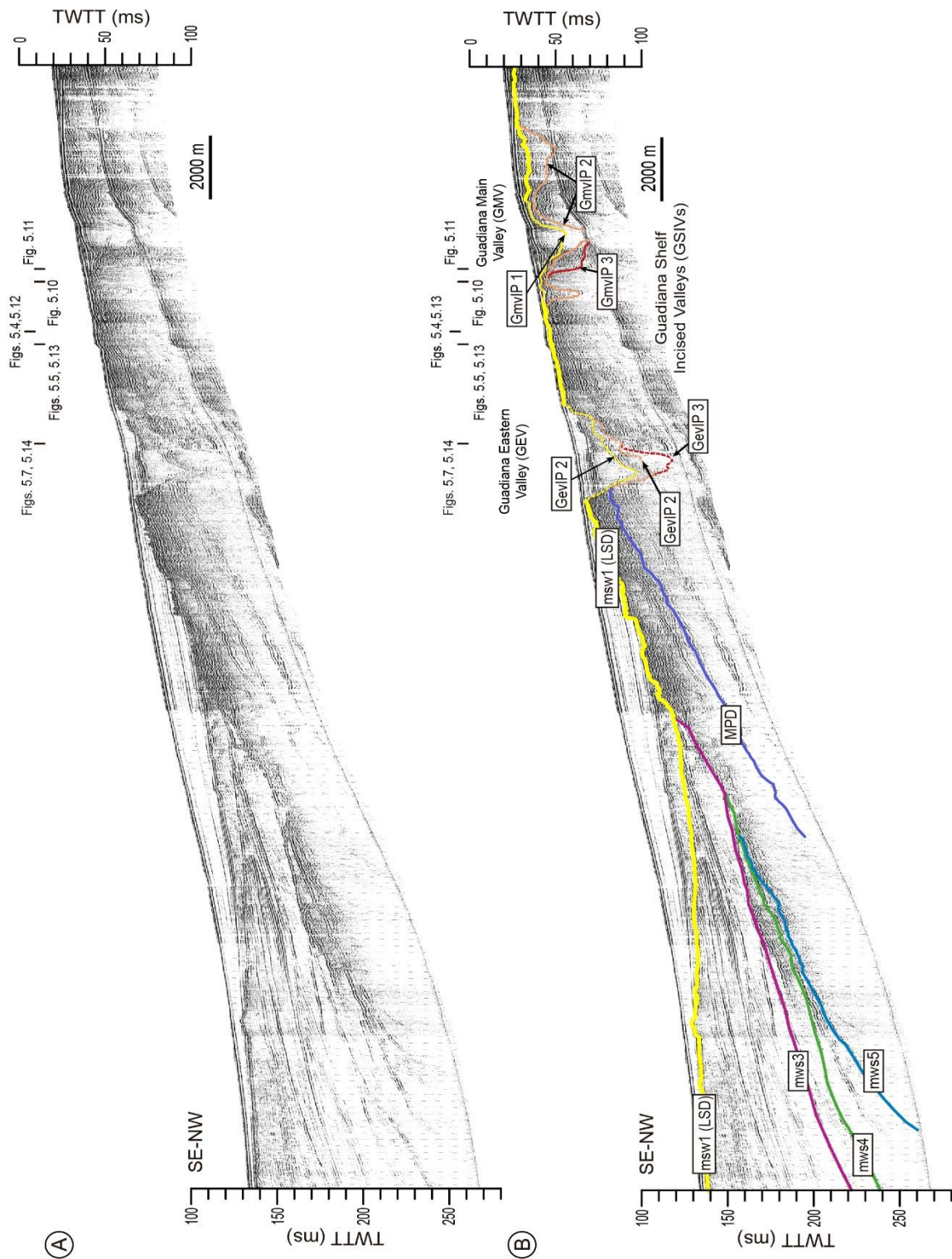


Figure 5.3: Downdip cross-shelf (SE-NW-oriented) sub-bottom seismic Uniboom source (Geopulse™) profile (A) and interpretation (B) showing the landward occurrence of two incised valley systems, formed by several incision phases, and their relationship with the major regional seismic horizons. Note how the MPD is cut by the incision phases. The color code and acronyms are indicated in Fig. 5.2, and the location of the seismic section is indicated in Figure 5.1. The crossings with Figures 5.4, 5.5, 5.7, 5.10, 5.11, 5.12, 5.13, and 5.14 are indicated here.

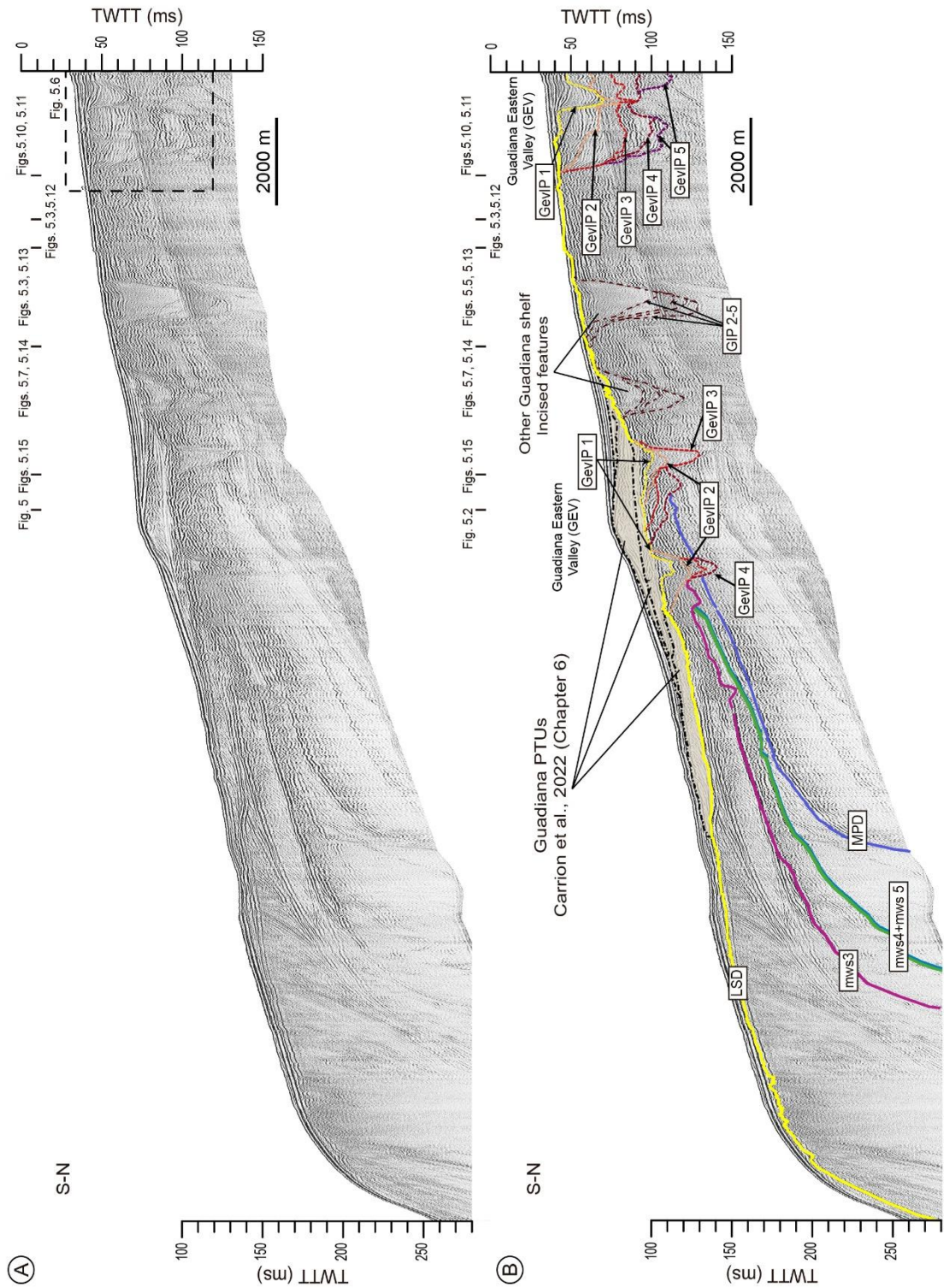


Figure 5.4: Down-dip cross-shelf (S-N-oriented) sub-bottom seismic Sparker profile (A) and interpretation (B) showing the landward occurrence of the Guadiana eastern incised valley system, formed by at least five incision phases, and its relationship with the major regional seismic horizons; other incised features not related with the two main valley systems that constitute the main scope of this chapter are also indicated. The color code and acronyms are indicated in Fig. 5.2, and the location of the seismic section is indicated in Figure 5.1. The location of Figure 5.6 (inset rectangle) and the crossings with Figures 5.2, 5.3, 5.5, 5.7, and 5.10 to 5.15 are indicated here.

The most recent incision phase (GmvIP 1) constitutes the main scope of this work, and its morphology and infilling will be presented in more detail afterwards. GmvIP1 seems to be genetically related with the most recent shelf-wide unconformity msw 1. During this phase, the GMV excavates the shelf at depths of 15 to 70 mbpsl, with maximum incision depths of 30 mbsf. It displays a well-marked asymmetrical V-shaped cross-section with one single thalweg. The infilling of GmvIP 1 shows a higher level of complexity than the previous incision phases, being composed of various seismic units characterized by a variable record of seismic facies with different amplitudes and continuities defining internal configurations ranging from sub-parallel to chaotic (Figs. 5.2, 5.3, and 5.5).

5.1.1.2 Incision phases in the Guadiana eastern valley

A maximum of five superimposed incision phases are identified in the GEV, labeled from older to younger as Guadiana eastern valley Incision Phases (GevIPs) 5 to 1 (Figs. 5.2 to 5.6).

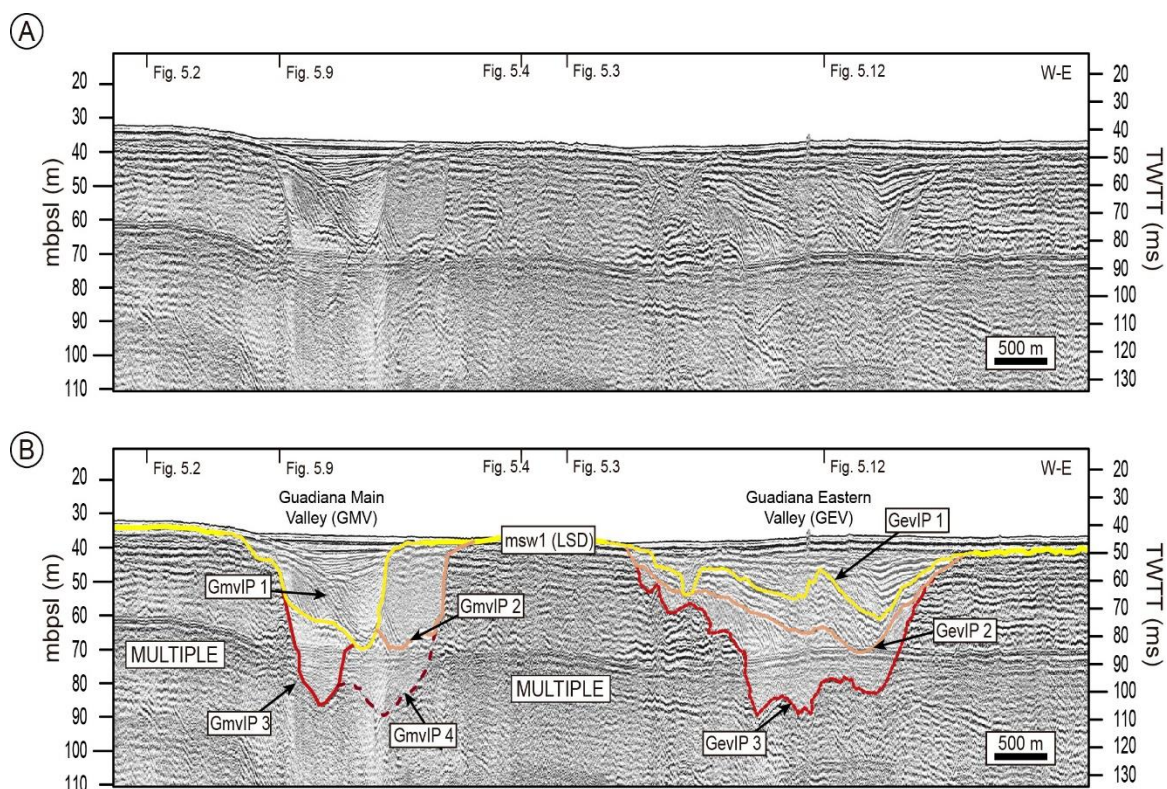


Figure 5.5: Along-shelf (W-E-oriented) sub-bottom Sparker profile showing the two main paleovalleys (A) and its interpretation (B) at around 30 m water depth. Here, four incision phases (GmvIPs 4 to 1) are identified in the GMV and at least three in the GEV (GevIPs 3 to 1). The occurrence of the multiple signal prevents a clear imaging of the lowermost incisions. The architecture of both valleys systems differs clearly. The GmvIPs are characterized by asymmetrical V-shaped geometries, whose thalwegs are laterally displaced. In contrast, the GevIPs are characterized by more symmetrical U-shaped cross sections that are vertically stacked. The color code and acronyms are indicated in Fig. 5.2, and the location of the seismic section is indicated in Figure 5.1. The crossings with Figures 5.2, 5.3, 5.4, 5.9, and 5.12 are indicated here.

The older incision phase GevIP 5 is poorly recognizable, as it could only be identified in a few seismic sections, where it is restricted to the the present-day inner shelf at 30 to 45 m below the present sea level (mbpsl; Figs. 5.4, and 5.6). GevIP 5 is bounded at the base by a moderate-amplitude seismic horizon, which truncates the underlying sub-parallel shelf seismic facies. The maximum incision reaches up to 65 meters below the seafloor (mbsf) (Figs. 5.4, and 5.6). The infilling of GevIP 5 is composed of a low- to medium-amplitude sub-parallel seismic configuration that mainly exhibits onlap terminations. A maximum width of 1,900 m could be measured. Nevertheless, the full width during this phase cannot be totally measured, as it seems to be partially eroded by the following incision phases (Fig. 5.6).

Incision phase GevIP 4 truncates the previous infilling and stacks vertically (Figs. 5.4, and 5.6). Its lower boundary is also characterized by a high-amplitude seismic horizon, which shows more continuity than the lower GevIP 5, allowing to be better identified below the shelf (Fig. 5.6). Maximum incision depths of this phase reach 50 mbsf below the middle shelf with a maximum measured width that reaches 1,750 m (Fig. 5.6). The infilling of this phase is characterized by a low- to medium-amplitude parallel seismic configuration that may exhibit intercalated chaotic facies (Fig. 5.6); locally, an upper sub-unit characterized by higher-amplitude seismic facies could be identified (Fig. 5.5).

Incision phase GevIP 3 is also bounded at the bottom by a high-amplitude seismic horizon that truncates the infilling of GevIP 4. This incision phase was broadly observed along the seismic sections (Figs. 5.2 to 5.6) and excavates the shelf with maximum incision depths that reach 50 mbsf (Figs. 5.3 to 5.6). This phase shows a maximum width of 2,900 m in some W-E sections (Fig. 5.5), and its infilling raises up to a maximum thickness of 40 m, characterized by a low-amplitude parallel seismic configuration that locally could be separated in two sub-units limited by high-amplitude reflections (Fig. 5.6). Cross-sectional morphologies of this phase display U-shaped geometries that range from symmetric to asymmetric (Figs. 5.2 to 5.6). Along coast-parallel seismic sections, GevIP3 exhibits a cross-sectional geometry with two marked thalwegs (Fig. 5.5).

The next incision phase (GevIP2) is identified excavating the present-day Guadiana Shelf at depths of 20 to 70 mbpsl. This phase truncates the previous GevIP3 (Figs. 5.2 to 5.6), and at the top, it is generally truncated by GevIP1 or by mws1 (Figs. 5.2 to 5.6). GevIP2 shows a maximum width of around 3,000 m in some W-E sections (Fig. 5.5). During this phase, channel cross-sections display symmetric to asymmetric U shapes (Figs. 5.2 to 5.6), where asymmetric shapes with laterally displaced valley thalwegs are more common (Fig. 5.5). The infilling of this phase raises up to a maximum thickness of 20 m, generally characterized by a low- to medium-amplitude parallel seismic configuration with onlap terminations (Figs. 5.5, and 5.6). This infilling can be divided into two sub-units, characterized by sub-parallel aggradational seismic facies and with increasing amplitudes in the upper sub-unit (Fig. 5.6).

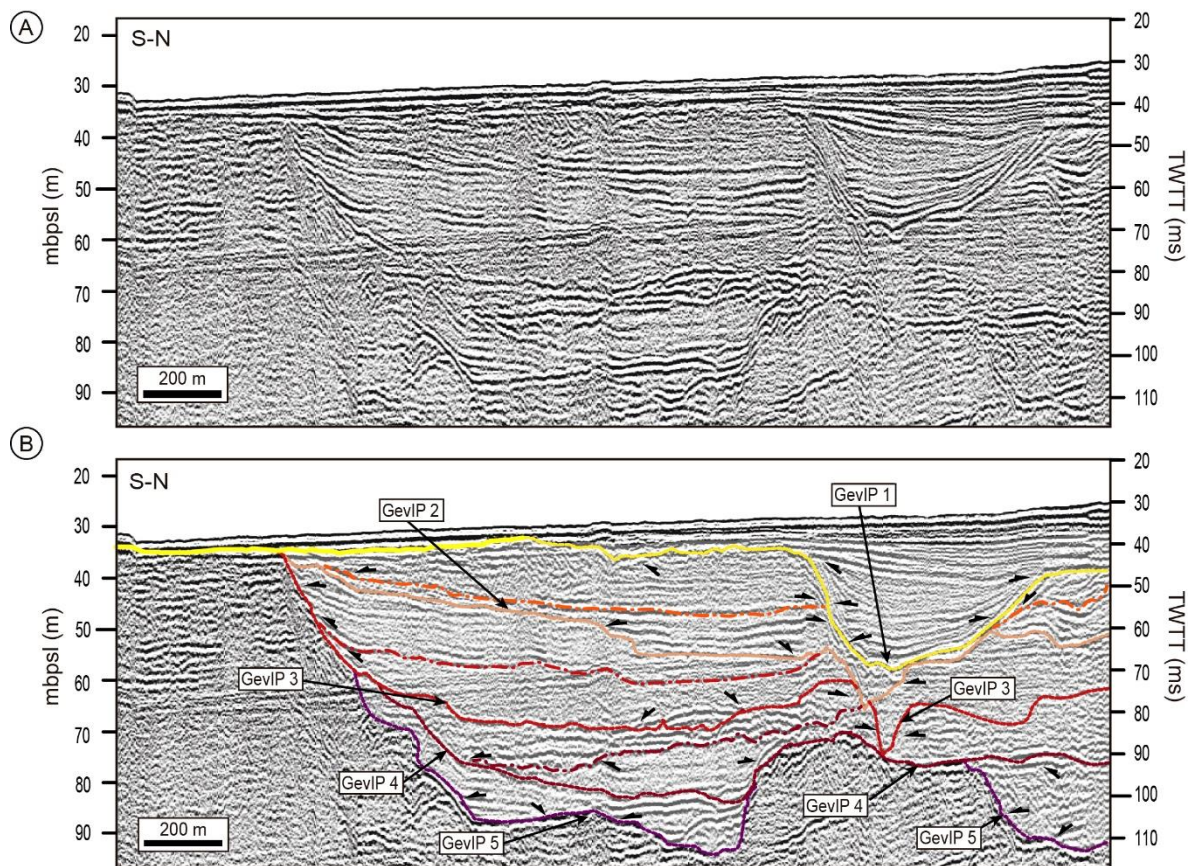


Figure 5.6: Downdip cross-shelf (S-N-oriented) sub-bottom seismic Sparker profile (A) and interpretation (B) focusing on the Guadiana eastern incised valley system, formed by at least five incision phases. The internal architecture of the different GevIPs is complex, with the occurrence of internal irregular surfaces and characterized by sub-parallel aggradational facies that may exhibit intercalated chaotic facies. The color code and acronyms are indicated in Fig. 5.2, and the location of the seismic section is indicated in Figures 5.1, and 5.4.

GevIP 1 excavates the shelf at depths of 20 to 65 mbpsl, with maximum incision depths of 30 mbsf. The width of GevIP 1 varies along the shelf, with a maximum width of around 3,000 m (Figs. 5.5, and 5.6). The cross-sectional geometries of GevIP1 show a variable spectrum, predominantly characterized by symmetric to asymmetric U-shaped sections where multiple thalwegs are occasionally observed, stacking vertically in relation to the previous incision phases (Figs. 5.5, and 5.6). The infilling also shows a higher level of complexity than the previous incision phases, being conformed of various seismic units characterized by a variable record of seismic facies with different amplitudes and continuities defining internal configurations ranging from sub-parallel to chaotic (Figs. 5.2 to 5.6).

5.1.2. Morphology of incised valleys related to the last shelf-wide unconformity (mws1)

The densely spaced, high-resolution grid of acoustic profiles (Fig. 5.1) allowed us to map the subsurface channels in great detail. Focusing on the two major paleovalleys carved during the last shelf-wide unconformity (mws1), the characterization of the morphology of

the most recent incision in both valleys was undertaken (Figs. 5.7, and 5.8). For that purpose, a detailed quantitative and qualitative analysis of the main geomorphologic parameters was carried out (Table 5.1; Fig. 5.8).

5.1.2.1 Guadiana Main Valley

The Guadiana Main Valley (Figs. 5.7, and 5.8; Table 5.1) is mapped along approximately 13 km in a N-S trend and has a sinuosity value of 1.05, an average width of 1500 m, and a maximum width of 2100 m. The valley trace commences at 35 mbpsl and ends at around 75 mbpsl. The maximum valley incision depth below the seafloor is 25 m and has an average maximum infilling thickness of 21 m. The valley excavates across the shelf, exhibiting an average gradient of 0.15°.

The GMV is characterized by an asymmetric V-shape geometry with a thalweg displaced to the western flank of the channel (Figs. 5.7, and 5.8; Table 5.1). The maximum gradients of the walls are ca. 6° for the western wall and 10° for the eastern wall (Table 5.1). However, on average, the gradients are higher in the western wall. Downslope, in the distal reaches of the valley, the thalweg occupies a more central position, and therefore the valley displays a more symmetrical cross-section (Fig. 5.8).

Values of valley width and area show relatively similar values from the proximal to the distal reaches (1400-1500 m). Only a slight decrease of the valley width is observed basinward. In addition, valley incision also decreases basinward from high values of ~25 m to minimum values of 15 m. The distal termination of the valley under the shelf is located below 50 mbpsl. The estimated width/depth ratio for this valley is 71.

5.1.2.2 Guadiana Eastern Paleovalley

The Guadiana Eastern Paleovalley (Figs. 5.7, and 5.8; Table 5.1) is mapped along 12 km in a N-S direction, where it exhibits a sinuosity of ~1.2. This valley is wider than the main valley, with an average width of ~3000 m and a maximum width of 3700 m. The identified valley trace commences at 44 mbpsl and ends at around 85 mbpsl. The maximum valley incision depth below the seafloor is 19 m and it has an average maximum infilling thickness of 14.3 m. The GEV also exhibits a higher average gradient than the GMV (~0.35°).

The GEV is characterized by a proximal near-to-symmetrical cross-section geometry that changes to asymmetrical downstream (Fig. 5.8). This change is caused because along the upper reaches of the GEV, two thalwegs could be identified, conferring a double U-shaped cross-sectional geometry (Fig. 5.8) that downslope seems to merge in a well-marked single thalweg which is displaced to the southeastern margin (Fig. 5.8; Table 5.1).

Table 5.1: Summary of the main morphometric characteristics of the two most recent incised valley incision phases characterized in the Guadiana Shelf study area.

V	Longitude (W)	Latitude (N)	L (m)	SL (m)	S	mD (mbpsl)	MD (mbpsl)	mDsf (mbsf)	MDsf (mbsf)	AvIT (m)	IM (m)	Im (m)	AvD (m)	MW (m)	AvW (m)
Main Channel	Start: 7°16'35.6"W	37°9'12.49"N	13347	12704	1.05	35	75	22	21	21.2	25	16	9.88	2115	1506
	End: 7°17'22.3"W	37°2'16"N													
Eastern channel	Start: 7°14'4.6"W	37°6'48.64"N	12300	10543	1.17	44	85	15	20	14.33	18	10	9.45	3766	2978
	End: 7°16'45.7"W	37°1'32.01"N													

V	VGr (°)	GrW (°)	GrE (°)	MGrW (°)	MGrE (°)	W/D	nThalweg	AvTs	MTs	mTs	Az (°)
Main Channel	0.15	3.63	2.75	6.04	10.2	151	1	0.35	0.45	0.22	184
Eastern channel	0.38	1.77	1.71	3.25	3.4	334	3	0.23	0.35	0.12	203
								0.77	0.74	0.8	
								0.74	0.57	0.89	

V: valleys; **L:** total length (distance between the shallowest and the deepest part of the valley measured along the valley); **SL:** straight length (shortest distance between the shallowest and the deepest part of the valley); **S:** sinuosity (relationship between the total and straight length); **mD:** minimum depth of the thalweg below the sea level (depth at which valley commences); **MD:** maximum depth of the thalweg below the sea level (depth at which valley ends); **mDsf:** minimum depth of the thalweg below the seafloor (depth at which valley commences); **MDsf:** maximum depth of the thalweg below the seafloor (depth at which valley ends); **MW:** maximum width (maximum horizontal distance perpendicular to the valley thalweg); **AvW:** average width (average value of valley width measured along the valley); **AvIT:** average maximum infilling thickness; **IM:** maximum valley incision (depth difference between the valley thalweg and the adjacent interfluves); **Im:** minimum valley incision (depth difference between the valley thalweg and the adjacent interfluves); **AvD:** average depth (measured in different cross-sections) **VGr:** average valley gradient (average angle measured between two points along the valley thalweg relative to horizontal); **GrW:** average gradient of the western valley wall (average angle measured between the shallowest and deepest points along the western valley wall relative to horizontal); **GrE:** average gradient of the eastern valley wall (average angle measured between the shallowest and deepest points along the eastern valley wall relative to horizontal); **MGrW:** maximum gradient of the western valley wall; **MGrE:** maximum gradient of the eastern valley wall; **Az:** azimuth (orientation relative to north between the starting and ending points); **nThalweg:** maximum number of thalweg per channel; **AvTs:** Average thalweg symmetry coefficient (0: totally asymmetrically to the west side; 0.5 : totally symmetrical; 1: totally asymmetrical to the east); **MTs:** maximum thalweg symmetry coefficient; **mTs:** minimum thalweg symmetry coefficient.

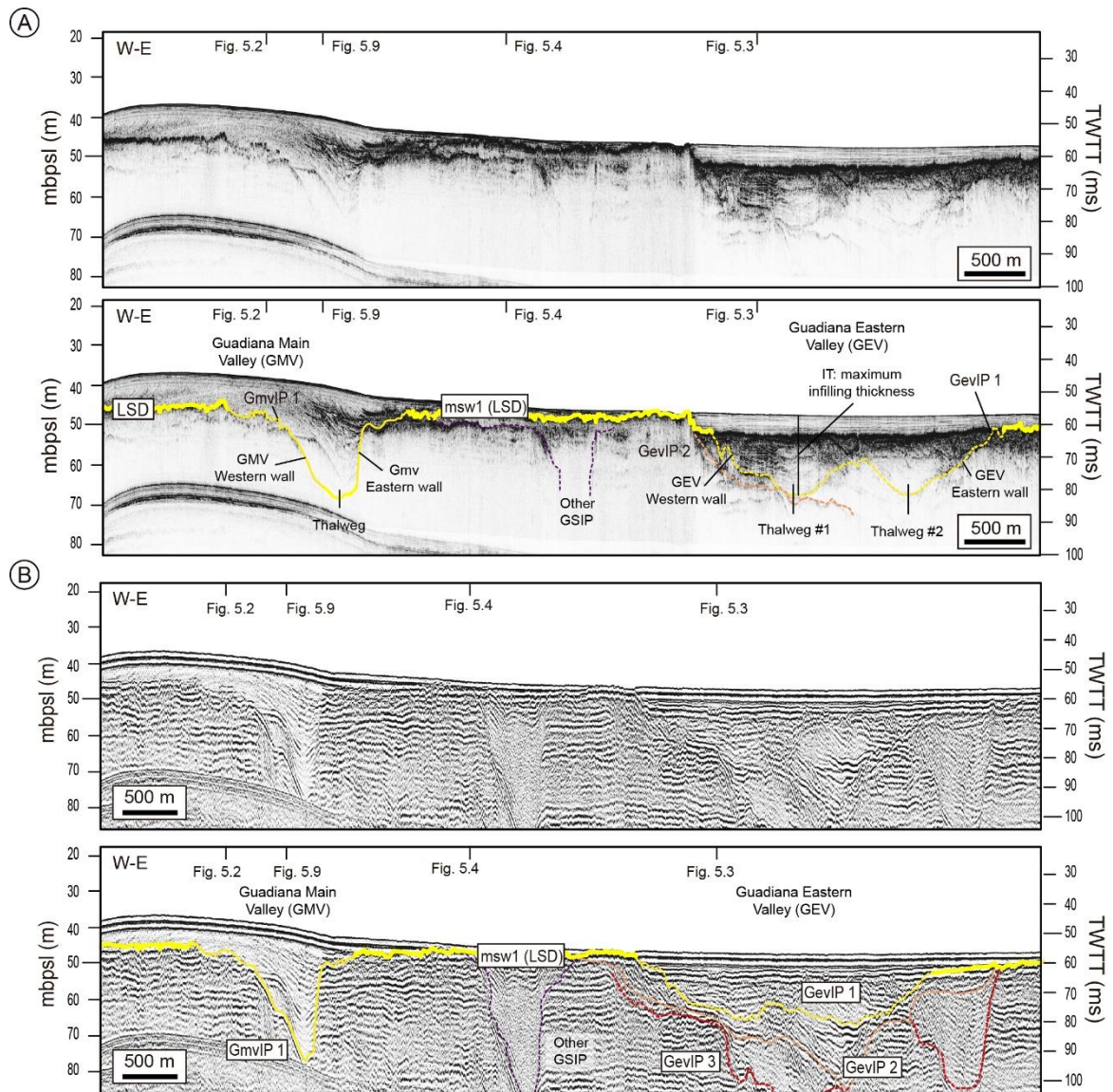


Figure 5.7: A) Along-shelf (W-E-oriented) sub-bottom acoustic profile (TOPAS) showing the two main paleovalleys (up) and its interpretation (below). B: The same along-shelf (W-E-oriented) profile shown in (A) but collected with a Sparker seismic source. Some of the geomorphologic features and measured parameters are indicated. Note the contrast in resolution between TOPAS and Sparker seismic profiles. The color code and acronyms are indicated in Fig. 5.2, and the location of the seismic section is indicated in Figure 5.1. The crossings with Figures 5.2, 5.3, 5.4, and 5.9 are indicated.

The maximum and average wall gradients do not exhibit significant differences between the western and eastern walls, with maximum values of 3.25° and 3.4° , respectively (Table 5.1). Values of valley width and area show homogeneous values from the proximal to the distal reaches (~ 2800 m). Valley incision depths increase basinward from values of ~ 10 - 15 m in proximal areas to maximum values of 20 m in distal areas.

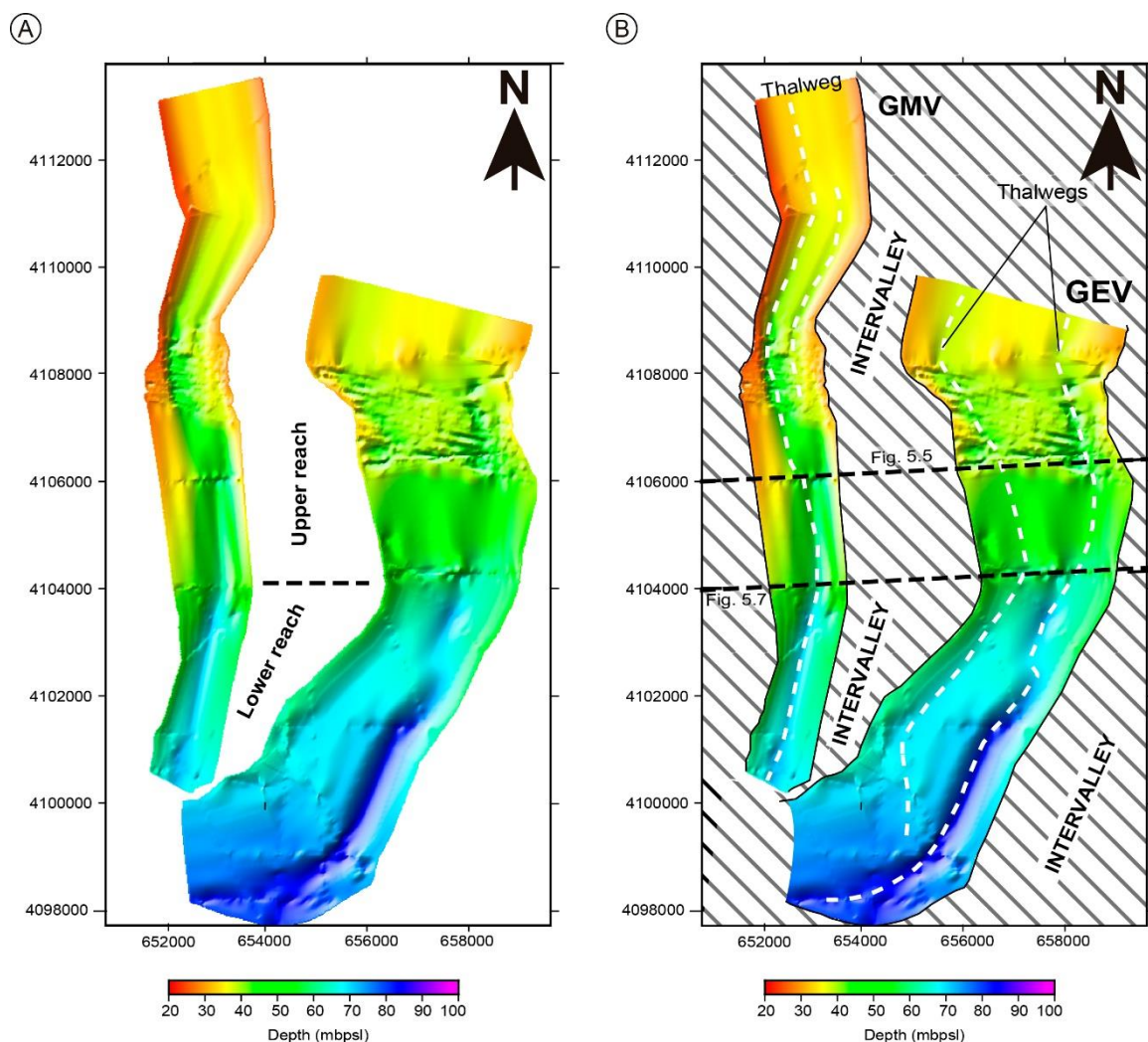


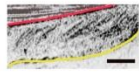
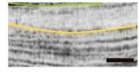





Figure 5.8: Interpolation model of fluvial channel morphology of the most recent incision phase of both studied valleys, providing a complete visualization of the morphology of the fluvial systems (A) and the interpretation of some geomorphologic features (B). The crossings with Figures 5.5, and 5.7 are indicated. The interpreted channel horizon data are shown in Figure 3.9 (Chapter 3).

5.1.3. The sedimentary infilling of the last incision phase

5.1.3.1 Seismic stratigraphy of the infilling

The sedimentary infilling of both valleys (GMV and GEV) could be mapped and characterized using the available database. The nature and geometry of the sedimentary infilling postdating the last incision phase exhibit remarkable differences between both valleys (Figs. 5.9 to 5.15). The proximal infilling in both valleys is composed of seismic units characterized by a variable record of seismic facies with lateral variations (Figs. 5.9 to 5.13). A classification of these major units based on their shape, stacking patterns, distribution, and internal architecture is presented below and summarized in Table 5.2.

Table 5.2: Summary table including the seismic facies, configuration, boundaries, geometry, interpretation, and acronyms for each seismic unit characterized in the studied incised valleys off the Guadiana River mouth.

Valley	Seismic sub-unit	Seismic image	Seismic configuration	Seismic Boundaries	Geometry	Interpretation
GMV	GmvU3		Amplitude: Medium to low Configuration: Semitransparent with lateral tangential-oblique reflections	Top: GmvL Termination: Toplap-Truncation Bottom: GmvIP1 Termination: Concordance / Downlap	Wedge/Channel-like infilling	Fluvial infilling with lateral accretion bars // Bayhead deltas
	GmvU2-2		Amplitude: Medium to low Configuration: Sub-parallel	Top: GmvT2 Termination: Toplap- Concordance Bottom: GmvL Termination: Onlap / Downlap / Concordance	Channel-like infilling	Estuarine central basin infilling
	GmvU2-1		Amplitude: Medium to low Configuration: Massive, non-stratified	Top: GmvT2 Termination: Toplap- Concordance Bottom: GmvL Termination: Onlap / Downlap / Concordance	Wedge	Shallow-marine sandy deltas
	GmvU1		Amplitude: High to medium Configuration: Sub-parallel	Top: GH Termination: Concordance Bottom: GmvT, Gev0, Gev1, GmvIP1 Termination: Concordance / Downlap	Sheet-like	Recent marine sedimentation
GEV	GevU3		Amplitude: Low to very low Configuration: Semitransparent with some weak sub-parallel reflections	Top: Gev2 Termination: Toplap-Erosion Bottom: GevIP 1 Termination: Onlap / Downlap / Concordance	Channel-like infilling	Low-energy estuarine infilling
	GevU2		Amplitude: Medium to low Configuration: Massive/ Chaotic	Top: Gev 1 Termination: Toplap-Erosion Bottom: Gev2 Termination: Concordance / Downlap	Mounds/Channel-like infilling	Estuarine-mouth massive sands // Channel infilling
	GevU1		Amplitude: Low Configuration: Chaotic to semitransparent with high amplitude reflections	Top: Gev0 Termination: Concordance/Toplap Bottom: Gev1 Termination: Downlap	Wedge/mound shaped	Paleobarrier

1) Guadiana Main Paleovalley (GMV) seismic stratigraphy.

Along the infilling of the GMV, three major seismic units could be distinguished, called from base to top as Guadiana Main Valley Units (GmvUs) 3 to 1 (Figs. 5.9 to 5.15; Table 5.2).

GmvU3. This seismic unit comprises the lower deposits identified along the GMV. It is bounded at the base by the highly reflective irregular seismic surface GmvIP 1, and at its top is truncated by a moderate-amplitude horizon labeled as GmvL. This unit is mostly characterized by a semi-transparent seismic configuration along the central area and by tangential-oblique internal reflections dipping laterally along the flanks of the unit (Figs. 5.9 to 5.13; Table 5.2). Along the GVM, this unit has a maximum thickness of 15 m in proximal valley areas (Fig. 5.9); the unit thickness decreases basinward, where it is few meters thick; distally, this unit thickens again reaching thickness values of 10 m for 9 km (Fig 5.9). In cross-section, GmvU3 exhibits a channel-like geometry where the thickness changes from maximum values of 20 m along the flanks in some sections (e.g., Fig. 5.11), to minimum values of few meters along the central part in other sections (e.g., Fig. 5.12). The seaward continuation of this unit is not imaged properly by the acoustic profiles (Fig. 5.9). Nevertheless, a lower body located below the proximal postglacial transgressive units (PTUs) and characterized by a semi-transparent acoustic response is interpreted as the distal part of this unit (Figs. 5.14, and 5.15).

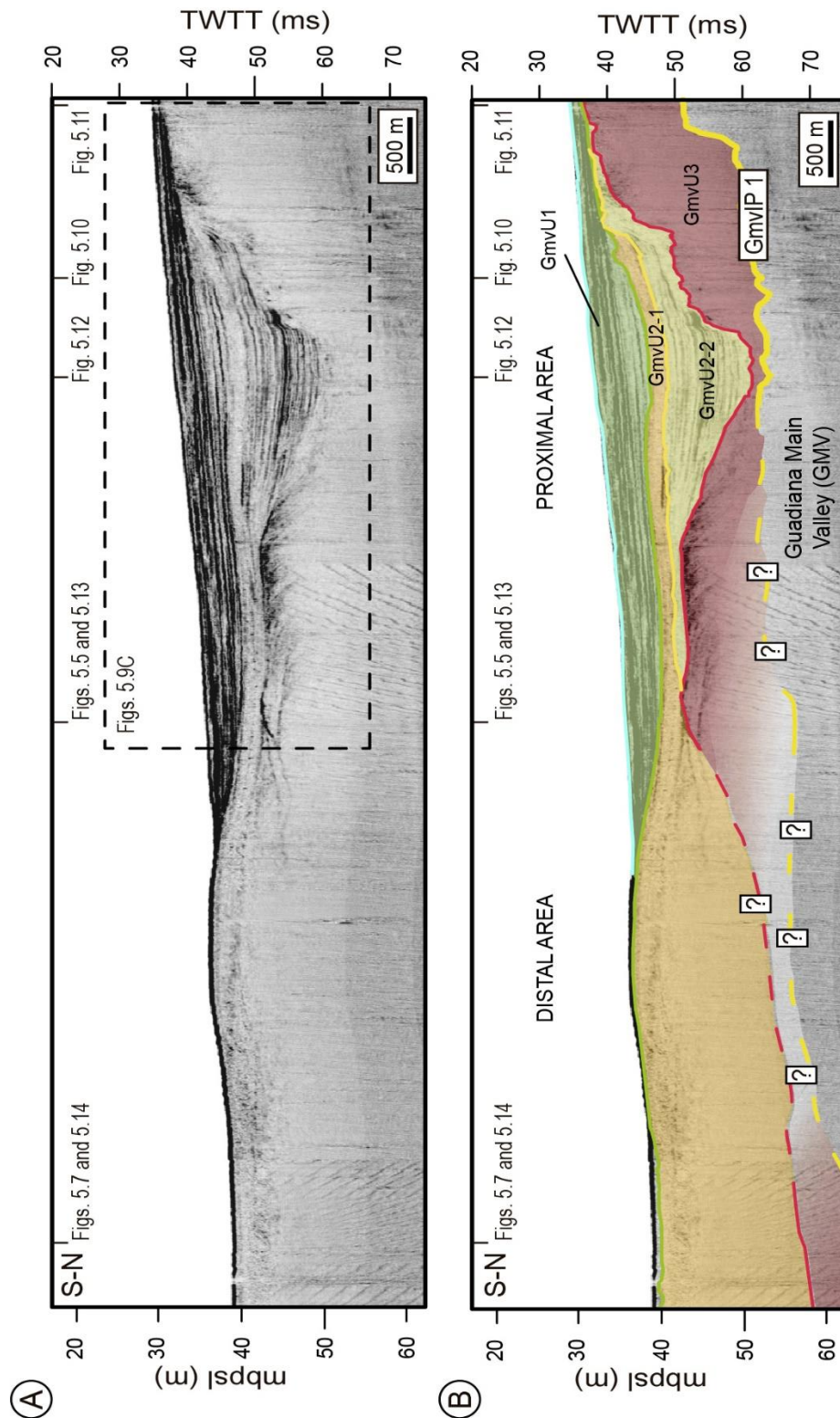


Figure 5.9: Downdip sub-bottom Parasound profile (A) and interpretation (B) oriented N-S along the Guadiana main valley showing the internal architecture along the GMV. C) Interpreted zoomed seismic window along the proximal area of the GMV (location indicated in Figure 5.9A). Here, the three major seismic units that compose the sedimentary infilling of the GMV could be identified. The units exhibit significant thickness variation along the valley. Note how the seismic sub-unit GmvU2-2 and the seismic unit GmvU1 are only characterized along the proximal valley segment.

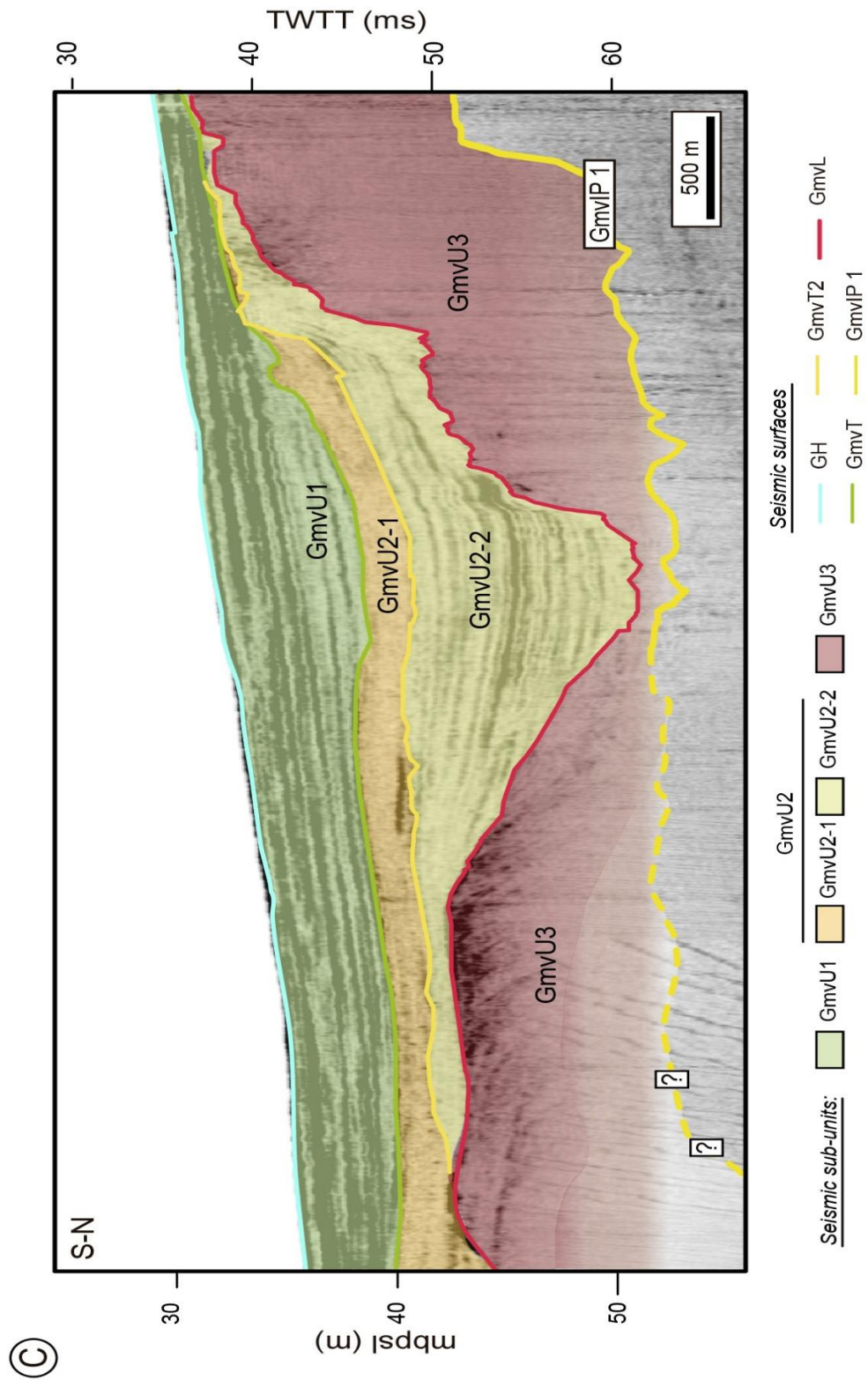


Figure 5.9: (Cont): Seismic sub-unit GmvU2-1 is not only restricted to the proximal areas; it extends basinward, where it builds up the uppermost part of a wedge-shaped deposit. The geometry of the lower unit GmvU3 could not be identified basinward due to poor seismic penetration. The color code and acronyms are indicated here, and the location of the seismic section is indicated in Figure 5.1. The crossings with Figures 5.5, 5.7, and 5.10 to 5.14 are also indicated.

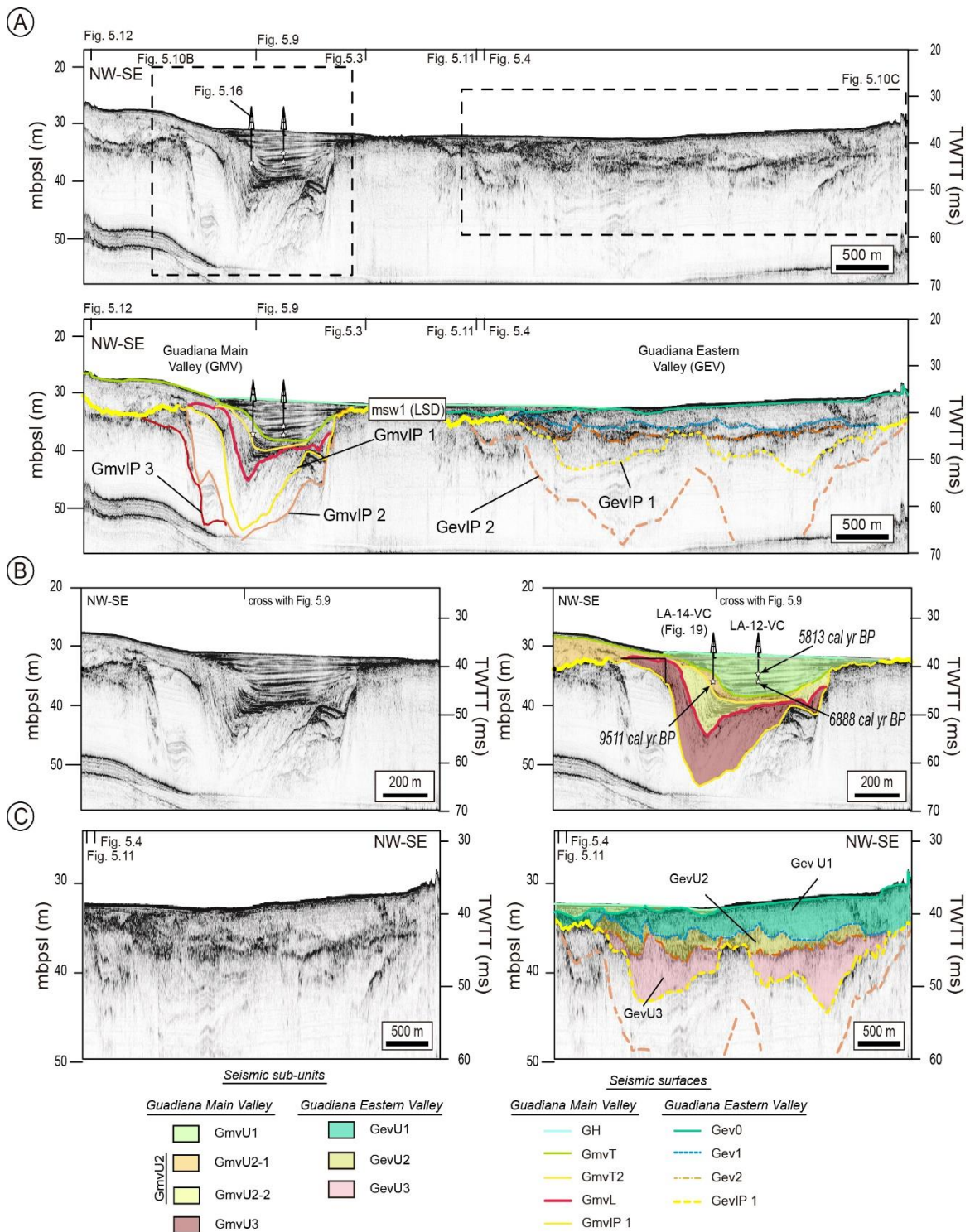


Figure 5.10: A) Along-shelf (NW-SE-oriented) sub-bottom acoustic profile showing the internal architecture of the infilling of the two studied paleovalleys (up) and its interpretation at around 30 m water depth. B and C) Zoomed seismic windows focusing on the architecture of the two different paleovalleys (left) and its interpretation (right). Their location is indicated in Figure 5.10A. Note the significant differences between the seismic facies of both valleys. Sediment cores LA-14-VC (Fig. 5.16) and LA-12-VC are indicated, and the available age datings are also shown. The color code and acronyms are indicated here, and the location of the seismic section is indicated in Figure 5.1. The crossings with Figures 5.3, 5.4, 5.9, 5.11, and 5.12 are also indicated.

GmvU2. The middle seismic unit (GmvU2) of the GMV infilling is bounded at the base by GmvL that marks the boundary with GmvU3, and at the top by a moderately reflective horizon labeled as GmvT, which at places coincides with the present-day seafloor (Figs. 5.9 to 5.15). Internally, GmvU2 could be separated into two sub-units labeled as GmvU2-2 and

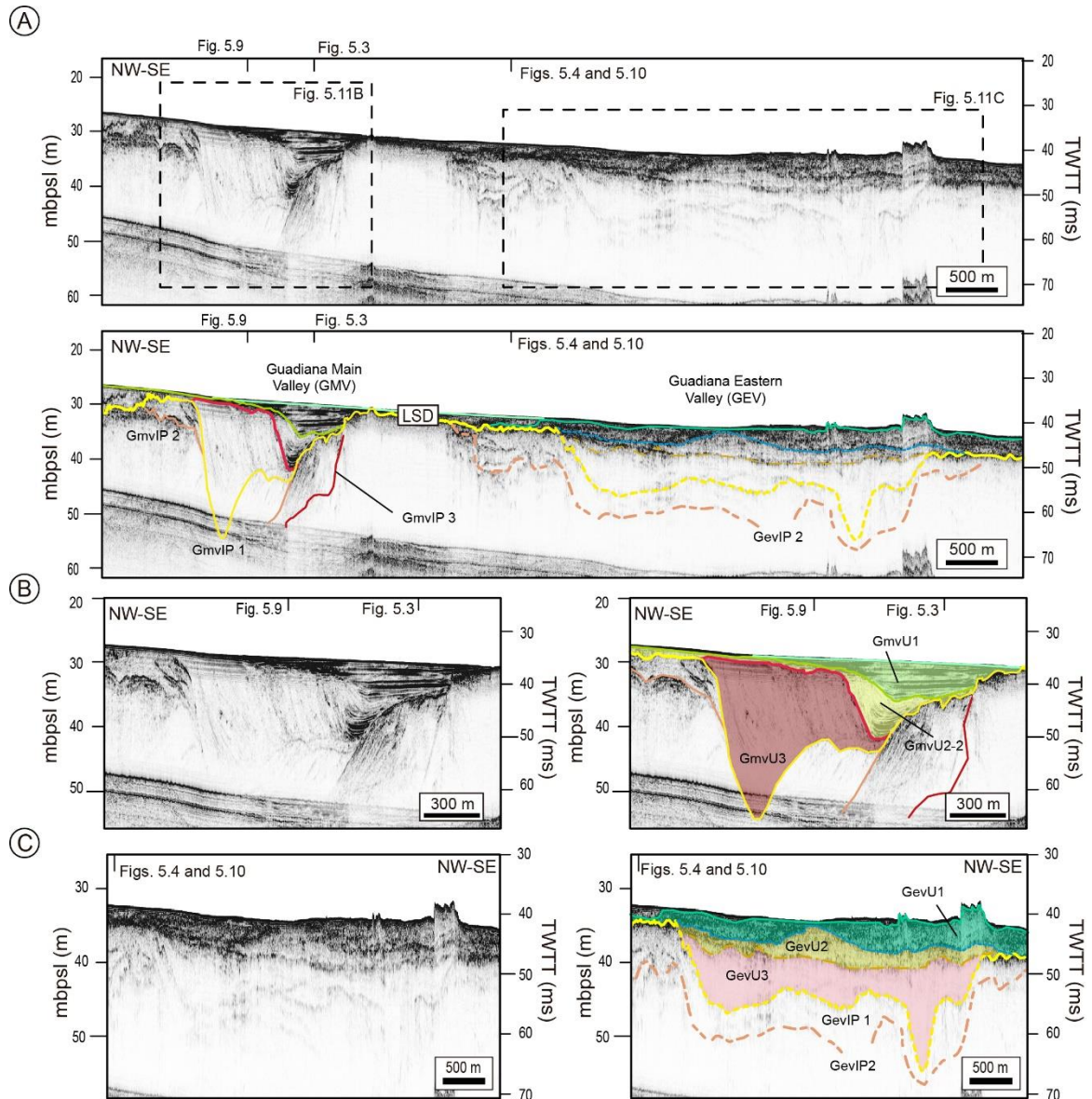


Figure 5.11: A) Along-shelf (NW-SE-oriented) sub-bottom acoustic profile showing the internal architecture of the infilling of the two studied paleovalleys (up) and its interpretation at around 30 to 35 m water depths. B and C) Zoomed seismic windows focusing on the architecture of the two different paleovalleys (left) and its interpretation (right). Their location is indicated in Figure 5.11A. Here, important characteristics are: well-defined tangential-oblique internal reflections dipping laterally in unit GmvU3; the absence of sub-unit GmvU2-1; the mounded patterns in GevU2 that protrude above the pre-existing relief; and the asymmetrical cross sections of both valleys. The color code and acronyms are indicated in Figures 5.9, and 5.10, and the location of the seismic section is indicated in Figure 5.1. The crossings with Figures 5.3, 5.4, 5.9, and 5.10 are also indicated.

GmvU2-1, based on their different seismic facies. The lower sub-unit GmvU2-2 is bounded at the top by a moderate-amplitude seismic horizon (GmvT2) (Figs. 5.9 to 12). This sub-unit is characterized by a well-defined sub-parallel seismic configuration that laterally evolves to massive (Figs. 5.9 to 5.15; Table 5.2). GmvU2-2 is restricted to the landward and

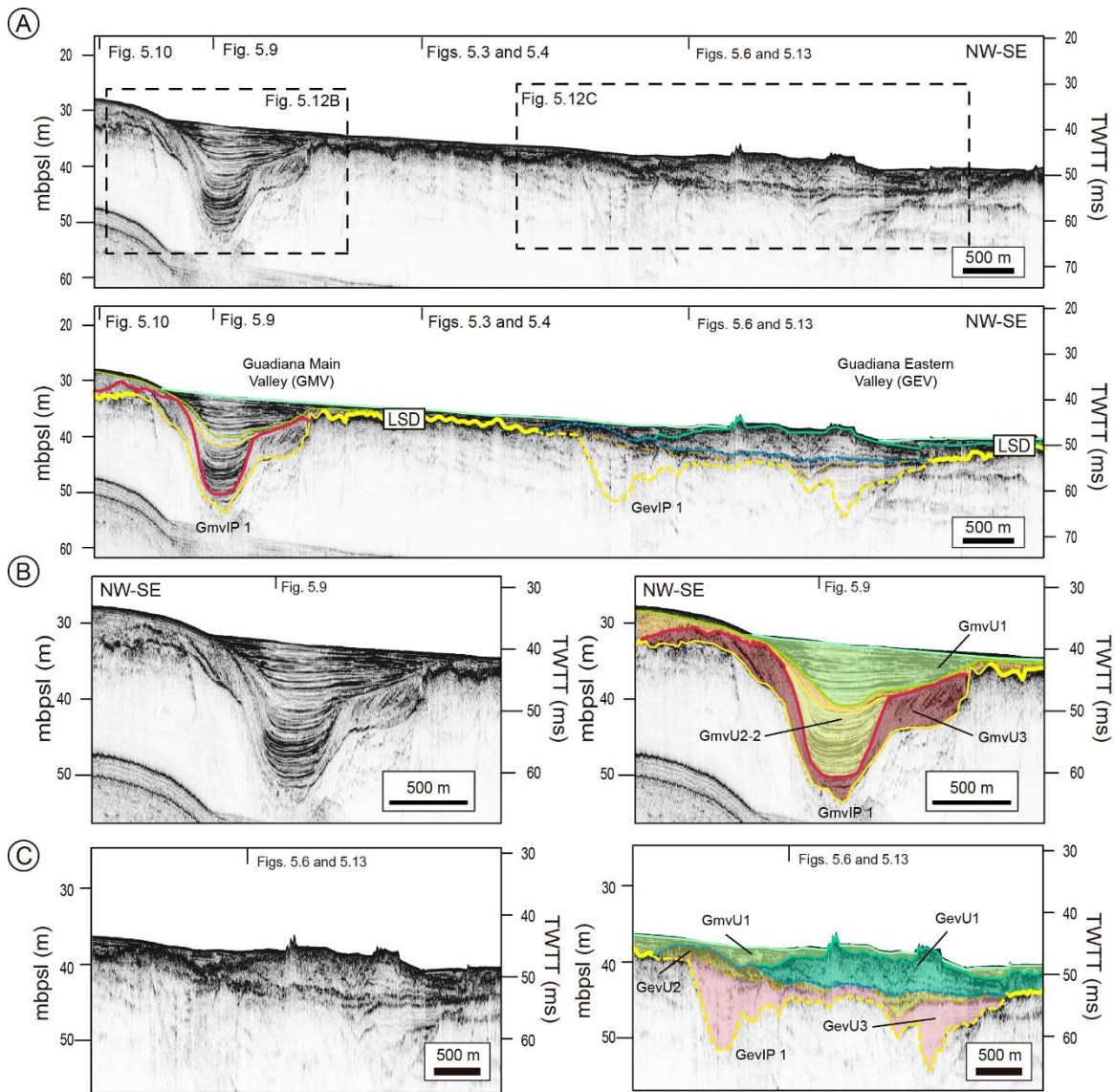


Figure 5.12: A) Along-shelf (NW-SE-oriented) sub-bottom acoustic profile showing the internal architecture of the infilling of the two studied paleovalleys (up) and its interpretation at around 33 to 40 m water depths. B and C) Zoomed seismic windows focusing on the architecture of the two different paleovalleys (left) and its interpretation (right). Their location is indicated in Figure 5.12A. Here, important characteristics are: sub-unit GmvU2-2 is characterized by a well-defined sub-parallel seismic configuration in the central areas of the GMV; sub-unit GmvU2-1 extends out of the valley westward; GmvU1 onlaps GevU1; the symmetrical V-shape cross section of GMV; and the two U-shaped geometries observed in the GEV. The color code and acronyms are indicated in Figures 5.9, and 5.10, and the location of the seismic section is indicated in Figure 5.1. The crossings with Figures 5.3, 5.4, 5.6, 5.9, 5.10, and 5.13 are also indicated.

central areas of the GMV (Fig. 5.9). In proximal areas (25-30 mbpsl), the unit is very thin (i.e., few meters thick), but it thickens basinward, where it might reach 12 m along the paleovalley central area, showing a wedge-shaped geometry. The upper sub-unit GmvU2-1 covers GmvU3 and GmvU2-2 (Fig. 5.10). In contrast to the lower sub-unit GmvU2-2, GmvU2-1 is not restricted to the proximal areas of the GMV, as it extends basinward. GmvU2-1 exhibits non-stratified seismic facies that extend seaward (Figs. 5.9 to 5.15; Table 5.2), where they construct the uppermost part of wedge-shaped deposits constituting the proximal PTUs (Figs. 5.14, and 5.15).

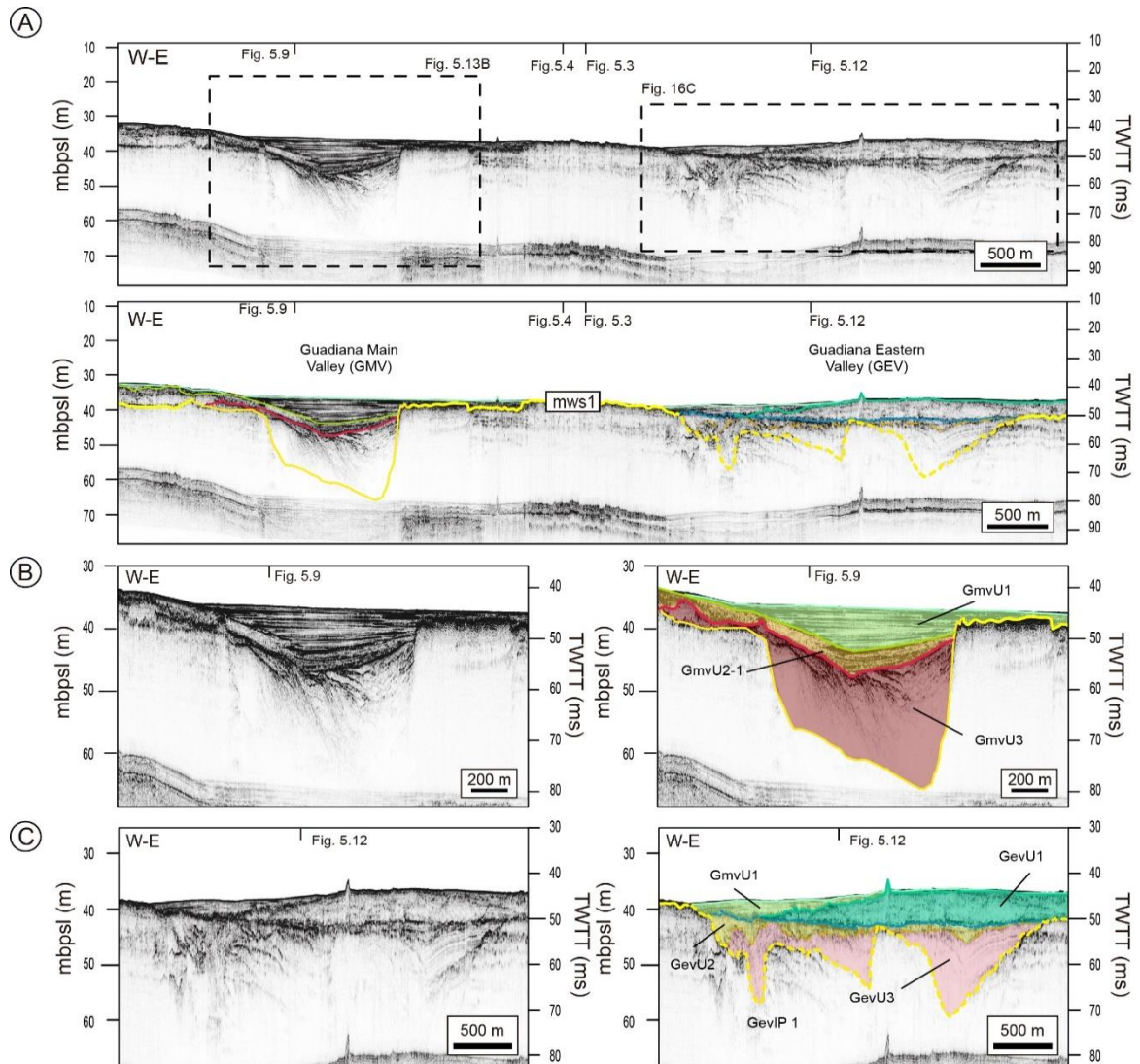


Figure 5.13: A) Along-shelf (W-E-oriented) sub-bottom acoustic profile showing the internal architecture of the infilling of the two studied paleovalleys (up) and its interpretation at around 40 m water depth. This acoustic section coincides with the Sparker seismic section shown in Figure 5.5. B and C) Zoomed seismic windows focusing on the architecture of the two different paleovalleys (left) and its interpretation (right). Their location is indicated in Figure 5.13A. Here, important characteristics are: the near-to-transparent seismic facies of the lower units (GmvU3 and GevU3); the restricted geometry of GevU2, infilling some channel-like depressions above GevU3; the well-developed mound geometry of GevU1; the asymmetrical V-shape cross section of the GMV, with the thalweg displaced eastward; and various thalwegs observed in the GEV. The color code and acronyms are indicated in Figures 5.9, and 5.10, and the location of the seismic section is indicated in Figure 5.1. The crossings with Figures 5.3, 5.4, 5.9, and 5.12 are also indicated.

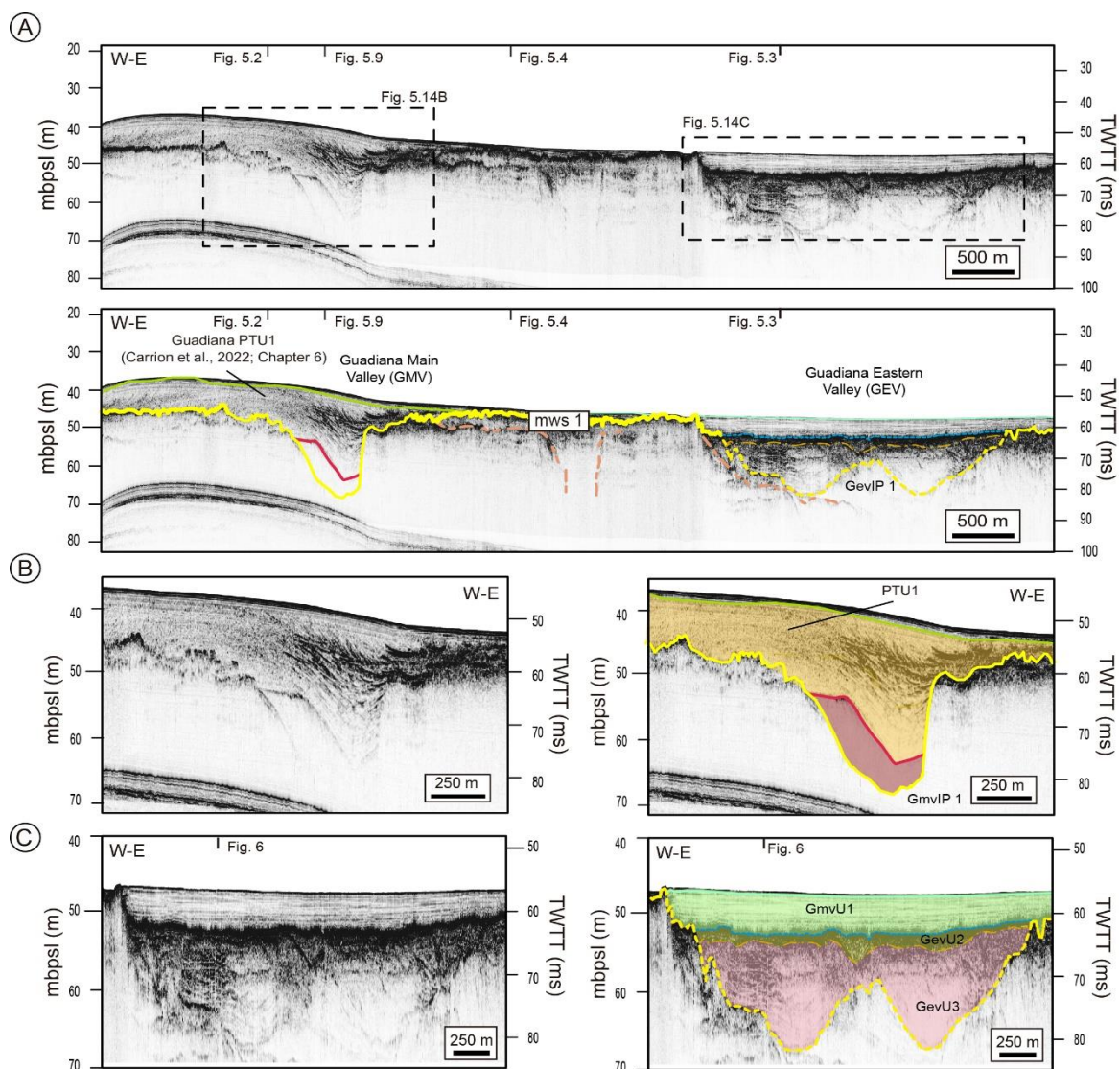


Figure 5.14: A) Along-shelf (W-E-oriented) sub-bottom acoustic profile showing the internal architecture of the infilling of the two studied paleovalleys (up) and its interpretation at around 50 m water depth. This seismic section coincides with Figure 5.7. B and C) Zoomed seismic windows focusing on the architecture of the two different paleovalleys (left) and its interpretation (right). Their location is indicated in Figure 5.14A. Here, important characteristics are: GmvU1 covering totally the GEV; GmvU2-1 exhibits non-stratified seismic facies that construct the uppermost part of wedge-shaped deposits related with the Guadiana PTU1 (Chapter 6); and semi-transparent seismic facies in GmvU3. The color code and acronyms are indicated in Figures 5.9, and 5.10, and the location of the seismic section is indicated in Figure 5.1. The crossings with Figures 5.2, 5.3, 5.4, and 5.9 are also indicated.

GmvU1. The uppermost unit is characterized by a high-amplitude, high-continuity sub-parallel seismic configuration (Figs. 5.9 to 5.13; Table 5.2). GmvU1 covers a subtle depression of the valley formed by the underlying units and also extends laterally through the intervalley areas (Figs. 5.10 to 5.13). This unit is bounded at the base by GmvT and at the top by the GH surface that coincides with the seafloor. The thickness of GmvU1

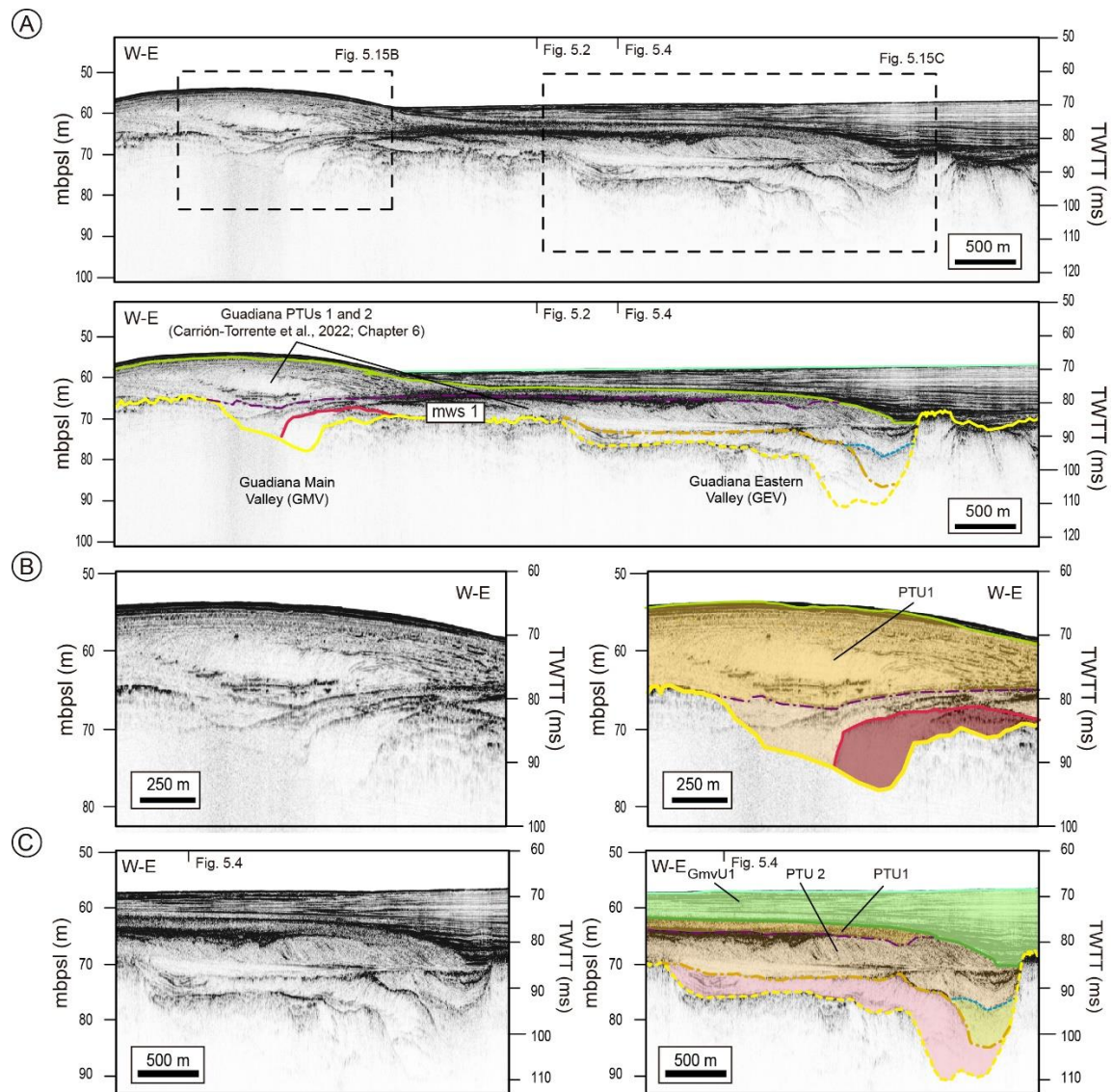


Figure 5.15: A) Along-shelf (W-E-oriented) sub-bottom acoustic profile showing the internal architecture of the infilling of the two studied paleovalleys (up) and its interpretation at around 60 m water depth. B and C) Zoomed seismic windows focusing on the architecture of the two different paleovalleys (left) and its interpretation (right). Their location is indicated in Figure 5.15A. Here, important characteristics are: the wedge-shaped deposits composing the proximal Guadiana PTUs 1 and 2 (Chapter 6), which offlap the underlying GEV; semi-transparent seismic facies of GmvU3; the close location of both valleys (~1 km); and the lower position of GEV respect to GMV. The color code and acronyms are indicated in Figures 5.9, and 5.10, and the location of the seismic section is indicated in Figure 5.1. The crossings with Figures 5.2, 5.3, 5.4, and 5.9 are also indicated.

describes a wedge-shaped geometry, with maximum thicknesses in the central part, where it reaches 6-7 m, and decreases landward (Fig. 5.9). Seaward, this unit downlaps with the upper boundary of the previous GmvU2 (Fig. 5.9).

2) Guadiana Eastern Paleovalley (GEV) seismic stratigraphy.

Three major seismic units characterize the infilling of the GEV, called from base to top as Guadiana eastern valley Units (GevUs) 3 to 1 (Figs. 5.10 to 5.15; Table 5.2).

GevU3. This unit comprises the lower deposits identified along the GEV. It is bounded at the base by the highly reflective irregular seismic horizon GevIP 1, and at its top is truncated by a moderately reflective horizon labeled as Gev2. It is generally characterized by a low- to very low-amplitude, moderate continuity, sub-parallel seismic configuration that is locally semi-transparent (Figs. 5.10 to 5.15; Table 5.2). The unit exhibits a channel geometry where the thickness does not show significant variations along the valley. Thickness displays a maximum average value of 10 m along both valley thalwegs (Figs. 5.10 to 5.13). A maximum thickness of 15 m is found in the eastern valley thalweg (Figs. 5.11, and 5.13). Seaward, this unit is offlapped by PTUs 1 and 2 (Carrión-Torrente et al., 2022), as these postglacial deposits extend laterally emanating from the main valley (Fig. 5.15).

GevU2. The second unit identified upward in the stratigraphic column is characterized at the base by an irregular high-amplitude seismic horizon (Gev2) that truncates the previous unit, and at the top by a flat to mound-shaped high-amplitude seismic horizon labeled as Gev1. This unit is mainly characterized by chaotic, reflective seismic facies, or locally by non-stratified, massive seismic facies (Figs. 5.10 to 5.15; Table 5.2). GevU2 partially infills the upper GEV section but also generates some mounded patterns that protrude above the pre-existing relief with a thickness that ranges from a maximum average value of ~5 m landward to less than 1 m basinward (Figs. 5.10 to 5.14). Seaward, GevU2 is offlapped by GmvU1 (Figs. 5.12, and 5.13) and by PTUs 1 and 2 (Carrión-Torrente et al., 2022; Chapter 6), which extend laterally from the GMV (Fig. 5.15).

GevU1. This unit is bounded at the base by a high-amplitude, irregular surface that separates GevU1 from the two previous units that comprise the GEV infilling (Gev1) and at the top by a high-amplitude surface labeled as Gev0 (Figs. 5.10 to 5.13). GevU1 shows a chaotic, highly reflective seismic configuration that shows some internal reflections (Figs. 5.10 to 5.13; Table 5.2). It has a mound-like geometry with a maximum thickness of around 5 m and laterally extends beyond the valley through the eastern intervalley area (Figs. 5.10 to 5.13). Moreover, this unit exhibits a limited along-valley seaward extension and cannot be identified in the distal seismic sections at ~15 km from the present coastline (Figs. 5.14, and 5.15).

5.1.3.2. Sedimentary facies and core descriptions

In order to study the sedimentary facies and to provide some chronostratigraphic constraints for the paleovalley infilling, we selected one sediment core collected in the Guadiana main valley (Fig. 5.16) considering its correlation with the seismic data. Sediment core LA-14-VC (Figs. 5.10, and 5.16) penetrates through GmvU1 and the upper part of unit GmvU2. Two AMS 14C dates were obtained at the base of sediment core LA-12-VC (Fig. 5.10), providing ages that place the formation of GmvU1 between 5563 and 7165 cal yr BP (Table 5.2.3; Fig. 5.10). The sedimentological analysis of

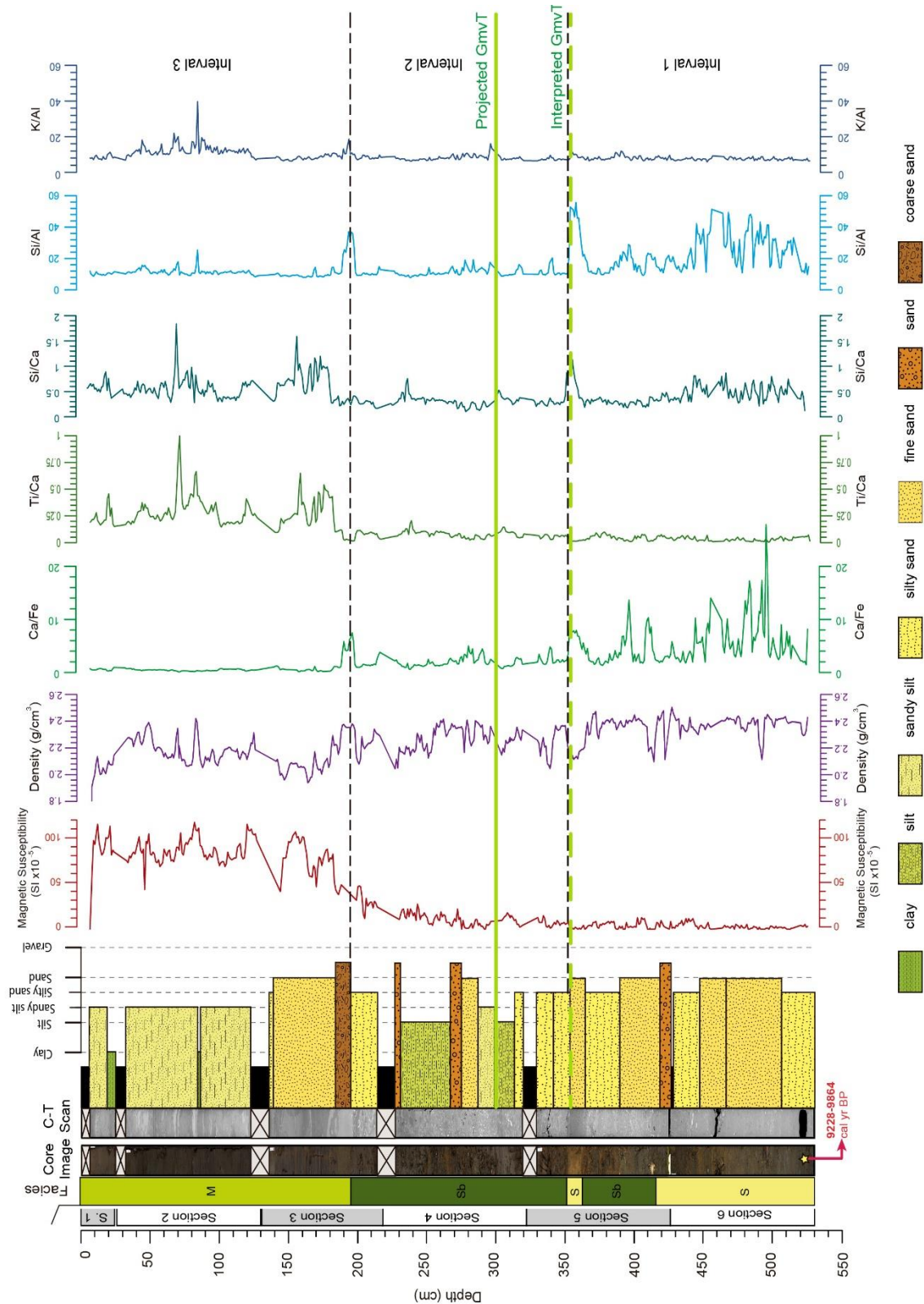


Figure 5.16: Photography, CT-scans, facies distribution, lithological description, control age points, grain size, physical properties (density and magnetic susceptibility logs), and XRF geochemical ratios of sediment core LA-14-VC, characterizing seismic units GmvU1 and GmvU2-1. The position of the sediment core is indicated in Figure 5.1 and its projection is indicated in Fig 5.10.

the sediment core (Fig. 5.16) allows us to distinguish three sedimentary facies types:

Facies S: Massive fine sands. This facies is composed of well-sorted fine-grained sands and silty sands with some granule- to pebble-sized bioclasts, mainly bivalves and gastropods. The facies is generally homogenous and massive (Fig. 5.16).

Facies Sb: Bioclastic sands. This facies is composed of highly fragmented granule- to pebble-sized bivalve shells and rounded rock grains, which are hosted in a mixture of fine to coarse sands and silts. This facies is poorly sorted and structureless (Fig. 5.16).

Facies M: Muds. This facies consists of silts and clays that exhibit some laminations and can include scarce, well-preserved shells and embedded silt nodules (Fig. 5.16).

From bottom to top, based on sedimentological, geophysical, and geochemical properties, three intervals can be distinguished in sediment core LA-14-VC (Fig. 5.16):

The lower interval (531-352 cm below the seafloor) is mainly characterized by sands (facies S) along the first 102 cm (531-428 cm) that are covered by 66 cm of fine and silty bioclastic sands (facies Sb). The upper part of this lower interval (362-352 cm) is dominated by well sorted sands (facies S; Fig. 5.16). This lower interval is geochemically characterized by high Ca/Fe values that decrease upward and by well-marked peaks in Si/Ca, Si/Al, and Ca/Fe ratios at the top, in coincidence with a decrease in the density log (Fig. 5.16).

The middle interval (352-195 cm below the seafloor) is dominated by facies Sb (Fig. 5.16). Geochemical and geophysical data along this interval do not exhibit any significant trend (Fig. 5.16).

The upper interval (195-0 cm below the seafloor) is characterized by a 10 cm homogenous sand layer (facies S) that is covered by a fining-upward laminated muddy sand interval with some intercalated clay and silt layers (facies M; 185-0 cm; Fig. 5.16). Geochemical data indicates a Si/Al peak at the base of this interval followed by upward increases in Ti/Ca and Si/Ca ratios (Fig. 5.16). In this interval, an increase of the magnetic susceptibility is observed with mean values of 100 SI x10e-5 (Fig. 5.16).

5.2 Discussion

5.2.1. Long-term development of incised valleys: Routes for shelf-margin growth

In many shallow-water settings, there is compelling evidence of the repeated reoccurrence of incised valleys, in which each incision phase is laterally associated to shelf-wide subaerial exposure and fluvial erosion surfaces (Labaune et al., 2010). Those major incision phases are related with periods of forced regressions leading into maximum shelf exposures; the prevailing hypothesis relates the episodes of shelf exposure to late Quaternary glacial lowstands, in response to base level drops of the order of 100 m (e.g., Foyle and Oertel, 1997; Burger et al., 2001; Brothers et al., 2020; Horozal et al., 2021). Those sea-level changes have been primarily guided by 100 ka relative sea-level cycles (Labaune et al., 2010; Tesson et al., 2011). However, in some settings, the influence of higher-

frequency sea-level cycles has been proposed to lead to repeated phases of channel incision (e.g., Xu et al., 2022; Liu et al., 2023).

Accordingly, we propose that the stratigraphic architecture of the two major studied incised valleys and their lateral relationships with well-defined shelf erosional unconformities likely reflect a major glacio-eustatic origin (Fig. 5.17). First, the studied incised valleys can be regarded as compound valley features, which contain a variable record of repeated incision and reoccupation (up to five) that can be connected to a cyclic process. In addition, stratigraphic evidence strongly suggests that these compound valleys are younger than the Middle Pleistocene Discontinuity (MPD); this major discontinuity was interpreted in the across-margin sedimentary record of the Gulf of Cadiz with an estimated age of 0.7-0.9 Ma (Hernández-Molina et al., 2002, 2016). Specifically, the tracing of the MPD towards the inner shelf reveals that the complex valley systems off the Guadiana River post-date that major unconformity. This pattern is compatible with observations from other margins, where widespread channel incisions are younger than 600-500 ka (Burger et al., 2001; Tesson et al., 2011).

Besides, seaward of the valleys, at least five shelf-wide unconformities (mws5 to mws 1) have been interpreted to reflect major sea-level lowerings to lowstands during the last 500 ka, conforming to a main 100 ka periodicity in response to late Quaternary glacial-interglacial cycles (Mestdagh et al., 2019). These unconformities represent the top boundaries of several shelf-margin wedges, which have been considered to be mainly constituted by forced-regressive deposits comprising Falling-Stage Systems Tracts (FSSTs) or secondarily Lowstand Systems Tracts (LSTs) in distal margin locations (Somoza et al., 1997; Hernández-Molina et al., 2000b; Lobo et al., 2005a). These unconformities tend to merge landward, becoming amalgamated with the most recent one (mws 1), which has been associated with the LGM lowstand (Lobo et al., 2018; Mestdagh et al., 2019). This mws 1 surface can be traced through the paleovalley systems, where it constitutes the most recent incision phase. Therefore, we can assume that older paleovalley incisions could be connected with older shelf-wide unconformities; this interpretation would link the main phases of incision in the studied paleovalleys to the different sea-level lowerings and lowstands during the last 500 ka, i.e., associated to Marine Isotopic Stages 12, 10, 8, 6, and 2. A similar stratigraphic scenario has been proposed in the Gulf of Lions shelf, where phases of valley incision on the inner shelf have been correlated seaward with the boundaries of regional prograding units on the middle to outer shelf, believed to represent forced regressive and lowstand wedges (Labaune et al., 2010; Tesson et al., 2011).

This hypothesis of 100 ka cycles leading the incision phases on the shelf provides a viable mechanism linking the entrenchment of fluvial valleys on the shelf over previously deposited regressive facies with the distal development of shelf-margin facies that should be regarded as shelf-margin deltas (Porebski and Steel, 2003). The seaward continuation of incised valley features in the study area can be observed up to water depths of ~80 mbpsl, probably as a consequence of the balance between seaward decreasing valley

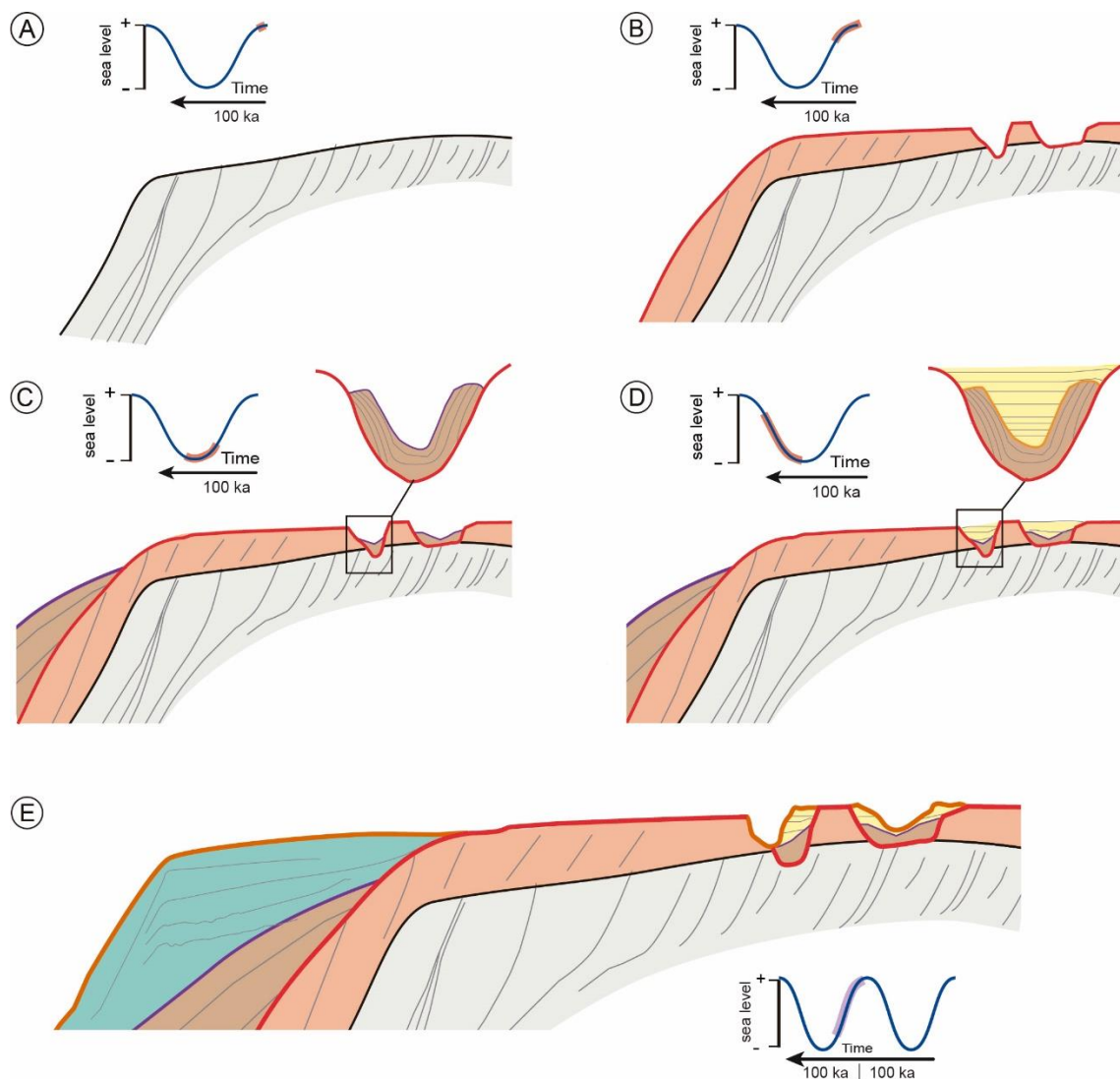


Figure 5.17: Synthetic model linking the initial formation of incised valleys, their subsequent infilling, and reincision with the generation of distal shelf-margin wedges. Cyclic sea-level changes are considered to be mostly driven by a dominant 100 ka periodicity. Here, only two successive cycles are represented.

incision as they approach a contemporaneous shelf- to shelf-margin shoreline (Blum et al., 2013) and transgressive reworking during subsequent sea-level rises.

Considering the connection established between phases of valley incision and development of shelf-margin wedges, we interpret the studied incised valleys as compound systems, resulting from a complex history of repeated avulsion and/or with periodic reoccupation of the fluvial system during consecutive glacio-eustatic cycles (Fig. 5.17), as reported in other large incised valleys (e.g., Horozal et al., 2021). This pattern results in amalgamated paleochannel complexes (Long et al., 2021) and differs from other shelves where buried channels overlap between different shoreface to shelfal deposits and occur in different places, so no reoccupation occurs (e.g., Foyle and Oertel, 1997; Burger et al., 2001; Weschenfelder et al., 2014; Mattheus et al., 2020). We interpret the pattern of reoccupation in the studied complex valleys as the result of: 1) limited accommodation on

the inner shelf, preventing vertical sequence stacking and favoring re-incision processes; this pattern contrasts with the middle to outer shelf, where increased subsidence has enabled the preservation of different shelf-margin wedges (Mestdagh et al., 2019), and could be possibly linked to the existence of a hinge point, delimiting the inner from the middle to outer shelf; and 2) occurrence of an indurated inner shelf, where pre-existing deposits have been cemented and/or armored (Lobo et al., 2018), largely preventing the reset of the drainage patterns.

Although both valleys can be regarded as examples of amalgamated complex valleys, where a major control of glacial-interglacial cycles on periodic incision is evidenced, we find a number of noticeable differences regarding their stratigraphic architectures, as the valleys differ in terms of shapes, number, and pattern of re-incision (Fig. 5.18). Those differences would suggest that both incised valleys have evolved differently during the late Quaternary due to the operation of distinct autocyclic processes.

The main valley is characterized by a maximum of 3-4 incision phases, which mostly exhibit V-shapes and tend to exhibit a multilateral stacking (Fig. 5.18), suggesting the occurrence of lateral shifting of the thalwegs axis between successive incisions, similar to the pattern documented in the Gulf of Lions (Labaune et al., 2010). This could also indicate the incomplete preservation of 100 ka depositional sequences in this valley system, as observed in other valley complexes where the correlation between major phases of incision and sea-level cycles is not one-to-one (e.g., Dubey et al., 2019). In this sense, the incisions in the main valley would be energetic and erosional, eventually resulting in the amalgamation of individual phases (Fig. 5.18). In addition, the existence of multilateral incisions would be compatible with the occurrence of limited channel avulsion. In contrast, in the eastern valley, at least five incision phases are identified; there, the incision phases tend to be U-shaped, and the valleys stack vertically in a multistorey fashion (Fig. 5.18). In contrast to the main valley, incisions in the eastern paleovalley would not result in the removal of previous incision phases, possibly in connection with less strong fluvial processes; also, the multistorey pattern is indicative of periodic reoccupation.

Apart from the different incision patterns exhibited by both valleys, we also find that their subsequent infillings exhibit different characteristics, involving the fingerprint of different depositional processes. Limited preservation of infilling facies in the main paleovalley and dominance of laterally accreting or chaotic deposits would reveal the preferential preservation of fluvial channel deposits, such as channel lags and/or point bars, which would mainly compose the Lowstand Systems Tracts (Horozal et al., 2021). This would indicate the removal of typical estuarine facies during successive incisions, as documented in the Gulf of Lions (Tesson et al., 2011). In contrast, the infillings of the eastern paleovalley are dominated by sub-parallel aggradational facies that may exhibit intercalated chaotic facies. These patterns are more indicative of mud-rich, low-energy tidally-influenced estuarine or coastal embayment depositional systems (Foyle and Oertel,

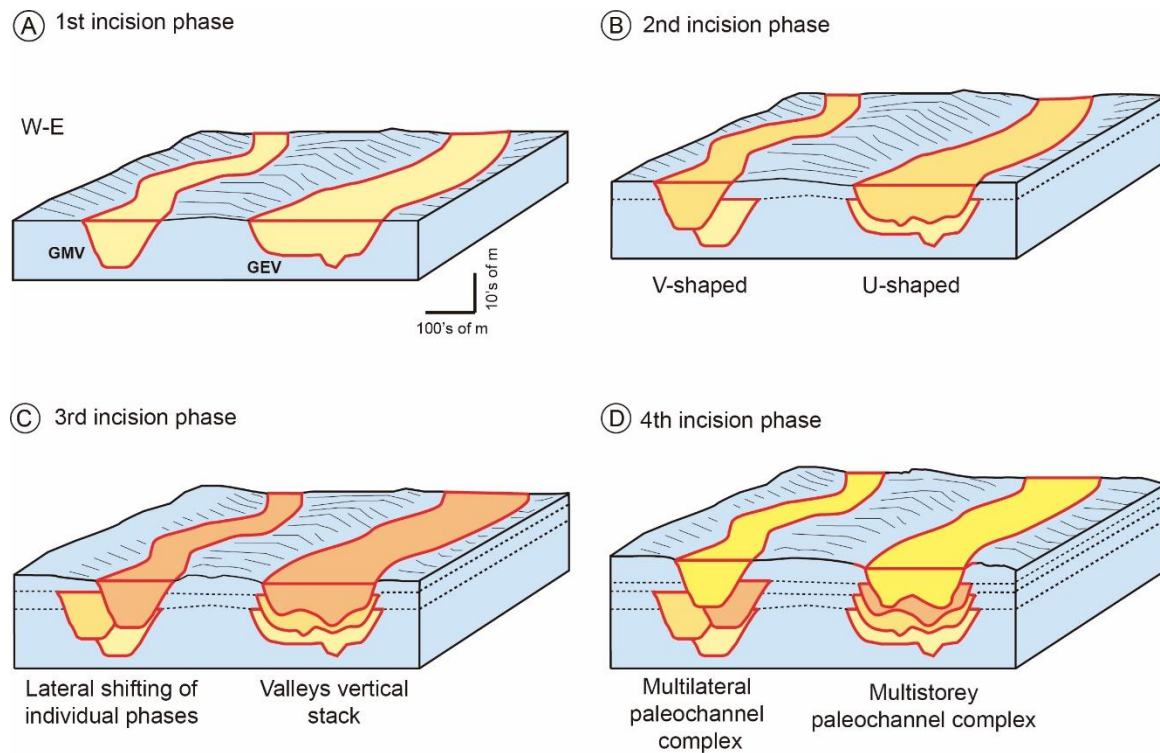


Figure 5.18: Schematic model of incised-valley architectural geometries identified in the two studied valleys. Here, four incision phases are observed, illustrating both valleys where the GMV mostly exhibits V-shapes that exhibit a multilateral stacking; in contrast, the GEV tends to be U-shaped, and the valleys stack vertically in a multistorey fashion.

1997; Tesson et al., 2010), with major preservation of central basin facies and occasional development of estuarine mouth sands composing the Transgressive System Tracts (Long et al., 2021). The boundaries between those estuarine facies could be interpreted as the product of estuarine ravinements (e.g., Foyle and Oertel, 1997). These observations are compatible with the differences found in the incision patterns and would indicate the persistence of the different depositional processes in both nearby valleys.

5.2.2. Valley morphology during the last sea-level lowstand: Some genetic constraints

The reconstruction of the morphology of the two study valleys during the last major incision phase enabled us to make some inferences concerning the paleogeographical configuration during periods of increased shelf exposure and related depositional environments. There are several factors claimed to influence the plan-view morphology of paleochannels, such as shelf gradients (Bae et al., 2018) or the mode of sediment transport; for example, low-sinuosity fluvial channels are typically related to bedload dominance and valley infilling by coarse-grained sediments (Alqahtani et al., 2017). Both valley trucks are characterized by rather straight patterns where no major meandering occurs. In this case, shelf gradients do not appear to influence significantly their plan-view patterns, as they tend to be developed over a low-gradient inner shelf. In contrast, both the elongation of

the valleys and their seaward terminations seem to be related to the existence of a marked contrast between an indurated inner shelf composed of coarse-grained bodies and a middle to outer shelf composed of more easily erodible materials; ultimately, the observed plan-view patterns have been attributed to strong confinement by the underlying geology (Lobo et al., 2018).

Both valleys differ in their main orientation, as the main valley is characterized by a well-defined N-S trend with slight bends along its course. However, the orientation of the eastern valley is more diverse, as northwards it is approximately N-S, becoming NE-SW oriented towards its distal termination. Ultimately, both valleys tend to converge towards their seaward pinch-outs, possibly suggesting that the eastern paleovalley acted as distributary of the main valley during lowered sea levels around the LGM. Eventually, during subsequent shelf flooding, both river mouths would have been located very close to the adjacent shoreline, forming a wide embayment. In fact, their converging pattern at the coastline closely resembles the present-day coastal pattern defined by the Tinto and Odiel rivers, developed along the northern coast of the Gulf of Cadiz E of the Guadiana River. In such system, a main river (Odiel) with a N-S orientation is tributed by the Tinto River along its left flank. The Odiel River is larger (140 versus 100 km) and extends over a wider drainage basin (2,300 versus 720 km²). The combined freshwater inflow is variable on a seasonal and annual basis, and in the final estuarine part, there is strong tidal influence (Borrego et al., 1995; Carro et al., 2019).

Cross-sectional shapes of the valleys are also remarkably different. Morphologic differences between nearby fluvial systems have been attributed to underlying structure and lithology, shelf gradients, and drainage basin characteristics (Klotsko et al., 2021). Taking into account the proximity of the valleys, the eventual influence of any of those factors is unlikely. However, different valley shapes are thought to condition hydrodynamics dictating sediment transport and deposition (Nordfjord et al., 2006; Chaumillon et al., 2008). We may suspect that depositional dynamics in each valley have been remarkably different. The main valley exhibits a well-defined V-shape and is narrower and deeper. In contrast, the eastern valley is characterized by a U-shaped cross-section, with a relatively wide bottom where two distinct thalwegs can be identified along most of its path. The higher width/depth ratio of this valley, together with the low sinuosity and slopes, can be compatible with the development of braided rivers (Nordfjord et al., 2005).

5.2.3. Variable patterns of postglacial infilling

Our high-resolution stratigraphic analysis strongly suggests that the two studied valleys do not only differ morphologically, but also in terms of infilling of the last incision phase related to the LGM. Those differences are noteworthy, considering the proximity of the valleys.

5.2.3.1. Tripartite infilling of the main valley

The detailed architecture observed within the post-LGM record of the main valley indicates the existence of three major evolutionary phases, comprising fluvio-deltaic, estuarine, and shallow-water environments (Fig. 5.19).

The basal facies (GmvU3) documented in the main valley are mostly characterized by a semi-transparent acoustic response with laterally dipping internal reflections (Fig. 5.19B). These laterally dipping facies have been attributed in other incised valleys to fluvial channel deposits, which are characteristic of the base of incised valley successions (Qiu et al., 2019); specifically, laterally migrating deposits can be interpreted as laterally accreted point bars (Green, 2009; Meckel and Mulcahy, 2016; Horozal et al., 2021). Its thin and patchy distribution along sections of the valley path could also be indicative of fluvial origin (Proust et al., 2010). These fluvial deposits tend to be deposited during lowstand conditions and thus compose the LST (Wellner and Bartek, 2003). However, wedge-shaped lateral channel migration facies are typical of meandering rivers (Proust et al., 2010; Wetzel et al., 2021). An alternative interpretation could be the interpretation of those facies as a bayhead delta (Figs. 5.19, and 5.20A), showing mostly seaward-directed progradations as reported in other fluvio-estuarine settings (e.g., Cartelle et al., 2022); also, lateral migrations advancing from both flanks can be generated in such protected depositional environments due to the generation of multiple lateral deltas (Maselli and Trincardi, 2013; Maselli et al., 2014). The fact that these facies show a proximal depocenter and basinward declining thickness could support that interpretation. Finally, the upper boundary of these fluvio-estuarine facies could be regarded as a bay ravinement (Fig. 5.20A), as documented in other valley infillings (Foyle and Oertel, 1997; Green, 2009).

The following upward facies (GmvU2-2) are typically characterized by sub-parallel seismic configuration in the central parts of the valley, evolving laterally to massive, non-stratified facies (Figs. 5.19, and 5.20A). This upward facies transition documents a significant change in depositional conditions, revealing the waning of fluvio-deltaic environment and the establishment of a protected lower-energy environment. Specifically, these facies could be interpreted as estuarine mud and sand alternations composing a central estuarine basin fill. Similar seismic facies in drowned valleys have been documented elsewhere (e.g., Weber et al., 2004a; Green, 2009; Graves et al., 2021). Laterally, these facies can evolve into side-attached channel margin deposits, such as tidal flats and coarser deposits that can extend into inter-channel areas. Internal high-amplitude surfaces within the proximal infilling of the central basin could indicate several transgressive ravinements.

Sub-unit GmvU2-1 exhibits non-stratified seismic facies that can be followed seaward, where they construct the uppermost part of wedge-shaped deposits constituting the proximal postglacial transgressive units (PTUs; Fig. 5.19A). These deposits represent shallow-water deltas formed during the course of the postglacial sea-level rise (Carrión-Torrente et al., 2022; Chapter 6). Ages collected from these PTUs integrated with ages extracted from

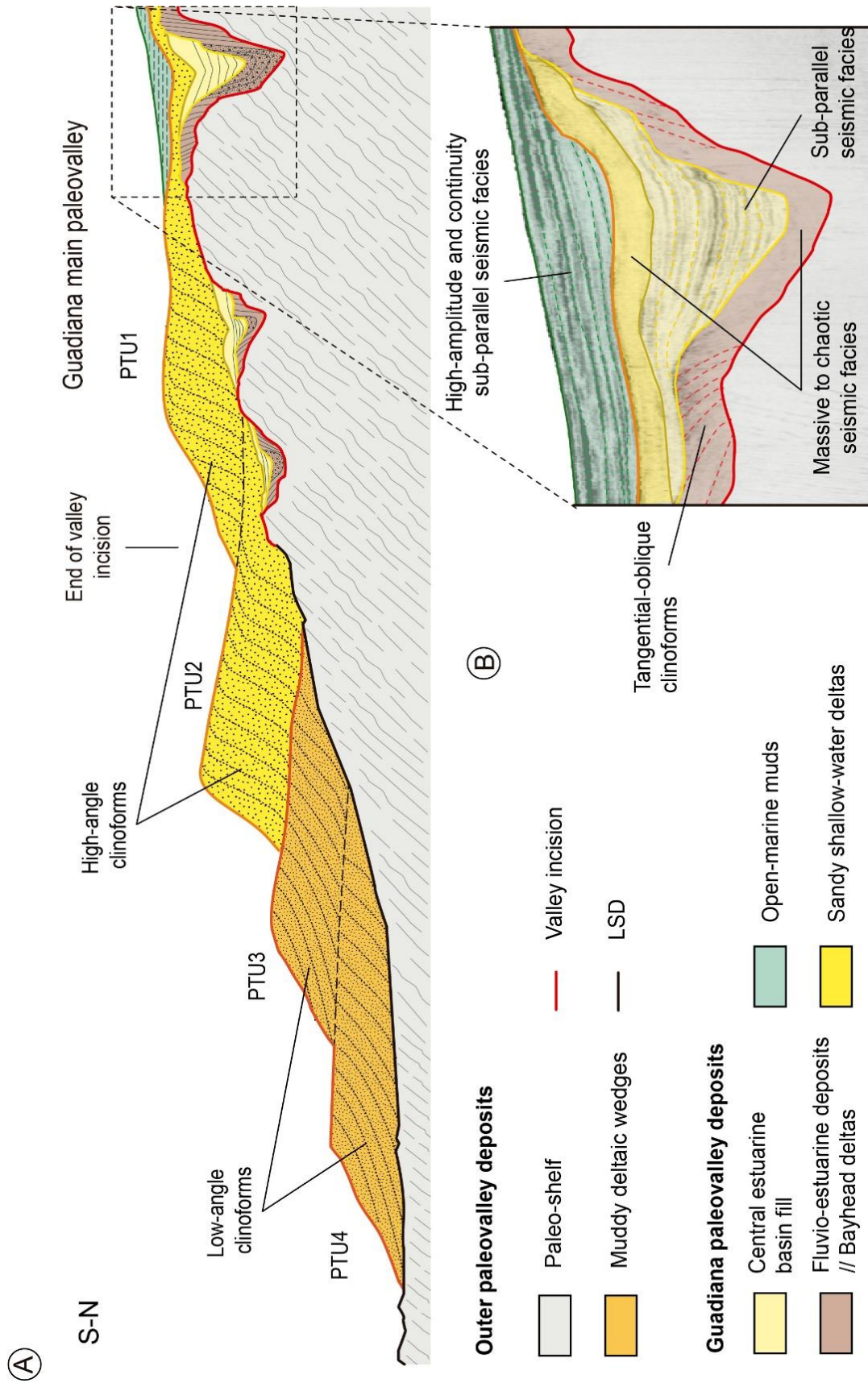


Figure 5.19: Synthetic along-valley sequence stratigraphic interpretation proposed for the Guadiana Main Valley and documenting the connection between proximal infilling facies and distal shallow-water deltas.

the valley infilling places the generation of these estuarine-to-shallow-water deposits in a transgressive context, as they extend from 18 ka to 8.5 ka BP (Fig. 5.21). Therefore, the middle facies of GmvU2 could be attributed to the TST of the last depositional sequence (Figs. 5.19, and 5.20A). The interpretation of this sub-unit as sandy shallow-water deltaic deposits is also supported by the sedimentological data obtained from the studied sediment core, which penetrates this unit for around 1.5 m (Fig. 5.16). This interval is strongly dominated by sandy facies (facies S and Sb). A well-marked peak on Ca/Fe, Si/Ca, and Si/Al ratios indicates an increase of terrigenous carbonates that would support this interpretation as shallow-water deltas.

The upper facies (GmvU1) also exhibits a sub-parallel configuration (Fig. 5.19A). These facies bury the last traces of the valley, extend laterally along the interfluves, and are partially buttressed distally by the shallow-water deltas. The horizontal layering and expanded distribution are characteristic of establishment of fully marine conditions in infilled incised valleys (Da Silva et al., 2016), usually in connection with the generation of marine muds with different origins (e.g., Estournès et al., 2012). In this particular setting, the valley was not completely infilled at the apex of the sea-level highstand, and this recent deposit has been defined as a mud entrapment (Figs. 5.19, and 5.20A) (Mendes et al., 2020). The sedimentary facies of this upper unit also support this interpretation, as the proportion of mud increases upwards (facies M), especially compared with the sandy facies that dominates the lower part of the core (Fig. 5.16). Ages of 6.8 and 5.8 cal Ka BP for this unit are compatible with the generation during the Holocene sea-level stabilization (Fig. 5.21), and therefore could be ascribed to the recent most HST. These deposits have been described regionally, where they constitute a number of muddy depocenters (e.g., Lobo et al., 2004b; Hanebuth et al., 2021).

5.2.3.2. Transgressive dominance in the eastern valley

In the eastern valley, the architecture of the most recent infilling phase is considerably simpler than the stratigraphic pattern found in the main valley, as basically two depositional environments can be recognized, evolving from an estuarine phase to an estuary-mouth to shallow-water environment.

The base of the valley infilling (GevU3) does not exhibit the lateral clinofolds characteristic of the main valley; only in distal locations, some wedge-shaped depositional bodies could be linked to remnants of fluvial deposition. In contrast, most of the valley is mainly filled by low-amplitude, sub-parallel reflections which locally exhibit sub-transparent acoustic responses. This pattern is typical of the backfilling of very low-energy estuarine settings (Fig. 5.20B), dominated by mud deposition with nearly continuous vertical aggradation, as documented elsewhere (e.g., Chaumillon et al., 2008; Green et al., 2013; Liu et al., 2017; Long et al., 2021). Locally, there is evidence that the low-energy estuarine infilling is offlapped by PTU 1, as this deposit extends laterally emanating from the

main valley. Considering the age (8.5 ka) of PTU 1, GevU3 is estimated to be a transgressive deposit.

Upward in the stratigraphic column, seismic unit GevU2 is characterized by a rather strong lower boundary and by reflective seismic facies, partially infilling the upper valley section but also generating some mounded patterns that protrude above the pre-existing

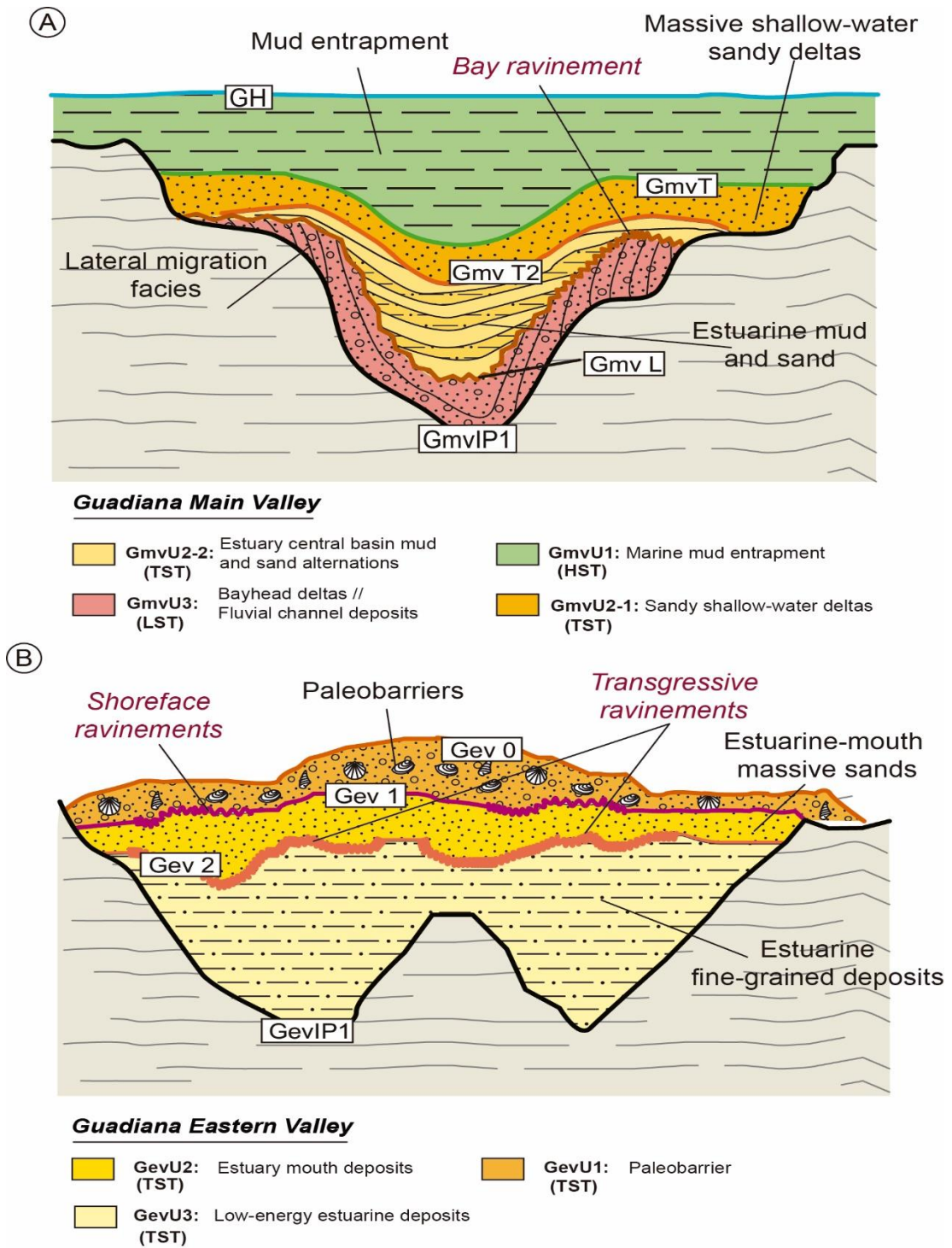


Figure 5.20: Idealized stratigraphic models for the incised valleys studied on the continental shelf of the study area, relating the seismic surfaces and units with their geological interpretation in the Guadiana main valley (A) and the Guadiana Eastern valley (B).

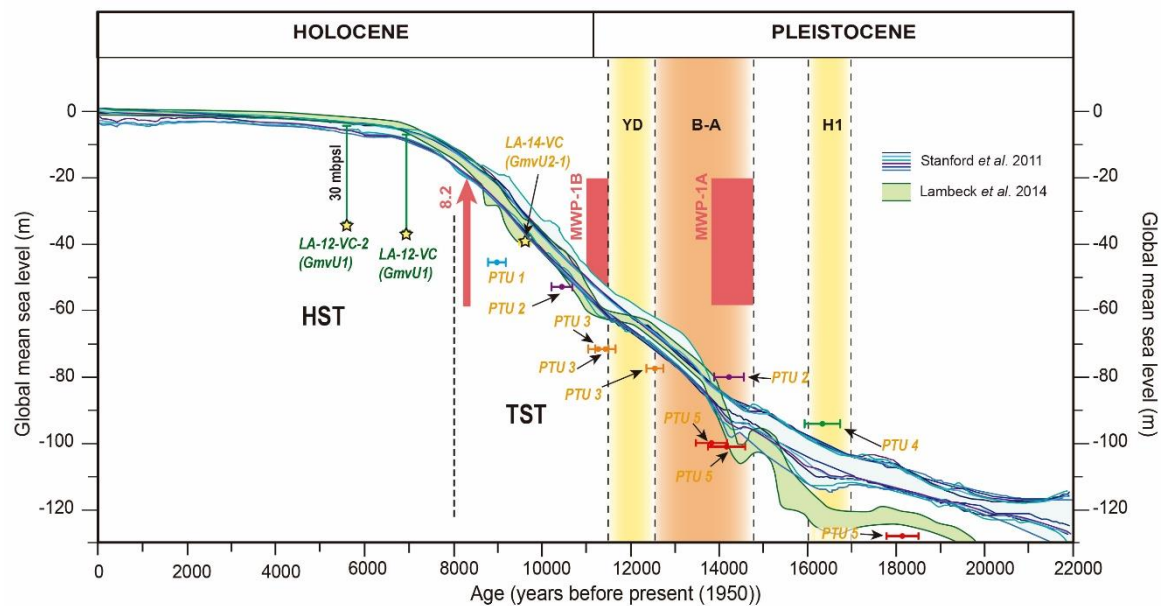


Figure 5.21: Chronology of the Guadiana main valley infilling seismic units (GmvU1 and GmvU2-1), with the transgressive seismic units (studied in the following Chapter 6) and correlation with the postglacial sea-level pattern. The major climatic events include: the Heinrich Event 1 (H1), the Bølling–Allerød warm period (B-A), and the Younger Dryas (YD) cold period, as well as the timing of Melt-Water Pulses (MWP) 1A and 1B and the 8.2 ka cooling event (in red). Plotted ages are named taking into account the coring site, the coring technique (VC stands for vibro coring), and the name of the seismic unit in which the samples were taken. The estimated water-depth locations of the Gulf of Cadiz transgressive clinoforms in relation to coeval sea levels are also indicated (Chapter 6).

relief. These facies are indicative of deposition of estuarine-mouth sand bodies (Fig. 5.20B), due to the landward rollover of a barrier system (e.g., Proust et al., 2010; Green et al., 2013; Liu et al., 2017). The base of these estuarine-mouth facies exhibits local signs of scouring that could be the product of transgressive ravinements (e.g., Nordfjord et al., 2006; Graves et al., 2021), either of tidal (distal) or wave origin (proximal) (Fig. 5.20B).

Overlying the recent most infill of the eastern estuary, a mounded, thick reflective deposit (GevU1) seems to exhibit a limited along-valley extension, possibly extending normal to the valley path. Equivalent valley-normal barriers have been documented in several Mediterranean incised valley settings, both in the Adriatic (Ronchi et al., 2018) and the Tyrrhenian seas (De Falco et al., 2022). Accordingly, this deposit could be attributed to the instauration of a shoreface to shallow-water sandy barrier, with the boundary with the estuary-mouth facies representing a shoreface ravinement still generated during transgressive conditions (Fig. 5.20B). As there is local evidence that GevU1 is overlapped by GmvU1, we consider that the formation of this shore-parallel barrier also occurred under transgressive conditions.

Therefore, most of the facies composing the infilling of the eastern valley are thought to compose the TST, including estuarine and shoreface-shelf depositional systems, with moderate remnants of fluvial lowstand deposition. Similar arrangements of facies infilling have been documented in other Atlantic estuaries (Foyle and Oertel, 1997; Estournès et al., 2012).

5.2.3.3. Variability of valley environments: hydrodynamics versus sediment supply conditions

Stratigraphic variability of nearby incised valleys is not common, but it has been reported occasionally. For example, it is thought that underlying geology and tectonics may play a significant role in modifying the expression of nearby valleys at regional spatial scales (Klotsko et al., 2021). In shorter spatial scales, structural control and/or antecedent morphology have led to very different valley morphologies (narrow versus wide, sheltered versus exposed), generating very different hydrodynamic regimes (Nordfjord et al., 2006; Menier et al., 2010), which in turn may interact with significant changes of sediment sources (Chaumillon et al., 2010; Cartelle et al., 2022). In other cases, stratigraphic variability may be strictly conditioned by the type of sediment supply, which can change from fluvial to marine-derived from one valley to another (Chaumillon and Weber, 2006). In the study area, the different facies exhibited by both infillings can be probably linked to the interplay between very different sediment supply conditions and also a variable role of the hydrodynamic regime. These different interactions could be possibly conditioned, to some extent, also by the different valley morphologies.

The main valley facies such as laterally accreting clinoforms and shallow-water deltas suggest strong fluvial supply irrespectively of the sea-level trend. Specifically, lateral accretion deposits are indicative of high rates of sediment supply (Maselli and Trincardi, 2013). Even during highstand conditions, the relict valley depression has been accumulating sediments from nearby fluvial sources. Therefore, this main valley can be considered a major path for fluvial sediment supply, not only at local but also at regional scale.

In contrast, the strong dominance of transgressive sediments within the eastern valley is suggestive of small sediment input (e.g., Qiu et al., 2019) and dominance of hydrodynamic agents in the generation of depositional systems. Indeed, the stratigraphic architecture of the eastern valley would be compatible with the development of wave-dominated incised valleys, where occasional development of barrier islands would have restricted inner lagoonal facies. This also stresses the similarities of the two studied valleys with the recent configuration of the combined Tinto-Odiel Estuary, which is partially protected by a well-developed sand spit (Carro et al., 2019). The comparison stresses the major influence of a longer valley possibly draining a much larger catchment, and a secondary valley with a reduced fluvial supply and dominated by coastal agents. The proximity of both valleys therefore suggests a major continued sediment contribution of the main valley and lateral sediment transport, which is eventually able to construct coastal barriers protecting the much more sediment-starved eastern valley.

5.2.3.4. Considerations about along-valley stratigraphic arrangement in the main valley

Stratigraphic architectures are considered to be variable along valley lengths, due to the influence of changing rates of sea-level rise (Green et al., 2013; Bae et al., 2018). However, there are few examples of along-valley stratigraphic facies arrangements. Some schematic descriptions were provided for the Trinity/Sabine incised valley system in the Gulf of Mexico (Thomas and Anderson, 1994). There, transgressive parasequences consisting of paired upper-bay and tidal inlet facies backstep within the valley in response to episodic valley flooding. A backstepping configuration of different estuarine deposits has been also inferred in the Manfredonia incised valley, Adriatic Sea, generated in response to short-term changes in sediment supply (Maselli and Trincardi, 2013). In comparison to those examples, the main valley in the study area stands out as a relevant example where it is possible to correlate along most of the valley length the infilling of incised valleys with the offshore transgressive stratigraphy, composed in this case by several shallow-water lithosomes. The most outstanding characteristic is the poor overlap between distal shallow-water deltas and the inner estuarine facies. The shallow-water deltas tend to develop mostly seaward of the valley and are the only features of the infilling that exhibit a characteristic backstepping pattern, likely reflecting either variable rates of sea-level rise or short-term changes of sediment supply (Carrión-Torrente et al., 2022; Chapter 6). In contrast, inner estuarine facies, although they exhibit a patchy distribution, tend to show a major depocenter in a proximal setting, landward of the shallow-water deltas. In this last case, the antecedent morphology seems to exert a higher influence on the distribution and focusing of estuarine facies.

CHAPTER

6

CHAPTER 6

Episodic deltaic development off the Guadiana River mouth during the postglacial transgression

The research work presented in the chapter is also a contribution to the paper:

Episodic postglacial deltaic pulses in the Gulf of Cádiz: Implications for the development of a transgressive shelf and driving environmental conditions.

Álvaro Carrión-Torrente^{1,2}, Francisco José Lobo¹, Ángel Puga-Bernabéu², Isabel Mendes³, Susana Lebreiro⁴, Marga García⁵, David Van Rooij⁶, María Luján⁷, María Isabel Reguera⁴

¹ *Department of Marine Geosciences, Instituto Andaluz de Ciencias de la Tierra–IACT, Spanish Research Council–CSIC and University of Granada–UGR, Avenida de las Palmeras 4, 18100 Armilla, Granada, Spain.*

² *Departamento de Estratigrafía y Paleontología, University of Granada, Granada, Spain.*

³ *Centre for Marine and Environmental Research–CIMA, Universidade do Algarve, Faro, Portugal.*

⁴ *Instituto Geológico y Minero de España–Centro Nacional, Spanish Research Council–CSIC, Madrid, Spain.*

⁵ *Oceanographic Centre of Cadiz, Spanish Institute of Oceanography–IEO, CSIC, Ministry of Science and Innovation, Cadiz, Spain.*

⁶ *Renard Centre of Marine Geology, Ghent University, Ghent, Belgium.*

⁷ *Department of Earth Sciences, University of Cadiz, Puerto Real, Spain.*

Published on:

Journal of Sedimentary Research, 92, 1116–1140

<https://doi.org/10.2110/jsr.2021.110>.

Received 30 September 2021; Accepted 3 August 2022.

Published Online: December 2022

JCR (2021): 2.481 (Q1)

Abstract

The postglacial sea-level rise after the Last Glacial Maximum provided ideal conditions to study the transgressive sedimentary response to sudden shelf flooding driven by different rates of sea-level rise. In this study, a high-resolution seismic stratigraphic interpretation and sedimentological analysis were conducted on data from the northern Gulf of Cadiz continental shelf (SW Iberian Peninsula), in order to: 1) understand the succession of sedimentary processes during each shelf flooding episode; and 2) explore the significance of variable rates of sea-level rise, sediment fluxes, and climatic conditions on the development of postglacial deposits.

Four backstepping seismic postglacial transgressive units (PTUs; 4 to 1 from oldest to youngest) that are linked to the retreating mouth of the Guadiana River were interpreted. Together, these seismic units display a wedge-shape geometry, are located over the inner to middle shelf, and overlie a regional unconformity formed during the Last Glacial Maximum. Each PTU can be divided into several sub-units with distinctive seismic facies that have a similar stratigraphic organization. Each PTU contains lower sub-units that are composed of low-angle tangential oblique clinoforms. The clinoforms are locally topped by a channelized sub-unit. The distal and/or lateral parts of the clinoforms are occasionally buried by sheet-like semitransparent subunits. The uppermost sub-units are present over the proximal and central parts of each seismic unit and are also sheet-like. PTUs can also be subdivided and described sedimentologically. Fine-grained sands with intercalated silty layers dominate the lower part of each PTU (lower clinoform sub-units). The upper part of each PTU (upper sheet-like sub-units) is characterised by reworked facies, composed of highly fragmented bioclasts within a mixture of silt and coarse to medium sand. Finally, mud deposits occur as a sediment drape over the PTUs.

The internal structure of each PTU reveals several phases of development under a general process of transgressive submergence in which both coastal and marine deposits were formed and eventually preserved. The initial phase involved the development of coarse-grained deltas in shallow water, which were locally eroded by a network of distributary channels. In a transitional phase, the infilling of distributary channels and the offshore export of fine-grained sediments is related to a change in sediment sources, possibly triggered by enhanced hydrodynamic processes. The final phase involved the reworking of fluvio-deltaic sediments by shoreface processes to generate a sediment sheet. Age correlation with a suite of postglacial sea-level curves indicates that the formation of the postglacial transgressive deposits is bracketed between 14 ka and 9 ka. The studied deposits were related to a period of reduced sea-level rise, culminating in the Younger Dryas event (two oldest PTUs), and to phases of enhanced sea-level rise, such as Meltwater Pulse (MWP) 1B (two youngest PTUs). In spite of high rates of sea-level rise over MWP-1B, each PTU exhibits progradation and preservation of much of the delta. The preservation of progradational deltaic units is likely caused by increased sediment supply during progradational pulses. Here it is suggested that those pulses of enhanced sediment

fluxes during MWP-1B were strongly driven by the overall climatic conditions in the SW of the Iberian Peninsula, probably resulting from enhanced rainfall runoff during humid periods and scarce land vegetation cover.

Key points

- Four transgressive postglacial units sourced in the Guadiana River retreating mouth were analysed.
- Each transgressive deposit is composed of deltaic clinoforms and shoreface reworking facies.
- Development of stratigraphy best explained by a transgressive submergence process.
- The pattern of sea-level rise is reflected in transgressive deposit geometry and composition.
- Deposit genesis guided by climatically-driven sediment fluxes under high sea-level rise rates.

6.1. Results

6.1.1. Seismic stratigraphy

The postglacial transgressive stratigraphy of the shelf off the Guadiana River mouth was believed to be constituted by four backstepping seismic units (named in this study as Postglacial Transgressive Units–PTUs) (Lobo et al., 2001), which are exposed on the Guadiana shelf in the middle shelf area (Fig. 6.1). However, an additional PTU was identified during this study, summing to a total amount of five PTUs. PTUs occur seaward of a system of N-S paleochannels located on the inner-middle shelf up to 75 m water depth, eroding older Pleistocene units (Chapter 5; Lobo et al., 2001, 2018; Gonzalez et al., 2004).

The studied deposits cover an irregular high-amplitude horizon (called SU, Fig. 6.2) that marks the erosional truncation of underlying Pleistocene oblique reflections, which has been interpreted as the paleo-topography of the LGM subaerial surface (Lobo et al., 2018).

6.1.1.1 Postglacial Seismic Units (PTUs): Internal Architecture and Seismic Facies

Each seismic unit contains a variable record of up to four different seismic sub-units (a to d) characterized by specific seismic facies and bounded by different seismic horizons (cl: clinoform horizon; ch: channel horizon; sh: sheet horizon; rw: reworked horizon) (Fig. 6.2).

PTU 4 lies above the regional unconformity SU (Figs. 6.2, and 6.3). Based on the seismic configuration, this unit can be divided into four sub-units: 4a, 4b, 4c, and 4d. Sub-unit 4a comprises the main body of PTU 4, and it is composed of gentle tangential-oblique clinoforms, mostly dipping SW, with gradients $\sim 0.7^\circ$ in the foresets, decreasing distally to less than 0.2° in the bottomsets (Fig. 6.3B; Table 6.1). Over the top of the clinoforms, sub-unit 4b is locally observed infilling a scoured, channel-like horizon.

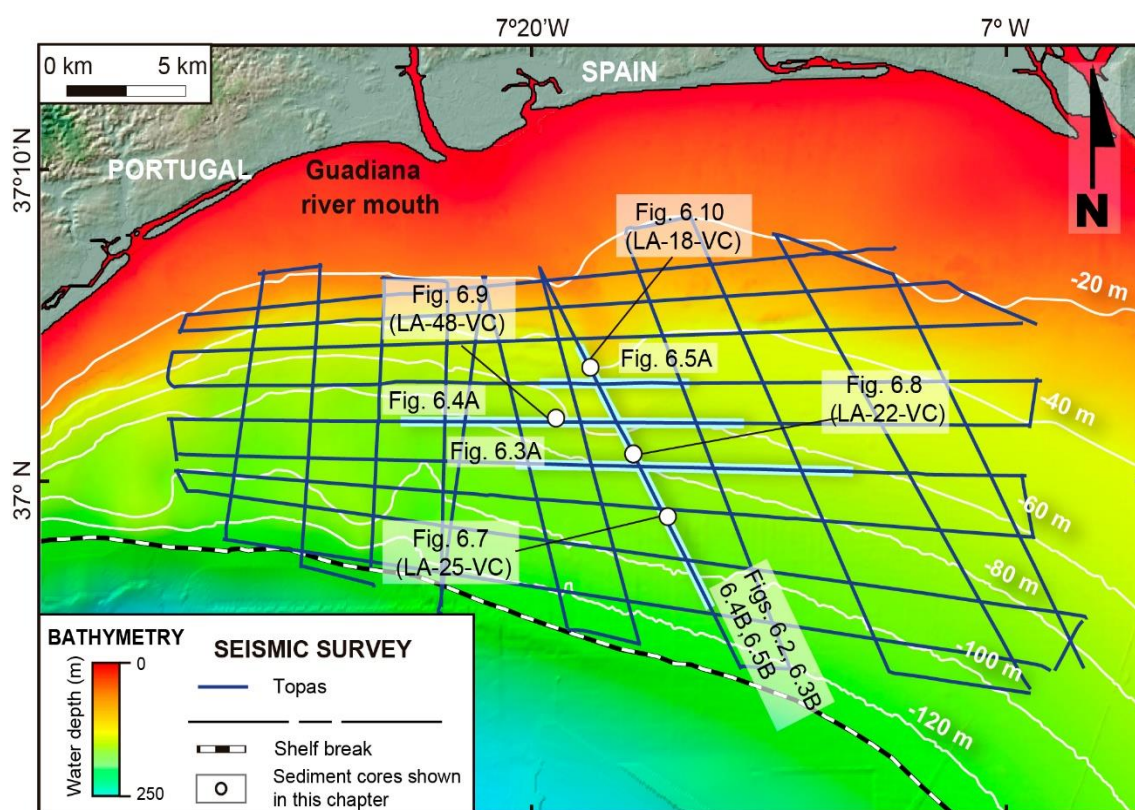






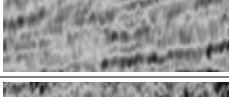











Figure 6.1: Location of the study area on the shelf offshore of the Guadiana River mouth, in the northern Gulf of Cadiz, showing the location of the seismic database and the selected core stations on the shelf in the study area offshore of the Guadiana River mouth (EMODnet Bathymetry Consortium, 2020). The location of Figures 6.2 to 6.5 is highlighted. The location of the sedimentological core stations showed in this chapter (Figs. 6.7 to 6.10) are also marked.

It is characterised by facies with a transparent to chaotic configuration and some weak internal reflections (Table 6.1). Laterally to sub-unit 4a, sub-unit 4c exhibits a sheet-like morphology onlapping the clinoforms of 4a, with transparent seismic facies that extend laterally over a few kilometers (Fig. 6.3A; Table 6.1). Sub-unit 4d extends across the proximal and central part of PTU 4 over the rest of the sub-units (Fig. 6.3B). It shows transparent seismic facies with some weak internal reflections (Table 6.1) and a thin (a few meters thick) sheet-like external shape with local superimposed undulations (Fig. 6.3).

PTU 3 is located landward of PTU 4 (Figs. 6.2, and 6.4). This unit can be divided into three sub-units: 3a, 3b, and 3d. Sub-unit 3a is characterised by a seismic facies composed of low-angle ($\sim 0.3^\circ$), parallel-oblique clinoforms dipping SW, downlapping onto the proximal parts of PTU 4 (Fig 6B; Table 6.1). Over the top of sub-unit 3a, sub-unit 3b fills a scoured channel-like horizon, showing a transparent to chaotic configuration with some weak internal reflections (Table 6.1). Overlying these sub-units, sub-unit 3d is a thin sheet-like body located over the central part of PTU 3, with a transparent seismic configuration and scattered weak internal reflections (Table 6.1; Fig. 6.4).

Episodic deltaic development off the Guadiana River mouth during the postglacial transgression

Table 6.1: Summary table including the seismic facies, configuration, boundaries, and acronyms for each seismic sub-unit identified in this study.

Unit	Sub-unit	Aspect	Seismic configuration	Lower boundary	Upper boundary
PTU4	4a		Amplitude: High to medium Configuration: Cliniforms Geometry: Wedge	Seismic Horizons: SU Termination: Downlap	Seismic Horizons: 4cl, 4ch Termination: Toplap/ Concordance/ Erosion
	4b		Amplitude: Medium to low Configuration: Transparent to chaotic with scattered internal reflections Geometry: Channel-like infilling	Seismic Horizons: 4ch, SU Termination: Onlap/Downlap	Seismic Horizons: 4cl Termination: Toplap/Erosion
	4c		Amplitude: Low Configuration: Transparent with scattered internal reflections Geometry: Sheet-like	Seismic Horizons: SU, 4cl Termination: Downlap, Onlap	Seismic Horizons: 4sh, Termination: Toplap
	4d		Amplitude: Very low Configuration: Transparent Geometry: Sheet-like	Seismic Horizons: 4cl, 4sh Termination: Concordance	Seismic Horizons: 4rw Termination: Erosion
PTU3	3a		Amplitude: High to medium Configuration: Cliniforms Geometry: Wedge	Seismic Horizons: SU, 4rw Termination: Downlap	Seismic Horizons: 3cl, 3ch Termination: Toplap/ Erosion
	3b		Amplitude: Medium Configuration: Chaotic Geometry: Channel-like infilling	Seismic Horizons: 3ch Termination: Erosion/Onlap/Downlap	Seismic Horizons: 3cl Termination: Toplap/Erosion
	3d		Amplitude: Low Configuration: Chaotic/Transparent Geometry: Sheet-like	Seismic Horizons: 3cl, SU Termination: Concordance	Seismic Horizons: 3rw, Termination: Toplap/ Erosion
PTU2	2a1		Amplitude: Medium to low Configuration: Cliniforms Geometry: Wedge	Seismic Horizons: SU, 3rw Termination: Downlap / Onlap	Seismic Horizons: 2cl Termination: Toplap/ Concordance/ Erosion
	2a2		Amplitude: Low Configuration: Cliniforms Geometry: Wedge/Mound	Seismic Horizons: SU, 3rw, 3cl, 2cl Termination: Downlap	Seismic Horizons: 2cl' Termination: Toplap/ Erosion
	2c		Amplitude: Very low Configuration: Transparent with scattered internal reflections Geometry: Sheet-like	Seismic Horizons: 2cl' Termination: Downlap, Onlap	Seismic Horizons: 2sh, Termination: Toplap
	2d		Amplitude: Low Configuration: Transparent with some internal reflections Geometry: Sheet-like	Seismic Horizons: 3cl, 2cl', SU Termination: Concordance	Seismic Horizons: 2rw Termination: Toplap
PTU1	1a1		Amplitude: Low Configuration: Transparent with some internal reflections Geometry: Wedge	Seismic Horizons: SU, 2rw Termination: Downlap / Onlap	Seismic Horizons: 2cl Termination: Toplap/ Concordance/Erosion
	1a2		Amplitude: Low-very low Configuration: Transparent with scattered internal reflections Geometry: Wedge/Mound	Seismic Horizons: SU, 1cl Termination: Downlap	Seismic Horizons: 1cl' Termination: Toplap/ Erosion
	1a3		Amplitude: Low to medium Configuration: Chaotic - Transparent with internal reflections Geometry: Wedge/Mound	Seismic Horizons: 1cl, 1cl', SU, 2rw Termination: Downlap	Seismic Horizons: 1cl'' Termination: Toplap
	1c		Amplitude: Low Configuration: Transparent with some internal reflections Geometry: Sheet-like	Seismic Horizons: 2cl', 2rw, SU, 1cl, 1cl'' Termination: Downlap, Onlap	Seismic Horizons: 1sh Termination: Toplap
	1d		Amplitude: Low Configuration: Transparent with some internal reflections Geometry: Sheet-like	Seismic Horizons: 1cl'', 1sh Termination: Concordance	Seismic Horizons: 1rw Termination: Toplap

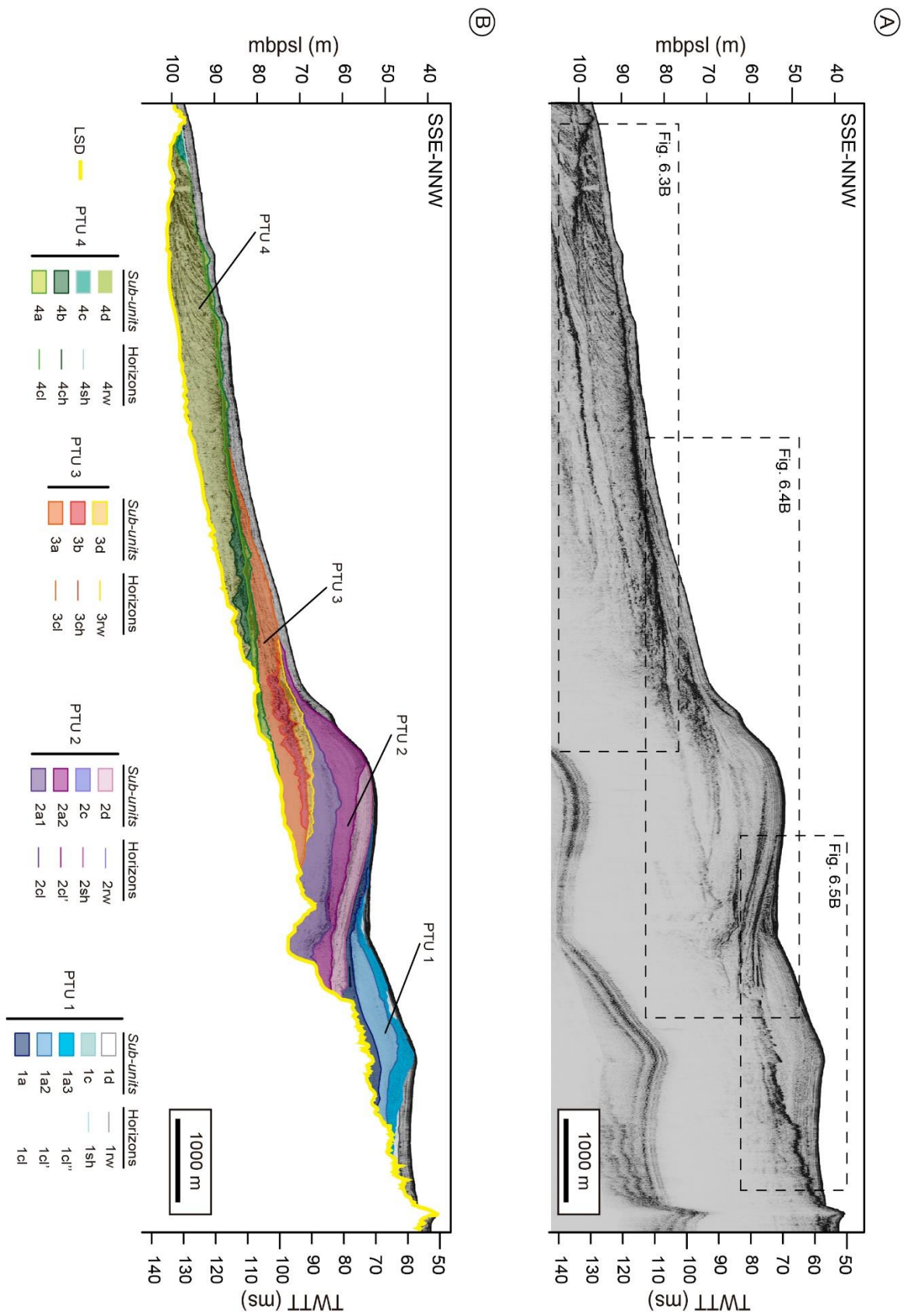


Figure 6.2: Representative downdip cross-shelf (SSE-NNW-oriented) sub-bottom seismic profile showing the general arrangement of backstepping seismic units (A) and their interpretation (B) offshore of the Guadiana River mouth. The color code and acronyms used in this chapter are also included. The location of the seismic section is indicated in Figure 6.1.

Episodic deltaic development off the Guadiana River mouth during the postglacial transgression

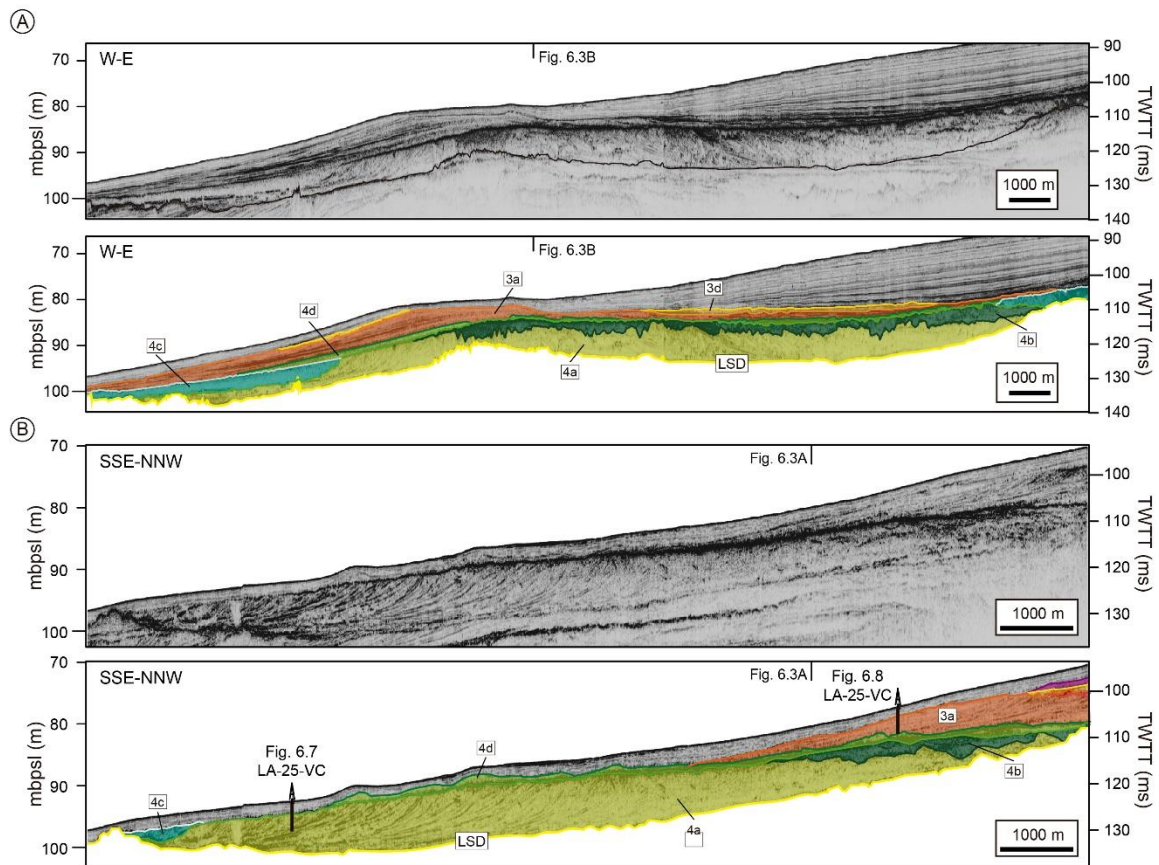


Figure 6.3: Representative sub-bottom profiles focusing on the Postglacial Transgressive Unit 4. A) W-E seismic line (up) and its interpretation (below). B) SSE-NNW seismic line (up) and its interpretation (below). Here, the important characteristics observed are: The clinoforms which compose the main body of PTU 4 (*sub-unit 4a*), mainly in the distal part of the unit; the channel features that characterize the proximal part of the body (*sub-unit 4b*); the transparent seismic facies that onlaps laterally to this body (*sub-unit 4c*); and the thin, and transparent facies, sheet-like body which integrates *sub-unit 4d*, where some superimposed undulations are observed. The location and penetration of sediment cores LA-25-VC (Fig. 6.7) and LA-22-VC (Fig. 6.8) are also indicated. The location of the seismic sections is indicated in Figure 6.1. The color code and acronyms are indicated in Figure 6.2.

PTU 2 is characterized mainly by a prograding wedge more than 20 m thick (Figs. 6.2, and 6.4). The lower part of this unit is composed of two prograding bodies (i.e., sub-units 2a1, and 2a2). Both sub-units are characterised by low-amplitude tangential-oblique clinoforms with angles in the proximal zones of $\sim 1^\circ$, decreasing distally to $0.3\text{--}0.4^\circ$ (Figs. 6.2, and 6.4; Table 6.1). These clinoforms dip in opposite directions (westward and eastward) (Fig. 6.4A). Sub-unit 2a1 is thinner and is completely covered by sub-unit 2a2. Laterally to this mound-shaped body, the sheet-like sub-unit 2c, with transparent seismic facies and some weak parallel internal reflections, onlaps the second prograding body (sub-unit 2a2; Fig. 6A; Table 6.1). Sub-unit 2d extends over the proximal and central part of PTU 2 and is restricted to the eastern sector (Fig. 6.4A).

PTU 1 covers the proximal part of PTU 2 (Figs. 6.2, and 6.5). The main core of PTU 1 is formed by three prograding sub-units (1a1, 1a2, and 1a3), which are covered by two other sub-units (1c and 1d), following a pattern similar to PTU 2. The three lower sub-units exhibit

prograding configurations (Table 6.1). Sub-unit 1a1 is characterized by low-amplitude reflections (Fig. 6.5), and its upper boundary is very irregular. Sub-unit 1a2 shows a similar configuration but with gradients up to 3°. Sub-unit 1a3 is formed by low-amplitude progradational reflections with gradients up to ~ 1° (Fig. 6.5; Table 6.1). Sub-unit 1c shows a sheet-like external shape and onlaps laterally onto sub-unit 1a3. It is characterized by a highly transparent configuration that extends laterally over a few kilometers (Fig. 6.5A; Table 6.1). Sub-unit 1d overlies sub-unit 1a3 and is located mainly in the central and proximal areas. It is a thin (a few meters thick) sheet-like unit with transparent seismic facies and some weak internal reflections (Table 6.1).

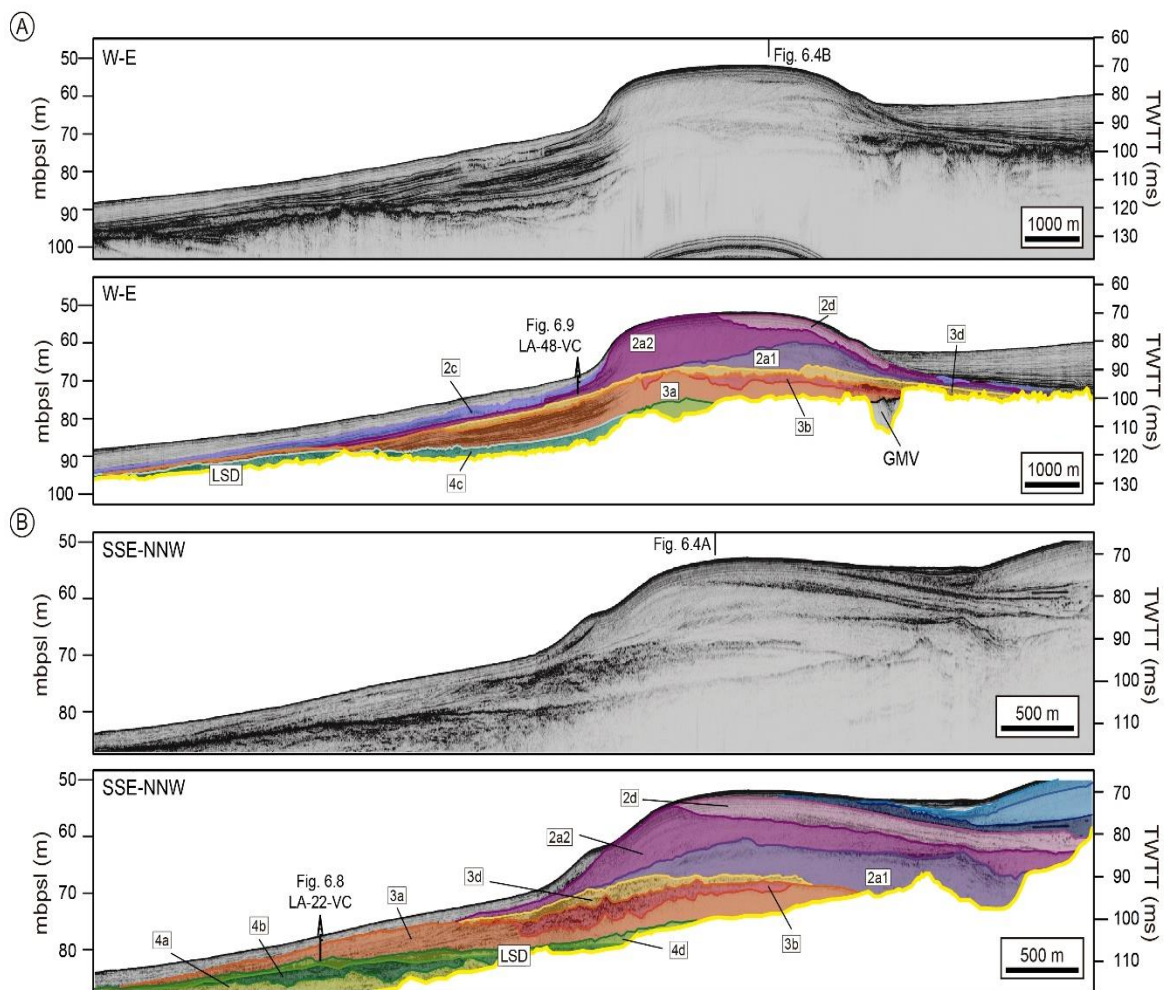


Figure 6.4: Representative sub-bottom profiles focusing on Postglacial Transgressive Units 3 and 2. A) W-E seismic line (up) and its interpretation (below). B) SSE-NNW seismic line (up) and its interpretation (below). Here, the remarked characteristics observed are: The low-angle clinofolds which compound the lower part of PTU3 (*sub-unit 3a*), and the two clinofolds bodies (with higher angles and dipping in opposite directions) that compound the most of PTU 2 (*sub-units 2a1 and 2a2*); the channel features with chaotic configuration that characterize the proximal part of the body (*sub-unit 3b*); the *sub-unit 2d*, which occurs over the proximal and central part of PTU 2, but is restricted only to the eastern sector; and the transparent seismic facies that onlaps laterally to sub-unit 2a2 (*sub-unit 2c*). The location and penetration of sediment cores LA-22-VC (Fig. 6.8) and LA-48-VC (Fig. 6.9) are also indicated. The location of the seismic sections is indicated in Figure 6.1. The color code and acronyms are indicated in Figure 6.2.

Episodic deltaic development off the Guadiana River mouth during the postglacial transgression

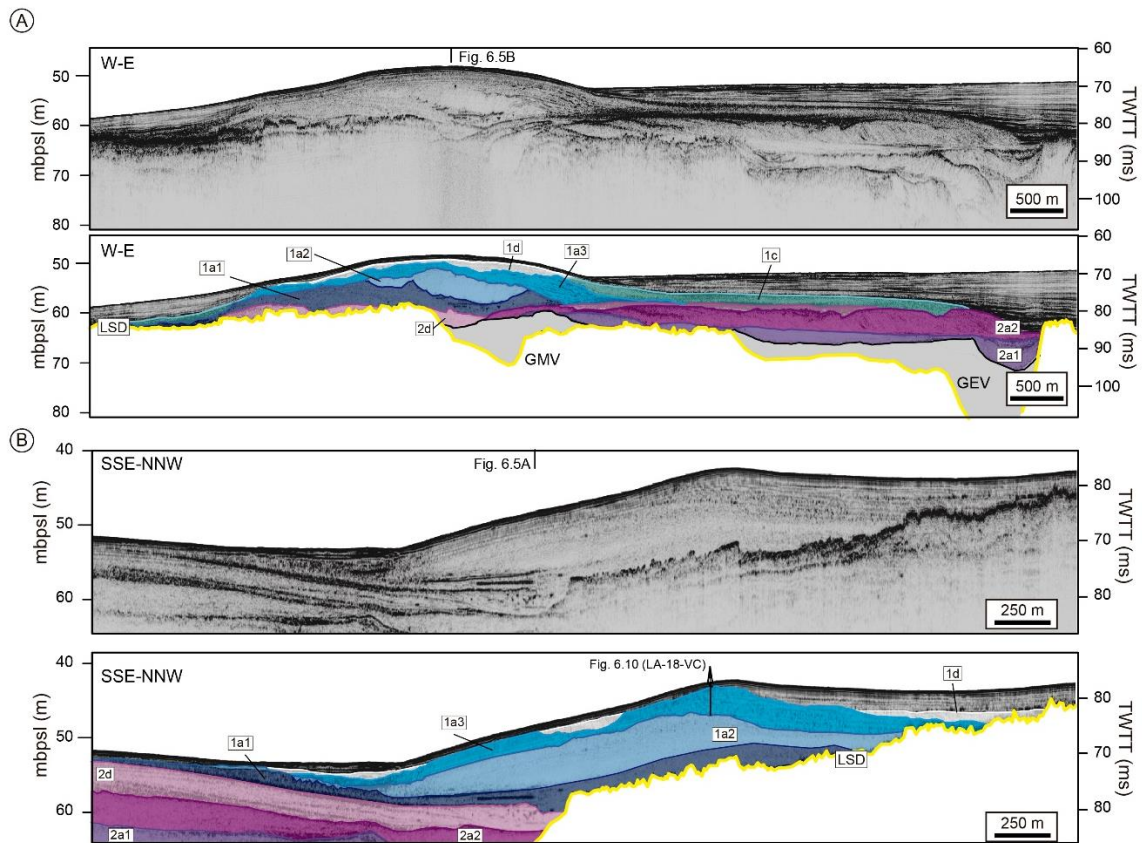


Figure 6.5: Representative sub-bottom profiles focusing on the Postglacial Transgressive Unit 1. A) W-E seismic line (up) and its interpretation (below). B) SSE-NNW seismic line (up) and its interpretation (below). Here, the remarked characteristics observed are: The three clinoform sub-units which form the main body of PTU 1 (i.e., sub-unit 1a1, 1a2 and 1a3); the sub-unit 1d, which occurs over the PTU 1; the transparent seismic facies that onlaps laterally to the main body of PTU 1 and is also lying over PTU 2 on the eastern sector (sub-unit 1c); and the incised-channel features located in the eastern sector, which contain parts of PTUs 2 and 3. The location and penetration of sediment core LA-18-VC (Fig. 6.10) are also indicated. The location of the seismic sections is indicated in Figure 6.1. The color code and acronyms are indicated in Figure 6.2.

6.1.1.2 Spatial Distribution

The studied deposits are located over the inner and middle continental shelf between 40 m and 100 m water depths (Figs. 6.2, and 6.6). In plan view, these units show a roughly ellipsoidal geometry (Fig. 6.6). Each individual unit shows wedge- or mound-shaped external shapes with a maximum thickness of 10-15 m in the central parts that decreases laterally. The depocenters of each unit are oriented ~ N90E, normal to the Guadiana River mouth. Nevertheless, each individual deposit varies slightly from this value.

PTU 4 is located over the middle shelf between 60 and 95 m water depths and covers an area of 212 km² (Fig. 6.6A, and 6.6B). It shows an elongated N85E distribution, extending 22 km in that direction and 7 km across the shelf (Fig. 6.6B). The main depocenter is displaced towards the east, showing a maximum thickness of around 10 m.

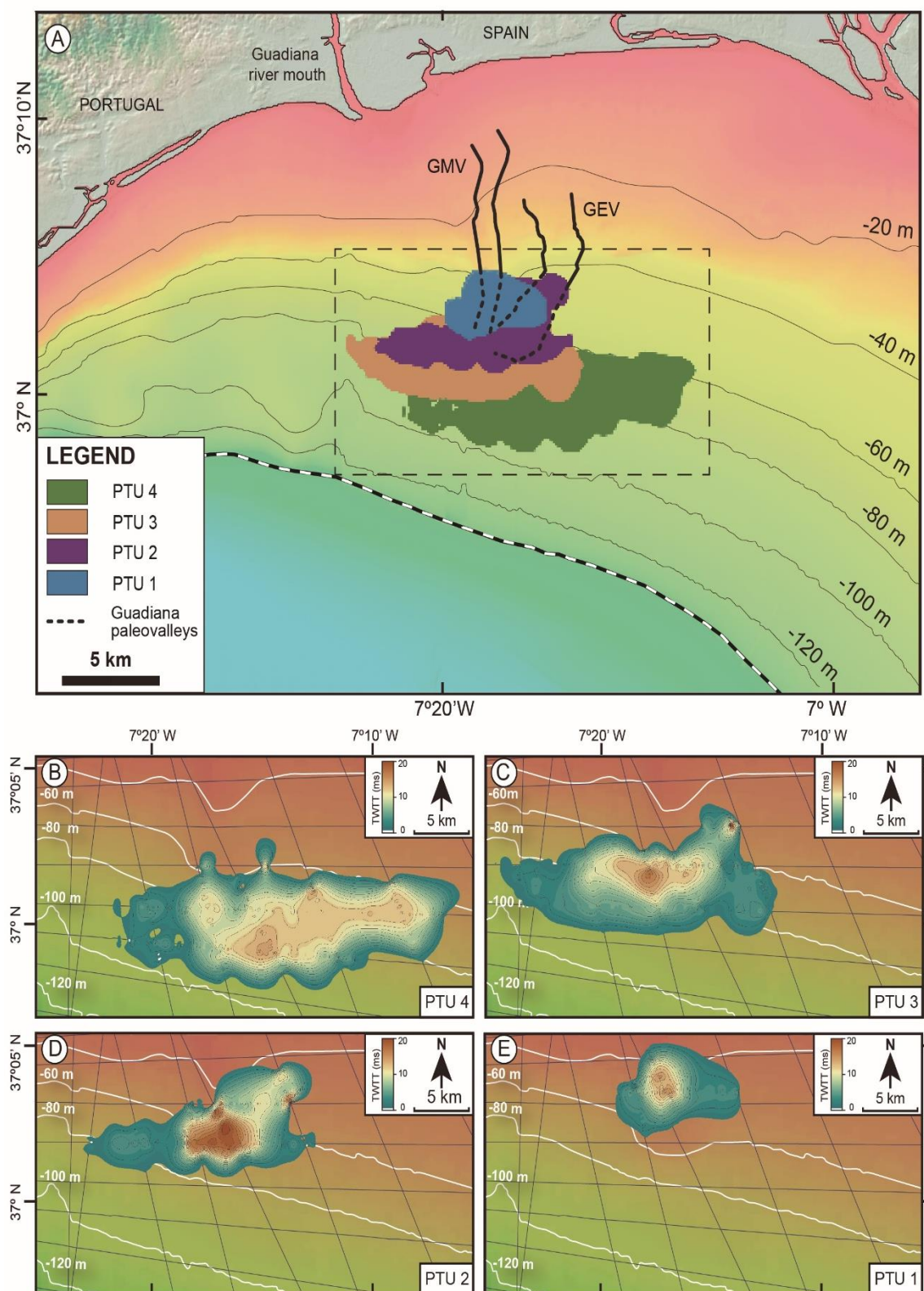


Figure 6.6: Spatial distribution and thickness of the studied deposits. A) Distribution maps of the PTUs showing the location of the main Guadiana paleovalley (GMV), the Guadiana Eastern paleovalley (GEV), the coastline, and the shelf bathymetry. The position of Figures 6.6B-E is indicated by the inset rectangle. B-D) Isochores map showing the spatial distribution and thickness in TWTT (ms) of the studied seismic units: B) PTU 4; C) PTU 3; D) PTU 2; E) PTU 1. The shelf bathymetry and the position of sub-bottom seismic lines are also represented.

PTU 3 is located over the middle shelf between 60 and 90 water depths, westward in relation to PTU 4, and extends over 149 km² (Fig. 6.6A, and 6.6C). Its distribution pattern is also elongated in a N90E trend extending for about 18 km, whereas across the shelf it extends for about 5.3 km (Fig. 6.6C). The main depocenter is located in the central area, with a maximum thickness of around 12 m.

PTU 2 is located over the inner-middle shelf between 50 and 75 m water depths (Fig. 6.6A, and 6.6D). Its spatial distribution shows a coverage smaller (106 km²) than the previous units, extending for 14 km in the N70E direction, and less than 5 km across shelf (Fig. 6.6D). Its maximum thickness (~ 18 m) occurs in the central part, decreasing abruptly towards the lateral margins.

PTU 1 exhibits a restricted areal distribution (38 km²) over the inner shelf at 40-55 m water depths (Fig. 6.6A, and 6.6E). In plan view, its distribution shows a N80E lobate shape with a maximum along-shelf length of around 8 km, and less than 5 km across shelf (Fig. 6.6E). The main depocenter is located slightly westward of the previous depocenters, with a maximum thickness of about 10 m (Figs. 6.5A, and 6.6E).

6.1.2. Sedimentological Analysis

6.1.2.1 Types of Sediment Facies

The results derived from the sedimentological analysis of sediment cores (Table 6.2) show that sedimentary facies in each unit exhibit a consistent pattern (Figs. 6.7, 6.8, 6.9, and 6.10). Three main types of facies were distinguished in the studied sediment cores.

Facies 1: Massive silty sands. This facies is composed of very well sorted fine-grained sands with abundant sand-size bioclasts and scattered shell fragments of centimetric scale intercalated with silty layers. Grains consist mainly of bivalve fragments and siliciclastic grains. This facies is generally massive, lacking sedimentary structures (Figs. 6.7F-G, 6.8F, 6.9F-G, and 6.10G), although parallel lamination to cross-lamination (Fig. 6.7E), bioturbation (Fig. 6.8F), and mottling (Fig. 6.7D) are locally observed.

Facies 2: Sandy gravels. This facies comprises granule- to pebble-size bioclasts, mainly highly fragmented bivalve shells, which are hosted in a mixture of coarse to fine sand mixed with silty sand. This facies is poorly sorted and structureless (Figs. 6.7B, 6.7C, 6.8B-D, 6.9D, and 6.10B).

Facies 3: Homogeneous muds. This facies consists of silt and clay without sedimentary structures and scarce well-preserved shells, some of them in life position (Figs. 6.7A, 6.8A, and 6.9A).

Table 6.2: Summary table of the studied sediment vibro cores, including their coordinates, length, and the water depths in which they were obtained.

Unit	Core ID	Geographic Coordinates		Water depth (m)	Core length (cm)
		Latitude (N)	Longitude (W)		
PTU4	LA-44-VC	36° 59. 115'	7° 17.429'	89	413.6
	LA-25-VC	36° 58.386'	7° 14. 697'	95	483.2
PTU 3	LA-22-VC	37° 00. 379'	7° 15. 926'	77	444.3
	LA-46-VC	37° 00. 596'	7° 17. 899'	67	399.7
PTU2	LA-48-VC	37° 01. 560'	7° 19. 104'	70.4	494.8
	LA-20-VC	37° 01. 599'	7° 16. 721'	52	70
PTU1	LA-18-VC	37° 03. 226'	7° 17. 736'	41	437.7

6.1.2.2 Core Descriptions

Sediment core LA-25-VC: This core is 480 cm long and penetrated PTU 4 (Figs. 6.1, and 6.3B; Table 6.2). From bottom to top, three intervals can be distinguished (Fig. 6.7). The lower interval (480-170 cm) is dominated by facies 1, where some lamination, bioturbation, mottling, and some dark layers are observed (Fig. 6.7D to 6.7G). Facies 1 can be assigned to sub-unit 4a. The middle interval (170-100 cm) is characterized by facies 2, whose matrix shows a darkish colour compared with the rest of the core (Fig. 6.7B, and 6.7C). This interval is also characterized by an upward, decreasing trend in the density log, continuous to the top of the core. Finally, the upper interval (100-0 cm) is characterized by homogeneous and structureless muds of facies 3. An increase in the magnetic susceptibility and a constant decrease in density is observed towards the core top. Facies 2 and 3 are correlated with post-transgressive sedimentation.

Sediment core LA-22-VC: This 440-cm-long sediment core penetrated PTU 3 (Figs. 6.1, and 6.4B; Table 6.2). From bottom to top, three intervals can be distinguished based on their dominant facies (Fig. 6.8). The lower interval (440-155 cm) is dominated by facies 1. In the middle part of this interval, between 370 and 335 cm depth, the sand is light brownish and bioturbated (Fig. 6.8F). In the upper part of this interval (230-185 cm), a coarsening-upward trend in the sand matrix is accompanied by an increase in content of shell fragment (Fig. 6.8D). The middle interval (155-75 cm) is characterized by facies 2 (Fig. 6.8B, 10C). The lower two thirds of the core (430-130 cm), characterized by facies 1 and facies 2 toward the top, are assigned to sub-unit 3a. The uppermost interval (75-0 cm) is a package of silts and clays (Facies 3) with scattered centimetric shells (≥ 2 cm) (Fig. 6.8A), and where magnetic susceptibility increases steadily towards the core top. The upper 130 cm is dominated by facies 2 and 3 and corresponds to post-transgressive sedimentation.

Episodic deltaic development off the Guadiana River mouth during the postglacial transgression

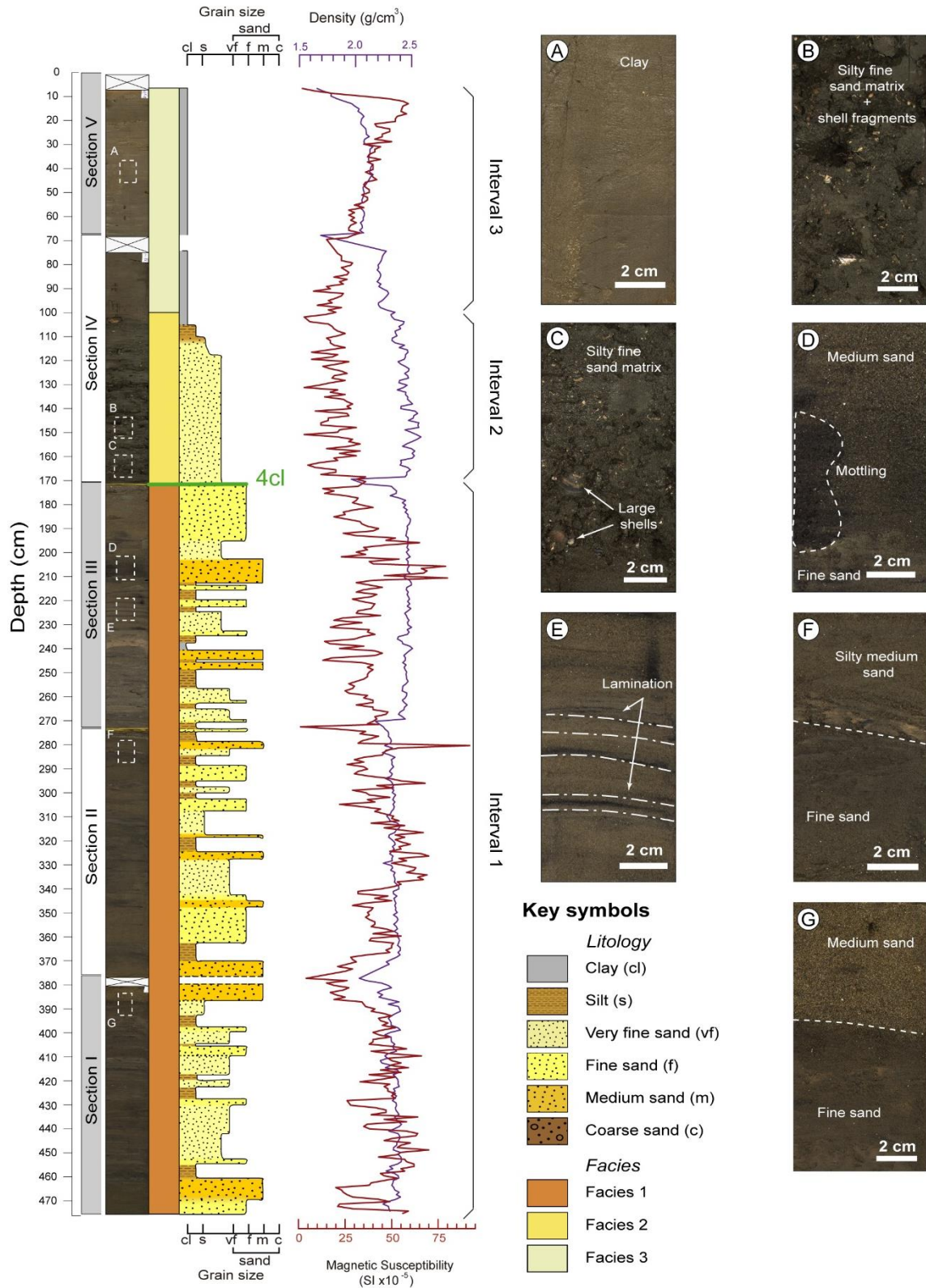


Figure 6.7: Photography, schematic sediment facies, and lithological description, control age points, density log, and magnetic susceptibility logs of sediment core LA-25-VC, characterizing seismic unit PTU 4. A) Homogeneous mud (facies 3); B, C) Silty sand mixed with highly fragmented bioclasts of bivalves, *Turritella* and *Ostrea* up 2 cm in length (facies 2); D) Massive medium to fine sand with mottling related to organic matter; E) Fine to medium sand with some silt laminae; F, G) Massive sands (facies 1).

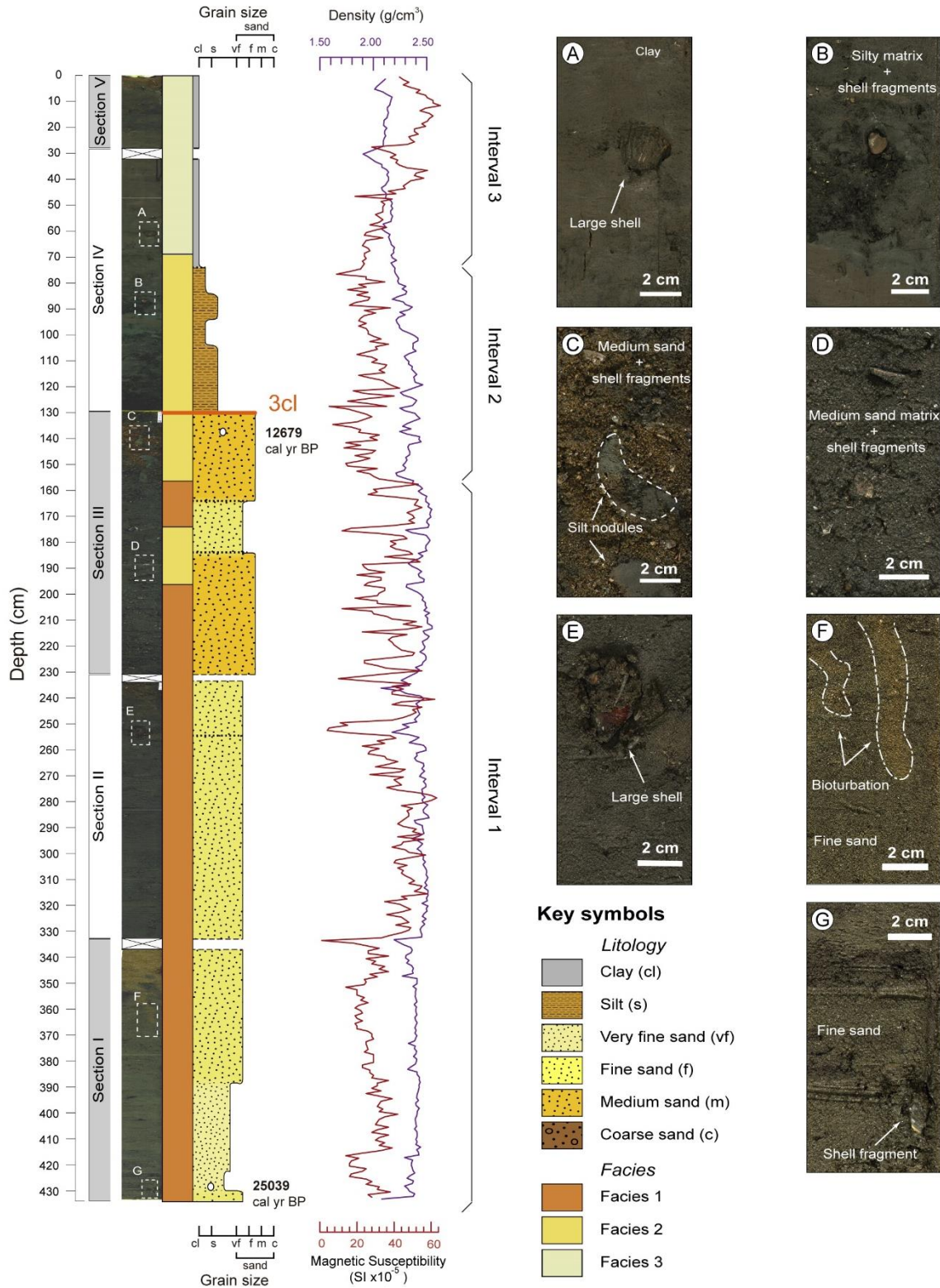


Figure 6.8: Photography, schematic facies, lithological description, control age points, density log, and magnetic susceptibility logs of sediment core LA-22-VC, characterizing seismic unit PTU 3. A) Muddy facies (facies 3) showing a large well-preserved 3-cm-long bivalve shell; B) Silty sand of facies 2 with 1 cm-long bivalve shell fragments (facies 2); C) Medium sand of facies 2 including a high amount of fragmented bioclasts of bivalves and *Turritella* and silt nodules; D) Medium sand including fragmented bioclasts like bivalves and *Turritella* up to 3 cm in length; E) Massive medium sand containing a large 5 cm bivalve shell and *Dentalium*; F) Bioturbation in fine to medium sand; G) Massive fine sand including a large bivalve shell fragment.

Sediment core LA-48-VC: This sediment core corresponds with PTU 2 and is located west of the other selected cores (Figs. 6.1, and 6.4A; Table 6.2). It has a total length of ~ 495 cm, and two main intervals can be distinguished according to their facies (Fig. 6.9). The first interval (495-90 cm) shows a relatively homogeneous composition reflected in the density log (Fig. 6.9). This interval is characterized by facies 1, does not exhibit primary sedimentary structures, and is correlated with seismic sub-units 2c and 2a2. A grain-size increase of the sand matrix is observed in the upper part of this interval (190-90 cm) (Fig. 6.9B). The second interval extends along the upper part of the core (90 to 0 cm) and is dominated by facies 3, where well-preserved shells with sizes larger than 5 cm are found (Fig. 6.9A). This interval is correlated with the post-transgressive sedimentation. The uppermost centimeters are characterized by a positive upward trend in magnetic susceptibility.

Sediment core LA-18-VC: This core corresponds with the uppermost part of PTU 1 (Figs. 6.1, and 6.5B; Table 6.2). It has a total length of about 440 cm and has a higher proportion of sand than the other sediment cores. Three intervals are distinguished according to the sedimentary facies. The lower interval (440-110 cm) is mainly dominated by facies 1, with two thin intervals characterized by facies 2 resting above erosional surfaces at 250-240 and 220-210 cm depths (Fig. 6.10). The second interval (110-30 cm) is characterized by facies 2 and is separated from the lower interval by a sharp erosional surface (Fig. 6.10B, and 6.10C). This interval can be subdivided into two minor intervals. From bottom to top, the first 35 cm (110-75 cm) are characterized by a silt layer without bioclasts. This silty layer is overlain by 40 cm of highly fragmented granule to pebble-size bioclasts in a coarse to medium sand matrix, which ends abruptly in a thin (5 cm) clay layer marked by a significant increase in the magnetic susceptibility (75-30 cm) (Fig. 6.10). Sub-unit 1a3 is mostly dominated by facies 1 with some intervals dominated by facies 2. The uppermost interval (30-0 cm) is characterized by facies 1. Recent sedimentation shows a marked increase of the sand fraction in contrast with the other studied cores.

6.1.2.3. Age Dates

Age values (Table 6.3) place the formation of the postglacial transgressive deposits between 13.8 and 9 ka. However, some age dates show anomalous values older than expected taking into account the sequence of ages and the overall chronostratigraphic scenario framed by postglacial sea-level changes and associated climatic changes. These anomalous age values were interpreted as the result of shell reworking, a process that is common to other postglacial transgressive settings (e.g., Aksu et al., 2016; Pretorius et al., 2019).

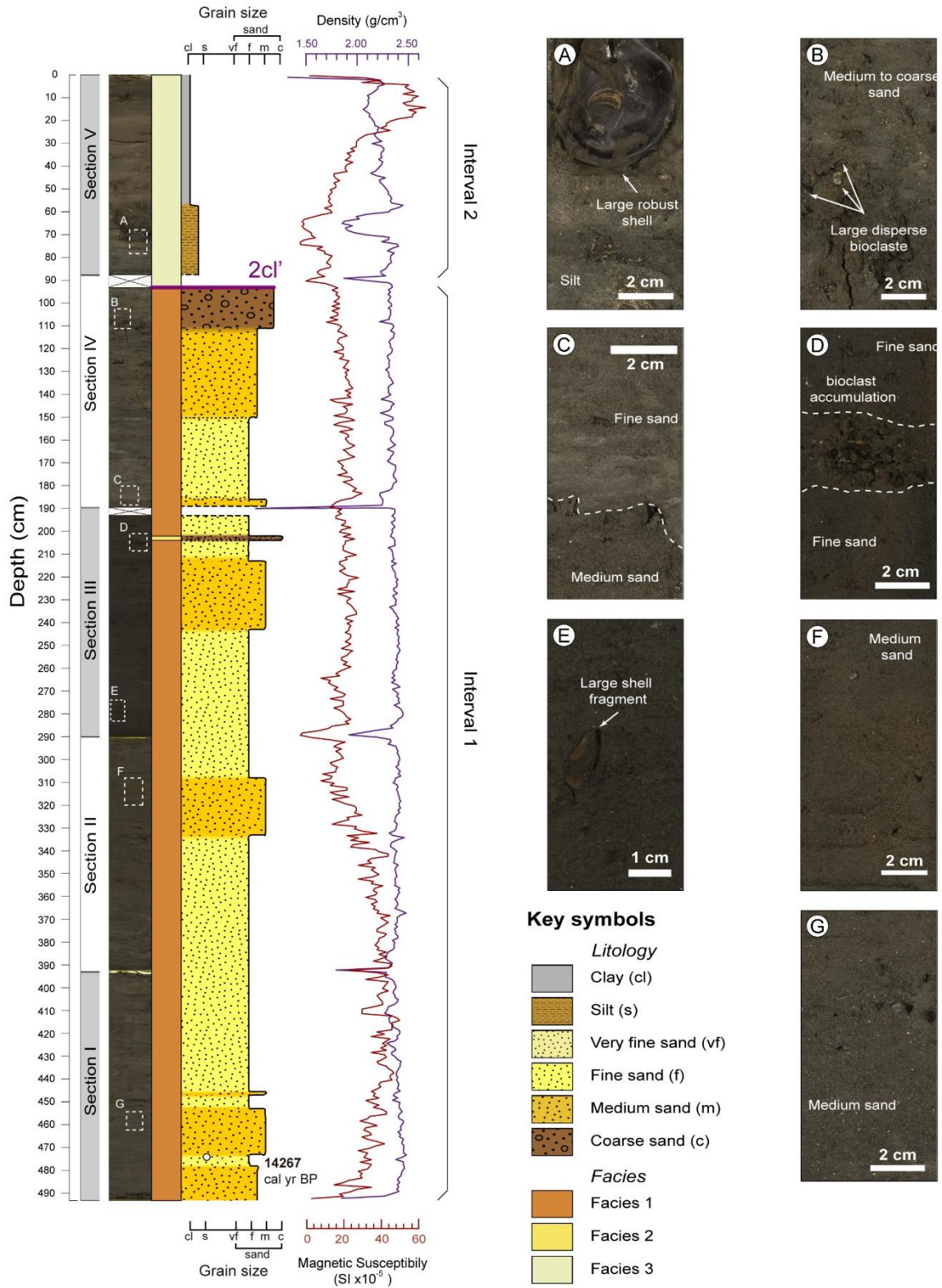


Figure 6.9: Photography, schematic facies, lithological description, control age points, density log, and magnetic susceptibility logs of sediment core LA-48-VC, characterizing seismic unit PTU 2. A) Silts (facies 3) containing a large well-preserved 5 cm *Ostrea* shell; B) Mixture of medium to coarse sand with scattered large bivalve and *Turritella* shell fragments up 2 cm in length; C) Medium to fine sand (facies 1); D) Bioclastic layer hosted in a fine sand interval; E) Massive fine sand of facies 1 including a large bivalve shell; F, G) Massive medium sand.

Episodic deltaic development off the Guadiana River mouth during the postglacial transgression

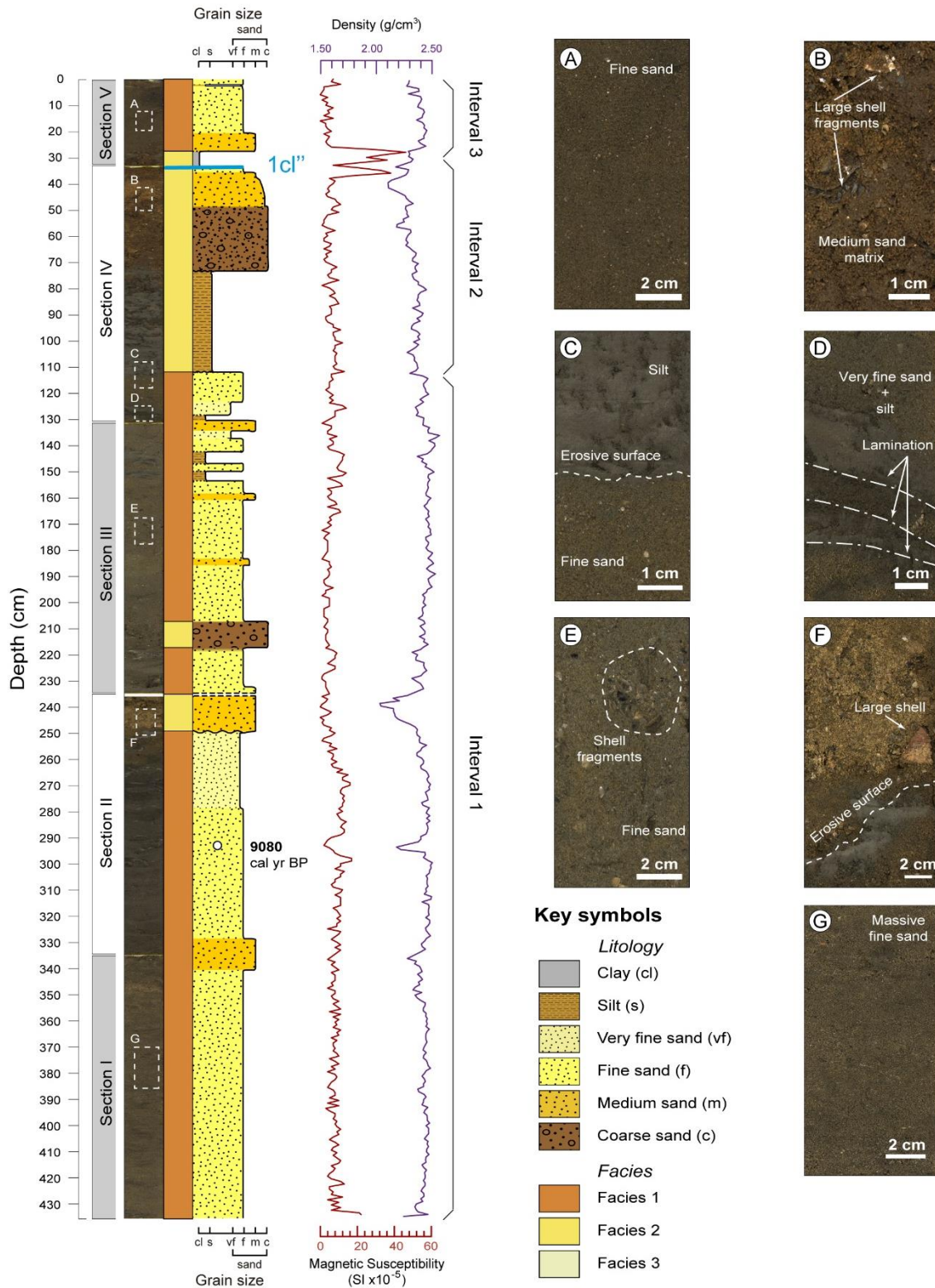


Figure 6.10: Photography, schematic facies, lithological description, control age points, density log, and magnetic susceptibility logs of sediment core LA-18-VC, characterizing seismic unit PTU 1. A) Massive fine sand of facies 1; B) Medium sand of Facies 2 with abundant fragmented bioclasts including *Pecten*; C) Erosional surface between fine sandy (Facies 1) and silty facies (Facies 2); D) Fine to medium sand of facies 1 showing some silt laminations; E) Massive fine sand of Facies 1 including some granule- to pebble-size shell fragments; F) Sandy gravels with bivalves and gastropods including a large shell; G) Massive fine sand of Facies 1.

Table 6.3: AMS radiocarbon data obtained on benthic foraminifera and shells in the studied sediment cores. Ages written in italics point out the anomalous results that provide ages older than expected.

Unit	Core ID	Depth in core (cm)	Sample material	$\delta^{13}\text{C}$ ‰	pMC	Conventional Age ^{14}C BP	cal yr BP (68.3%-1s)	cal yr BP (95.4%-2s)	Median probability ^(a)	Relative area under probability distribution 1.000 ^(c)
PTU1	LA-18-VC	292.3	Shells	4.8 ± 1	34.21 ± 0.21	8620 ± 50	8985 - 9179	8885-9284	9080	1
PTU2	LA-20-VC	8.5	Shells	3.3 ± 0.6	93.11 ± 0.32	575 ± 30	<i>post 1950</i> ^(b)	<i>post 1950</i> ^(b)		
		46	Shell alone	-2.2 ± 0.7	29.69 ± 0.19	9760 ± 60	10409 - 10643	10273-10739	10521	1
	LA-48-VC	475.3	Foraminifera	-5 ± 0.6	20.40 ± 0.18	12740 ± 70	<i>14080 - 14410</i>	<i>13983-14653</i>	<i>14267</i>	<i>1 (68.3%) and 0.992 (95.4%)</i>
PTU3	LA-46-VC	199.5	Shells	-0.5 ± 0.7	27.7 ± 0.19	10310 ± 60	11180 - 11387	11097-11554	11291	1
		199.5	Shells	-1.18 ± 1.5	27.26 ± 0.13	10441 ± 38	11347 - 11586	11255 - 11695	11469	1
	LA-22-VC	136.3	Shells	0.7 ± 0.4	24.42 ± 0.18	11330 ± 60	12604 - 12747	12448-12830	12679	1
		428.9	Foraminifera	-9.7 ± 0.6	6.73 ± 0.13	21670 ± 160	<i>24817 - 25256</i>	<i>24591-25496</i>	<i>25039</i>	<i>1</i>
PTU4	LA-44-VC	226.4	Shell alone	-1.1 ± 0.5	17.04 ± 0.15	14210 ± 80	<i>16202 - 16503</i>	<i>15967-16770</i>	<i>16355</i>	<i>1</i>

(a) Online program Calib.8.2, which uses the marine20.14c calibration dataset recommended for marine samples limited to 603-50,788 14C year BP (Stuiver et al. 2021; Heaton et al. 2020)

(b) No valid radioC age between 603 and 50779 yrs BP for this calibration curve

(c) Heaton et al. 2020.

6.2 Discussion

6.2.1. Development of the Transgressive Stratigraphic Architecture

6.2.1.1 Depositional Environments and Processes

In the study area, the internal organization and seismic facies of each PTU likely represent a succession of distinct depositional systems during each phase of shelf inundation bounded by flooding surfaces (Fig. 6.11).

The bulk of each unit is constituted by wedge-shaped, seaward-prograding clinofolds (i.e., sub-units a). Similar seismic facies have been documented in diverse postglacial transgressive architectures, where they are generically related to prograding bodies (Shinn et al., 2007; Maselli et al., 2011; Engelbrecht et al., 2020) or more specifically to ancient deltaic systems (Gensous and Tesson, 2003; Labaune et al., 2005; Berné et al., 2007). Accordingly, in the study area, such clinofolds are interpreted to represent the establishment of a coastal regime, during which shallow-water, coarse-grained river-dominated deltas formed (Fig. 6.11A). This interpretation is also favored by: 1) the clinofold sedimentary facies, which are predominantly constituted by silty sands; 2) the fact that these transgressive clinofolds were developed seaward of an infilled incised valley attributed to the older course of the Guadiana River (Lobo et al., 2018); and 3) the

Episodic deltaic development off the Guadiana River mouth during the postglacial transgression

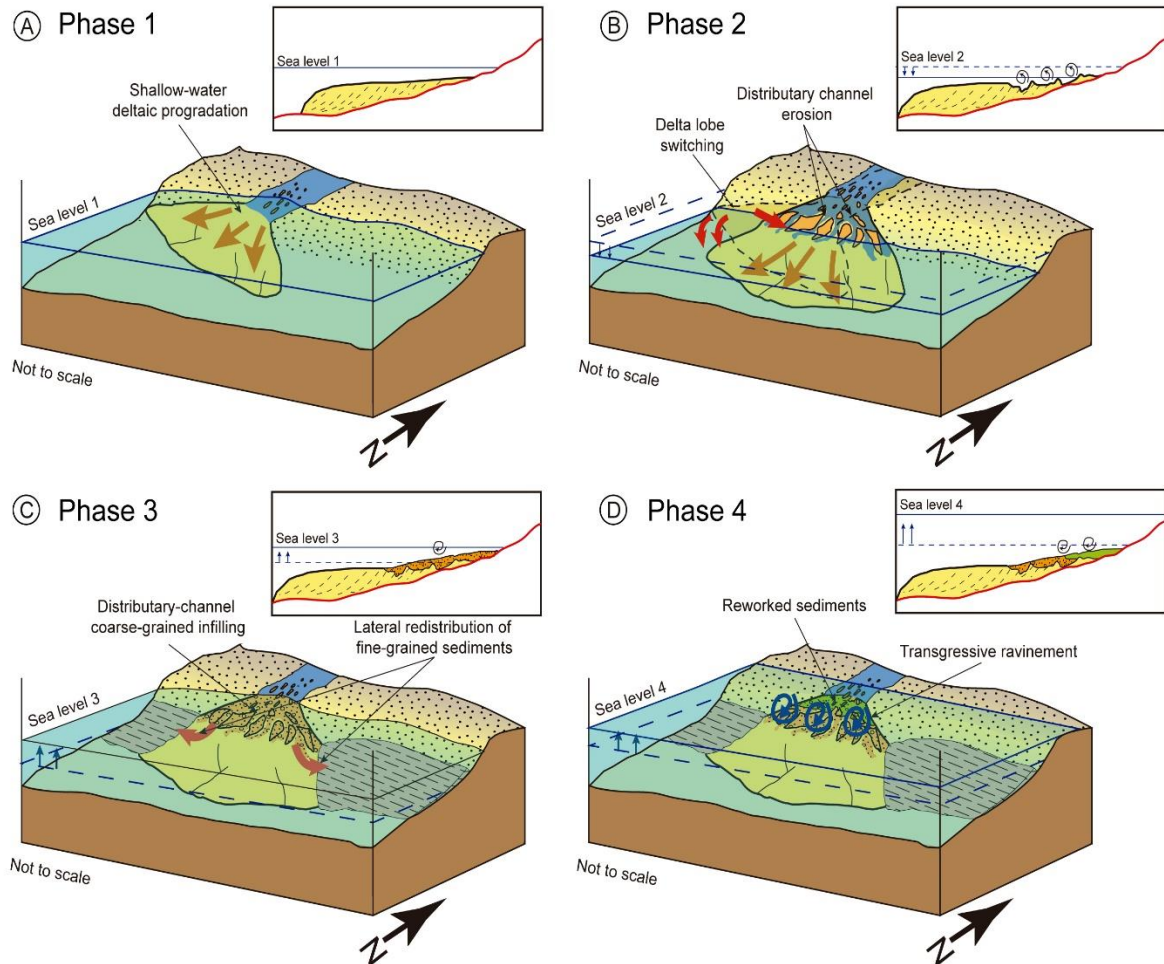


Figure 6.11: Schematic block diagrams and cross sections showing the model of sedimentary evolution proposed for the formation of a generic transgressive deposit associated with the postglacial retreat of the Guadiana River mouth. Dashed lines and blue arrows show the position of sea level in the previous phases. A) Phase of clinoform body development (i.e., *sub-units a*), representing the establishment of a coastal regime, during which shallow-water, coarse-grained river-dominated deltas formed; B) Phase of delta-top distributary-channel formation following construction of transgressive delta; C) Phase of infilling of erosional channels (i.e., *sub-units b*) over the proximal areas of the clinoforms and fine-grained sediment export to construct distal sediment sheets (i.e., *sub-units c*); D) Final evolutionary phase of each transgressive deposit, characterized by shoreface reworking (i.e., *sub-units d*) of the previous fluvio-deltaic depositional system.

ages indicate that the clinoform deposits occurred in a range of water depths up to 15-20 m below contemporaneous sea levels, suggesting that clinoform development may have occurred in shallow-water environments with upward development limited by storm wave base.

Slight differences between the types of clinoforms may be related to the sandier or muddier composition of the deltaic clinoform wedges (i.e., *sub-units a*). Thus, the older clinoforms of PTUs 4 and 3 exhibit shallower slope and lesser amounts of sand; these facies resemble tangential oblique or parallel oblique deltaic progradation characteristic of muddy or moderate sand content clinothermes (e.g., Gökaşan et al., 2005; Pellegrini et al.,

2015; Dyer et al., 2021). In contrast, steeper and sandier clinofolds characteristic of PTUs 2 and 1 seem to be equivalent to constructional phases of sandy deltas, such as those recognized in southeast Africa offshore of the Thukela River (Engelbrecht et al., 2020).

The internal architecture of the deltaic wedges is more complex in some of the seismic units, such as PTUs 2 and 1. These units have lateral bidirectional progradation and internal truncation surfaces, interpreted to be the result of delta lobe switching and abandonment, as is found in southeast Africa transgressive deltaic bodies (e.g., Engelbrecht et al., 2020; Dyer et al., 2021).

The occasional occurrence of infilled erosional channels (i.e., sub-units b) over the proximal parts of the clinofolds is not common in postglacial transgressive architectures. Instead, similar facies are typically attributed to the topsets of lowstand deltaic deposits (Trincardi et al., 1994; Storms et al., 2008). Channel fills in the central parts of depositional bodies formed during transgressive stages have been observed in relation to radial seaward progradation and the development of fan-shaped geometries (Gökaşan et al., 2005; Engelbrecht et al., 2020). These channel units have been interpreted as delta-top distributary channels formed during phases of transgressive delta construction (Dyer et al., 2021). I favor a similar interpretation in the study area (Fig. 6.11B). The stratigraphic position and proximal location of sub-units b, in relation to the underlying clinofolds, drive us to interpret them as distributary channels formed during important normal regressions in an otherwise overall transgressive system.

Semitransparent, sheet-like facies that drape the clinofolds (i.e., sub-units c), extend beyond the edges of the underlying clinofolds. According to our knowledge, this kind of deposit and its stratigraphic relationship with underlying clinofolds is not common in other studies of transgressive deposits. Sub-units c do not completely cover the clinofolds; rather, they onlap laterally, without interfingering, and clearly postdate the clinofolds which would have been fed by the distributary channels. Consequently, a fluvial origin is not likely, and some change in the sediment sources needs to be invoked, so that these deposits can be formed above an inactive delta front. In addition, superimposed bedforms indicative of a mobile carpet (as evidenced in the Gulf of Lions, Bassetti et al., 2006) are not observed; therefore, sub-units c are also not considered to be the product of sediment reworking.

Taking into account the draping geometry and lack of internal reflections, these facies may indicate a low-energy environment dominated by mud, as documented in the South African shelf (Engelbrecht et al., 2020) or the southeastern Yellow Sea (Shinn et al., 2007). Since these sub-units c are found down-dip of the channelized facies (sub-units b), a process of sediment partitioning could have taken place, involving retention of the coarse-grained fraction in the distributary channels, and coeval offshore fine-grained sediment dispersal by the action of oceanographic agents such as waves, tides, and/or currents (Fig. 6.11C). It is proposed that sub-units c could be interpreted as the result of a type of sediment gravity flow induced either by wave (wave-supported gravity flows) or tidal

motions (estuarine fluid muds) (e.g., Parsons et al., 2007). The winnowing of fine-grained sediments in the distributary channels would form sediment plumes in the shelf environment, which would be eventually redistributed laterally by the Gulf of Cadiz Current (Bellanco and Sánchez-Leal, 2016), leading to the generation of extensive mud blankets far beyond the confined location of the deltaic clinoforms.

Upper chaotic facies documented in a number of paleo-deltaic systems are interpreted as sandy bedforms originated from ancient shorelines or delta fronts (e.g., Berné et al., 2007). However, in the study area the uppermost sub-units d in each seismic unit occur over erosional truncations. Truncations on top of underlying clinoforms are interpreted as the product of ravinement (Shinn et al., 2007). The sub-units observed over the truncations closely resemble the pattern identified on several sectors of the Italian shelves, where sheet-like transparent units are interpreted as reworked (lower shoreface) sand sheets (Tortora, 1996). These sheets may develop asymmetric patterns on their tops, interpreted as dunes formed during the reworking of the sandy layer (Masselli et al., 2011). Similarly, in our study area, these upper sub-units are considered as the by-product of the reworking of the original clinoforms during transgressive ravinement (Fig. 6.11D), generating scattered bedforms along the central area of sub-unit 4d (Fig. 6.3).

The observed architectures in the studied PTUs are in agreement with the preservation of both paralic (coastal) and marine components that compose transgressive deposits (Saito, 1994; Tortora, 1996). However, PTUs identified on the Guadiana shelf exhibit a diverse and rich internal stratigraphic organization, unparalleled in many other postglacial transgressive deltaic systems that tend to exhibit, as a general rule, a more monotonous stratigraphy and composition (e.g., Gensous and Tesson, 2003; Maselli et al., 2011)

In the present study, the lower component would be composed of shallow-water deltaic clinoforms and facies associated with the full establishment of fluvio-deltaic depositional systems (seismic facies or sub-units a). The upper chaotic facies with local development of undulations would represent marine deposits as a consequence of transgressive ravinement (seismic sub-units d).

However, in the study area the transition between the deltaic systems and the marine deposits would be more complex than in other transgressive settings. Such transition is represented not only by a wave ravinement surface but also by a significant change of sediment sources involving the dearth of deltaic construction and the establishment of a process of sediment partitioning involving channel infilling and offshore export of fine-grained sediments (seismic sub-units b and c).

6.2.1.2 Implications for Transgressive Development

The postglacial sedimentary record on the Guadiana shelf displays several distinct characteristics in terms of the preservation and internal architecture of individual deposits in transgressive deltaic settings. A number of indications would signal the importance of high sediment fluxes during each transgressive phase. These indications include: 1) an

unusually large number of transgressive deposits; 2) occurrence of proximal infilled channels; and 3) occurrence of delta lobe switching.

Many transgressive shelf-wide settings are low-accumulation settings due to the strong prevalence of transgressive ravinement. As a consequence, Atlantic transgressive settings tend to be composed of erosional morphologies, such as coastal terraces, transgressive lags and bedforms, and/or remnants of coastal deposits such as barriers (e.g., Nordfjord et al., 2009; Cooper et al., 2016; Ximenes Neto et al., 2018; Gomes et al., 2020). Preservation of single transgressive wedges has been reported on the New Jersey shelf (Nordfjord et al., 2009) and the Galician shelf (Lantzsch et al., 2010). The dominance of transgressive ravinement may even occur on wide shelves, where the development of deltaic deposits in the transgressive systems tract is also uncommon (Puchała et al., 2011).

Transgressive packages also exhibit low preservation potential of deltaic deposits on shelves fed by short, mountainous streams such as the Californian shelf (Spinelli and Field, 2003; Hogarth et al., 2012). There, clinof orm wedges of restricted distribution have been identified in specific sectors (Grossman et al., 2006; Klotsko et al., 2015). Also, the well-studied transgressive record of the South African shelf is strongly dominated by nondeltaic shoreline-connected deposits (e.g., Pretorius et al., 2019; Green et al., 2020). However, in river-dominated sectors of the southeastern African shelf, several phases of transgressive deltaic progradation have been reported to occur intercalated within the major postglacial shelf flooding phases (Engelbrecht et al., 2020; Dyer et al., 2021).

Significant development of transgressive deltaic deposits in water depths equivalent to those of the study area, and with transgressive ages younger than 14.5 ka, is found only in several Mediterranean settings. These settings are regarded as ideal delta-forming environments, due to the sediment supply conditions and redistribution of river-borne sediments by oceanographic processes (Anthony et al., 2014). For example, three individual deposits have been described in the Gulf of Lions (Gensous and Tesson, 2003; Labaune et al., 2005) and two to three individual transgressive deposits in the Adriatic Sea (Storms et al., 2008; Maselli et al., 2011).

In comparison to all those settings, the number (four) of transgressive deposits identified in the middle to inner shelf setting of the study area seems to be higher, and would imply faster responses of the Guadiana fluvial system to external driving factors in comparison to the sedimentary response of larger fluvial systems, such as the Po or the Rhône river systems. Other stratigraphic evidence that suggests a significant influence of fluvio-deltaic processes include the presence of proximal distributary channels on top of the clinof orms and identification of delta switching processes in the younger PTUs. The identification of delta-top distributary channels in postglacial transgressive architectures has been related with extensive periods of delta progradation under normal regressive conditions (Dyer et al., 2021). That interpretation is favored in the study area, because these distributary channels are identified in PTUs 4 and 3, whose formation is related to a prolonged sea-level slowdown (see subsequent discussion about sea-level change trends).

Delta lobe switching and abandonment occurring in an overall transgressive context can be produced by pure autocyclic processes, due to lateral shifting of river courses (Berné et al., 2007; Zecchin et al., 2015; Dyer et al., 2021). However, such a hypothesis cannot be tested in the study area, because evidences of delta lobe switching are restricted to the younger PTUs 2 and 1, where preserved distributary channels are not found. Alternatively, delta lobe switching has also been related to changing sediment fluxes to the deltaic realm due to variations in the frequency and magnitude of flood events driven by transitions between humid and dry climates (Berné et al., 2007; Dyer et al., 2021). A similar interpretation could be valid for PTUs 2 and 1, since their formation is roughly coeval with a period of increased frequency of large-magnitude floods after the Younger Dryas event in southern Iberia (more details in a subsequent discussion about the role of sediment fluxes).

Another significant difference between the postglacial record of the Guadiana shelf and most Mediterranean settings, which exhibit similar arrangements of transgressive stacking patterns, is the formation of reworked facies overlying prodeltaic clinoforms. In most Mediterranean examples, these facies are poorly documented at the seismic scale (e.g., Gensous and Tesson, 2003; Berné et al., 2007; Maselli et al., 2011). This significant difference could be explained by considering the oceanographic setting. Several facts would account for the distinctive influence of the oceanographic regime in the Gulf of Cadiz:

a) In the present-day Gulf of Cadiz, wave remobilization may extend to several tens of meters water depths (e.g., Dolbeth et al., 2007; Gutiérrez-Mas et al., 2009).

b) The estimated water depth of the Gulf of Cadiz transgressive clinoforms, in relation to coeval sea levels, indicate wave-base levels 10-20 m deep.

c) The Guadiana shelf clinoforms exhibit an heterolithic coarse-grained composition, in contrast to other Mediterranean clinoforms, which tend to be finer-grained (Pellegrini et al., 2015).

d) The elongated depocenters of each unit, specially marked in PTUs 4 and 3, would attest to the influence of an active shelf current circulation, represented at present day by the dominant Gulf of Cadiz Current (Bellanco and Sánchez-Leal, 2016).

Therefore, the sedimentary architecture of the postglacial transgressive deposits in the Guadiana shelf area resulted from the combination of relatively significant fluvial sediment fluxes and a wave-dominated setting with active along-shelf currents, in contrast to most Mediterranean settings where: 1) possibly, the larger drainage basins were less dynamic in their sedimentary response; and 2) hydrodynamic conditions were of lower energy. As a consequence, the observed architecture of the postglacial transgressive deposits is more compatible with a transgressive submergence process rather than with a process of in-place drowning (i.e., overstepping), which seems to be the preferential mechanism in transgressive records dominated by the preservation of barriers and associated deposits (e.g., Pretorius et al., 2019; Green et al., 2020).

6.2.2. Chronological Framework of the Postglacial Transgression: Implications for Driving Processes

6.2.2.1 The Importance of Sea-Level Change Trends

The occurrence of each phase of transgressive development and the sea-level pattern in continental shelves shows a great diversity around the world. In general terms, under the absence or scarcity of age control, depths of occurrence of transgressive deposits or shorelines are compared with the glacio-eustatic stepped sea-level rise (Fig. 6.12). With such constraints, major phases of clinoform development are assumed to be related with periods of reduced sea-level rise or stillstands (Zecchin et al., 2015) such as the Younger Dryas (Gensous and Tesson, 2003; Boyer et al., 2005; Berné et al., 2007; Maselli et al., 2011), or during steps punctuating MWP (Zecchin et al., 2015; Engelbrecht et al., 2020; De Santis et al., 2020; Dyer et al., 2021). In wave-dominated settings, shoreline complexes have also been related to sea-level stability (Green et al., 2014). Under that scheme, major periods of shelf drowning are supposed to be driven by periods of enhanced sea-level rise, such as MWP-1A and 1B (Fig. 6.12) (Pellegrini et al., 2015; Green et al., 2014; Zecchin et al., 2015).

However, the development of transgressive deposits also occurs during moderately high rates of sea-level rise (up to 10 mm/year). This occurs during the sea-level rise postdating the Younger Dryas (Berné et al., 2007) and during the sea-level deceleration after MWP-1B (Fig. 6.12) (Gensous and Tesson, 2003; Boyer et al., 2005; Storms et al., 2008; Schattner et al., 2020; Maselli et al., 2011; De Falco et al., 2015).

In the most extreme cases, the development of transgressive deposits has even been related to periods of sustained sea-level rises with rates up to 60 mm/year during the MWP-1A (Fig. 6.12). For example, coastal barrier-lagoon systems (Storms et al., 2008; De Santis et al., 2020) and prograding bodies (Maselli et al., 2011) have been reported in the Adriatic Sea, and low-energy marine deposits in the Gulf of Lions (Labaune et al., 2005). In California, the generation of a clinoform wedge was also related to the abrupt sea-level rise of MWP-1B (Fig. 6.12) (Grossman et al., 2006).

The formation of the studied PTUs 4 to 1 is framed by the overall sea-level rise in the 14-9 ka interval (Fig. 6.12). In general, most of the ages exhibit a coherent pattern; however, some anomalous results provide ages older than expected, with values located well above the contemporary sea-level positions (Fig. 6.12; Table 6.3). One of the anomalous results corresponds with the age value of PTU 4 (16.3 ka; Fig. 6.12; Table 6.3), which is considerably older than the termination age of preceding PTU 5, framed between 13.8 and 14.3 ka (Lobo et al., 2015). The ages of the younger PTU 3 between 11.2 and 12.7 ka are in agreement with a genesis during the Younger Dryas event, a period of reduced sea-level rise (Fig. 6.12; Table 6.3). Consequently, it is inferred that the formation of PTU 4 occurred between 12.7 and 13.8 ka, possibly during MWP-1A but after the phase of accelerated sea-level rise between 14.5 and 14 ka (Stanford et al., 2011; Lambeck et al., 2014). Conversely, the

Episodic deltaic development off the Guadiana River mouth during the postglacial transgression

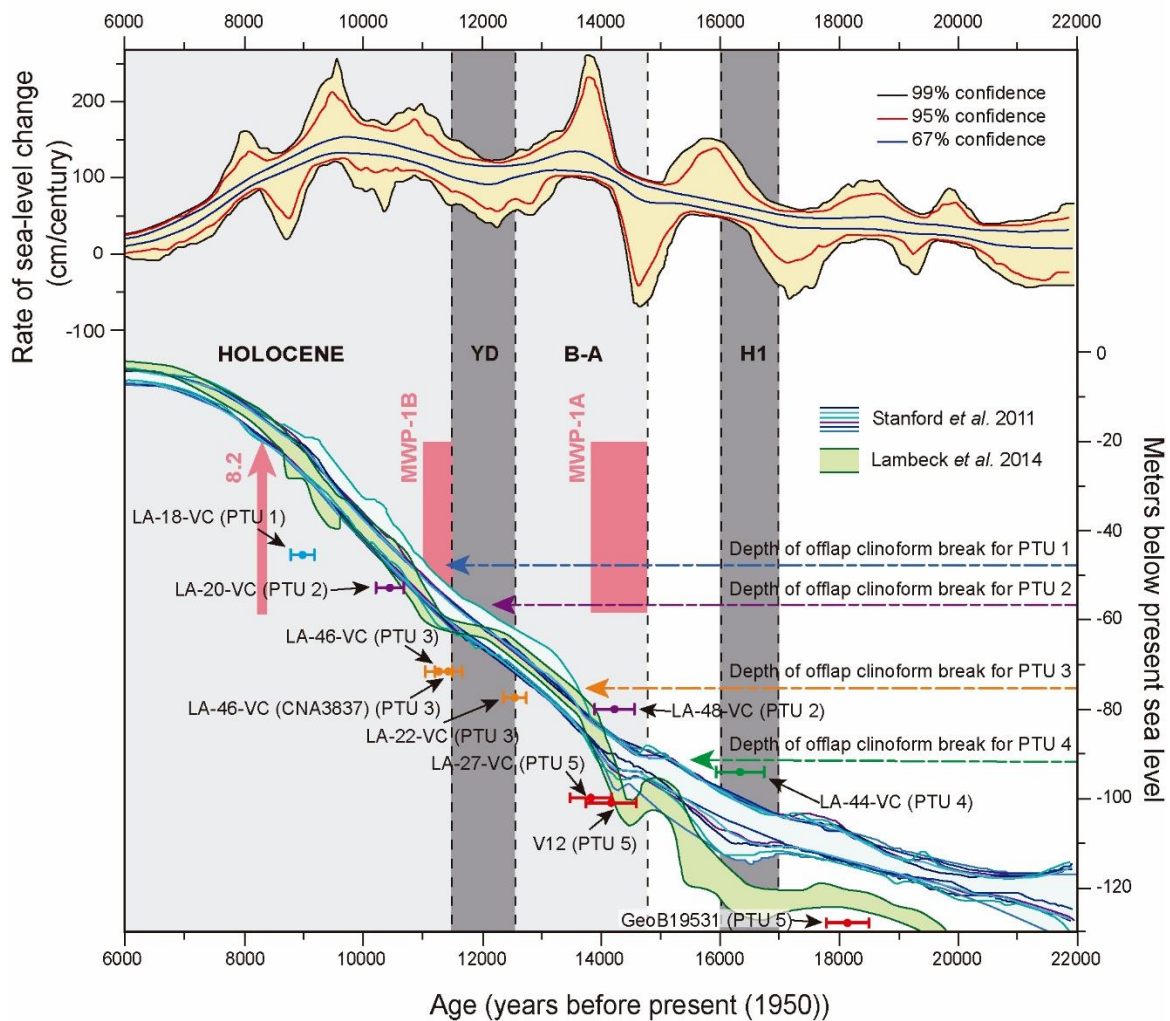


Figure 6.12: Proposed chronology of transgressive seismic units (including ages of PTU 5 after Lobo et al., 2015) and correlation with the postglacial sea-level pattern (rate of sea-level change above and amplitude of sea-level change below). The major climatic events include: Heinrich Event 1 (H1), the Bølling–Allerød warm period (B-A) and the Younger Dryas (YD) cold period, as well as the timing of Melt-Water Pulses (MWP) 1A and 1B and the 8.2 ka cooling event (in red). Plotted ages are named taking into account the coring site, the coring technique (VC stands for vibro coring), and the name of the seismic unit in which the samples were taken. The estimated water-depth locations of the Gulf of Cadiz transgressive clinoforms in relation to coeval sea levels are also indicated.

ages of the most recent PTUs (2 and 1) would place them in a period of high rates of sea-level rise during MWP-1B, between 11.5 and 8.8 ka (Stanford et al., 2011).

The proposed chronological framework supports the idea that PTUs 4 and 3 are genetically related, and that PTUs 2 and 1 are also genetically related. Thus, the formation of PTUs 4 and 3 possibly took place in an interval bracketed by two periods of very high sea-level rise during MWPs-1A and 1B, when rates of sea-level rise were generally lower than 15 mm/year (Stanford et al., 2011). Therefore, these two units are related to a period of deceleration or slowdown during the deglaciation that culminated in the Younger Dryas event. This is similar to other transgressive settings such as the Gulf of Lions or the Adriatic

Sea (Gensous and Tesson, 2003; Maselli et al., 2011). These periods of reduced sea-level rise are assumed to be related to major phases of clinoform development (Zecchin et al., 2015). This is compatible with our observations, since these two older transgressive units exhibit more elongated patterns, wider distribution and a finer-grained composition than the two younger units, suggesting genetic conditions favorable for clinoform development.

In contrast to the sea-level conditions of the older transgressive deposits, the two more recent PTUs (2 and 1) are assumed to be related to an overall period of enhanced sustained sea-level rise during MWP-1B, with rates of sea-level change of around 20 mm/year and even higher (Stanford et al., 2011). This connection with high rates of sea-level rise is also reflected in the geometry and composition of such units, which are more confined and exhibit higher percentages of sands than the older transgressive deposits.

6.2.2.1 The Role of Sediment Fluxes in the River Basin

As discussed above, the formation of PTUs 2 and 1 seems to be related with high rise rates of sea level. Indeed, under such circumstances, major increases in sediment supply may guide the formation of postglacial transgressive deposits rather than the primary control of sea-level changes. These changes in sediment flux might have been the result of rapid climatic changes (Berné et al., 2007; Labaune et al., 2008) influencing vegetation cover and subsequently the total discharge (Maselli et al., 2011). Other interpretations stress the importance of: 1) antecedent slope and geology, as they may influence the rate of transgression and the ravinement processes, particularly in transgressive systems composed mainly of barriers (Storms et al., 2008; Pretorius et al., 2016); and 2) uplift rates greater than sea-level rise rates (Grossman et al., 2006; Hogarth et al., 2012).

Assuming preferential development during conditions of rapid sea-level rise, phases of increased precipitation and sediment input have been invoked to trigger the development of deltaic deposition during transgressive intervals (Puchała et al., 2011). Specifically, phases of enhanced sediment supply could have been fostered by meltwater pulses (Labaune et al., 2008; Lebreiro et al., 2009). With relevance for the study area, periods of increased fluvial activity in Spain related to anomalous rainfall (Trigo and DaCamara, 2000) extend back to the postglacial transgression. In fact, the two older periods of increased frequency of large-magnitude floods postdate the Younger Dryas event (10.75-10.24 and 9.62-8.785 ka) (Thorndycraft and Benito, 2006; Benito et al., 2008). The increase in flood frequency after the Younger Dryas event has been related to large-scale atmospheric circulation changes and climatic transitions (Benito et al., 2008) in relation to the return of westerly storm tracks to Iberian latitudes (Thorndycraft and Benito, 2006). After these two main flooding periods, a hiatus in the paleoflood record until 2.9 ka, with no major increases in the flood frequency, has been reported (Thorndycraft and Benito, 2006).

These flooding phases probably involved spatially diverse climatic trends, with colder and more arid climates in central Iberia and more temperate and humid in western

(Morellón et al., 2018), southwestern (Dorado Valiño et al., 2002), and southern (Mesa-Fernández et al., 2018) Iberia. In fact, the period between 10.8 and 7 ka is regarded as dominated by increasingly humid conditions in western and southern Iberia, with enhanced runoff inputs interrupted by arid events (Carrión, 2002; Rodrigues et al., 2009, 2010; Mesa-Fernández et al. 2018; Morellón et al., 2018).

At a smaller scale and with relevance for the present study, expansions and declines of forests in the Guadiana Estuary since 13 ka provide indications of climatic variability. Temperate to warm, moist climates occurred during the Allerød interstadial and between 9 and 5 ka. Drier conditions were prevalent during the Younger Dryas and the early Holocene (Fletcher et al., 2007). These general climatic conditions in SW Iberia seem to be in agreement with our chronostratigraphic scenario, assuming that sediment supply in the southern Iberian Peninsula is strongly driven by rainfall during humid periods because the land vegetation cover is scarce. Thus, the formation of PTUs 2 and 1 were dated postdating the Younger Dryas event to humid climates prevailing in SW Iberia, and by extension, in the Guadiana drainage basin. Conditions of increased humidity during the early Holocene after the Younger Dryas event possibly accentuated allocyclic processes, leading to channel abandonment and delta lobe switching during the younger PTUs. Also in the Guadiana Estuary, an accelerated phase of infilling by clayey sediments was initiated at ca. 9.8 ka (Boski et al., 2002). This trend also seems to be compatible with the transgressive record on the shelf, since the formation of PTUs 2 and 1, which exhibit a sandier composition than the older transgressive deltas, occurred at the timing of fine-grained sediment trapping in the estuary.

CHAPTER

7

CHAPTER 7:

Conclusions/*Conclusiones*

7.1 Conclusions

The results and subsequent discussions presented across the three main chapters of this PhD thesis reveal a comprehensive understanding of the formation of incised valleys and transgressive deposits. The integration of diverse fluvial sources, consideration of sedimentary dynamics, and recognition of the influence of antecedent topography collectively contribute to a better comprehension of the controlling factors that drove the evolution of these systems in response to late Quaternary glacio-eustatic changes. These insights provide a foundation for future research into sedimentary processes. The thesis has addressed its overarching aim by drawing the following conclusions related to each specific objective in each chapter:

Conclusions of Chapter 4: Incised valleys on the Algarve Shelf

- Seismic stratigraphic evidence correlated with age-constrained regional stratigraphic horizons and limited recent sediment data have revealed the existence of a network of incised valleys off the Gilão-Almargem Estuary, a small fluvial drainage system in the eastern Algarve shelf, northern margin of the Gulf of Cadiz. The occurrence of such sediment routing system mostly limited to the paleo-inner shelf likely reveals the operation of distinct driving factors modulating the primary glacio-eustatic factor, usually considered as the primary control on incised-valley development, and enabling the formation of abundant incised valleys in a currently low supply setting.
- The dendritic inner-shelf valley network shows no signs of tectonic control. A number of stratigraphic evidences drive us to interpret the inner-shelf paleovalleys as a simple system formed during the last glacial cycle; fluvial incision is likely to have occurred during falling sea-level leading into the Last Glacial Maximum, whereas the incised valley infill took place during the postglacial transgression. The stratigraphic architecture reveals the frequent occurrence of coarse-grained sediment bodies like estuarine bars, estuary-mouth sand plough, and coastal barriers, and a second phase of incision interpreted as tidal inlets/channels. Its inner location strongly suggests that at least the recent phase of infilling is Holocene in age.
- The formation of the inner shelf paleovalleys was strongly determined by background geology, where the occurrence of a flat, lithified paleo-inner shelf bounded seaward by a break of slope conditioned the formation of small-sized incised valleys. Subsequently, the infilling of the valleys took place under a context of high rates of sea-level rise and limited fluvial supply at the start of the Holocene. The paleogeographic

configuration during this final phase of the postglacial transgression likely involved the development of a dendritic system, with numerous barriers interrupted by tidal inlets or scours in a mixed estuarine system.

Conclusions of Chapter 5: Incised valleys on the Guadiana shelf

- The studied incised valleys exhibit amalgamated stratigraphic architectures influenced by glacio-eustatic cycles, underlying geology, and sediment supply dynamics. The long-term stratigraphic architecture of the studied incised valleys, particularly their compound nature with up to five incision phases, is attributed to valley reoccupation in response to 100 ka glacio-eustatic sea-level cycles. The complex valley architecture and their physiographic location are compatible with the existence of a link between phases of valley incision and distal development of shelf-margin deltaic wedges; therefore, the studied valleys constitute key pathways enabling the sediment transfer toward the distal shelf domain, contributing to the long-term margin growth. In spite of the overarching sea-level influence, the two studied valleys display distinct reoccupation and infilling patterns within a relatively small geographic area. The main valley adjusted via lateral avulsion in response to high-energetic fluvial events, with preferential preservation of fluvial channel deposits; in contrast, the eastern valley exhibits a multi-storey pattern that would indicate the periodic reestablishment of estuarine conditions.

- The straight plan-view morphology of the paleovalleys is influenced by the underlying geology and the contrast between an indurated inner shelf and a more erodible middle to outer shelf. Differences in cross-sectional shapes, with the main valley exhibiting a V-shape and the eastern valley a U-shape, are likely attributed to underlying structure, lithology, and hydrodynamics, possibly indicating distinct sediment transport and depositional dynamics. The arrangement of the two valleys likely resembles the present-day coastal pattern constituted by the Tinto and Odiel rivers, with the occurrence of a main fluvial valley and a tributary valley coalescing near the coastline.

- The patterns of postglacial infilling also exhibit significant differences, evidencing the operation of different governing agents. The post-LGM infilling of the Guadiana main valley comprises fluvio-deltaic, estuarine, and shallow-water deposits, revealing distinct sedimentary conditions during its development. The dominance of laterally accreting clinofolds and seaward correlation with shallow-water deltas suggests strong fluvial dominance irrespective of the sea-level trend. In contrast, the infilling of the Guadiana eastern valley is simpler with estuarine and shoreface-shelf depositional systems, highlighting variability in sediment supply and hydrodynamics during its development. The eastern valley is mainly filled by transgressive sediments, which indicates smaller sediment input and hydrodynamic control. This stratigraphic variability could be assigned to the establishment of a coastal system where the main valley would provide most of the sediment supply, which would be laterally redistributed by eastward-directed coastal

dynamics, enabling the generation of coastal barriers at the mouth of the eastern valley, with subsequent development of low-energy conditions in the back barrier setting. Besides, the stratigraphic arrangement along the length of the main valley evidences the physical continuity between the estuarine infilling of the valley and the offshore transgressive stratigraphy, emphasizing the role of antecedent morphology in influencing the distribution of estuarine facies.

Conclusions of Chapter 6: Episodic deltaic development off the Guadiana River mouth during the postglacial transgression

- The rich stratigraphic architecture of four postglacial transgressive units (PTUs) recognized in the northern margin of the Gulf of Cadiz off the Guadiana River reveals the occurrence of several major phases of development, indicating a high variability in the driving factors in the Gulf of Cadiz; in contrast, many other postglacial transgressive settings tend to be largely dominated by a prevailing controlling factor, such as fluvial sediment supply, hydrodynamic activity, or antecedent topography, resulting in generally more homogeneous sedimentary processes and products.

- The initial phase was the establishment of shallow-water, coarse-grained, river-dominated deltas. These deltas were subsequently eroded by distributary channels formed during normal regressions, punctuating the overall transgressive interval. Transitional phases between normal regressions and resumed transgressions involved the filling of distributary channels and the offshore export and lateral redistribution of fine-grained sediments due to enhanced hydrodynamic activity. The last phase was driven by shoreface reworking of previous fluvio-deltaic depositional systems and the formation of wave-ravinement surfaces. The sedimentary architecture of the postglacial transgressive deposits on the Guadiana shelf involves both enhanced deposition as well as subsequent preservation of reworked facies. This stratigraphic pattern likely resulted from the combination of relatively significant sediment fluxes generating normal regressions during different rates of sea-level rise and an active oceanographic regime with wave and/or tidal reworking in the nearshore and along-shelf redistribution by currents. As a result, the observed transgressive architectures are best explained by a transgressive submergence process.

- The formation of PTUs located on the Guadiana Shelf is framed within the 14-9 ka interval; the chronostratigraphic framework provides important clues to the variable influences of controlling factors of transgressive development, suggesting that both rates of sea-level rise and sediment fluxes played significant yet contrasting roles. Thus, the older PTUs (4 and 3) seem to be related to periods of reduced sea-level rise, such as the terminal part of MWP-1A and the Younger Dryas event. Meanwhile, the younger PTUs (2

and 1) are related with the MWP-1B, a period of high rate of sea-level rise during the deglaciation.

- The genesis of PTUs 2 and 1 is attributed primarily to the overall climatic conditions established in SW Iberia after the Younger Dryas that triggered significant changes in sediment supply in the river basin. Those phases of enhanced sediment supply probably resulted from increased rainfall runoff during humid periods and scarce land vegetation cover.

- The prevailing influence of those controlling factors has been modified through time, and is reflected in the morphology, distribution patterns, and lithologies of PTUs. Thus, more extended deposit distributions and fine-grained compositions tend to occur during enhanced sea-level dominance. In contrast, more confined distributions and coarse-grained compositions seem to be the result of enhanced sediment fluxes.

7.2 Conclusiones

Los resultados y discusiones presentados a lo largo de los tres capítulos que conforman el grueso de esta tesis doctoral revelan una comprensión integral de la formación de valles encajados y depósitos transgresivos. La integración de distintas fuentes fluviales, la consideración de las distintas dinámicas sedimentarias y el reconocimiento de la influencia de la topografía antecedente contribuyen colectivamente a una mejor comprensión de los factores que controlaron la evolución de estos sistemas en respuesta a los cambios glacio-eustáticos durante el Cuaternario tardío, sentando las bases para futuras investigaciones sobre procesos sedimentarios. La tesis ha abordado sus objetivos generales extrayendo las siguientes conclusiones relacionadas con cada objetivo específico en cada capítulo:

Conclusiones del Capítulo 4: Incised valleys on the Algarve inner shelf

- Una amplia red de valles encajados frente al estuario de los ríos Gilão y Almargem, un pequeño sistema de drenaje fluvial situado en la plataforma este del Algarve, en el margen norte del Golfo de Cádiz, ha sido caracterizada a través de una detallada interpretación sísmica junto con datos de testigos de sondeos y correlacionada con superficies estratigráficas regionales. La presencia de dicho sistema de transferencia de sedimento, principalmente limitado a la plataforma interna, sugiere la interacción conjunta de distintos factores de control secundarios que han modulado los cambios glacio-eustáticos, habitualmente considerados como el control primario en el desarrollo de los valles encajados. Como consecuencia de dicha interacción, se ha posibilitado la formación y preservación de dichos valles en un contexto actualmente con bajo aporte de sedimento.

- La red dendrítica de valles encajados en la plataforma interna no muestra signos de control tectónico. Diversas evidencias estratigráficas nos llevan a interpretar los paleovalles de la plataforma interna como un sistema simple formado durante el último ciclo glacial; la incisión fluvial probablemente ocurrió durante el descenso del nivel del mar que condujo al Último Máximo Glacial, mientras que el relleno de los valles encajados tuvo lugar durante la transgresión postglacial. La arquitectura estratigráfica revela la frecuente presencia de cuerpos sedimentarios de grano grueso, como barras estuarinas o barreras costeras, y una segunda fase de incisión interpretada como canales mareales. Su ubicación fisiográfica sugiere firmemente que al menos la fase reciente de relleno es de edad Holocena.

- La formación de los paleovalles de la plataforma interna estuvo determinada por la geología previa, donde la presencia de una paleo-plataforma interna litificada y de baja inclinación, limitada hacia el mar por una ruptura de pendiente, condicionó la formación de valles encajados de pequeño tamaño. Posteriormente, el relleno de los

valles tuvo lugar en un contexto de altas tasas de subida del nivel del mar y aporte fluvial muy limitado al inicio del Holoceno. La configuración paleogeográfica durante esta fase final de la transgresión postglacial probablemente implicó el desarrollo de un sistema dendrítico, con numerosas barreras interrumpidas por canales o surcos de marea en un sistema estuarino mixto.

Conclusiones del Capítulo 5: Valles encajados en la plataforma del Guadiana

- Los valles encajados estudiados en la plataforma frente al río Guadiana exhiben arquitecturas estratigráficas amalgamadas influenciadas por los ciclos glacio-eustáticos, la geología previa y la dinámica de aporte de sedimentos. La arquitectura estratigráfica a largo plazo de los valles encajados estudiados, en particular su naturaleza compuesta con hasta cinco fases de incisión, se atribuye a la reocupación de los valles en respuesta a ciclos glacio-eustáticos del nivel del mar de 100 ka. La compleja arquitectura de los valles y su ubicación fisiográfica son compatibles con la existencia de una conexión entre las fases de incisión del valle y el desarrollo distal de cuñas deltaicas en la plataforma media y externa; por lo tanto, los valles estudiados constituyen vías clave que permiten la transferencia de sedimentos hacia el dominio distal de la plataforma, contribuyendo al crecimiento a largo plazo del margen. A pesar de la influencia generalizada del nivel del mar, los dos valles estudiados muestran patrones distintos de reocupación y relleno dentro de un área geográfica relativamente pequeña. El valle principal se ajustó mediante procesos de avulsión lateral en respuesta a eventos fluviales de alta energía, con la preservación preferencial de depósitos de canales fluviales; en cambio, el valle oriental exhibe un patrón de apilamiento vertical varios niveles que indicaría el restablecimiento periódico de condiciones estuarinas.

- La morfología en planta recta de los paleovalles está influenciada por la geología previa y el contraste entre una plataforma interna litificada y una plataforma media y externa más erosionable. Las diferencias morfológicas de las secciones transversales, con el valle principal en forma en V y el valle oriental en forma en U, se atribuyen probablemente a la estructura subyacente, la litología y la hidrodinámica, lo que posiblemente indica diferentes dinámicas de transporte y depósito de sedimentos. La disposición de los dos valles se asemeja al patrón costero actual constituido por los ríos Tinto y Odiel, caracterizado por un valle fluvial principal y un valle tributario que confluyen cerca de la costa.

- Los patrones de relleno postglacial también presentan diferencias significativas que evidencian la acción de diferentes agentes de control. El relleno postglacial del valle principal del Guadiana comprende depósitos fluvio-deltaicos, estuarinos y de aguas someras, los cuales indican condiciones sedimentarias distintas durante su desarrollo. La predominancia de clinofomas que acrecionan lateralmente y la correlación hacia el mar con deltas de aguas someras sugieren un fuerte dominio fluvial independientemente de

la tendencia de variación del nivel del mar. En cambio, el relleno del valle oriental del Guadiana es más simple, con sistemas deposicionales estuarinos y costeros, lo que pone de manifiesto la variabilidad en el aporte de sedimentos y las condiciones hidrodinámicas durante su desarrollo. El valle oriental está principalmente relleno con sedimentos transgresivos, lo que indica un menor aporte fluvial y un control hidrodinámico. Esta variabilidad estratigráfica podría atribuirse al establecimiento de un sistema costero donde el valle principal proporcionaría la mayor parte del aporte de sedimentos, los cuales serían redistribuidos lateralmente por la dinámica costera hacia el este, permitiendo la generación de barreras costeras en la desembocadura del valle oriental y el posterior desarrollo de condiciones de baja energía en el ambiente de tras-barrera. Además, la disposición estratigráfica a lo largo de la longitud del valle principal evidencia la continuidad física entre el relleno estuarino del valle y la estratigrafía transgresiva mar adentro, destacando el papel de la morfología previa en la distribución de las facies estuarinas.

Conclusiones del Capítulo 6: Desarrollo deltaico episódico en la desembocadura del río Guadiana durante la transgresión postglacial

- La diversa arquitectura estratigráfica de cuatro unidades transgresivas postglaciales (UTP) reconocidas en el margen norte del Golfo de Cádiz frente al río Guadiana muestra la ocurrencia de varias fases principales de desarrollo, indicando una alta variabilidad en los factores de control en el Golfo de Cádiz; en cambio, muchos contextos transgresivos postglaciales tienden a estar ampliamente dominados por un factor de control predominante, como el aporte de sedimento fluvial, la actividad hidrodinámica o la topografía antecedente, lo cual da lugar a procesos y productos sedimentarios generalmente más homogéneos.

- La fase inicial fue determinada por el establecimiento de deltas de grano grueso dominados por la acción fluvial en aguas someras. Estos deltas fueron posteriormente erosionados por canales distributarios formados durante regresiones normales, interrumpiendo el intervalo transgresivo general. Las fases de transición entre regresiones normales y la recuperación de las transgresiones implicaron el relleno de los canales distributarios y la exportación y redistribución lateral de sedimentos finos mar adentro debido a una mayor actividad hidrodinámica. La última fase fue impulsada por el retrabajamiento de los sistemas fluvio-deltaicos previos y la formación de superficies de retrabajamiento por la acción del oleaje. La arquitectura sedimentaria de los depósitos transgresivos postglaciales en la plataforma del Guadiana implica tanto un mayor depósito como la posterior preservación de facies retrabajadas. Este patrón estratigráfico probablemente fue el resultado de la combinación de flujos de sedimentos particularmente significativos que generaron regresiones normales durante diferentes tasas de aumento del nivel del mar y un régimen oceanográfico activo con

retrabajamiento por olas y/o mareas en la zona litoral y redistribución a lo largo de la plataforma por corrientes. Como resultado, las arquitecturas transgresivas observadas se explican mediante un proceso de sumersión transgresiva.

- La formación de las UTP ubicadas en la Plataforma del Guadiana se enmarca en el intervalo de 14 a 9 ka; el marco cronoestratigráfico proporciona indicios importantes sobre las influencias variables de los factores de control del desarrollo transgresivo, sugiriendo que tanto las tasas de ascenso del nivel del mar como los flujos de sedimentos desempeñaron roles significativos, aunque contrastados. Así, las UTP más antiguas (4 y 3) parecen estar relacionadas con períodos de menor subida del nivel del mar, como la parte terminal del *MWP-1A* y el evento del Dryas Reciente. Por su parte, las UTP más recientes (2 y 1) están relacionadas con el *MWP-1B*, un período de alta tasa de aumento del nivel del mar durante la deglaciación.

- La génesis de las UTP 2 y 1 se atribuye principalmente a las condiciones climáticas generales establecidas en el suroeste de Iberia después del Dryas Reciente que provocaron cambios significativos en el aporte de sedimentos en la cuenca fluvial. Esas fases de mayor aporte de sedimento probablemente resultaron del aumento de la escorrentía de lluvia durante períodos húmedos y de la escasa cobertura vegetal.

- La influencia predominante de esos factores de control ha sido modificada a lo largo del tiempo y se refleja en la morfología, los patrones de distribución y las litologías de las UTP. Por lo tanto, las distribuciones de depósitos más extensas y componentes de grano fino tienden a ocurrir durante condiciones de estabilidad del nivel del mar. Por el contrario, las distribuciones más confinadas y los componentes de grano grueso parecen ser el resultado de mayores flujos de sedimentos.

REFERENCES

References

- Aksu, A.E., Hiscott, R.N., & Yaltrak, C. (2016). Early Holocene age and provenance of a mid-shelf delta lobe south of the Strait of Bosphorus, Turkey, and its link to vigorous Black Sea outflow. *Marine Geology*, 380, 113-137. <https://doi.org/10.1016/j.margeo.2016.07.003>.
- Allen, G.P., & Truilhe, G. (1988). Stratigraphic and Facies Model of a Transgressing Estuarine Valley Fill in the Gironde Estuary (France). In: James, D.P., & Leckie, D.A. (Eds.), *Sequences, Stratigraphy, Sedimentology Surface and Subsurface*. Canadian Society of Petroleum Geologists memoirs, 15, pp. 575-575.
- Allen, G.P., & Posamentier, H.W. (1991). Facies and the stratal patterns in incised valleys: examples from the recent Gironde Estuary (France) and the Cretaceous Viking Formation. American Association of Petroleum Geologists, Annual Meeting, Program with Abstract, 534-534.
- Allen, G.P., & Posamentier, H.W. (1992). On the origin and subsequent modification of incised valleys. American Association of Petroleum Geologists, annual Convention, Calgary, Canada, Program with Abstract, 70-70.
- Allen, G.P., & Posamentier, H.W. (1994). Transgressive Facies and Sequence Architecture in Mixed Tide- and Wave-Dominated Incised Valleys: Example from the Gironde Estuary, France. In: Dalrymple, R.W., Boyd, R.J., & Zaitlin, B.A. (Eds.), *Incised-Valley Systems: Origin and Sedimentary Sequences*. SEPM Society for Sedimentary Geology Special Publication, 51, pp. 225-240. <https://doi.org/10.2110/pec.94.12.0225>.
- Allen, G.P., Castaing, P., Feral, A., Klingebiel, A., & Vigneaux, M. (1970). Contribution à l'étude des facies de comblement et interprétation paléogéographique de l'évolution des milieux sédimentaires récents et actuels de l'estuaire de la Gironde. *Bulletin de l'institut de Géologie du Bassin d'Aquitaine*, 8, 99-155.
- Alqahtani, F.A., Jackson, C.A.L., Johnson, H.D., & Som, M.R.B. (2017). Controls on the geometry and evolution of humid-tropical fluvial systems: Insights from 3D Seismic Geomorphological Analysis of the Malay Basin, Sunda Shelf, Southeast Asia. *Journal of Sedimentary Research*, 87(1), 17-40. <https://doi.org/10.2110/jsr.2016.88>.
- Ambar, I., Armi, L., Bower, A., & Ferreira, T. (1999). Some aspects of time variability of the Mediterranean Water off south Portugal. *Deep Sea Research Part I: Oceanographic Research Papers*, 46(7), 1109-1136. [https://doi.org/10.1016/S0967-0637\(99\)00006-0](https://doi.org/10.1016/S0967-0637(99)00006-0).
- Andrade, C. (1990). O ambiente de barreira da Ria Formosa (Algarve, Portugal). Unpublished PhD dissertation, Department of Geology, University of Lisbon, 645 pp.

References

- Anthony, E.J., Marriner, N., & Morhange, C. (2014). Human influence and the changing geomorphology of Mediterranean deltas and coasts over the last 6000 years: From progradation to destruction phase? *Earth-Science Reviews*, 139, 336-361. <https://doi.org/10.1016/j.earscirev.2014.10.003>.
- Aquino da Silva, A.G., Statterger, K., Schwarzer, K., & Vital, H. (2016). Seismic stratigraphy as an indicator of late Pleistocene and Holocene sea-level changes on the NE Brazilian continental shelf. *Journal of South American Earth Sciences*, 70, 188-197. <https://doi.org/10.1016/j.jsames.2016.05.001>.
- Ashley, G.M., & Sheridan, R.E. (1994). Depositional Model for Valley Fills on a Passive Continental Margin. In: Dalrymple, R.W., Boyd, R.J., & Zaitlin, B.A. (Eds.), *Incised-Valley Systems: Origin and Sedimentary Sequences*. SEPM Society for Sedimentary Geology Special Publication, 51, pp. 285-301. <https://doi.org/10.2110/pec.94.12.0285>.
- Bae, S.H., Kong, G.S., Lee, G.S., Yoo, D.G., & Kim, D.C. (2018). Incised channel morphology and depositional fill of the paleo-Seomjin River in the continental shelf of the South Sea, Korea. *Quaternary International*, 468, 49-61. <https://doi.org/10.1016/j.quaint.2017.03.053>.
- Baldy, P. (1977). *Géologie du plateau continental portugaise (au sud du cap de Sines)*. Thèse de 3ème Cycle, Université Paris VI, 113 pp.
- Baraza, J., Ercilla, G., & H. Nelson, C.H. (1999). Potential geologic hazards on the eastern Gulf of Cadiz slope (SW Spain). *Marine Geology*, 155, 191-215. [https://doi.org/10.1016/S0025-3227\(98\)00147-9](https://doi.org/10.1016/S0025-3227(98)00147-9).
- Bard, E., Hamelin, B., & Fairbanks, R.G. (1990). U-Th ages obtained by mass spectrometry in corals from Barbados: sea level during the past 130,000 years. *Nature*, 346, 456-458. <https://doi.org/10.1038/346456a0>.
- Bard, E., Hamelin, B., Arnold, M., Montaggioni, L., Cabioch, G., Faure, G., & Rougerie, F. (1996). Deglacial sea-level record from Tahiti corals and the timing of global meltwater discharge. *Nature*, 382, 241-244. <https://doi.org/10.1038/382241a0>.
- Bard, E., Hamelin, B., & Delanghe-Sabatier, D. (2010). Deglacial Meltwater Pulse 1B and Younger Dryas Sea Levels Revisited with Boreholes at Tahiti. *Science*, 327, 1235-1237. <https://doi.org/10.1126/science.1180557>.
- Bartolomé, R., Gràcia, E., Stich, D., Martínez-Lorient, S., Klaeschen, D., de Lis Mancilla, F., Iacono, C., Dañobeitia, J.J., & Zitellini, N. (2012). Evidence for active strike-slip faulting along the Eurasia-Africa convergence zone: Implications for seismic hazard in the southwest Iberian margin. *Geology*, 40, 495-498. <https://doi.org/10.1130/g33107.1>.

- Bassetti, M.A., Jouet, G., Dufois, F., Berné, S., Rabineau, M., & Taviani, M. (2006). Sand bodies at the shelf edge in the Gulf of Lions (Western Mediterranean): Deglacial history and modern processes. *Marine Geology*, 234, 93-109. <https://doi.org/10.1016/j.margeo.2006.09.010>.
- Belknap, D.F., & Kraft, J.C. (1985). Influence of antecedent geology on stratigraphic preservation potential and evolution of Delaware's barrier systems. *Marine Geology*, 63, 235-262. [https://doi.org/10.1016/0025-3227\(85\)90085-4](https://doi.org/10.1016/0025-3227(85)90085-4).
- Bellanco, M.J., & Sánchez-Leal, R.F. (2016). Spatial distribution and intra-annual variability of water masses on the Eastern Gulf of Cadiz seabed. *Continental Shelf Research*, 128, 26-35. <https://doi.org/10.1016/j.csr.2016.09.001>.
- Benito, G., Thorndycraft, V.R., Rico, M., Sánchez-Moya, Y., & Sopena, A. (2008). Palaeoflood and floodplain records from Spain: Evidence for long-term climate variability and environmental changes. *Geomorphology*, 101, 68-77. <https://doi.org/10.1016/j.geomorph.2008.05.020>.
- Berends, C.J., Köhler, P., Lourens, L.J., & van de Wal, R.S.W. (2021). On the Cause of the Mid-Pleistocene Transition. *Reviews of Geophysics*, 59, e2020RG000727. <https://doi.org/10.1029/2020RG000727>.
- Berné, S., Jouet, G., Bassetti, M.A., Dennielou, B., & Taviani, M. (2007). Late Glacial to Preboreal sea-level rise recorded by the Rhône deltaic system (NW Mediterranean). *Marine Geology*, 245, 65-88. <https://doi.org/10.1016/j.margeo.2007.07.006>.
- Blum, M.D., & Price, D.M. (1998). Quaternary Alluvial Plain Construction in Response to Glacio-Eustatic and Climatic Controls, Texas Gulf Coastal Plain. In: Kocurek, G. (Ed.), *Relative Role of Eustacy, Climate, and Tectonism in Continental Rocks*. SEPM Society for Sedimentary Geology Special Publication, 59, pp. 31-49. <https://doi.org/10.2110/pec.98.59.0031>.
- Blum, M. D., & Törnqvist, T. E. (2000). Fluvial responses to climate and sea-level change: A review and look forward. *Sedimentology*, 47, 2-48. <https://doi.org/10.1046/j.1365-3091.2000.00008.x>.
- Blum, M., Martin, J., Milliken, K., & Garvin, M. (2013). Paleovalley systems: Insights from Quaternary analogs and experiments. *Earth-Science Reviews*, 116, 128-169. <https://doi.org/10.1016/j.earscirev.2012.09.003>.
- Borenäs, K.M., Wåhlin, A.K., Ambar, I., & Serra, N. (2002). The Mediterranean outflow splitting-a comparison between theoretical models and CANIGO data. *Deep Sea Research Part II: Topical Studies in Oceanography*, 49, 4195-4205. [https://doi.org/10.1016/S0967-0645\(02\)00150-9](https://doi.org/10.1016/S0967-0645(02)00150-9).

References

- Borrego, J., Morales, J.A., & Pendon, J.G. (1995). Holocene Estuarine Facies along the Mesotidal Coast of Huelva, South-Western Spain. In: Flemming, B.W., & Bartholomä, A. (Eds.), *Tidal Signatures in Modern and Ancient Sediments*. International Association of Sedimentologists Special Publication, 24, pp. 151-170. <https://doi.org/10.1002/9781444304138.ch10>.
- Boski, T., Moura, D., Veiga-Pires, C., Camacho, S., Duarte, D., Scott, D.B., & Fernandes, S.G. (2002). Postglacial sea-level rise and sedimentary response in the Guadiana Estuary, Portugal/Spain border. *Sedimentary Geology*, 150, 103-122. [https://doi.org/10.1016/S0037-0738\(01\)00270-6](https://doi.org/10.1016/S0037-0738(01)00270-6).
- Boski, T., Camacho, S., Moura, D., Fletcher, W., Wilamowski, A., Veiga-Pires, C., Correia, V., Loureiro, C., & Santana, P. (2008). Chronology of the sedimentary processes during the postglacial sea level rise in two estuaries of the Algarve coast, Southern Portugal. *Estuarine, Coastal and Shelf Science*, 77, 230-244. <https://doi.org/10.1016/j.ecss.2007.09.012>.
- Bosnic, I., Cascalho, J., Taborda, R., Drago, T., Hermínio, J., Rosa, M., Dias, J., & Garel, E. (2017). Nearshore sediment transport: Coupling sand tracer dynamics with oceanographic forcing. *Marine Geology*, 385, 293-303. <https://doi.org/10.1016/j.margeo.2017.02.004>.
- Boyd, R. (2010). Transgressive wave-dominated coasts. In: James N.P., & Dalrymple R.W. (Eds.), *Facies models 4*. St. John's: Geological Association of Canada, pp. 265-294.
- Boyd, R., Dalrymple, R.W., & Zaitlin, B.A. (2006). Estuarine and Incised-Valley Facies Models. In: Posamentier, H. W., & Walker, R. G. (Eds.), *Facies Models Revisited*. SEPM Society for Sedimentary Geology Special Publication, 84, pp. 171-235. <https://doi.org/10.2110/pec.06.84.0171>.
- Boyer, J., Duvail, C., le Strat, P., Gensous, B., & Tesson, M. (2005). High resolution stratigraphy and evolution of the Rhône delta plain during Postglacial time, from subsurface drilling data bank. *Marine Geology*, 222-223, 267-298. <https://doi.org/10.1016/j.margeo.2005.06.017>.
- Brothers, L.L., Foster, D.S., Pendleton, E.A., & Baldwin, W.E. (2020). Seismic stratigraphic framework of the continental shelf offshore Delmarva, U.S.A.: Implications for Mid-Atlantic Bight Evolution since the Pliocene. *Marine Geology*, 428, 106287. <https://doi.org/10.1016/j.margeo.2020.106287>.
- Brown Jr, L.F., & Fisher, W.L. (1977). Seismic-Stratigraphic Interpretation of Depositional Systems: Examples from Brazilian Rift and Pull-Apart Basins. In: Payton, C.E. (Ed.), *Seismic Stratigraphy - Applications to Hydrocarbon Exploration*. American Association of Petroleum Geologists, 26, pp. 213-248. <https://doi.org/10.1306/M26490C14>.

- Bruun, P.M. (1962). Sea-Level Rise as a Cause of Shore Erosion. *Journal of the Waterways and Harbors Division*, 88, 117-132. <https://doi.org/10.1061/JWHEAU.0000252>.
- Burger, R.L., Fulthorpe, C.S., & Austin, A.J. (2001). Late Pleistocene channel incisions in the southern Eel River Basin, northern California: implications for tectonic vs. eustatic influences on shelf sedimentation patterns. *Marine Geology*, 177, 317-330. [https://doi.org/10.1016/S0025-3227\(01\)00166-9](https://doi.org/10.1016/S0025-3227(01)00166-9).
- Burgess, P.M., Steel, R.J., & Granjeon, D. (2008). Stratigraphic Forward Modeling of Basin-Margin Clinoform Systems: Implications for Controls on Topset and Shelf Width and Timing of Formation of Shelf-Edge Deltas. In: Hampson, G.J., Steel, R.J., Burgess, P.M., & Dalrymple, R.W. (Eds.), *Recent Advances in Models of Siliciclastic Shallow-Marine Stratigraphy*. SEPM Society for Sedimentary Geology Special Publication, 90, pp. 35–45. <https://doi.org/10.2110/pec.08.90.0035>.
- Carlin, J.A., Dellapenna, T.M., Strom, K., & Noll, C.J. (2015). The influence of a salt wedge intrusion on fluvial suspended sediment and the implications for sediment transport to the adjacent coastal ocean: A study of the lower Brazos River TX, USA. *Marine Geology*, 359, 134-147. <https://doi.org/10.1016/j.margeo.2014.11.001>
- Carlson, A.E., & Clark P.U. (2012). Ice sheet sources of sea level rise and freshwater discharge during the last deglaciation: Reviews of Geophysics, *Journal of the Waterways and Harbour Division*, 50, 1-72. <https://doi.org/10.1029/2011RG000371>.
- Carrión, J.S. (2002). Patterns and processes of Late Quaternary environmental change in a montane region of southwestern Europe. *Quaternary Science Reviews*, 21, 18-19. [https://doi.org/10.1016/S0277-3791\(02\)00010-0](https://doi.org/10.1016/S0277-3791(02)00010-0).
- Carrión-Torrente, Á., Lobo, F.J., Puga-Bernabéu, Á., Mendes, I., Lebreiro, S., García, M., van Rooij, D., Luján, M., Reguera, M.I., & Antón, L. (2022). Episodic postglacial deltaic pulses in the Gulf of Cadiz: Implications for the development of a transgressive shelf and driving environmental conditions. *Journal of Sedimentary Research*, 92, 1116-1140. <https://doi.org/10.2110/jsr.2021.110>.
- Carrión-Torrente, Á., Lobo, F.J., Puga-Bernabéu, Á., Luján, M., Mendes, I., Hanebuth, T.J.J., Lebreiro, S., García, M., Reguera, M. I., Antón, L., van Rooij, D., & Cerrillo-Escoriza, J. (2023). Incised valleys on the Algarve inner shelf, northern Gulf of Cadiz margin: Stratigraphic architecture and controlling factors in a low fluvial supply setting. *Continental Shelf Research*, 266, 105095. <https://doi.org/10.1016/J.CSR.2023.105095>.
- Carro, B., Borrego, J., & Morales, J.A. (2019). Estuaries of the Huelva Coast: Odiel and Tinto Estuaries (SW Spain). In: Morales, J.A. (Ed.), *The Spanish Coastal Systems: Dynamic Processes, Sediments and Management*. Springer International Publishing, pp. 543-564. https://doi.org/10.1007/978-3-319-93169-2_23.

References

- Cartelle, V., García-Moreiras, I., Martínez-Carreño, N., Muñoz Sobrino, C., & García-Gil, S. (2022). The role of antecedent morphology and changing sediment sources in the postglacial palaeogeographical evolution of an incised valley: The sedimentary record of the Ría de Arousa (NW Iberia). *Global and Planetary Change*, 208, 103727. <https://doi.org/10.1016/J.GLOPLACHA.2021.103727>.
- Cattaneo, A., & Steel, R.J. (2003). Transgressive deposits: A review of their variability. *Earth-Science Reviews*, 62, 187-228. [https://doi.org/10.1016/S0012-8252\(02\)00134-4](https://doi.org/10.1016/S0012-8252(02)00134-4)
- Catuneanu, O. (2002). Sequence stratigraphy of clastic systems: concepts, merits, and pitfalls. *Journal of African Earth Sciences*, 35, 1-43. [https://doi.org/10.1016/S0899-5362\(02\)00004-0](https://doi.org/10.1016/S0899-5362(02)00004-0).
- Catuneanu, O. (2006). *Principles of Sequence Stratigraphy*. 1st Edition, Elsevier, Amsterdam, 388 pp.
- Catuneanu, O. (2017). Sequence Stratigraphy: Guidelines for a Standard Methodology. In: Montenari, M. (Ed.), *Stratigraphy and Timescales*. Academic Press, 2, pp. 1-57. <https://doi.org/10.1016/BS.SATS.2017.07.003>.
- Catuneanu, O. (2019a). Model-independent sequence stratigraphy. *Earth-Science Reviews*, 188, 312-388. <https://doi.org/10.1016/j.earscirev.2018.09.017>
- Catuneanu, O. (2019b). Scale in sequence stratigraphy. *Marine and Petroleum Geology*, 106, 128-159. <https://doi.org/10.1016/j.marpetgeo.2019.04.026>
- Catuneanu, O. (2022) *Principles of Sequence Stratigraphy*. 2nd Edition, Elsevier, Amsterdam, 494 pp.
- Catuneanu, O., Abreu, V., Bhattacharya, J.P., Blum, M.D., Dalrymple, R.W., Eriksson, P.G., Fielding, C.R., Fisher, W.L., Galloway, W.E., Gibling, M.R., Giles, K.A., Holbrook, J.M., Jordan, R., Kendall, C.G.S.C., Macurda, B., Martinsen, O.J., Miall, A.D., Neal, J.E., Nummedal, D., ... Winker, C. (2009). Towards the standardization of sequence stratigraphy. *Earth-Science Reviews*, 92, 1-33. <https://doi.org/10.1016/j.earscirev.2008.10.003>
- Catuneanu, O., Bhattacharya, J.P., Blum, M.D., Dalrymple, R.W., Eriksson, P.G., Fielding, C.R., Fisher, W.L., Galloway, W.E., Gianolla, P., Gibling, M.R., Giles, K.A., Holbrook, J.M., Jordan, R., Kendall, C.G.St.C., Macurda, B., Martinsen, O.J., Miall, A.D., Nummedal, D., Posamentier, H.W., Pratt, B.R., Shanley, K.W., Steel, R.J., Strasser, A., Tucker, M.E. (2010). Sequence stratigraphy: common ground after three decades of development. *First break*, 28, 21-34. <https://doi.org/10.3997/1365-2397.2010002>.

- Catuneanu, O., Galloway, W.E., Kendall, C.G.S.C., Miall, A.D., Posamentier, H.W., Strasser, A., & Tucker, M.E. (2011). Sequence Stratigraphy: Methodology and nomenclature. *Newsletters on Stratigraphy*, 44, 173-245. <https://doi.org/10.1127/0078-0421/2011/0011>.
- Chaumillon, E., & Weber, N. (2006). Spatial variability of modern incised valleys on the French Atlantic coast: comparison between the Charente and the Lay-Sèvre incised valleys. In: Dalrymple, R.W., Leckie, D.A., & Tillman, R.W. (Eds.), *Incised Valleys in Time and Space*. SEPM Society for Sedimentary Geology Special Publication, 85, pp. 57–85. <https://doi.org/10.2110/pec.06.85.0057>.
- Chaumillon, E., Proust, J.-N., Menier, D., & Weber, N. (2008). Incised-valley morphologies and sedimentary-fills within the inner shelf of the Bay of Biscay (France): A synthesis. *Journal of Marine Systems*, 72, 383-396. <https://doi.org/10.1016/j.jmarsys.2007.05.014>.
- Chaumillon, E., Tessier, B., & Reynaud, J.-Y. (2010). Stratigraphic records and variability of incised valleys and estuaries along French coasts. *Bulletin de La Société Géologique de France*, 181, 75-85. <https://doi.org/10.2113/gssgfbull.181.2.75>.
- Ciavola, P., Taborda, R., Ferreira, Ó., & Dias, J.A. (1997). Field Measurements of Longshore Sand Transport and Control Processes on a Steep Meso-Tidal Beach in Portugal. *Journal of Coastal Research*, 13, 1119-1129. <http://www.jstor.org/stable/4298720>.
- Clark, P., Dyke, A., Shakun, J., Carlson, A., Clark, J., Wohlfarth, B., Mitrovica, J., Hostetler, S., & McCabe, A. (2009). The Last Glacial Maximum. *Science*, 325, 710-714. <https://doi.org/10.1126/science.1172873>.
- Cooper, J.A.G., Green, A.N., Meireles, R.P., Klein, A.H.F., Souza, J., & Toldo, E.E. (2016). Sandy barrier overstepping and preservation linked to rapid sea level rise and geological setting. *Marine Geology*, 382, 80-91. <https://doi.org/10.1016/j.margeo.2016.10.003>.
- Costa, M., Silva, R., and Vitorino, J. (2001). Contribuição para o estudo do clima de agitação marítima na costa Portuguesa: Proceedings of 2as Jornadas Portuguesas de Engenharia Costeira e Portuária, Sines, Portugal (2001), CD-ROM.
- Criado-Aldeanueva, F., García-Lafuente, J., Navarro, G., & Ruiz, J. (2009). Seasonal and interannual variability of the surface circulation in the eastern Gulf of Cadiz (SW Iberia). *Journal of Geophysical Research: Oceans*, 114, C01011. <https://doi.org/10.1029/2008jc005069>.
- Dadey, K.A., Janecek, T.R., & Klaus, A. (1992). Dry-bulk density: its use and determination. *Proceedings of the Ocean Drilling Program, Scientific Results*, 12, 551-554.

References

- Dalrymple, R.W. (2006). Incised Valleys in Time and Space: An Introduction to the Volume and an Examination of the Controls on Valley Formation and Filling. In: Dalrymple, R.W., Leckie, D.A., & Tillman, R.W. (Eds.), *Incised Valleys in Time and Space*. SEPM Society for Sedimentary Geology Special Publication, 85, pp. 5–12. <https://doi.org/10.2110/pec.06.85.0005>.
- Dalrymple, R.W. (2010). Introduction to siliciclastic facies models. In: James N.P., & Dalrymple R.W. (Eds.), *Facies models 4*. St. John's: Geological Association of Canada, pp. 59-72.
- Dalrymple, R.W., Zaitlin, B.A., & Boyd, R. (1992). Estuarine facies models; conceptual basis and stratigraphic implications. *Journal of Sedimentary Research*, 62, 1130-1146. <https://doi.org/10.1306/D4267A69-2B26-11D7-8648000102C1865D>.
- Dalrymple, R.W., Boyd, R., & Zaitlin, B.A. (1994a). History of Research, Types and Internal Organisation of Incised-Valley Systems: Introduction to the Volume. In: Dalrymple, R.W., Leckie, D.A., & Tillman, R.W. (Eds.), *Incised-Valley Systems: Origin and Sedimentary Sequences*. SEPM Society for Sedimentary Geology Special Publication, 51, pp. 3-10. <https://doi.org/10.2110/pec.94.12.0003>.
- Dalrymple, R.W., Boyd, R., & Zaitlin, B.A. (1994b). *Incised-Valley Systems: Origin and Sedimentary Sequences*. SEPM Society for Sedimentary Geology Special Publication, 51, 391 pp. <https://doi.org/10.2110/pec.94.12>.
- Dalrymple, R.W., Leckie, D.A., & Tillman, R.W. (2006). *Incised Valleys in Time and Space*. SEPM Society for Sedimentary Geology Special Publication, 85, 349 pp. <https://doi.org/10.2110/pec.06.85>.
- Dana, J. D. (1880). *Manual of Geology: Treating of the Principles of the Science with Special Reference to American Geological History*. 3rd Edition, New York, Ivison, Blakeman, Taylor and Company, 911 pp.
- Darmadi, Y., Willis, B.J., & Dorobek, S.L. (2007). Three-Dimensional Seismic Architecture of Fluvial Sequences on the Low-Gradient Sunda Shelf, Offshore Indonesia. *Journal of Sedimentary Research*, 77, 225-238. <https://doi.org/10.2110/jsr.2007.024>.
- De Falco, G., Antonioli, F., Fontolan, G., Lo Presti, V., Simeone, S., & Tonielli, R. (2015). Early cementation and accommodation space dictate the evolution of barrier system during the Holocene. *Marine Geology*, 369, 52-66. <https://doi.org/10.1016/j.margeo.2015.08.002>.
- De Falco, G., Carannante, A., del Vais, C., Gasperini, L., Pascucci, V., Sanna, I., Simeone, S., & Conforti, A. (2022). Evolution of a single incised valley related to inherited geology, sea level rise and climate changes during the Holocene (Tirso river, Sardinia, western Mediterranean Sea). *Marine Geology*, 451, 106885. <https://doi.org/10.1016/J.MARGEO.2022.106885>.

- De Oliveira Júnior, L., Relvas, P., & Garel, E. (2022). Kinematics of surface currents at the northern margin of the Gulf of Cádiz. *Ocean Science*, 18, 1183-1202. <https://doi.org/10.5194/OS-18-1183-2022>.
- De Santis, V., Caldara, M., & Pennetta, L. (2020). Transgressive architecture of coastal barrier systems in the ofanto incised valley and its surrounding shelf in response to stepped sea-level rise. *Geosciences*, 10, 497. <https://doi.org/10.3390/geosciences10120497>.
- Del Río, L., Plomaritis, T.A., Benavente, J., Valladares, M., & Ribera, P. (2012). Establishing storm thresholds for the Spanish Gulf of Cádiz coast. *Geomorphology* 143-144, 13-23. <https://doi.org/10.1016/j.geomorph.2011.04.048>.
- Delgado, J., Nieto, J.M., & Boski, T. (2010). Analysis of the spatial variation of heavy metals in the Guadiana Estuary sediments (SW Iberian Peninsula) based on GIS-mapping techniques. *Estuarine, Coastal and Shelf Science*, 88, 71-83. <https://doi.org/10.1016/j.ecss.2010.03.011>
- Demarest, J.M., & Kraft, J.C. (1987). Stratigraphic record of Quaternary sea levels: implications for more ancient strata. In: Nummedal, D., Pilkey, O.H., & Howard, J.D. (Eds.), *Sea-Level Fluctuation and Coastal Evolution*. SEPM Society for Sedimentary Geology Special Publication, 41, pp. 223-239. <https://doi.org/10.2110/pec.87.41.0223>.
- Dewey, J.F., Helman, M.L., Knott, S.D., Turco, E., & Hutton, D.H.W. (1989). Kinematics of the western Mediterranean. Geological Society, London, Special Publications, 45, pp. 265-283. <https://doi.org/10.1144/GSL.SP.1989.045.01.15>.
- Dolbeth, M., Ferreira, Ó., Teixeira, H., Marques, J., Dias, J., & Pardal, M. (2007). Beach morphodynamic impact on a macrobenthic community along a subtidal depth gradient. *Marine Ecology-Progress Series*, 352, 113-124. <https://doi.org/10.3354/meps07040>.
- Dorado Valiño, M., Valdeolmillos Rodríguez, A., Blanca Ruiz Zapata, M., José Gil García, M., & de Bustamante Gutiérrez, I. (2002). Climatic changes since the Late-glacial/Holocene transition in La Mancha Plain (South-central Iberian Peninsula, Spain) and their incidence on Las Tablas de Daimiel marshlands. *Quaternary International*, 93-94, 73-84. [https://doi.org/10.1016/S1040-6182\(02\)00007-1](https://doi.org/10.1016/S1040-6182(02)00007-1).
- Duarte, D., Roque, C., Ng, Z.L., Hernández-Molina, F.J., Magalhães, V.H., Silva, S., & Llave, E. (2022). Structural control and tectono-sedimentary evolution of the Gulf of Cadiz, SW Iberia since the late Miocene: Implications for contourite depositional system. *Marine Geology*, 449, 106818. <https://doi.org/10.1016/j.margeo.2022.106818>.
- Dubey, K.M., Chaubey, A.K., Mahale, V.P., & Karisiddaiah, S.M. (2019). Buried channels provide keys to infer Quaternary stratigraphic and paleo-environmental changes: A case study from the west coast of India. *Geoscience Frontiers*, 10, 1577-1595. <https://doi.org/10.1016/j.gsf.2018.09.016>.

References

- Duggen, S., Hoernle, K., den Bogaard, P., Rüpke, L., & Morgan, J.P. (2003). Deep roots of the Messinian salinity crisis. *Nature*, 422, 602-606. <https://doi.org/10.1038/nature01553>.
- Dyer, S.E., Green, A.N., Cooper, J.A.G., Hahn, A., & Zabel, M. (2021). Response of a wave-dominated coastline and delta to antecedent conditioning and fluctuating rates of postglacial sea-level rise. *Marine Geology*, 434, 106435. <https://doi.org/10.1016/j.margeo.2021.106435>.
- EMODnet Bathymetry Consortium, 2020. EMODnet Digital Bathymetry (DTM). EMODnet Bathymetry Consortium. <https://doi.org/10.12770/bb6a87dd-e579-4036-abe1-e649cea9881a>.
- Engelbrecht, L., Green, A.N., Cooper, J.A. G., Hahn, A., Zabel, M., & Mackay, C.F. (2020). Construction and evolution of submerged deltaic bodies on the high energy SE African coastline: The interplay between relative sea level and antecedent controls. *Marine Geology*, 424, 106170. <https://doi.org/10.1016/j.margeo.2020.106170>.
- Estournès, G., Menier, D., Guillocheau, F., le Roy, P., Paquet, F., & Goubert, E. (2012). The paleo-Etel River incised valley on the Southern Brittany inner shelf (Atlantic coast, France): Preservation of Holocene transgression within the remnant of a middle Pleistocene incision? *Marine Geology*, 329-331, 75-92. <https://doi.org/10.1016/j.margeo.2012.08.005>.
- Fairbanks, R.G. (1989). A 17,000-year glacio-eustatic sea level record: influence of glacial melting rates on the Younger Dryas event and deep-ocean circulation. *Nature*, 342, 637-642. <https://doi.org/10.1038/342637a0>.
- Féniès, H., & Lericolais, G. (2005). Architecture interne d'une vallée incisée sur une côte à forte énergie de houle et de marée (vallée de la Leyre, côte aquitaine, France). *Comptes Rendus - Geoscience*, 337, 1257-1266. <https://doi.org/10.1016/j.crte.2005.06.005>.
- Fernández, M., Berástegui, X., Puig, C., García-Castellanos, D., Jurado, M.J., Torné, M., & Banks, C. (1998). Geophysical and geological constraints on the evolution of the Guadalquivir foreland basin, Spain. *Geological Society, London, Special Publications*, 134, 29-48. <https://doi.org/10.1144/gsl.sp.1998.134.01.03>.
- Fernández-Salas, L.M., Rey, J., Pérez-Vázquez, E., Ramírez, J.L., Hernández-Molina, F.J., Somoza, L., de Andrés, J.R., & Lobo, F.J. (1999). Morphology and characterisation of the relict facies on the internal continental shelf in the Gulf of Cadiz, between Ayamonte and Huelva (southern Iberian Peninsula). *Boletín Del Instituto Español de Oceanografía*, 15, 123-132. <http://hdl.handle.net/10261/320023>.

- Fernández-Salas, L.M., Lobo, F.J., Hernández-Molina, F.J., Somoza, L., Rodero, J., Díaz del Río, V., & Maldonado, A. (2003). High-resolution architecture of late Holocene highstand prodeltaic deposits from southern Spain: the imprint of high-frequency climatic and relative sea-level changes. *Continental Shelf Research*, 23, 1037-1054. [https://doi.org/10.1016/S0278-4343\(03\)00120-1](https://doi.org/10.1016/S0278-4343(03)00120-1).
- Ferreira, Ó., Matias, A., & Pacheco, A. (2016). The East Coast of Algarve: a Barrier Island Dominated Coast. *Thalassas*, 32, 75-85. <https://doi.org/10.1007/s41208-016-0010-1>.
- Fisher, A. G. (1961), Stratigraphic record of transgressing seas in light of sedimentation on Atlantic coast of New Jersey. *American Association of Petroleum Geologists Bulletin*, 45, 1656-1667. <https://doi.org/10.1306/BC743717-16BE-11D7-8645000102C1865D>.
- Fletcher, W.J., Boski, T., & Moura, D. (2007). Palynological evidence for environmental and climatic change in the lower Guadiana valley, Portugal, during the last 13 000 years. *The Holocene*, 17, 481-494. <https://doi.org/10.1177/0959683607077027>.
- Folk, R.L. (1954). The distinction between grain size and mineral composition in sedimentary-rock nomenclature. *The Journal of Geology*, 62, 344-359. <https://www.jstor.org/stable/30065016>.
- Foyle, A.M., & Oertel, G.F. (1997). Transgressive systems tract development and incised-valley fills within a Quaternary estuary-shelf system: Virginia inner shelf, USA. *Marine Geology*, 137, 227-249. [https://doi.org/10.1016/s0025-3227\(96\)00092-8](https://doi.org/10.1016/s0025-3227(96)00092-8).
- García, C. M., Prieto, L., Vargas, M., Echevarría, F., García-Lafuente, J., Ruiz, J., & Rubín, J.P. (2002). Hydrodynamics and the spatial distribution of plankton and TEP in the Gulf of Cádiz (SW Iberian Peninsula). *Journal of Plankton Research*, 24, 817 - 833. <https://doi.org/10.1093/plankt/24.8.817>.
- García-Lafuente, J., Delgado, J., Criado-Aldeanueva, F., Bruno, M., del Río, J., & Miguel Vargas, J. (2006). Water mass circulation on the continental shelf of the Gulf of Cádiz. *Deep Sea Research Part II: Topical Studies in Oceanography*, 53, 1182-1197. <https://doi.org/10.1016/j.dsr2.2006.04.011>.
- Gardner James, V., & Kidd Robert, B. (1987). Sedimentary processes on the northwestern Iberian continental margin viewed by long-range side-scan sonar and seismic data. *Journal of Sedimentary Petrology*, 57, 397-407. <https://doi.org/10.1306/212f8b43-2b24-11d7-8648000102c1865d>.
- Garel, E., Laiz, I., Drago, T., & Relvas, P. (2016). Characterisation of coastal counter-currents on the inner shelf of the Gulf of Cadiz. *Journal of Marine Systems*, 155, 19-34. <https://doi.org/10.1016/j.jmarsys.2015.11.001>.

References

- Gensous, B., & Tesson, M. (2003). L'analyse des dépôts postglaciaires et son application à l'étude des séquences de dépôt du Quaternaire terminal sur la plate-forme au large du Rhône (Golfe du Lion). *Bulletin de la Société Géologique de France*, 174, 401-419. <https://doi.org/10.2113/174.4.423>.
- Gibling, M.R. (2006). Width and thickness of fluvial channel bodies and valley fills in the geological record: A literature compilation and classification. *Journal of Sedimentary Research*, 76, 731-770. <https://doi.org/10.2110/jsr.2006.060>.
- Goff, J.A., & Nordfjord, S. (2004). Interpolation of fluvial morphology using channel-oriented coordinate transformation: A case study from the New Jersey shelf. *Mathematical Geology*, 36, 643-658. <https://doi.org/10.1023/B:MATG.0000039539.84158.cd>.
- Goff, J.A., Austin, J.A., Gulick, S., Nordfjord, S., Christensen, B., Sommerfield, C., Olson, H., & Alexander, C. (2005). Recent and modern marine erosion on the New Jersey outer shelf. *Marine Geology*, 216, 275-296. <https://doi.org/10.1016/j.margeo.2005.02.015>.
- Gökaşan, E., Tur, H., Ecevitoglu, B., Görüm, T., Türker, A., Tok, B., Çağlak, F., Birkan, H., & Şimşek, M. (2005). Evidence and implications of massive erosion along the Strait of İstanbul (Bosphorus). *Geo-Marine Letters*, 25, 324-342. <https://doi.org/10.1007/s00367-005-0216-3>.
- Gomes, M.P., Vital, H., Stattegger, K., & Schwarzer, K. (2016). Bedrock control on the Assu Incised Valley morphology and sedimentation in the Brazilian Equatorial Shelf. *International Journal of Sediment Research*, 31, 181-193. <https://doi.org/10.1016/j.ijsrc.2015.04.002>.
- Gomes, M.P., Vital, H., & Droxler, A.W. (2020) Terraces, reefs, and valleys along the Brazil northeast outer shelf: deglacial sea-level archives? *Geo-Marine Letters*, 40, 699-711. <https://doi.org/10.1007/s00367-020-00666-4>.
- González, R., & Dias, J.M.A. (2004). Sediment Dispersal Patterns on the Northern Gulf of Cadiz Shelf: Which Areas are Influenced by Anthropogenic Sand Starvation? *Journal of Coastal Research*, 39, 446-449. <https://www.jstor.org/stable/25741613>.
- González, R., Dias, J.A., & Ferreira, O. (2001). Recent Rapid Evolution of the Guadiana Estuary Mouth (Southwestern Iberian Peninsula). *Journal of Coastal Research*, 34, 516-527. <http://www.jstor.org/stable/25736317>.
- Gonzalez, R., Dias, J.M. A., Lobo, F., & Mendes, I. (2004). Sedimentological and paleoenvironmental characterisation of transgressive sediments on the Guadiana Shelf (Northern Gulf of Cadiz, SW Iberia). *Quaternary International*, 120, 133-144. <https://doi.org/10.1016/j.quaint.2004.01.012>.

- González, R., Araújo, M. F., Burdloff, D., Cachão, M., Cascalho, J., Corredeira, C., Dias, J. M. A., Fradique, C., Ferreira, J., Gomes, C., Machado, A., Mendes, I., & Rocha, F. (2007). Sediment and pollutant transport in the Northern Gulf of Cadiz: A multi-proxy approach. *Journal of Marine Systems*, 68, 1-23. <https://doi.org/10.1016/j.jmarsys.2006.10.007>.
- Gràcia, E., Dañobeitia, J., Vergés, J., Bartolomé, R., & Córdoba, D. (2003). Crustal architecture and tectonic evolution of the Gulf of Cadiz (SW Iberian margin) at the convergence of the Eurasian and African plates. *Tectonics*, 22, 1033. <https://doi.org/10.1029/2001tc901045>.
- Grant, K.M., Rohling, E. J., Bar-Matthews, M., Ayalon, A., Medina-Elizalde, M., Ramsey, C.B., Satow, C., & Roberts, A.P. (2012). Rapid coupling between ice volume and polar temperature over the past 150,000 years. *Nature*, 491, 744-747. <https://doi.org/10.1038/nature11593>.
- Grant, K.M., Rohling, E.J., Bronk Ramsey, C., Cheng, H., Edwards, R.L., Florindo, F., Heslop, D., Marra, F., Roberts, A.P., Tamisiea, M.E., & Williams, F. (2014). Sea-level variability over five glacial cycles. *Nature Communications*, 5, 5076. <https://doi.org/10.1038/ncomms6076>.
- Graves, L.G., Driscoll, N.W., & Maloney, J.M. (2021). Tectonic and eustatic control on channel formation, erosion, and deposition along a strike-slip margin, San Diego, California, USA. *Continental Shelf Research*, 231, 104571. <https://doi.org/10.1016/J.CSR.2021.104571>.
- Green, A.N. (2009). Palaeo-drainage, incised valley fills and transgressive systems tract sedimentation of the northern KwaZulu-Natal continental shelf, South Africa, SW Indian Ocean. *Marine Geology*, 263, 46-63. <https://doi.org/10.1016/j.margeo.2009.03.017>.
- Green, A.N., Dladla, N., & Garlick, G.L. (2013). Spatial and temporal variations in incised valley systems from the Durban continental shelf, KwaZulu-Natal, South Africa. *Marine Geology*, 335, 148-161. <https://doi.org/10.1016/j.margeo.2012.11.002>.
- Green, A.N., Cooper, J.A.G., & Salzmann, L. (2014). Geomorphic and stratigraphic signals of postglacial meltwater pulses on continental shelves. *Geology*, 42, 151-154. <https://doi.org/10.1130/G35052.1>.
- Green, A.N., Cooper, J.A.G., & Salzmann, L. (2018). The role of shelf morphology and antecedent setting in the preservation of palaeo-shoreline (beachrock and aeolianite) sequences: the SE African shelf. *Geo-Marine Letters*, 38, 5-18. <https://doi.org/10.1007/s00367-017-0512-8>.
- Green, A.N., Cooper, J.A.G., Dlamini, N.P., Dladla, N.N., Parker, D., & Kerwath, S.E. (2020). Relict and contemporary influences on the postglacial geomorphology and evolution of a current swept shelf: The Eastern Cape Coast, South Africa. *Marine Geology*, 427, 106230. <https://doi.org/10.1016/j.margeo.2020.106230>.

References

- Greene Jr., D.L., Rodriguez, A.B., & Anderson, J.B. (2007). Seaward-Branching Coastal-Plain and Piedmont Incised-Valley Systems Through Multiple Sea-Level Cycles: Late Quaternary Examples from Mobile Bay and Mississippi Sound, U.S.A. *Journal of Sedimentary Research*, 77, 139-158. <https://doi.org/10.2110/jsr.2007.016>.
- Grossman, E.E., Eittrheim, S.L., Field, M.E., & Wong, F.L. (2006). Shallow stratigraphy and sedimentation history during high-frequency sea-level changes on the central California shelf. *Continental Shelf Research*, 26, 1217-1239. <https://doi.org/10.1016/j.csr.2006.04.001>.
- Gutierrez, B.T., Uchupi, E., Driscoll, N.W., & Aubrey, D.G. (2003). Relative sea-level rise and the development of valley-fill and shallow water sequences in Nantucket sound, Massachusetts. *Marine Geology*, 193, 295-314. [https://doi.org/10.1016/S0025-3227\(02\)00665-5](https://doi.org/10.1016/S0025-3227(02)00665-5).
- Gutiérrez-Mas, J.M., Hernández-Molina, F.J., & López Aguayo, F. (1996). Holocene sedimentary dynamics on the Iberian continental shelf of the Gulf of Cadiz (SW Spain). *Continental Shelf Research*, 16, 1635-1653. [https://doi.org/10.1016/0278-4343\(96\)00010-6](https://doi.org/10.1016/0278-4343(96)00010-6).
- Gutiérrez-Mas, J.M., López-Arroyo, J., & Morales, J.A. (2009). Recent marine lithofacies in Cadiz Bay (SW Spain): Sequences, processes and control factors. *Sedimentary Geology*, 218, 31-47. <https://doi.org/10.1016/j.sedgeo.2009.04.002>.
- Gutscher, M.-A., Malod, J., Rehault, J.-P., Contrucci, I., Klingelhoefer, F., Mendes-Victor, L., & Spakman, W. (2002). Evidence for active subduction beneath Gibraltar. *Geology*, 30, 1071-1074. [https://doi.org/10.1130/0091-7613\(2002\)030<1071:EFASBG>2.0.CO;2](https://doi.org/10.1130/0091-7613(2002)030<1071:EFASBG>2.0.CO;2).
- Hanebuth, T.J.J., King, M.L., Mendes, I., Lebreiro, S., Lobo, F.J., Oberle, F.K., Antón, L., Ferreira, P.A., & Reguera, M.I. (2018). Hazard potential of widespread but hidden historic offshore heavy metal (Pb, Zn) contamination (Gulf of Cadiz, Spain). *The Science of the Total Environment*, 637-638, 561-576. <https://doi.org/10.1016/j.scitotenv.2018.04.352>.
- Hanebuth, T. J. J., King, M. L., Lobo, F. J., & Mendes, I. (2021). Formation history and Material Budget of Holocene Shelf Mud Depocenters in the Gulf of Cadiz. *Sedimentary Geology*, 421, 105956. <https://doi.org/10.1016/j.sedgeo.2021.105956>.
- Harrison, S., Smith, D. E., & Glasser, N. F. (2019). Late Quaternary meltwater pulses and sea level change. *Journal of Quaternary Science*, 34, 1-15. <https://doi.org/10.1002/jqs.3070>.
- Hays, J.D., Imbrie, J., & Shackleton, N.J. (1976). Variations in the Earth's Orbit: Pacemaker of the Ice Ages. *Science*, 194, 1121-1132. <https://doi.org/10.1126/science.194.4270.1121>.

- Heaton, T.J., Köhler, P., Butzin, M., Bard, E., Reimer, R.W., Austin, W.E.N., Bronk Ramsey, C., Grootes, P.M., Hughen, K.A., Kromer, B., Reimer, P.J., Adkins, J., Burke, A., Cook, M.S., Olsen, J., & Skinner, L.C. (2020). Marine20—the marine radiocarbon age calibration curve (0–55,000 cal BP). *Radiocarbon*, 62, 779–820. <https://doi.org/10.1017/RDC.2020.68>.
- Helland-Hansen, W., & Martinsen, O.J. (1996) Shoreline trajectories and sequences: Description of variable depositional-dip scenarios. *Journal of Sedimentary Research*, 66, 670–688. <https://doi.org/10.1306/D42683DD-2B26-11D7-8648000102C1865D>.
- Hernández-Molina, F. J., Roque, C., Lobo, F., Somoza, L., & Díaz del Río, V. (2000a). La cuña progradante infralitoral del Holoceno Superior de Faro-Tavira. *Geogaceta*, 27, 219–222.
- Hernández-Molina, F. J., Somoza, L., & Lobo, F. (2000b). Seismic stratigraphy of the Gulf of Cádiz continental shelf: a model for Late Quaternary very high-resolution sequence stratigraphy and response to sea-level fall. In: Hunt, D., & Gawthorpe, R.L.G. (Eds.), *Sedimentary Responses to Forced Regressions*. Geological Society, London, Special Publication, 172, pp. 329–363. <https://doi.org/10.1144/gsl.sp.2000.172.01.15>.
- Hernández-Molina, F.J., Somoza, L., Vázquez, J.T., Lobo, F., Fernández-Puga, M.C., Llave, E., & Díaz-del-Río, V. (2002). Quaternary stratigraphic stacking patterns on the continental shelves of the southern Iberian Peninsula: their relationship with global climate and paleoceanographic changes. *Quaternary International*, 92, 5–23. [https://doi.org/10.1016/S1040-6182\(01\)00111-2](https://doi.org/10.1016/S1040-6182(01)00111-2).
- Hernández-Molina, J., Llave, E., Somoza, L., Fernández-Puga, M. C., Maestro, A., León, R., Medialdea, T., Barnolas, A., García, M., del Río, V. D., Fernández-Salas, L. M., Vázquez, J. T., Lobo, F., Dias, J. M. A., Rodero, J., & Gardner, J. (2003). Looking for clues to paleoceanographic imprints: A diagnosis of the Gulf of Cadiz contourite depositional systems. *Geology*, 31, 19–22. [https://doi.org/10.1130/0091-7613\(2003\)031<0019:LFCTPI>2.0.CO;2](https://doi.org/10.1130/0091-7613(2003)031<0019:LFCTPI>2.0.CO;2).
- Hernández-Molina, F. J., Llave, E., Stow, D. A. V., García, M., Somoza, L., Vázquez, J. T., Lobo, F. J., Maestro, A., Díaz del Río, V., León, R., Medialdea, T., & Gardner, J. (2006). The contourite depositional system of the Gulf of Cádiz: A sedimentary model related to the bottom current activity of the Mediterranean outflow water and its interaction with the continental margin. *Deep Sea Research Part II: Topical Studies in Oceanography*, 53, 1420–1463. <https://doi.org/10.1016/j.dsr2.2006.04.016>.
- Hernández-Molina, F. J., Sierro, F. J., Llave, E., Roque, C., Stow, D. A. v, Williams, T., Lofi, J., van der Schee, M., Arnáiz, A., Ledesma, S., Rosales, C., Rodríguez-Tovar, F. J., Pardo-Igúzquiza, E., & Brackenkridge, R. E. (2016). Evolution of the gulf of Cadiz margin and southwest Portugal contourite depositional system: Tectonic, sedimentary and paleoceanographic implications from IODP expedition 339. *Marine Geology*, 377, 7–39. <https://dx.doi.org/10.1016/j.margeo.2015.09.013>.

References

- Hogarth, L. J., Driscoll, N. W., Babcock, J. M., & Orange, D. L. (2012). Transgressive deposits along the actively deforming Eel River Margin, Northern California. *Marine Geology*, 303-306, 99-114. <https://doi.org/10.1016/J.MARGEО.2012.02.005>.
- Holbrook, J. M., & Bhattacharya, J. P. (2012). Reappraisal of the sequence boundary in time and space: Case and considerations for an SU (subaerial unconformity) that is not a sediment bypass surface, a time barrier, or an unconformity. *Earth-Science Reviews*, 113, 271-302. <https://doi.org/10.1016/j.earscirev.2012.03.006>.
- Horozal, S., Chae, S., Seo, J. M., Lee, S. M., Han, H. S., Cukur, D., Kim, E. D., & Son, J. H. (2021). Quaternary evolution of the southeastern Korean continental shelf, East Sea: Paleo-incised valley and channel systems. *Marine and Petroleum Geology*, 128, 105011. <https://doi.org/10.1016/j.marpetgeo.2021.105011>.
- Hunt, D., & Tucker, M. E. (1992). Stranded parasequences and the forced regressive wedge systems tract: deposition during base-level fall. *Sedimentary Geology*, 81, 1-9. [https://doi.org/10.1016/0037-0738\(92\)90052-S](https://doi.org/10.1016/0037-0738(92)90052-S).
- Joekel, R.M. (1999) Tectonic Uplift and Climate Change. *Bulletin of the American Meteorological Society*, 80, 936.
- Kearey, P., Brooks, M., & Hill, I. (2013). *An Introduction to Geophysical Exploration*. John Wiley & Sons. Blackwell Publishing. 288 pp.
- Klotsko, S., Driscoll, N., Kent, G., & Brothers, D. (2015). Continental shelf morphology and stratigraphy offshore San Onofre, California: The interplay between rates of eustatic change and sediment supply. *Marine Geology*, 369, 116-126. <https://doi.org/10.1016/j.margeo.2015.08.003>.
- Klotsko, S., Skakun, M., Maloney, J., Gusick, A., Davis, L., Nyers, A., & Ball, D. (2021). Geologic controls on paleodrainage incision and morphology during sea level lowstands on the Cascadia shelf in Oregon, USA. *Marine Geology*, 434, 106444. <https://doi.org/10.1016/j.margeo.2021.106444>.
- Kraft, J. C. (1971). Sedimentary facies patterns and geologic history of a Holocene marine transgression. *Geological Society of America Bulletin*, 2131-2158. [https://doi.org/10.1130/0016-7606\(1971\)82\[2131:sfpageh\]2.0.co;2](https://doi.org/10.1130/0016-7606(1971)82[2131:sfpageh]2.0.co;2).
- Kraft, J.C., Chrzasrowski, M.J., Belknap, D.F., Toscano, M.A., & Fletcher, C.H. (1987). The transgressive barrier-lagoon coast of Delaware: morphostratigraphy, sedimentary sequences and responses to relative rise in sea level. In: Nummedal, D., Pilkey, O.H., Howard, J.D. (Eds.), *Sea-Level Fluctuation and Coastal Evolution*. SEPM Society for Sedimentary Geology Special Publication, 41, pp. 129-143. <https://doi.org/10.2110/pec.87.41.0129>.

- Labaune, C., Jouet, G., Berné, S., Gensous, B., Tesson, M., & Delpeint, A. (2005). Seismic stratigraphy of the Deglacial deposits of the Rhône prodelta and of the adjacent shelf. *Marine Geology*, 222-223, 299-311. <https://doi.org/10.1016/j.margeo.2005.06.018>.
- Labaune, C., Tesson, M., & Gensous, B. (2008). Variability of the transgressive stacking pattern under environmental changes control: Example from the Post-Glacial deposits of the Gulf of Lions inner-shelf, Mediterranean, France. *Continental Shelf Research*, 28, 1138-1152. <https://doi.org/10.1016/j.csr.2008.02.016>.
- Labaune, C., Tesson, M., Gensous, B., Parize, O., Imbert, P., & Delhaye-Prat, V. (2010). Detailed architecture of a compound incised valley system and correlation with forced regressive wedges: Example of Late Quaternary Têt and Agly rivers, western Gulf of Lions, Mediterranean Sea, France. *Sedimentary Geology*, 223, 360-379. <https://doi.org/10.1016/j.sedgeo.2009.12.001>.
- Lambeck, K., & Chappell, J. (2001). Sea Level Change Through the Last Glacial Cycle. *Science*, 292, 679-686. <https://doi.org/10.1126/science.1059549>.
- Lambeck, K., Esat, T.M., & Potter, E.K. (2002). Links between climate and sea levels for the past three million years. *Nature*, 419, 199-206. <https://doi.org/10.1038/nature01089>.
- Lambeck, K., Rouby, H., Purcell, A., Sun, Y., & Sambridge, M. (2014). Sea level and global ice volumes from the Last Glacial Maximum to the Holocene. *Proceedings of the National Academy of Sciences of the United States of America*, 111, 15296-15303. <https://doi.org/10.1073/pnas.1411762111>.
- Lantzsch, H., Hanebuth, T.J.J., & Henrich, R. (2010). Sediment recycling and adjustment of deposition during deglacial drowning of a low-accumulation shelf (NW Iberia). *Continental Shelf Research*, 30, 1665-1679. <https://doi.org/10.1016/j.csr.2010.06.013>.
- Lebreiro, S.M., Moreno, J.C., Abrantes, F.F., & Pflaumann, U. (1997). Productivity and paleoceanographic implications on the Tore Seamount (Iberian Margin) during the last 225 kyr: Foraminiferal evidence. *Paleoceanography*, 12, 718-727. <https://doi.org/10.1029/97PA01748>.
- Lebreiro, S.M., Voelker, A.H.L., Vizcaino, A., Abrantes, F.G., Alt-Epping, U., Jung, S., Thouveny, N., & Gràcia, E. (2009). Sediment instability on the Portuguese continental margin under abrupt glacial climate changes (last 60kyr). *Quaternary Science Reviews*, 28, 3211-3223. <https://doi.org/10.1016/j.quascirev.2009.08.007>.
- Leckie, D.A. (1994). Canterbury Plains, New Zealand-Implications for Sequence Stratigraphic Models1. *American Association of Petroleum Geologists Bulletin*, 78, 1240-1256. <https://doi.org/10.1306/A25FEABD-171B-11D7-8645000102C1865D>.

References

- Lericolais, G., Berné, S., & Féliès, H. (2001). Seaward pinching out and internal stratigraphy of the Gironde incised valley on the shelf (Bay of Biscay). *Marine Geology*, 175, 183-197. [https://doi.org/10.1016/S0025-3227\(01\)00134-7](https://doi.org/10.1016/S0025-3227(01)00134-7).
- Lericolais, G., Auffret, J.P., & Bourillet, J.F. (2003). The Quaternary Channel River: Seismic stratigraphy of its palaeo-valleys and deeps. *Journal of Quaternary Science*, 18, 245-260. <https://doi.org/10.1002/jqs.759>.
- Li, C., Wang, P., Sun, H., Zhang, J., Fan, D., & Deng, B. (2002). Late Quaternary incised-valley fill of the Yangtze delta (China): its stratigraphic framework and evolution. *Sedimentary Geology*, 152, 133-158. [https://doi.org/10.1016/S0037-0738\(02\)00066-0](https://doi.org/10.1016/S0037-0738(02)00066-0).
- Li, C.L., Coullin, P., Bernheim, A., Joliot, V., Auffray, C., Zoroob, R., & Perbal, B. (2006). Integration of Myeloblastosis Associated Virus proviral sequences occurs in the vicinity of genes encoding signaling proteins and regulators of cell proliferation. *Cell Communication and Signaling*, 4, 1-15. <https://doi.org/10.1186/1478-811X-4-1>.
- Li, G., Li, P., Liu, Y., Qiao, L., Ma, Y., Xu, J., & Yang, Z. (2014). Sedimentary system response to the global sea level change in the East China Seas since the last glacial maximum. *Earth-Science Reviews*, 139, 390-405. <https://doi.org/10.1016/j.earscirev.2014.09.007>.
- Liu, J. P., Milliman, J., Gao, S., & Cheng, P. (2004). Holocene development of the Yellow River subaqueous delta, North Yellow Sea. *Marine Geology*, 209, 45-67. <https://doi.org/10.1016/j.margeo.2004.06.009>.
- Liu, J., Saito, Y., Kong, X., Wang, H., Wen, C., Yang, Z., & Nakashima, R. (2010). Delta development and channel incision during marine isotope stages 3 and 2 in the western South Yellow Sea. *Marine Geology*, 278, 54-76. <https://doi.org/10.1016/j.margeo.2010.09.003>.
- Liu, S., Goff, J.A., & Austin, J.A. (2017). Seismic morphology and infilling structure of the buried channel system beneath the inner shelf off western Long Island, New York: Accessing clues to palaeo-estuarine and coastal processes. *Marine Geology*, 387, 12-30. <https://doi.org/10.1016/j.margeo.2017.03.004>.
- Liu, S., Feng, A., & Liu, Y. (2023). Buried channels under the northern Bohai Sea: Evidence for a great Bohai Paleolake during the late MIS3. *Marine and Petroleum Geology*, 155, 106413. <https://doi.org/10.1016/J.MARPETGEO.2023.106413>.
- Llave, E., Hernández-Molina, F.J., Somoza, L., Stow, D.A.V., & del Río, V. (2007). Quaternary evolution of the contourite depositional system in the gulf of Cadiz. *Geological Society Special Publication*, 276, 49-79. <https://doi.org/10.1144/GSL.SP.2007.276.01.03>.

- Lobo, F.J., Hernández-Molina, F.J., Somoza, L., & Díaz del Río, V. (1999). Palaeoenvironments, relative sea-level changes and tectonic influence on the Quaternary seismic units of the Huelva continental shelf (Gulf of Cadiz, southwestern Iberian Peninsula). *Boletín Del Instituto Español de Oceanografía*, 15, 161-180.
- Lobo, F. J., Hernández-Molina, F.J., Somoza, L., Rodero, J., Maldonado, A., & Barnolas, A. (2000). Patterns of bottom current flow deduced from dune asymmetries over the Gulf of Cadiz shelf (southwest Spain). *Marine Geology*, 164, 91-117. [https://doi.org/10.1016/S0025-3227\(99\)00132-2](https://doi.org/10.1016/S0025-3227(99)00132-2).
- Lobo, F.J., Hernández-Molina, F.J., Somoza, L., & Díaz del Río, V. (2001). The sedimentary record of the post-glacial transgression on the Gulf of Cadiz continental shelf (Southwest Spain). *Marine Geology*, 178, 171-195. [https://doi.org/10.1016/S0025-3227\(01\)00176-1](https://doi.org/10.1016/S0025-3227(01)00176-1).
- Lobo, F.J., Plaza, F., González, R., Dias, J.M.A., Kapsimalis, V., Mendes, I., & Díaz del Río, V. (2004a). Estimations of bedload sediment transport in the Guadiana Estuary (SW Iberian Peninsula) during low river discharge periods. *Journal of Coastal Research*, 41, 12-26. <http://hdl.handle.net/10261/318847>.
- Lobo, F. J., Sánchez, R., González, R., Dias, J. M. A., Hernández-Molina, F. J., Fernández-Salas, L. M., Díaz del Río, V., & Mendes, I. (2004b). Contrasting styles of the Holocene highstand sedimentation and sediment dispersal systems in the northern shelf of the Gulf of Cadiz. *Continental Shelf Research*, 24, 461-482. <https://doi.org/10.1016/j.csr.2003.12.003>.
- Lobo, F.J., Dias, J.M.A., Hernández-Molina, F.J., González, R., Fernández-Salas, L.M., & Díaz-Del-Río, V. (2005a). Late Quaternary shelf-margin wedges and upper slope progradation in the Gulf of Cadiz margin (SW Iberian Peninsula). In: Hodgson, D.M., & Flint, S.S. (Eds.), *Submarine Slope Systems: Processes and Products*. Geological Society, London, Special Publications, 244, pp. 7-25. <https://doi.org/10.1144/GSL.SP.2005.244.01.02>.
- Lobo, F.J., Fernández-Salas, L.M., Hernández-Molina, F.J., González, R., Dias, J.M. A., Díaz del Río, V., & Somoza, L. (2005b). Holocene highstand deposits in the Gulf of Cadiz, SW Iberian Peninsula: A high-resolution record of hierarchical environmental changes. *Marine Geology*, 219, 109-131. <https://doi.org/10.1016/j.margeo.2005.06.005>.
- Lobo, F.J., Roy, P. Le, Mendes, I., & Sahabi, M. (2014). Chapter 9 The Gulf of Cádiz continental shelves. Geological Society, London, *Memoirs*, 41, 109-130. <https://doi.org/10.1144/M41.9>.
- Lobo, F.J., Mendes, I., García, M., Reguera, M.I., Antón, L., Lebreiro, S., van Rooij, D., Luján, M., Fernández-Puga, M.C., & Dias, J.M.A. (2015). A progradational pulse during the initial postglacial shelf drowning in the northern Gulf of Cadiz. VIII Simposio sobre el Margen Ibérico Arlántico (MIA15), volumen de comunicaciones, 619-622.

References

- Lobo, F.J., García, M., Luján, M., Mendes, I., Reguera, M.I., & van Rooij, D. (2018). Morphology of the last subaerial unconformity on a shelf: insights into transgressive ravinement and incised valley occurrence in the Gulf of Cádiz. *Geo-Marine Letters*, 38, 33-45. <https://doi.org/10.1007/s00367-017-0511-9>.
- Lofi, J., Voelker, A. H.L., Ducassou, E., Hernández-Molina, F.J., Sierro, F.J., Bahr, A., Galvani, A., Lourens, L.J., Pardo-Igúzquiza, E., Pezard, P., Rodríguez-Tovar, F.J., & Williams, T. (2016). Quaternary chronostratigraphic framework and sedimentary processes for the Gulf of Cadiz and Portuguese Contourite Depositional Systems derived from Natural Gamma Ray records. *Marine Geology*, 377, 40-57. <https://doi.org/10.1016/J.MARGE0.2015.12.005>.
- Long, J.H., Hanebuth, T.J.J., Alexander, C.R., & Wehmiller, J.F. (2021). Depositional Environments and Stratigraphy of Quaternary Paleochannel Systems Offshore of the Georgia Bight, Southeastern U.S.A. *Journal of Coastal Research*, 37, 883-905. <https://doi.org/10.2112/JCOASTRES-D-20-00088.1>.
- Lopes, F.C., Cunha, P.P., le Gall, B. (2006). Cenozoic seismic stratigraphy and tectonic evolution of the Algarve margin (offshore Portugal, southwestern Iberian Peninsula). *Marine Geology*. 231, 1-36. <https://doi.org/10.1016/j.margeo.2006.05.007>.
- López-Galindo, A., Rodero, J., & Maldonado, A. (1999). Surface facies and sediment dispersal patterns: southeastern Gulf of Cadiz, Spanish continental margin. *Marine Geology*, 155, 83-98. [https://doi.org/10.1016/S0025-3227\(98\)00142-X](https://doi.org/10.1016/S0025-3227(98)00142-X).
- Luján, M., Lobo, F.J., Mestdagh, T., Vázquez, J.T., Fernández-Puga, M.C., & Van Rooij D. (2020). Pliocene-Quaternary Deformational Structures in the Eastern Algarve Continental Shelf, Gulf of Cadiz. *Geogaceta* 67, 3-6.
- Lyell, C. (1853). *Principles of Geology; or, the Modern Changes of the Earth and its Inhabitants Considered as Illustrations of Geology*. 9th Edition, Boston, Little, Brown, and Company, 835 pp.
- Madelain, F. (1970). Influence de la topographie du fond sur l'écoulement méditerranéen entre le Détroit de Gibraltar et le Cap Saint-Vincent. *Cahiers océanographiques*, 22, 43-61.
- Maher, B.A., & Thompson, R. (1995). Paleorainfall Reconstructions from Pedogenic Magnetic Susceptibility Variations in the Chinese Loess and Paleosols. *Quaternary Research*, 44, 383-391. <https://doi.org/10.1006/qres.1995.1083>.
- Maldonado, A., & Nelson, C.H. (1999). Interaction of tectonic and depositional processes that control the evolution of the Iberian Gulf of Cadiz margin. *Marine Geology*, 155, 217-242. [https://doi.org/10.1016/S0025-3227\(98\)00148-0](https://doi.org/10.1016/S0025-3227(98)00148-0).

- Maldonado, A., Somoza, L., & Pallarés, L. (1999). The Betic orogen and the Iberian-African boundary in the Gulf of Cadiz: geological evolution (central North Atlantic). *Marine Geology*, 155, 9-43. [https://doi.org/10.1016/S0025-3227\(98\)00139-X](https://doi.org/10.1016/S0025-3227(98)00139-X).
- Maldonado, A., Rodero, J., Pallarés, L., Pérez, L., Somoza, L., Medialdea, T., Hernández-Molina, F.J., & Lobo, F.J. (2003). Mapa Geológico de la Plataforma Continental Española y Zonas Adyacentes. Escala 1:200.000. Cádiz. Instituto Geológico y Minero de España, Madrid.
- Martin, J., Cantelli, A., Paola, C., Blum, M., & Wolinsky, M. (2011). Quantitative Modeling of the Evolution and Geometry of Incised Valleys. *Journal of Sedimentary Research*, 81, 64-79. <https://doi.org/10.2110/jsr.2011.5>.
- Martínez-Carreño, N., & García-Gil, S. (2017). Reinterpretation of the Quaternary sedimentary infill of the Ría de Vigo, NW Iberian Peninsula, as a compound incised valley. *Quaternary Science Reviews*, 173, 124-144. <https://doi.org/10.1016/j.quascirev.2017.08.015>.
- Maselli, V., & Trincardi, F. (2013). Large-scale single incised valley from a small catchment basin on the western Adriatic margin (central Mediterranean Sea). *Global and Planetary Change*, 100, 245-262. <https://doi.org/10.1016/j.gloplacha.2012.10.008>.
- Maselli, V., Hutton, E.W., Kettner, A.J., Syvitski, J.P.M., & Trincardi, F. (2011). High-frequency sea level and sediment supply fluctuations during Termination I: An integrated sequence-stratigraphy and modeling approach from the Adriatic Sea (Central Mediterranean). *Marine Geology*, 287, 54-70. <https://doi.org/10.1016/j.margeo.2011.06.012>.
- Maselli, V., Trincardi, F., Asioli, A., Ceregato, A., Rizzetto, F., & Taviani, M. (2014). Delta growth and river valleys: the influence of climate and sea level changes on the South Adriatic shelf (Mediterranean Sea). *Quaternary Science Reviews*, 99, 146-163. <https://doi.org/10.1016/j.quascirev.2014.06.014>.
- Mat Yusoff, H.H., Johnson, H.D., Lonergan, L., Whittaker, A.C., & Abu Bakar, A. (2023). Seismic stratigraphy of Late Pleistocene incised valleys and adjacent environments, eastern Central Luconia Province, offshore north-west Borneo. *Sedimentology*, 71, 319-354. <https://doi.org/10.1111/sed.13138>.
- Matias, H., Kress, P., Terrinha, P., Mohriak, W., Menezes, P.T.L., Matias, L., Santos, F., & Sandnes, F. (2011). Salt tectonics in the western Gulf of Cadiz, southwest Iberia. *The American Association of Petroleum Geologists Bulletin*, 95, 1667-1698. <https://doi.org/10.1306/01271110032>.
- Mattheus, C.R., & Rodriguez, A.B. (2011). Controls on late quaternary incised-valley dimension along passive margins evaluated using empirical data. *Sedimentology*, 58, 1113-1137. <https://doi.org/10.1111/j.1365-3091.2010.01197.x>.

References

- Mattheus, C.R., Rodriguez, A.B., Greene, D.L., Simms, A.R., & Anderson, J.B. (2007) Control of upstream variables on incised-valley dimension. *Journal of Sedimentary Research*, 77, 213-224. <https://doi.org/10.2110/jsr.2007.022>.
- Mattheus, C.R., Ramsey, K. W., & Tomlinson, J.L. (2020). The evolution of coastal-plain incised valleys over multiple glacio-eustatic cycles: Insights from the inner continental shelf of Delaware, U.S.A. *Journal of Sedimentary Research*, 90, 1510-1526. <https://doi.org/10.2110/jsr.2020.69>.
- Meckel, T.A., & Mulcahy, F.J. (2016). Use of novel high-resolution 3D marine seismic technology to evaluate Quaternary fluvial valley development and geologic controls on shallow gas distribution, inner shelf, Gulf of Mexico. *Interpretation*, 4, 35-49. <https://doi.org/10.1190/int-2015-0092.1>.
- Medialdea, T., Vegas, R., Somoza, L., Vázquez, J.T., Maldonado, A., Díaz-del-Río, V., Maestro, A., Córdoba, D., & Fernández-Puga, M.C. (2004). Structure and evolution of the "Olistostrome" complex of the Gibraltar Arc in the Gulf of Cádiz (eastern Central Atlantic): evidence from two long seismic cross-sections. *Marine Geology*, 209, 173-198. <https://doi.org/10.1016/j.margeo.2004.05.029>.
- Mélières, F. (1974). *Recherches sur la dynamique sédimentaire du Golfe de Cadix (Espagne)*. Thèse d'état de l'Université Pierre et Marie Curie, Paris, 235 pp.
- Mendes, I., Dias, J.A., Schönfeld, J., Ferreira, Ó., Rosa, F., Gonzalez, R., & Lobo, F. J. (2012). Natural and human-induced Holocene paleoenvironmental changes on the Guadiana shelf (northern Gulf of Cadiz). *The Holocene*, 22, 1011-1024. <https://doi.org/10.1177/0959683612437867>.
- Mendes, I., Lobo, F. J., Hanebuth, T.J. J., López-Quirós, A., Schönfeld, J., Lebreiro, S., Reguera, M.I., Antón, L., & Ferreira, Ó. (2020). Temporal variability of flooding events of Guadiana River (Iberian Peninsula) during the middle to late Holocene: Imprints in the shallow-marine sediment record. *Palaeogeography, Palaeoclimatology, Palaeoecology*, 556, 109900. <https://doi.org/10.1016/j.palaeo.2020.109900>.
- Menier, D., Tessier, B., Proust, J.-N., Baltzer, A., Sorrel, P., & Traini, C. (2010). The Holocene transgression as recorded by incised-valley infilling in a rocky coast context with low sediment supply (southern Brittany, western France). *Bulletin de La Société Géologique de France*, 181, 115-128. <https://doi.org/10.2113/gssgfbull.181.2.115>.
- Mesa-Fernández, J.M., Jiménez-Moreno, G., Rodrigo-Gámiz, M., García-Alix, A., Jiménez-Espejo, F.J., Martínez-Ruiz, F., Scott Anderson, R., Camuera, J., & Ramos-Román, M.J. (2018). Vegetation and geochemical responses to Holocene rapid climate change in the Sierra Nevada (southeastern Iberia): The Laguna Hondera record. *Climate of the Past*, 14, 1687-1706. <https://doi.org/10.5194/cp-14-1687-2018>.

- Mestdagh, T., Lobo, F.J., Llave, E., Hernández-Molina, F.J., & van Rooij, D. (2019). Review of the late Quaternary stratigraphy of the northern Gulf of Cadiz continental margin: New insights into controlling factors and global implications. *Earth-Science Reviews*, 198, 102944. <https://doi.org/10.1016/j.earscirev.2019.102944>
- Mestdagh, T., Lobo, F.J., Llave, E., Hernández-Molina, F.J., García-Ledesma, A., Puga-Bernabéu, Á., Fernández-Salas, L.M., & Rooij, D. van. (2020). Late Quaternary multi-genetic processes and products on the northern Gulf of Cadiz upper continental slope (SW Iberian Peninsula). *Marine Geology*, 427, 106214. <https://doi.org/10.1016/j.margeo.2020.106214>.
- Miall, A.D. (1996). *The geology of fluvial deposits: sedimentary facies, basin analysis and petroleum geology*. Springer-Verlag, Inc., Heidelberg, 582 pp.
- Miall, A.D. (2010). *The geology of stratigraphic sequences*. Springer International Publishing, Berlin, 522pp. <https://doi.org/10.1007/978-3-642-05027-5>.
- Miall, A.D. (2014). *Fluvial depositional systems*. Springer International Publishing, Berlin, 316 pp. <https://doi.org/10.1007/978-3-319-00666-6>.
- Milliman, J.D., & Syvitski, J.P.M. (1992). Geomorphic/Tectonic Control of Sediment Discharge to the Ocean: The Importance of Small Mountainous Rivers. *The Journal of Geology*, 100, 525-544. <https://doi.org/10.1086/629606>.
- Mitchum Jr., R.M. (1977). Seismic stratigraphy and global changes of sea level. Part 11: Glossary of terms used in seismic stratigraphy. In: Payton, C.E. (Ed.), *Seismic Stratigraphy - Applications to Hydrocarbon Exploration*. American Association of Petroleum Geologists Memoir, 26, pp. 205-212. <https://doi.org/10.1306/M26490C13>.
- Mitchum, R.M., & Van Wagoner, J.C. (1991). High-frequency sequences and their stacking patterns: sequence-stratigraphic evidence of high-frequency eustatic cycles. *Sedimentary Geology*, 70, 131-160. [https://doi.org/10.1016/0037-0738\(91\)90139-5](https://doi.org/10.1016/0037-0738(91)90139-5).
- Mitchum, R.M., Vail, P.R., & Sandgrew, J.B. (1977). Seismic stratigraphy and global changes of sea level, part 6: stratigraphic interpretation of seismic reflection patterns in depositional sequences. In: Payton, C.E. (Ed.), *Seismic Stratigraphy - Applications to Hydrocarbon Exploration*. American Association of Petroleum Geologists Memoir, 26, pp. 117-134. <https://doi.org/10.1306/M26490C8>.
- Morales, J.A. (1997). Evolution and facies architecture of the mesotidal Guadiana River delta (S.W. Spain-Portugal). *Marine Geology*, 138, 127-148. [https://doi.org/10.1016/S0025-3227\(97\)00009-1](https://doi.org/10.1016/S0025-3227(97)00009-1).
- Morales, J.A., & Garel, E. (2019). The Guadiana River Delta. In: Morales, J.A. (Ed.), *The Spanish Coastal Systems: Dynamic Processes, Sediments and Management*. Springer International Publishing, pp. 565-581. https://doi.org/10.1007/978-3-319-93169-2_24.

References

- Morales, J.A., Pendón, J.G., & Borrego, J. (1994). Origen y evolución de flechas litorales recientes en la desembocadura del estuario mesomareal del río Guadiana (Huelva, SO de España). *Revista de La Sociedad Geológica de España*, 7, 155-167
- Morales, J.A., Borrego, J., Jiménez, I., Monterde, J., & Gil, N. (2001). Morphostratigraphy of an ebb-tidal delta system associated with a large spit in the Piedras Estuary mouth (Huelva Coast, Southwestern Spain). *Marine Geology*, 172, 225-241. [https://doi.org/10.1016/S0025-3227\(00\)00135-3](https://doi.org/10.1016/S0025-3227(00)00135-3).
- Morales, J.A., Rodríguez-Ramírez, A., & Sedrati, M. (2019). Beaches of Huelva. In: Morales, J.A. (Ed.), *The Spanish Coastal Systems: Dynamic Processes, Sediments and Management*. Springer International Publishing, pp. 335-359. https://doi.org/10.1007/978-3-319-93169-2_15.
- Mulder, T., Lecroart, P., Hanquiez, V., Marches, E., Gonthier, E., Guedes, J.-C., Thiébot, E., Jaaidi, B., Kenyon, N., Voisset, M., Perez, C., Sayago, M., Fuchey, Y., & Bujan, S. (2006). The western part of the Gulf of Cadiz: contour currents and turbidity currents interactions. *Geo-Marine Letters*, 26, 31-41. <https://doi.org/10.1007/s00367-005-0013-z>.
- Nelson, C.H., Baraza, J., Maldonado, A., Rodero, J., Escutia, C., & Barber Jr., J.H. (1999). Influence of the Atlantic inflow and Mediterranean outflow currents on Late Quaternary sedimentary facies of the Gulf of Cadiz continental margin. *Marine Geology*, 155, 99-129. [https://doi.org/10.1016/S0025-3227\(98\)00143-1](https://doi.org/10.1016/S0025-3227(98)00143-1).
- Nelson, H.F., & Bray, E.E. (1970). Stratigraphy and history of the Holocene sediments in the Sabine-High Island area, Gulf of Mexico. In: Morgan, J.P., & Shaver, R.H. (Eds.), *Deltaic Sedimentation Modern and Ancient*. SEPM Society for Sedimentary Geology Special Publication, 15, pp. 48-78. <https://doi.org/10.2110/pec.70.11.0048>.
- Nicholls, R.J., Birkemeier, W.A., & Lee, G. (1998). Evaluation of depth of closure using data from Duck, NC, USA: *Marine Geology*, 148, 179-201. [https://doi.org/10.1016/S0025-3227\(98\)00011-5](https://doi.org/10.1016/S0025-3227(98)00011-5).
- Nordfjord, S., Goff, J.A., Austin, J.A., & Sommerfield, C.K. (2005). Seismic geomorphology of buried channel systems on the New Jersey outer shelf: assessing past environmental conditions. *Marine Geology*, 214, 339-364. <https://doi.org/10.1016/j.margeo.2004.10.035>.
- Nordfjord, S., Goff, J.A., Austin, J.A., & Gulick, S.P.S. (2006). Seismic Facies of Incised-Valley Fills, New Jersey Continental Shelf: Implications for Erosion and Preservation Processes Acting During Latest Pleistocene-Holocene Transgression. *Journal of Sedimentary Research*, 76, 1284-1303. <https://doi.org/10.2110/jsr.2006.108>.

- Nordfjord, S., Goff, J.A., Austin, J.A., & Duncan, L.S. (2009). Shallow stratigraphy and complex transgressive ravinement on the New Jersey middle and outer continental shelf. *Marine Geology*, 266, 232-243. <https://doi.org/10.1016/j.margeo.2009.08.010>
- Nummedal, D., & Swift, D.J.P. (1987). Transgressive stratigraphy at sequence-bounding unconformities: some principles derived from Holocene and Cretaceous examples. In: Nummedal, D., Pilkey, O.H., & Howard, J.D. (Eds.), *Sea-Level Fluctuation and Coastal Evolution*. SEPM Society for Sedimentary Geology Special Publication, 41, pp. 241-260. <https://doi.org/10.2110/pec.87.41.0241>.
- Pacheco, A., Ferreira, Ó., Williams, J.J., Garel, E., Vila-Concejo, A., & Dias, J.A. (2010). Hydrodynamics and equilibrium of a multiple-inlet system. *Marine Geology*, 274, 32-42. <https://doi.org/10.1016/j.margeo.2010.03.003>.
- Palanques, A., Díaz, J. I., & Farrán, M. (1995). Contamination of heavy metals in the suspended and surface sediment of the Gulf of Cadiz (Spain): the role of sources, currents, pathways and sinks. *Oceanologica Acta*, 18, 469-477. <http://hdl.handle.net/10261/243390>.
- Paquet, F., Menier, D., Estournès, G., Bourillet, J.F., Leroy, P., & Guillocheau, F. (2010). Buried fluvial incisions as a record of Middle-Late Miocene eustasy fall on the Armorican Shelf (Bay of Biscay, France). *Marine Geology*, 268, 137-151. <https://doi.org/10.1016/j.margeo.2009.11.002>.
- Parsons, J.D., Friedrichs, C.T., Traykovski, P.A., Mohrig, D., Imran, J., Syvitski, J.P.M., Parker, G., Puig, P., Buttles, J.L., & García, M.H. (2007). The Mechanics of Marine Sediment Gravity Flows. In: Nittrouer, C.A., Austin, J.A., Field, M.E., Kravitz, J.H., Syvitski, J.P.M., & Wiberg, P.L. (Eds.), *Continental Margin Sedimentation*. International Association of Sedimentologists Special Publications, 37, pp. 275-337. <https://doi.org/10.1002/9781444304398.CH6>.
- Payton, C.E. (1977). *Seismic Stratigraphy - Applications to Hydrocarbon Exploration*: Tulsa, American Association of Petroleum Geologists Memoir, 26, 516 pp.
- Pellegrini, C., Maselli, V., Cattaneo, A., Piva, A., Ceregato, A., & Trincardi, F. (2015). Anatomy of a compound delta from the post-glacial transgressive record in the Adriatic Sea. *Marine Geology*, 362, 43-59. <https://doi.org/10.1016/j.margeo.2015.01.010>.
- Peltier, W., & Fairbanks, R.G. (2006). Global glacial ice volume and Last Glacial Maximum duration from an extended Barbados Sea level record. *Quaternary Science Reviews*, 25, 3322-3337. <https://doi.org/10.1016/j.quascirev.2006.04.010>.
- Peltier, W.R., Argus, D.F., & Drummond, R. (2015). Space geodesy constrains ice age terminal deglaciation: The global ICE-6G_C (VM5a) model. *Journal of Geophysical Research: Solid Earth*, 120, 450-487. <https://doi.org/10.1002/2014JB011176>.

References

- Pendón, J.G., Morales, J.A., Borrego, J., Jimenez, I., & Lopez, M. (1998). Evolution of estuarine facies in a tidal channel environment, SW Spain: evidence for a change from tide- to wave-domination. *Marine Geology*, 147, 43-62. [https://doi.org/10.1016/S0025-3227\(98\)00006-1](https://doi.org/10.1016/S0025-3227(98)00006-1).
- Pilkey Jr., O.H., W.J. Neal, J.H. Monteiro, & J.M.A. Dias. (1989). Algarve Barrier Islands: A Noncoastal-Plain System in Portugal. *Journal of Coastal Research*, 5, 239-261. <http://www.jstor.org/stable/4297527>.
- Plint, A.G. (1988). Sharp-Based Shoreface Sequences and 'Offshore Bars' in the Cardium Formation of Alberta: Their Relationship to Relative Changes in Sea Level. In: Wilgus, C.K., Hastings, B.S., Kendall, C.G.C., Posamentier, H.W., Ross, C.A., & Van Wagoner, J.C. (Eds.), *Sea-Level Changes: An Integrated Approach*. SEPM Society for Sedimentary Geology Special Publication, 42, pp. 357-370. <https://doi.org/10.2110/pec.88.01.0357>.
- Plomaritis, T.A., Benavente, J., Laiz, I., & Del Río, L. (2015). Variability in storm climate along the Gulf of Cadiz: the role of large scale atmospheric forcing and implications to coastal hazards. *Climate Dynamics*, 45, 2499-2514. <https://doi.org/10.1007/s00382-015-2486-4>.
- Porebski, S.J., & Steel, R.J. (2003). Shelf-margin deltas: their stratigraphic significance and relation to deepwater sands. *Earth-Science Reviews*, 62, 283-326. [https://doi.org/10.1016/S0012-8252\(02\)00161-7](https://doi.org/10.1016/S0012-8252(02)00161-7).
- Portela, L.I., Ramos, S., & Teixeira, A.T. (2013). Effect of salinity on the settling velocity of fine sediments of a harbour basin. *Journal of Coastal Research*, 65, 1188-1193. <https://doi.org/10.2112/SI65-201.1>.
- Posamentier, H.W. (2001). Lowstand Alluvial Bypass Systems: Incised vs. Unincised. *American Association of Petroleum Geologists Bulletin*, 85, 1771-1793. <https://doi.org/10.1306/8626D06D-173B-11D7-8645000102C1865D>.
- Posamentier, H.W., & Vail, P.R. (1988). Eustatic Controls on Clastic Deposition II-Sequence and Systems Tract Models. In: Wilgus, C.K., Hastings, B.S., Kendall, C.G.StC., Posamentier, H.W., Ross, C.A., & Van Wagoner, J.C (Eds.), *Sea-Level Changes: An Integrated Approach*. SEPM Society for Sedimentary Geology Special Publication, 42, pp. 125-154. <https://doi.org/10.2110/pec.88.01.0125>.
- Posamentier, H.W., Jervey, M.T., Vail, P.R. (1988). Eustatic controls on clastic deposition. I. Conceptual framework. In: Wilgus, C.K., Hastings, B.S., Kendall, C.G.StC., Posamentier, H.W., Ross, C.A., Van Wagoner, J.C. (Eds.), *Sea Level Changes: An Integrated Approach*. SEPM Society for Sedimentary Geology Special Publication, 42, pp. 109-124. <https://doi.org/10.2110/pec.88.01.0109>.

- Posamentier, H.W., Allen, G.P., James, D.P., & Tesson, M. (1992). Forced regressions in a sequence stratigraphic framework: concepts, examples, and exploration significance. *American Association of Petroleum Geologists Bulletin*, 76, 1687 - 1709. <https://dx.doi.org/10.1306/bdff8aa6-1718-11d7-8645000102c1865d>.
- Pretorius, L., Green, A.N., & Cooper, A. (2016). Submerged shoreline preservation and ravinement during rapid postglacial sea-level rise and subsequent "slowstand." *Bulletin of the Geological Society of America*, 128, 1059-1069. <https://doi.org/10.1130/B31381.1>.
- Pretorius, L., Green, A.N., Cooper, J.A.G., Hahn, A., & Zabel, M. (2019). Outer- to inner-shelf response to stepped sea-level rise: Insights from incised valleys and submerged shorelines. *Marine Geology*, 416, 105979. <https://doi.org/10.1016/j.margeo.2019.105979>.
- Price, J.F., Baringer, M.O., Lueck, R.G., Johnson, G.C., Ambar, I., Parrilla, G., Cantos, A., Kennelly, M. A., & Sanford, T. B. (1993). Mediterranean Outflow Mixing and Dynamics. *Science*, 259, 1277-1282. <https://doi.org/10.1126/science.259.5099.1277>.
- Proust, J.-N., Menier, D., Guillocheau, F., Guennoc, P., Bonnet, S., Rouby, D., & Corre, C. (2001). Les vallées fossiles de la baie de la Vilaine: nature et évolution du prisme sédimentaire côtier du Pléistocène armoricain. *Bulletin de la Société Géologique de France*, 172, 737-749. <https://doi.org/10.2113/172.6.737>.
- Proust, J.-N., Renault, M., Guennoc, P., & Thion, I. (2010). Sedimentary architecture of the Loire River drowned valleys of the French Atlantic shelf. *Bulletin de La Société Géologique de France*, 181(2), 129-149. <https://doi.org/10.2113/gssgfbull.181.2.129>.
- Puchała, R.J., Porbski, S.J., Śliwiński, W.R., & August, C. J. (2011). Pleistocene to Holocene transition in the central basin of the Gulf of Thailand, based on geoacoustic survey and radiocarbon ages. *Marine Geology*, 288, 103-111. <https://doi.org/10.1016/j.margeo.2011.08.007>.
- Qiu, J., Liu, J., Saito, Y., Yin, P., Zhang, Y., Liu, J., & Zhou, L. (2019). Seismic morphology and infilling architecture of incised valleys in the northwest South Yellow Sea since the last glaciation. *Continental Shelf Research*, 179, 52-65. <https://doi.org/10.1016/j.csr.2019.04.008>.
- Ramos, A., Fernández, O., Terrinha, P., & Muñoz, J.A. (2016). Extension and inversion structures in the Tethys-Atlantic linkage zone, Algarve Basin, Portugal. *International Journal of Earth Sciences*, 105, 1663-1679. <https://doi.org/10.1007/s00531-015-1280-1>.
- Ramos, A., Fernández, O., Muñoz, J.A., & Terrinha, P. (2017). Impact of basin structure and evaporite distribution on salt tectonics in the Algarve Basin, Southwest Iberian margin. *Marine and Petroleum Geology*, 88, 961-984. <https://doi.org/10.1016/j.marpetgeo.2017.09.028>.

References

- Ramos, A., Fernández, O., Terrinha, P., Muñoz, J.A., & Arnaiz, Á. (2020). Paleogeographic evolution of a segmented oblique passive margin: the case of the SW Iberian margin. *International Journal of Earth Sciences*, 109, 1871-1895. <https://doi.org/10.1007/s00531-020-01878-w>.
- Rampino, M.R., & Sanders, J.E. (1980). Holocene transgression in south-central Long Island, New York: *Journal of Sedimentary Petrology*, 50, 1063-1080.
- Reading, H.G., & Collinson, J.D. (1996). Clastic Coasts. In: Reading, H.G. (Ed.), *Sedimentary Environments: Processes, Facies and Stratigraphy*. Blackwells, Cornwall, pp. 154-231.
- Reijnenstein, H., Posamentier, H., & Bhattacharya, J. (2011). Seismic geomorphology and high-resolution seismic stratigraphy of inner-shelf fluvial, estuarine, deltaic, and marine sequences, Gulf of Thailand. *American Association of Petroleum Geologists Bulletin*, 95, 1959-1990. <https://doi.org/10.1306/03151110134>.
- Rey, J., & Medialdea, T. (1989). Morfología y sedimentos recientes del margen continental de Andalucía Occidental. In: Díaz del Olmo, F., Rodríguez-Vidal, J. (Eds.). *El Cuaternario de Andalucía occidental*. AEQUA Monografías, 1, pp. 133-144.
- Reynaud, J., Tessier, B., Proust, J.-N., Dalrymple, R., Bourillet, J.-F., Batist, M., Lericolais, G., Berne, S., & Marsset, T. (1999). Architecture and sequence stratigraphy of a Late Neogene incised valley at the shelf margin, Southern Celtic Sea. *Journal of Sedimentary Research*, 69, 351-364. <https://doi.org/10.2110/jsr.69.351>.
- Richter, T.O., Gaast, S., van der Koster, B., Vaars, A., Gieles, R., Stigter, H.C., de Haas, H., & van der Weering, T.C.E. (2006). The Avaatech XRF Core Scanner: technical description and applications to NE Atlantic sediments. In: Rothwell, R.G. (Ed.), *New Techniques in Sediment Core Analysis*. Geological Society, London, Special Publications, 267, pp. 39-50. <https://doi.org/10.1144/GSL.SP.2006.267.01.03>
- Rocha, F., Boski, T., Gomes, C., Moura, D., & Veiga-Pires, C.C. (2004). Characterization of the sedimentary environment of the Gilão River mouth, based on sedimentological and mineralogical analysis. *Thalassas* 20, 31-37. <http://hdl.handle.net/10400.1/2627>.
- Rodero, J., Pallares, L., & Maldonado, A. (1999). Late Quaternary seismic facies of the Gulf of Cadiz Spanish margin: depositional processes influenced by sea-level change and tectonic controls. *Marine Geology*, 155, 131-156. [https://doi.org/10.1016/S0025-3227\(98\)00144-3](https://doi.org/10.1016/S0025-3227(98)00144-3).
- Rodrigues, T., Grimalt, J.O., Abrantes, F.G., Flores, J. A., & Lebreiro, S.M. (2009). Holocene interdependences of changes in sea surface temperature, productivity, and fluvial inputs in the Iberian continental shelf (Tagus mud patch). *Geochemistry, Geophysics, Geosystems*, 10, Q07U06. <https://doi.org/10.1029/2008GC002367>.

- Rodrigues, T., Grimalt, J.O., Abrantes, F., Naughton, F., & Flores, J.A. (2010). The last glacial-interglacial transition (LGIT) in the western mid-latitudes of the North Atlantic: Abrupt sea surface temperature change and sea level implications. *Quaternary Science Reviews*, 29, 1853-1862. <https://doi.org/10.1016/j.quascirev.2010.04.004>.
- Rodríguez Ramírez, A., Ruiz, F., Caceres, L.M., Rodríguez Vidal, J., Pino, R., & Muñoz, J.M. (2003). Analysis of the recent storm record in the southwestern Spanish coast: implications for littoral management. *The Science of the Total Environment*, 303, 189-201. [https://doi.org/10.1016/S0048-9697\(02\)00400-X](https://doi.org/10.1016/S0048-9697(02)00400-X).
- Rodriguez, A., Anderson, J., & Simms, A. (2005). Terrace Inundation as an Autocyclic Mechanism for Parasequence Formation: Galveston Estuary, Texas, U.S.A. *Journal of Sedimentary Research*, 75, 608-620. <https://doi.org/10.2110/jsr.2005.050>.
- Ronchi, L., Fontana, A., Correggiari, A., & Asioli, A. (2018). Late Quaternary incised and infilled landforms in the shelf of the northern Adriatic Sea (Italy). *Marine Geology*, 405, 47-67. <https://doi.org/10.1016/j.margeo.2018.08.004>.
- Roque, C., Hernández-Molina, F.J., Lobo, F.J., Somoza, L., Díaz del Río, V., Vázquez, J.T., & Dias, J. (2010). Geomorphology of the Eastern Algarve proximal continental margin (South Portugal, SW Iberia Peninsula): sedimentary dynamics and its relationship with the last asymmetrical eustatic cycle. *Ciências Da Terra*, 17, 7-28.
- Rosa, F., Rufino, M., Ferreira, Ó., Matias, A., Brito, A., & Gaspar, M. (2013). The influence of coastal processes on inner shelf sediment distribution: The Eastern Algarve Shelf (Southern Portugal). *Geologica Acta*, 11, 59-73. <https://doi.org/10.1344/105.000001755>.
- Rosenbaum, G., Lister, G.S., & Duboz, C. (2002). Relative motions of Africa, Iberia and Europe during Alpine orogeny. *Tectonophysics*, 359, 117-129. [https://doi.org/10.1016/S0040-1951\(02\)00442-0](https://doi.org/10.1016/S0040-1951(02)00442-0).
- Rothwell, R.G., & Croudace, I.W. (2015). Twenty Years of XRF Core Scanning Marine Sediments: What Do Geochemical Proxies Tell Us? In: Croudace I.W., & Rothwell, R.G. (Eds.), *Micro-XRF Studies of Sediment Cores. Developments in Paleoenvironmental Research*, 17, pp. 25-102. https://doi.org/10.1007/978-94-017-9849-5_2.
- Roveri, M., Flecker, R., Krijgsman, W., Lofi, J., Lugli, S., Manzi, V., Sierro, F.J., Bertini, A., Camerlenghi, A., De Lange, G., Govers, R., Hilgen, F.J., Hübscher, C., Meijer, P.T., & Stoica, M. (2014). The Messinian Salinity Crisis: Past and future of a great challenge for marine sciences. *Marine Geology*, 352, 25-58. <https://doi.org/10.1016/j.margeo.2014.02.002>.
- Roy, P.S., Cowell, P.J., Ferland, M.A., & Thom, B.G. (1994). Wave-dominated coasts. In: Carter, R.W.G., Woodroffe, C.D. (Eds.), *Coastal Evolution: Late Quaternary Shoreline Morphodynamics*. Cambridge University Press, pp. 121-186 <https://doi.org/10.1017/CBO9780511564420.006>.

References

- Ruddiman, W.F. (2013). Tectonic uplift and climate change. Springer Science & Business Media, 535pp. <https://doi.org/10.1007/978-1-4615-5935-1>.
- Saito, Y. (1994). Shelf sequence and characteristic bounding surfaces in a wave-dominated setting: Latest Pleistocene-Holocene examples from Northeast Japan. *Marine Geology*, 120, 105-127. [https://doi.org/10.1016/0025-3227\(94\)90080-9](https://doi.org/10.1016/0025-3227(94)90080-9).
- Sanders, J., & Kumar, N. (1975). Evidence of Shoreface Retreat and In-Place "Drowning" During Holocene Submergence of Barriers, Shelf off Fire Island, New York. *Geological Society of America Bulletin*, 86, 65–76. [https://doi.org/10.1130/0016-7606\(1975\)86<65:EOSRAI>2.0.CO;2](https://doi.org/10.1130/0016-7606(1975)86<65:EOSRAI>2.0.CO;2).
- Schattner, U., José Lobo, F., López-Quirós, A., dos Passos Nascimento, J.L., & de Mahiques, M.M. (2020). What feeds shelf-edge clinoforms over margins deprived of adjacent land sources? An example from southeastern Brazil. *Basin Research*, 32, 293-301. <https://doi.org/10.1111/bre.12397>.
- Schumm, S.A., & Brakenridge, G. R. (1987). River responses. In: Ruddiman, W.F., & Wright, H.E. (Eds.), *North America and Adjacent Oceans During the Last Deglaciation. The Geology of North America*, K-3, pp. 221-240. <https://doi.org/10.1130/DNAG-GNA-K3.221>.
- Sheriff, R.E., & Geldart, L.P. (1995). *Exploration Seismology*. 2nd Edition, Cambridge University Press. 628 pp. <https://doi.org/10.1017/CBO9781139168359>.
- Shinn, Y. J., Chough, S. K., Kim, J. W., & Woo, J. (2007). Development of depositional systems in the southeastern Yellow Sea during the postglacial transgression. *Marine Geology*, 239, 59-82. <https://doi.org/10.1016/j.margeo.2006.12.007>.
- Siddall, M.E., Rohling, E. J., Almogi-Labin, A., Hemleben, C., Meischner, D., Schmelzer, I., & Smeed, D. (2003). Sea-level fluctuations during the last glacial cycle. *Nature*, 423, 853-858. <https://doi.org/10.1038/nature01690>.
- Simms, A., Anderson, J., Taha, Z., & Rodriguez, A. (2006). Overfilled versus Underfilled Incised Valleys: examples from the Quaternary Gulf of Mexico. In: Dalrymple, R.W., Leckie, D.A., & Tillman, R.W. (Eds.), *Incised Valleys in Time and Space*. SEPM Society for Sedimentary Geology Special Publication, 85, pp. 117–139. <https://doi.org/10.2110/pec.06.85.0117>.
- Sloss, L.L., Krumbein, W.C., & Dapples, E.C. (1949). Integrated facies analysis 1. In: Longwell, C.R., Moore, R.C., McKee, E.D., Müller, S.W., Spieker, E.M., Wood, H.E., Sloss, L.L., Krumbein, W.C., & Dapples, E.C. (Eds.), *Sedimentary Facies in Geologic History*. Geological Society of America memoir, 39, pp. 91–124. <https://doi.org/10.1130/MEM39-p91>.

- Somoza, L., Hernández-Molina, F.J., de Andrés, J.R., & Rey, J. (1997). Continental shelf architecture and sea-level cycles: Late Quaternary high-resolution stratigraphy of the Gulf of Cádiz, Spain. *Geo-Marine Letters*, 17, 133-139. <https://doi.org/10.1007/s003670050018>.
- Sousa, C., Boski, T., Gomes, A., Pereira, L., Lampreia, J., & Oliveira, S. (2014). Holocene reconstruction of the Ria Formosa coastal lagoon (south of Portugal) based on a pre-Holocene paleosurface digital model. *Comunicações Geológicas*, 101, 635-639.
- Sousa, C., Boski, T., & Pereira, L. (2019). Holocene evolution of a barrier island system, Ria Formosa, South Portugal. *The Holocene* 29, 64-76. <https://doi.org/10.1177/0959683618804639>.
- Spanish National Geographic Institute, 2015. Mapa Topográfico Nacional 1:50.000 ráster de España, MTN50 ráster.
- Spinelli, G.A., & Field, M.E. (2003). Controls of tectonics and sediment source locations on along-strike variations in transgressive deposits on the northern California margin. *Marine Geology*, 197, 35-47. [https://doi.org/10.1016/S0025-3227\(03\)00116-6](https://doi.org/10.1016/S0025-3227(03)00116-6).
- Srivastava, S.P., Schouten, H., Roest, W.R., Klitgord, K.D., Kovacs, L. C., Verhoef, J., & Macnab, R. (1990). Iberian plate kinematics: A jumping plate boundary between Eurasia and Africa. *Nature*, 344, 756 - 759. <https://doi.org/10.1038/344756a0>.
- Stanford, J.D., Hemingway, R., Rohling, E.J., Challenor, P.G., Medina-Elizalde, M., & Lester, A.J. (2011). Sea-level probability for the last deglaciation: A statistical analysis of far-field records. *Global and Planetary Change*, 79, 193-203. <https://doi.org/10.1016/j.gloplacha.2010.11.002>.
- Stanley, D.J. (1995), A global sea-level curve for the late Quaternary: the impossible dream? *Marine Geology*, 125, 1-6. [https://doi.org/10.1016/0025-3227\(95\)00057-6](https://doi.org/10.1016/0025-3227(95)00057-6).
- Storms, J.E.A., Weltje, G.J., Terra, G. J., Cattaneo, A., & Trincardi, F. (2008). Coastal dynamics under conditions of rapid sea-level rise: Late Pleistocene to Early Holocene evolution of barrier-lagoon systems on the northern Adriatic shelf (Italy). *Quaternary Science Reviews*, 27, 1107-1123. <https://doi.org/10.1016/j.quascirev.2008.02.009>.
- Strong, N., & Paola, C. (2008). Valleys That Never Were: Time Surfaces Versus Stratigraphic Surfaces. *Journal of Sedimentary Research*, 78, 579-593. <https://doi.org/10.2110/jsr.2008.059>.
- Stuiver, M., Reimer, P.J., & Reimer, R.W. (2021). Calib 8.2. *Radiocarbon*, 35, 215-230. <http://calib.org>
- Summerfield, M.A. (1985). Plate tectonics and landscape development on the African continent. In: Morisawa, M., & Hack, J.T. (Eds.) *Tectonic Geomorphology*. Allen and Unwin, Boston, MA, pp. 27-51.

References

- Swift, D.J.P. (1968). Coastal Erosion and Transgressive Stratigraphy. *The Journal of Geology*, 76, 444-456. <http://www.jstor.org/stable/30064653>
- Swift, D.J.P. (1975). Barrier-island genesis: evidence from the central Atlantic shelf, eastern U.S.A. *Sedimentary Geology*, 14, 1-43. [https://doi.org/10.1016/0037-0738\(75\)90015-9](https://doi.org/10.1016/0037-0738(75)90015-9).
- Swift, D.J.P. (1976). Coastal sedimentation. In: Stanley, D.J., & Swift, D.J.P. (Eds.), *Marine Sediment Transport and Environmental Management*. Wiley, New York, pp. 255-310.
- Syvitski, J.P.M., & Milliman, J.D. (2007). Geology, Geography, and Humans Battle for Dominance over the Delivery of Fluvial Sediment to the Coastal Ocean. *The Journal of Geology*, 115, 1-19. <https://doi.org/10.1086/509246>
- Talling, P.J. (1998). How and where do incised valleys form if sea level remains above the shelf edge? *Geology* 26, 87-90. [https://doi.org/10.1130/0091-7613\(1998\)026<0087:HAWDIV>2.3.CO;2](https://doi.org/10.1130/0091-7613(1998)026<0087:HAWDIV>2.3.CO;2).
- Tan, M., Zhu, X., Liu, Q., Zhang, Z., & Liu, W. (2020). Multiple fluvial styles in Late Miocene post-rift successions of the offshore Bohai Bay Basin (China): Evidence from a seismic geomorphological study. *Marine and Petroleum Geology*, 113, 104173. <https://doi.org/10.1016/j.marpetgeo.2019.104173>.
- Tanabe, S., Nakanishi, T., Ishihara, Y., & Nakashima, R. (2015). Millennial-scale stratigraphy of a tide-dominated incised valley during the last 14 kyr: Spatial and quantitative reconstruction in the Tokyo Lowland, central Japan. *Sedimentology*, 62, 1837-1872. <https://doi.org/10.1111/sed.12204>.
- Telford, R.J., Heegaard, E., & Birks, H.J.B. (2004). The intercept is a poor estimate of a calibrated radiocarbon age. *The Holocene*, 14, 296-298. <https://doi.org/10.1191/0959683604hl707fa>.
- Terrinha, P. (1998). Structural geology and tectonic evolution of the Algarve Basin, south Portugal. Ph.D. Thesis, Imperial College London, 430 pp.
- Terrinha, P., Matias, L., Vicente, J., Duarte, J., Luís, J., Pinheiro, L., Lourenço, N., Diez, S., Rosas, F., Magalhães, V., Valadares, V., Zitellini, N., Roque, C., & Víctor, L.M. (2009). Morphotectonics and strain partitioning at the Iberia-Africa plate boundary from multibeam and seismic reflection data. *Marine Geology*, 267, 156-174. <https://doi.org/10.1016/j.margeo.2009.09.012>.
- Tessier, B. (2012). Stratigraphy of Tide-Dominated Estuaries. In: Davis Jr., R.A., Dalrymple, R.W. (Eds.), *Principles of Tidal Sedimentology*. Springer Netherlands, Dordrecht, pp. 109-128. https://doi.org/10.1007/978-94-007-0123-6_6.
- Tesson, M., Labaune, C., Gensous, B. (2005). Small rivers contribution to the Quaternary evolution of a Mediterranean littoral system: The western gulf of Lion, France. *Marine Geology*, 223, 299-311. <https://doi.org/10.1016/j.margeo.2005.06.021>.

- Tesson, M., Labaune, C., Gensous, B., & Delhay-Prat, V. (2010). Quaternary compound incised valleys of the Roussillon coast (SE France): correlation of seismic data with core data. *Bulletin de La Société Géologique de France*, 181, 183-196. <https://doi.org/10.2113/gssgfbull.181.2.183>.
- Tesson, M., Labaune, C., Gensous, B., Suc, J.-P., Melinte-Dobrinescu, M., Parize, O., Imbert, P., & Delhay-Prat, V. (2011). Quaternary "Compound" Incised Valley in a Microtidal Environment, Roussillon Continental Shelf, Western Gulf of Lions, France. *Journal of Sedimentary Research*, 81, 708-729. <https://doi.org/10.2110/jsr.2011.59>.
- Tesson, M., Posamentier, H., & Gensous, B. (2015). Compound incised-valley characterization by high-resolution seismics in a wave-dominated setting: Example of the Aude and Orb rivers, Languedoc inner shelf, Gulf of Lion, France. *Marine Geology*, 367, 1-21. <https://doi.org/10.1016/j.margeo.2015.05.004>.
- Thanh, N.T., Liu, P.J., Dong, M.D., Nhon, D.H., Cuong, D.H., Dung, B.V., Phach, P. van, Thanh, T.D., Hung, D.Q., & Nga, N.T. (2018). Late Pleistocene-Holocene sequence stratigraphy of the subaqueous Red River delta and the adjacent shelf. *Science of the Earth*, 40, 271-287. <https://doi.org/10.15625/0866-7187/40/3/12618>.
- Thomas, M.A., & Anderson, J.B. (1994). Sea-level controls on the facies architecture of the Trinity/Sabine incised-valley system, Texas continental shelf. In: Dalrymple, R.W., Boyd, R., & Zaitlin, B.A. (Eds.), *Incised-valley Systems: Origin and Sedimentary Sequences*. SEPM Society for Sedimentary Geology Special Publication, 51, pp. 63-82. <https://doi.org/10.2110/pec.94.12.0063>.
- Thorndycraft, V.R., & Benito, G. (2006). The Holocene fluvial chronology of Spain: evidence from a newly compiled radiocarbon database. *Quaternary Science Reviews*, 25, 223-234. <https://doi.org/10.1016/j.quascirev.2005.07.003>.
- Tjallingii, R., Stattegger, K., Wetzel, A., & van Phach, P. (2010). Infilling and flooding of the Mekong River incised valley during deglacial sea-level rise. *Quaternary Science Reviews*, 29, 1432-1444. <https://doi.org/10.1016/j.quascirev.2010.02.022>
- Torelli, L., Sartori, R., & Zitellini, N. (1997). The giant chaotic body in the Atlantic Ocean off Gibraltar: new results from a deep seismic reflection survey. *Marine and Petroleum Geology*, 14, 125-138. [https://doi.org/10.1016/S0264-8172\(96\)00060-8](https://doi.org/10.1016/S0264-8172(96)00060-8).
- Törnqvist, T., Wortman, S., Mateo, Z., Milne, G., & Swenson, J. (2006). Did the last sea level lowstand always lead to cross-shelf valley formation and source-to-sink sediment flux? *Journal of Geophysical Research: Earth Surface*, 111, F04002. <https://doi.org/10.1029/2005JF000425>.

References

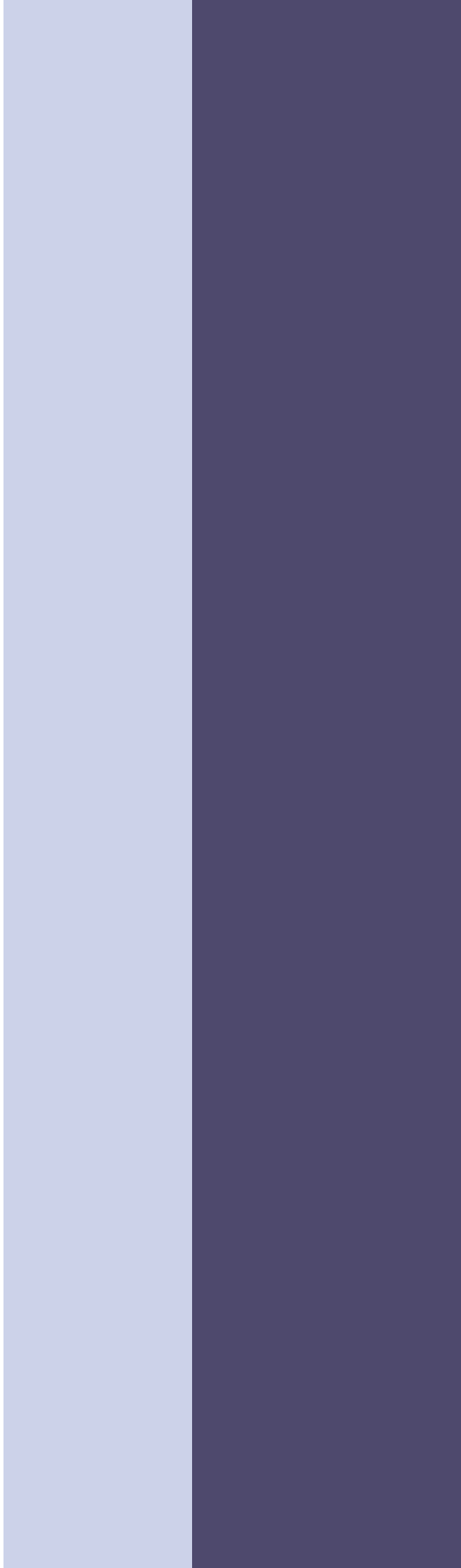
- Tortora, P. (1996). Depositional and erosional coastal processes during the last postglacial sea-level rise; an example from the central Tyrrhenian continental shelf (Italy). *Journal of Sedimentary Research*, 66, 391-405. <https://doi.org/10.1306/D4268356-2B26-11D7-8648000102C1865D>.
- Trigo, R.M., & DaCamara, C.C. (2000). Circulation weather types and their influence on the precipitation regime in Portugal. *International Journal of Climatology*, 20: 1559-1581. [https://doi.org/10.1002/1097-0088\(20001115\)20:13<1559::AID-JOC555>3.0.CO;2-5](https://doi.org/10.1002/1097-0088(20001115)20:13<1559::AID-JOC555>3.0.CO;2-5).
- Trincardi, F., Cattaneo, A., Alessandra, A., Correggiari, A., & Langone, L. (1996). Stratigraphy of the late-Quaternary deposits in the Central Adriatic basin and the record of short-term climatic events. *Memorie-Istituto Italiano Di Idrobiologia*, 55, 39-70.
- Trincardi, F., Correggiari, A., & Roveri, M. (1994). Late Quaternary transgressive erosion and deposition in a modern epicontinental shelf: The Adriatic semienclosed basin. *Geo-Marine Letters*, 14, 41-51. <https://doi.org/10.1007/BF01204470>.
- Vail, P.R. (1987) Seismic Stratigraphy Interpretation Procedures. In: Bally, A.W. (Ed.), *Atlas of Seismic Stratigraphy*, American Association of Petroleum Geologists Studies in Geology, 1, pp. 1-10.
- Vail, P.R., Mitchum, R.M., & Sangree, J.B. (2002). Concepts of depositional sequences. In: Armentrout, J., & Rosen, N.C. (Eds.), *Sequence Stratigraphic Models for Exploration and Production: Evolving Methodology, Emerging Models, and Application Histories*. 22nd Annual Gulf Coast Section SEPM Foundation Bob F. Perkins Research Conference Proceedings, pp.19-32. <https://doi.org/10.5724/gcs.02.22>.
- Val-Peón, C., Santisteban, J.I., López-Sáez, J.A., Weniger, G.-C., & Reicherter, K. (2021). Environmental Changes and Cultural Transitions in SW Iberia during the Early-Mid Holocene. *Applied Sciences*, 11, 3580. <https://doi.org/10.3390/app11083580>.
- Van Wagoner, J.C., Posamentier, H.W., Mitchum, R.M., Vail, P.R., Sarg, J.F., Loutit, T.S., & Hardenbol, J. (1988). An Overview of the Fundamentals of Sequence Stratigraphy and Key Definitions. In: Wilgus, C.K., Hastings, B.S., Kendall, C.G.StC., Posamentier, H.W., Ross, C.A., & Van Wagoner, J.C (Eds.), *Sea-Level Changes: An Integrated Approach*. SEPM Society for Sedimentary Geology Special Publication, 42, pp. 39-45. <https://doi.org/10.2110/pec.88.01.0039>.
- Van Wagoner J.C., Mitchum R.M., Campion K.M., & Rahmanian V.D. (1990). Siliciclastic Sequence Stratigraphy in Well Logs, Cores, and Outcrops: Concepts for High-Resolution Correlation of Time and Facies. *American Association of Petroleum Geologists Methods in Exploration Series*, 7, 55. <https://doi.org/10.1017/S0016756800017866>.
- Vanney, J.R., & Mougénot, D. (1982). La plate-forme continentale du Portugal et les provinces adjacentes: Analyse géomorphologique. *Geo-Marine Letters*, 2, 109. <https://doi.org/10.1007/BF02462809>.

- Vázquez, J.T., Fernández-Puga, M.C., Medialdea, T., Díaz del Rio, V., Fernández-Salas, L.M., Llave, E., Lobo, F.J., Lopes, F.C., Maldonado, A., Somoza, L., & Palomino, D. (2010). Fracturación normal durante el Cuaternario Superior en la plataforma continental septentrional del Golfo de Cádiz (SO de Iberia). 1ª Reunión Ibérica Sobre Tectónica Activa y Paleosismología.
- Veiga-Pires, C.C., Moura, D., Pedro, P., Correia, V., Duarte, D., & Boski, T. (2000). Gilão and Almagem Rivers evolution during Late Quaternary - Preliminary results. *INQUA Newsletters*, 22, 79-80.
- Vila-Concejo, A., Matias, A., Pacheco, A., Ferreira, Ó., & Dias, J.A. (2006). Quantification of inlet-hazards in barrier island systems. An example from the Ria Formosa (Portugal). *Continental Shelf Research*, 26, 1045-1060. <https://doi.org/10.1016/j.csr.2005.12.014>.
- Walker, R.G. (1990) Facies modeling and sequence stratigraphy. *Journal of Sedimentary Research*, 60, 777-786. <https://doi.org/10.1306/212F926E-2B24-11D7-8648000102C1865D>.
- Wang, R., Colombera, L., Mountney, N.P. (2019). Geological controls on the geometry of incised-valley fills: Insights from a global dataset of late-Quaternary examples. *Sedimentology* 66, 2134-2168. <https://doi.org/10.1111/sed.12596>.
- Wang, R., Colombera, L., & Mountney, N.P. (2020). Quantitative analysis of the stratigraphic architecture of incised-valley fills: A global comparison of Quaternary systems. *Earth Sciences Reviews*, 200, 102988. <https://doi.org/10.1016/j.earscirev.2019.102988>.
- Weaver, P.P.E., Wynn, R.B., Kenyon, N.H., & Evans, J. (2000). Continental margin sedimentation, with special reference to the north-east Atlantic margin. *Sedimentology*, 47, 239-256. <https://doi.org/10.1046/j.1365-3091.2000.0470s1239.x>.
- Weber, N., Chaumillon, E., Tesson, M., & Garlan, T. (2004a). Architecture and morphology of the outer segment of a mixed tide and wave-dominated-incised valley, revealed by HR seismic reflection profiling: the paleo-Charente River, France. *Marine Geology*, 207, 17-38. <https://doi.org/10.1016/j.margeo.2004.04.001>.
- Weber, N., Chaumillon, E., Tesson, M. (2004b). Enregistrement de la dernière remontée du niveau marin dans l'architecture interne d'une vallée incisée: le Pertuis Breton (Charente-Maritime). *Comptes Rendus Geoscience*, 336, 1273-1282. <https://doi.org/10.1016/j.crte.2004.07.007>.
- Wellner, R.W., & Bartek, L.R. (2003). The Effect of Sea Level, Climate, and Shelf Physiography on the Development of Incised-Valley Complexes: A Modern Example From the East China Sea. *Journal of Sedimentary Research*, 73, 926-940. <https://doi.org/10.1306/041603730926>.

References

- Weschenfelder, J., Baitelli, R., Corrêa, I.C.S., Bortolin, E.C., & dos Santos, C.B. (2014). Quaternary incised valleys in southern Brazil coastal zone. *Journal of South American Earth Sciences*, 55, 83-93. <https://doi.org/10.1016/j.jsames.2014.07.004>.
- Wetzel, A., Feldens, A., Unverricht, D., Stattegger, K., & Tjallingii, R. (2021). Late Pleistocene sea-level changes and the formation and fill of bent valleys incised into the shelf of the western South China Sea. *Journal of Asian Earth Sciences*, 206, 104626. <https://doi.org/10.1016/j.jseaes.2020.104626>.
- Wilgus, C.K., Hastings, B.S., Kendall, C.G.C., Posamentier, H.W., Ross, C.A., & Van Wagoner, J.C. (1988). *Sea-Level Changes: An Integrated Approach*. SEPM Society for Sedimentary Geology Special Publication, 42, 407 pp. <https://doi.org/10.2110/pec.88.01>
- Ximenes Neto, A.R., Pessoa, P.R.S., Pinheiro, L. de S., & de Moraes, J.O. (2021). Seismic stratigraphy of a partially filled incised valley on a semi-arid continental shelf, Northeast Brazil. *Geo-Marine Letters*, 41, 18. <https://doi.org/10.1007/s00367-021-00687-7>.
- Xu, C., Wang, H., Mou, X., Wu, X., Wang, Y., Li, X., Zhang, Y., Kong, X., Cong, J., & Ning, Z. (2022). Sea level change determined paleochannel development on the continental shelf of the southern East China Sea since MIS 5. *Palaeogeography, Palaeoclimatology, Palaeoecology*, 606, 111242. <https://doi.org/10.1016/J.PALAEO.2022.111242>.
- Zaitlin, B.A., Dalrymple, R.W., & Boyd, R. (1994). The Stratigraphic Organization of Incised-Valley Systems Associated with Relative Sea-Level Change. In: Dalrymple, R.W., Boyd, R., & Zaitlin, B.A. (Eds.), *Incised-Valley Systems: Origin and Sedimentary Sequences*. SEPM Society for Sedimentary Geology Special Publication, 51, pp. 45-60. <https://doi.org/10.2110/pec.94.12.0045>.
- Zecchin, M., & Catuneanu, O. (2013). High-resolution sequence stratigraphy of clastic shelves I: Units and bounding surfaces. *Marine and Petroleum Geology*, 39, 1-25. <https://doi.org/10.1016/j.marpetgeo.2012.08.015>.
- Zecchin, M., Gordini, E., & Ramella, R. (2015). Recognition of a drowned delta in the northern Adriatic Sea, Italy: Stratigraphic characteristics and its significance in the frame of the early Holocene sea-level rise. *Holocene*, 25, 1027-1038. <https://doi.org/10.1177/0959683615575358>.
- Zitellini, N., Gràcia, E., Matias, L., Terrinha, P., Abreu, M.A., DeAlteriis, G., Henriët, J.P., Dañobeitia, J.J., Masson, D.G., Mulder, T., Ramella, R., Somoza, L., & Diez, S. (2009). The quest for the Africa-Eurasia plate boundary west of the Strait of Gibraltar. *Earth and Planetary Science Letters*, 280, 13-50. <https://doi.org/10.1016/j.epsl.2008.12.005>.

APPENDIX



APPENDIX: Figures and tables

Figures:

- [1] **Figure 1.1:** Sequence stratigraphic surfaces and systems tract beds developed during a full cycle of relative sea-level change in a clastic shelf/ramp setting. Continental to offshore deposits are considered (Adapted from Zecchin and Catuneanu, 2013).
- [2] **Figure 1.2:** Stratigraphic architectures of worldwide incised-valley fills, illustrating the seismostratigraphic variability (bounding surfaces and system tracts) between them. The examples are grouped by the hydrodynamic regimes from wave- to tide-dominated. A) Changjiang valley, China (Li et al., 2006); B) Paleo-Nakagawa valley, Japan (Tanabe et al., 2015); C) Gironde estuary, France (Allen and Posamentier, 1994) D) Vilaine valley, France (Chaumillon et al., 2008); E) Paleo-Chao Praya valley, Gulf of Thailand (Reijnenstein et al., 2015); F) Adriatic Sea, Italy (Ronchi et al., 2018); G) Trinity-San Jacinto incised valley, USA (Rodriguez et al., 2005) H) Gulf of Lyon, France (Tesson et al., 2015); I) New Jersey shelf, USA (Nordfjord et al., 2006); J) Durban shelf, South Africa (Green et al., 2013).
- [3] **Figure 1.3:** Examples of stratigraphic organization of postglacial transgressive deposits. The relative position of each example is based on the prevailing sedimentation/erosion ratio in each setting (up and left, where sedimentation is higher than erosion). A) Gulf of Lions, characterized by high rates of sediment supply (adapted from Gensous and Tesson, 2003). B) Central Adriatic margin, also characterized by high rates of sediment supply. ES1, regional unconformity; S1 and S2, regional surfaces, each recording a specific interval of sea-level rise; Si, internal surface of erosion (adapted from Maselli et al., 2011). C) Offshore San Onofre, California characterized by a reduced amount of transgressive depositional bodies, possibly because of lower sediment inputs (adapted from Klotsko et al., 2015). D) East China Sea, where the transgressive architecture is strongly influenced by the hydrodynamic regime. TBL, transgressive boundary layer (adapted from Li et al., 2014). E) Durban shelf, eastern South Africa, characterized by the preferential development of barrier and backbarrier deposits (adapted from Pretorius et al., 2019). F) Continental shelf off New Jersey, characterized by a major role of transgressive ravinement. "R" horizon, a composite product of erosion, forms the base of three seismically recognized sedimentary deposits of latest Pleistocene-Holocene age older than the LGM. "T" horizon, the transgressive ravinement associated with Holocene sea-level rise (adapted from Nordfjord et al., 2009). Highstand systems tracts (HST) are represented in green, and transgressive deposits are represented in yellow-orange. The different transgressive units are designated differently according to their sequential order in each location. mfs, maximum-flooding surface; TS, transgressive surface.
- [4] **Figure 1.4:** A) Schematic global mean sea level curve from the last 3.5 Ma (modified from Berends et al., 2021). The position of the Mid-Pleistocene Transition (MPT) is indicated. B) Schematic late Quaternary sea-level curve showing 100 ka glacio-eustatic cycles from the last 450 ka (Modified from Grant et al., 2014, and Mestdagh et al., 2019). Marine Isotopic Stages (MISs) 2–11 are highlighted. C) The pattern of postglacial sea-level rise, with indication of major climatic events such as: Heinrich Event 1 (H1), the Bølling–Allerød warm period (B-A), and the Younger Dryas (YD) cold period. Timing of Melt-Water Pulses (MWP) 1A and 1B and the 8.2 ka cooling event (in red) are also indicated. Sea-level curve is modified from Lambeck et al. (2014).
- [5] **Figure 1.5:** Schematic diagrams of different incised-valley-fill dimensions corresponding to passive margins (A) and active margins (B). Along passive margins (A), the scale of incised-valley fills associated with large and small drainage-basin areas is compared (taken from Wang et al., 2019).
- [6] **Figure 2.1:** A) Geographical location of the Gulf of Cádiz within the general context of the NE Atlantic Ocean. B) Physiographic domains along the Gulf of Cádiz.

- [7] **Figure 2.2:** Long-term geological evolution of the Gulf of Cádiz: A) geological setting during the Late Jurassic and Early Cretaceous; B) interpretative cross-section during the Late Jurassic and Early Cretaceous; C) geological setting during the Early-Middle Miocene; and D) interpretative cross-section during the Early-Middle Miocene. Adapted from Maldonado and Nelson (1999).
- [8] **Figure 2.3:** Location of the study area on the northern Gulf of Cadiz. Topo-bathymetric map showing the main rivers and pathways of the main water masses and currents. Topography from Spanish National Geographic Institute, 2015 (MTN50 raster). Bathymetry from EMODnet Bathymetry Consortium, 2020. The position of Figure 2.4 is indicated here.
- [9] **Figure 2.4:** A) Bathymetric map showing the study area (Chapter 4) on the eastern Algarve Shelf (Portugal), offshore the Gilão-Almargem Estuary, in the northern Gulf of Cadiz. Bathymetry from EMODnet Bathymetry Consortium, 2020. B) Bathymetric map showing the study area (Chapters 5 and 6) off the Guadiana River mouth in the northern Gulf of Cadiz. Bathymetry from EMODnet Bathymetry Consortium, 2020.
- [10] **Figure 2.5:** Map showing the surficial sediment distribution on the shelf in the study area (extracted from González et al., 2004). The position of Figure 2.6 is indicated here.
- [11] **Figure 2.6:** A) Map showing the sediment distribution on the shelf in the study area offshore of the Guadiana River mouth (extracted from González et al., 2004) and the Gilão River basin. B) Map showing the sediment distribution on the shelf in the study area off the Guadiana River mouth (extracted from González et al., 2004).
- [12] **Figure 2.7:** Late Quaternary sequences (U1-U5) and sequence stratigraphic surfaces on the northern Gulf of Cadiz continental margin, from the middle slope to the shelf. Taken from Mestdagh et al., (2019). MIS: Marine Isotopic Stage.
- [13] **Figure 2.8:** A) Geomorphological interpretation of the most recent subaerial unconformity surface, featuring two distinct domains (inner versus outer shelf) bounded by a clear physiographic boundary. Major valley incision seems to be constrained to the inner shelf landward of the boundary. B) 3D scheme of the last subaerial unconformity, highlighting the distinct geomorphological boundary between the inner and outer shelf. Most of the inner shelf exhibits an extensive physiographic high, interpreted as indurated facies resistant to erosion. More significant erosion occurred to the east, where an arc-shaped embayment was possibly developed. Most of the outer shelf shows a planar pattern, indicative of widespread transgressive ravinement. Taken from Lobo et al. (2018).
- [14] **Figure 3.1:** Outline of the methodology followed throughout the PhD thesis.
- [15] **Figure 3.2:** Different types of seismic data used in this PhD thesis: A) Topographic Parametric Sonar sub-bottom acoustic profiles; B) Parasound sub-bottom acoustic profiles; C) Sparker single-channel seismic profiles; and D) Uniboom source seismic profiles
- [16] **Figure 3.3:** Location of high-resolution TOPAS seismic profiles on the shelf offshore the Guadiana River mouth (EMODnet Bathymetry Consortium, 2020).
- [17] **Figure 3.4:** Location of the grid of Parasound seismic profiles on the shelf in the study area along the northern Gulf of Cádiz shelf (EMODnet Bathymetry Consortium, 2020).
- [18] **Figure 3.5:** Location of the grid of high-resolution sparker seismic profiles on the shelf in the study area offshore of the Guadiana River mouth (EMODnet Bathymetry Consortium, 2020).
- [19] **Figure 3.6:** Location of the grid of vintage Uniboom seismic profiles on the shelf in the study area along the northern Gulf of Cádiz shelf (EMODnet Bathymetry Consortium, 2020).
- [20] **Figure 3.7:** Location of sediment core stations on the shelf in the study area along the northern Gulf of Cádiz shelf (EMODnet Bathymetry Consortium, 2020). The position of sediment cores shown in this PhD thesis is also indicated.
- [21] **Figure 3.8:** Sediment sampling devices deployed during LASEA 2013 AND CADISED 2015 oceanographic surveys: A) Grab Sampler; B) Giant Box Corer, C) Rumohr Corer; D) Gravity Corer, E) Piston Corer, F) Vibrocorer.

- [22] **Figure 3.9:** A: The Guadiana main Incised valley studied in Chapter 5: (up) Interpreted channel horizon data transformed into channel coordinate space. (center) Linear interpolation along three paths on each side interim to the edges and thalweg. (down) Completed interpolation in channel space using planar interpolation within an optimal triangulation of the values shown in (center). B: The Guadiana Eastern Incised valley studied in Chapter 5: (up) Interpreted channel horizon data transformed into channel coordinate space. (center) Linear interpolation along three paths on each side interim to the edges and thalweg. (down) Completed interpolation in channel space using planar interpolation within an optimal triangulation of the values shown in (center).
- [23] **Figure 3.10:** Sketches summarizing the main morphometric parameters measured in the two incised paleovalleys that comprise the main scope of Chapter 5 of this PhD thesis. A) Paleovalley in plain view. B) Cross-section of a paleovalley.
- [24] **Figure 4.1:** Location of the seismic database on the shelf in the study area offshore of the Gilão-Almargem Estuary (EMODnet Bathymetry Consortium, 2020). The location of Figure 4.2 is indicated in the inset rectangle, and the location of Figures 4.3 to 4.8 is highlighted.
- [25] **Figure 4.1:** Spatial distribution and schematic cross-sections of the different incised valley features identified along the Algarve inner shelf off the Gilão-Almargem Estuary. The trace of the main fluvial valley, which can be considered the seaward extension of the Gilão River, is also represented. Background information consists of shelf bathymetry, the Last Subaerial Discontinuity (LSD) slope break line, and the position of sub-bottom seismic lines. UBI: Upper boundary of infilling; IPs 1 and 2: Incised phases 1 and 2.
- [26] **Figure 4.3:** A) Coast-parallel (SSW-NNE-oriented) sub-bottom seismic Uniboom source (Geopulse™) profile focusing on the proximal inner-shelf paleovalley system (up) and its interpretation (below). B, C, D) Interpreted zoomed seismic windows of the different paleovalleys. Their location is indicated in Figure 4.3A. Here, the important characteristics observed are: the occurrence of highly reflective seismic facies in the intervalley areas with local identifications of well-marked erosional truncations; the distinctive seismic facies which compose the infilling of the paleovalleys, with sub-parallel facies infilling the older incision phase (ISU 2) and with chaotic facies with local occurrences of lateral migrations infilling the younger incision (ISU 1); the asymmetric shape of the younger phase IP 1, with thalwegs displaced laterally; and the thin, laterally extensive reflective unit covering the incisions. The color code and acronyms are indicated here, and the location of the seismic section is indicated in Figure 4.1. IPs 1 and 2: Incised phases 1 and 2; UBI: Upper boundary of infilling; UBS: Upper boundary of sheet-like unit.
- [27] **Figure 4.4:** Along-shelf (W-E-oriented) sub-bottom acoustic profile showing the main inner-shelf paleovalley (A) and its interpretation (B) at around 30 m water depth. The infilling of the lower incision phase (ISU 2) is very complex, with the occurrence of erosional irregular surfaces and chaotic mounds intercalated within sub-parallel seismic facies. The younger incision phase is asymmetrical, with the thalwegs displaced eastward. The infilling of the younger incision phase exhibits a chaotic seismic configuration. The upper reflective unit is not laterally continuous at this location. The location of the seismic section is indicated in Figure 4.1 and the color code and acronyms are indicated in Figure 4.3.
- [28] **Figure 4.5:** Along-shelf (W-E-oriented) sub-bottom seismic profiles focusing on the main inner-shelf paleovalley. A) TOPAS acoustic profile (left) and its interpretation (right). B) Sparker profile (left) and its interpretation (right). In the acoustic profile, the lack of penetration prevents the recognition of the oldest incision phase and its infilling. The reflective sheet-shaped unit that covers the paleovalley and its infilling is very thick (10 meters) at this location, where an internal high-amplitude reflection separates two sheet-like deposits. The color code and acronyms are indicated in Figure 4.3. The location of the seismic section is indicated in Figure 4.1. The crossings with Figures 4.6, and 4.7 are also indicated.
- [29] **Figure 4.6:** Downdip cross-shelf (S-N oriented) Sparker profile (A) and interpretation (B) showing the occurrence of valleys landward and seaward of the break of slope that establishes the seaward boundary of the paleo-inner shelf. Landward of the break of slope, the main inner shelf paleovalley is observed at an approximate depth of 40 to 80 ms (more details of this valley are provided in figure 4.7). Seaward of the break of slope, several valley features occur at water depths of 39 m. Here, the paleovalleys seem to be covered by blocky, highly reflective seismic facies, and the lateral flanks of the valleys are not easily

identified. The location of the seismic section is indicated in Figure 4.1 and the color code and acronyms are indicated in Figure 4.3. The location of Figure 4.7 (inset rectangle), and the crossings with Figures 4.5, and 4.8 are also indicated.

- [30] **Figure 4.7:** Dondip cross-shelf (S-N-oriented) Sparker profile showing the main inner-shelf paleovalley (A) and its interpretation (B). The paleovalley occurs landward of the break of slope, and is characterized by two phases of incision and infilling. The second incision phase is asymmetric and is mostly covered by non stratified seismic facies. The reflective unit covering the paleovalley and its infilling is relatively thick here (maximum thickness of 10 m) and exhibits some landward-directed prograding reflectors. The color code and acronyms are indicated in Figure 4.3. The location of the seismic section is indicated in Figures 4.1, and 4.6. The crossing with Figure 4.5 is also indicated.
- [31] **Figure 4.8:** A) W-E-oriented sub-bottom acoustic profile including the projected position of the studied sediment core GeoB19508. The location of the seismic section is indicated in Figure 4.1. The crossing with Figure 4.6 is also indicated. B) Photography, facies distribution, lithological description, control age points, grain size statistical parameters (mean, sorting, skewness and kurtosis), and carbonate content of sediment core GeoB19508, characterizing the distal termination of an incised valley. The position of the sediment core is indicated in Figures 4.1, and 4.2.
- [32] **Figure 4.9:** Synthetic seismic and sequence stratigraphic interpretation for the northern Gulf of Cadiz. A) Late Quaternary sequences and sequence stratigraphic surfaces on the northern Gulf of Cadiz continental margin, from the middle slope to shelf (taken from Mestdagh et al., 2019), and the last 430 ka BP sea-level curve. Marine Isotopic Stages (MIS) 2 to 11 are highlighted. Colors are according to the proposed hypothesis in this work: post-channel fill deposits: blue; MIS 2-LGM: yellow; MIS 6: orange. B) Schematic model and cross section showing the proposed model for a simple valley framed in the last glacial cycle. C) Schematic model and cross section showing the proposed model for a compound valley framed during the two last glacial cycles.
- [33] **Figure 4.10:** Idealized stratigraphic model for the incised valleys recognized on the inner shelf of the study area, relating the seismic surfaces and units with their geological interpretation.
- [34] **Figure 4.11:** Proposed paleogeographic reconstruction of the study area at ~10 ka BP where multiple sandy islands are interrupted by numerous tidal inlets in several channels showing a coastal pattern, which is similar to that of the present-day Ria Formosa Barrier Island System. The position of seismic lines and the studied sediment core are indicated and the red lines correspond with the width of IP 1 along the different incised valleys.
- [35] **Figure 5.1:** A) Bathymetric map of the study area including the location of the shelf seismic database (EMODnet Bathymetry Consortium, 2020). The location of Figure 5.1B is indicated in the inset rectangle, and the location of Figures 5.2 to 5.5 is highlighted. The shelf break and 20-meter bathymetric contours are included. B) Zoom window of the map shown in (A), highlighting the location of Figures 5.2 to 5.16.
- [36] **Figure 5.2:** Dondip cross-shelf (SE-NW-oriented) sub-bottom seismic Uniboom source (Geopulse™) profile (A) and interpretation (B) showing the occurrence of two incised valley systems landward below the postglacial transgressive units (PTUs), studied in Chapter 6, and the margin-wide scale (mws) surfaces defined by Mestdagh et al. (2019) seaward. The color code and acronyms are indicated here, and the location of the seismic section is indicated in Figure 5.1. The crossings with Figures 5.4, 5.5, 5.9, 5.13, and 5.15 are indicated. The age of the major seismic horizons is also shown. GMV: Gadiana main valley; GEV: Gadiana eastern valley; IPs: Incised phases; mws 1 to 5: margin-wide surfaces; LSD: Last Subaerial Discontinuity; MPD: Mid-Pleistocene Disconformity.
- [37] **Figure 5.3:** Dondip cross-shelf (SE-NW-oriented) sub-bottom seismic Uniboom source (Geopulse™) profile (A) and interpretation (B) showing the landward occurrence of two incised valley systems, formed by several incision phases, and their relationship with the major regional seismic horizons. Note how the MPD is cut by the incision phases. The color code and acronyms are indicated in Fig. 5.2, and the location of the seismic section is indicated in Figure 5.1. The crossings with Figures 5.4, 5.5, 5.7, 5.10, 5.11, 5.12, 5.13, and 5.14 are indicated here.

- [38] **Figure 5.4:** Downdip cross-shelf (S-N-oriented) sub-bottom seismic Sparker profile (A) and interpretation (B) showing the landward occurrence of the Guadiana eastern incised valley system, formed by at least five incision phases, and its relationship with the major regional seismic horizons; other incised features not related with the two main valley systems that constitute the main scope of this chapter are also indicated. The color code and acronyms are indicated in Fig. 5.2, and the location of the seismic section is indicated in Figure 5.1. The location of Figure 5.6 (inset rectangle) and the crossings with Figures 5.2, 5.3, 5.5, 5.7, and 5.10 to 5.15 are indicated here.
- [39] **Figure 5.5:** Along-shelf (W-E-oriented) sub-bottom Sparker profile showing the two main paleovalleys (A) and its interpretation (B) at around 30 m water depth. Here, four incision phases (GmvIPs 4 to 1) are identified in the GMV and at least three in the GEV (Gevs 3 to 1). The occurrence of the multiple signal prevents a clear imaging of the lowermost incisions. The architecture of both valleys systems differs clearly. The GmvIPs are characterized by asymmetrical V-shaped geometries, whose thalwegs are laterally displaced. In contrast, the GevIPs are characterized by more symmetrical U-shaped cross sections that are vertically stacked. The color code and acronyms are indicated in Fig. 5.2, and the location of the seismic section is indicated in Figure 5.1. The crossings with Figures 5.2, 5.3, 5.4, 5.9, and 5.12 are indicated here.
- [40] **Figure 5.6:** Downdip cross-shelf (S-N-oriented) sub-bottom seismic Sparker profile (A) and interpretation (B) focusing on the Guadiana eastern incised valley system, formed by at least five incision phases. The internal architecture of the different GevIPs is complex, with the occurrence of internal irregular surfaces and characterized by sub-parallel aggradational facies that may exhibit intercalated chaotic facies. The color code and acronyms are indicated in Fig. 5.2, and the location of the seismic section is indicated in Figures 5.1, and 5.4.
- [41] **Figure 5.7:** A) Along-shelf (W-E-oriented) sub-bottom acoustic profile (TOPAS) showing the two main paleovalleys (up) and its interpretation (below). B: The same along-shelf (W-E-oriented) profile shown in (A) but collected with a Sparker seismic source. Some of the geomorphologic features and measured parameters are indicated. Note the contrast in resolution between TOPAS and Sparker seismic profiles. The color code and acronyms are indicated in Fig. 5.2, and the location of the seismic section is indicated in Figure 5.1. The crossings with Figures 5.2, 5.3, 5.4, and 5.9 are indicated.
- [42] **Figure 5.8:** Interpolation model of fluvial channel morphology of the most recent incision phase of both studied valleys, providing a complete visualization of the morphology of the fluvial systems (A) and the interpretation of some geomorphologic features (B). The crossings with Figures 5.5, and 5.7 are indicated. The interpreted channel horizon data are shown in Figure 3.9 (Chapter 3).
- [43] **Figure 5.9:** Downdip sub-bottom Parasound profile (A) and interpretation (B) oriented N-S along the Guadiana main valley showing the internal architecture along the GMV. C) Interpreted zoomed seismic window along the proximal area of the GMV (location indicated in Figure 5.9A). Here, the three major seismic units that compose the sedimentary infilling of the GMV could be identified. The units exhibit significant thickness variation along the valley. Note how the seismic sub-unit GmvU2-2 and the seismic unit GmvU1 are only characterized along the proximal valley segment. Seismic sub-unit GmvU2-1 is not only restricted to the proximal areas; it extends basinward, where it builds up the uppermost part of a wedge-shaped deposit. The geometry of the lower unit GmvU3 could not be identified basinward due to poor seismic penetration. The color code and acronyms are indicated here, and the location of the seismic section is indicated in Figure 5.1. The crossings with Figures 5.5, 5.7, and 5.10 to 5.14 are also indicated.
- [44] **Figure 5.10:** A) Along-shelf (NW-SE-oriented) sub-bottom acoustic profile showing the internal architecture of the infilling of the two studied paleovalleys (up) and its interpretation at around 30 m water depth. B and C) Zoomed seismic windows focusing on the architecture of the two different paleovalleys (left) and its interpretation (right). Their location is indicated in Figure 5.10A. Note the significative differences between the seismic facies of both valleys. Sediment cores LA-14-VC (Fig. 5.16) and LA-12-VC are indicated, and the available age datings are also shown. The color code and acronyms are indicated here, and the location of the seismic section is indicated in Figure 5.1. The crossings with Figures 5.3, 5.4, 5.9, 5.11, and 5.12 are also indicated.

- [45] **Figure 5.11:** A) Along-shelf (NW-SE-oriented) sub-bottom acoustic profile showing the internal architecture of the infilling of the two studied paleovalleys (up) and its interpretation at around 30 to 35 m water depths. B and C) Zoomed seismic windows focusing on the architecture of the two different paleovalleys (left) and its interpretation (right). Their location is indicated in Figure 5.11A. Here, important characteristics are: well-defined tangential-oblique internal reflections dipping laterally in unit GvmU3; the absence of sub-unit GmvU2-1; the mounded patterns in GevU2 that protrude above the pre-existing relief; and the asymmetrical cross sections of both valleys. The color code and acronyms are indicated in Figures 5.9, and 5.10, and the location of the seismic section is indicated in Figure 5.1. The crossings with Figures 5.3, 5.4, 5.9, and 5.10 are also indicated.
- [46] **Figure 5.12:** A) Along-shelf (NW-SE-oriented) sub-bottom acoustic profile showing the internal architecture of the infilling of the two studied paleovalleys (up) and its interpretation at around 33 to 40 m water depths. B and C) Zoomed seismic windows focusing on the architecture of the two different paleovalleys (left) and its interpretation (right). Their location is indicated in Figure 5.12A. Here, important characteristics are: sub-unit GmvU2-2 is characterized by a well-defined sub-parallel seismic configuration in the central areas of the GMV; sub-unit GmvU2-1 extends out of the valley westward; GmvU1 onlaps GevU1; the symmetrical V-shape cross section of GMV; and the two U-shaped geometries observed in the GEV. The color code and acronyms are indicated in Figures 5.9, and 5.10, and the location of the seismic section is indicated in Figure 5.1. The crossings with Figures 5.3, 5.4, 5.6, 5.9, 5.10, and 5.13 are also indicated.
- [47] **Figure 5.13:** A) Along-shelf (W-E-oriented) sub-bottom acoustic profile showing the internal architecture of the infilling of the two studied paleovalleys (up) and its interpretation at around 40 m water depth. This acoustic section coincides with the Sparker seismic section shown in Figure 5.5. B and C) Zoomed seismic windows focusing on the architecture of the two different paleovalleys (left) and its interpretation (right). Their location is indicated in Figure 5.13A. Here, important characteristics are: the near-to-transparent seismic facies of the lower units (GmvU3 and GevU3); the restricted geometry of GevU2, infilling some channel-like depressions above GevU3; the well-developed mound geometry of GevU1; the asymmetrical V-shape cross section of the GMV, with the thalweg displaced eastward; and various thalwegs observed in the GEV. The color code and acronyms are indicated in Figures 5.9, and 5.10, and the location of the seismic section is indicated in Figure 5.1. The crossings with Figures 5.3, 5.4, 5.9, and 5.12 are also indicated.
- [48] **Figure 5.14:** A) Along-shelf (W-E-oriented) sub-bottom acoustic profile showing the internal architecture of the infilling of the two studied paleovalleys (up) and its interpretation at around 50 m water depth. This seismic section coincides with Figure 5.7. B and C) Zoomed seismic windows focusing on the architecture of the two different paleovalleys (left) and its interpretation (right). Their location is indicated in Figure 5.14A. Here, important characteristics are: GmvU1 covering totally the GEV; GmvU2-1 exhibits non-stratified seismic facies that construct the uppermost part of wedge-shaped deposits related with the Guadiana PTU1 (Chapter 6); and semi-transparent seismic facies in GmvU3. The color code and acronyms are indicated in Figures 5.9, and 5.10, and the location of the seismic section is indicated in Figure 5.1. The crossings with Figures 5.2, 5.3, 5.4, and 5.9 are also indicated.
- [49] **Figure 5.15:** A) Along-shelf (W-E-oriented) sub-bottom acoustic profile showing the internal architecture of the infilling of the two studied paleovalleys (up) and its interpretation at around 60 m water depth. B and C) Zoomed seismic windows focusing on the architecture of the two different paleovalleys (left) and its interpretation (right). Their location is indicated in Figure 5.15A. Here, important characteristics are: the wedge-shaped deposits composing the proximal Guadiana PTUs 1 and 2 (Chapter 6), which offlap the underlying GEV; semi-transparent seismic facies of GmvU3; the close location of both valleys (~1 km); and the lower position of GEV respect to GMV. The color code and acronyms are indicated in Figures 5.9, and 5.10, and the location of the seismic section is indicated in Figure 5.1. The crossings with Figures 5.2, 5.3, 5.4, and 5.9 are also indicated.

- [50] **Figure 5.16:** Photography, CT-scans, facies distribution, lithological description, control age points, grain size, physical properties (density and magnetic susceptibility logs), and XRF geochemical ratios of sediment core LA-14-VC, characterizing seismic units GmvU1 and GmvU2-1. The position of the sediment core is indicated in Figure 5.1 and its projection is indicated in Fig 5.10.
- [51] **Figure 5.17:** Synthetic model linking the initial formation of incised valleys, their subsequent infilling, and reincision with the generation of distal shelf-margin wedges. Cyclic sea-level changes are considered to be mostly driven by a dominant 100 ka periodicity. Here, only two successive cycles are represented.
- [52] **Figure 5.18:** Schematic model of incised-valley architectural geometries identified in the two studied valleys. Here, four incision phases are observed, illustrating both valleys where the GMV mostly exhibits V-shapes that exhibit a multilateral stacking; in contrast, the GEV tends to be U-shaped, and the valleys stack vertically in a multistorey fashion.
- [53] **Figure 5.19:** Synthetic along-valley sequence stratigraphic interpretation proposed for the Guadiana Main Valley and documenting the connection between proximal infilling facies and distal shallow-water deltas.
- [54] **Figure 5.20:** Idealized stratigraphic models for the incised valleys studied on the continental shelf of the study area, relating the seismic surfaces and units with their geological interpretation in the Guadiana main valley (A) and the Guadiana Eastern valley (B).
- [55] **Figure 5.21:** Chronology of the Guadiana main valley infilling seismic units (GmvU1 and GmvU2-1), with the transgressive seismic units (studied in the following Chapter 6) and correlation with the postglacial sea-level pattern. The major climatic events include: the Heinrich Event 1 (H1), the Bølling–Allerød warm period (B-A), and the Younger Dryas (YD) cold period, as well as the timing of Melt-Water Pulses (MWP) 1A and 1B and the 8.2 ka cooling event (in red). Plotted ages are named taking into account the coring site, the coring technique (VC stands for vibro coring), and the name of the seismic unit in which the samples were taken. The estimated water-depth locations of the Gulf of Cadiz transgressive clinofolds in relation to coeval sea levels are also indicated (Chapter 6).
- [56] **Figure 6.1:** Location of the study area on the shelf offshore of the Guadiana River mouth, in the northern Gulf of Cadiz, showing the location of the seismic database and the selected core stations on the shelf in the study area offshore of the Guadiana River mouth (EMODnet Bathymetry Consortium, 2020). The location of Figures 6.2 to 6.5 is highlighted. The location of the sedimentological core stations showed in this chapter (Figs. 6.7 to 6.10) are also marked.
- [57] **Figure 6.2:** Representative downdip cross-shelf (SSE-NNW-oriented) sub-bottom seismic profile showing the general arrangement of backstepping seismic units (A) and their interpretation (B) offshore of the Guadiana River mouth. The color code and acronyms used in this chapter are also included. The location of the seismic section is indicated in Figure 6.1.
- [58] **Figure 6.3:** Representative sub-bottom profiles focusing on the Postglacial Transgressive Unit 4. A) W-E seismic line (up) and its interpretation (below). B) SSE-NNW seismic line (up) and its interpretation (below). Here, the important characteristics observed are: The clinofolds which compose the main body of PTU 4 (*sub-unit 4a*), mainly in the distal part of the unit; the channel features that characterize the proximal part of the body (*sub-unit 4b*); the transparent seismic facies that onlaps laterally to this body (*sub-unit 4c*); and the thin, and transparent facies, sheet-like body which integrates *sub-unit 4d*, where some superimposed undulations are observed. The location and penetration of sediment cores LA-25-VC (Fig. 6.7) and LA-22-VC (Fig. 6.8) are also indicated. The location of the seismic sections is indicated in Figure 6.1. The color code and acronyms are indicated in Figure 6.2.

- [59] **Figure 6.4:** Representative sub-bottom profiles focusing on Postglacial Transgressive Units 3 and 2. A) W-E seismic line (up) and its interpretation (below). B) SSE-NNW seismic line (up) and its interpretation (below). Here, the remarked characteristics observed are: The low-angle clinoforms which compound the lower part of PTU3 (*sub-unit 3a*), and the two clinoforms bodies (with higher angles and dipping in opposite directions) that compound the most of PTU 2 (*sub-units 2a1 and 2a2*); the channel features with chaotic configuration that characterize the proximal part of the body (*sub-unit 3b*); the *sub-unit 2d*, which occurs over the proximal and central part of PTU 2, but is restricted only to the eastern sector; and the transparent seismic facies that onlaps laterally to sub-unit 2a2 (*sub-unit 2c*). The location and penetration of sediment cores LA-22-VC (Fig. 6.8) and LA-48-VC (Fig. 6.9) are also indicated. The location of the seismic sections is indicated in Figure 6.1. The color code and acronyms are indicated in Figure 6.2.
- [60] **Figure 6.5:** Representative sub-bottom profiles focusing on the Postglacial Transgressive Unit 1. A) W-E seismic line (up) and its interpretation (below). B) SSE-NNW seismic line (up) and its interpretation (below). Here, the remarked characteristics observed are: The three clinoform sub-units which form the main body of PTU 1 (i.e., *sub-unit 1a1, 1a2 and 1a3*); the sub-unit 1d, which occurs over the PTU 1; the transparent seismic facies that onlaps laterally to the main body of PTU 1 and is also lying over PTU 2 on the eastern sector (*sub-unit 1c*); and the incised-channel features located in the eastern sector, which contain parts of PTUs 2 and 3. The location and penetration of sediment core LA-18-VC (Fig. 6.10) are also indicated. The location of the seismic sections is indicated in Figure 6.1. The color code and acronyms are indicated in Figure 6.2.
- [61] **Figure 6.6:** Spatial distribution and thickness of the studied deposits. A) Distribution maps of the PTUs showing the location of the main Guadiana paleovalley (GMV), the Guadiana Eastern paleovalley (GEV), the coastline, and the shelf bathymetry. The position of Figure 6.6B-E is indicated by the inset rectangle. B-D) Isochores map showing the spatial distribution and thickness in TWTT (ms) of the studied seismic units: B) PTU 4; C) PTU 3; D) PTU 2; E) PTU 1. The shelf bathymetry and the position of sub-bottom seismic lines are also represented.
- [62] **Figure 6.7:** Photography, schematic sediment facies, and lithological description, control age points, density log, and magnetic susceptibility logs of sediment core LA-25-VC, characterizing seismic unit PTU 4. A) Homogeneous mud (facies 3); B, C) Silty sand mixed with highly fragmented bioclasts of bivalves, *Turritella* and *Ostrea* up 2 cm in length (facies 2); D) Massive medium to fine sand with mottling related to organic matter; E) Fine to medium sand with some silt laminae; F, G) Massive sands (facies 1).
- [63] **Figure 6.8:** Photography, schematic facies, lithological description, control age points, density log, and magnetic susceptibility logs of sediment core LA-22-VC, characterizing seismic unit PTU 3. A) Muddy facies (facies 3) showing a large well-preserved 3-cm-long bivalve shell; B) Silty sand of facies 2 with 1 cm-long bivalve shell fragments (facies 2); C) Medium sand of facies 2 including a high amount of fragmented bioclasts of bivalves and *Turritella* and silt nodules; D) Medium sand including fragmented bioclasts like bivalves and *Turritella* up to 3 cm in length; E) Massive medium sand containing a large 5 cm bivalve shell and *Dentalium*; F) Bioturbation in fine to medium sand; G) Massive fine sand including a large bivalve shell fragment.
- [64] **Figure 6.9:** Photography, schematic facies, lithological description, control age points, density log, and magnetic susceptibility logs of sediment core LA-48-VC, characterizing seismic unit PTU 2. A) Silts (facies 3) containing a large well-preserved 5 cm *Ostrea* shell; B) Mixture of medium to coarse sand with scattered large bivalve and *Turritella* shell fragments up 2 cm in length; C) Medium to fine sand (facies 1); D) Bioclastic layer hosted in a fine sand interval; E) Massive fine sand of facies 1 including a large bivalve shell; F, G) Massive medium sand.

- [65] **Figure 6.10:** Photography, schematic facies, lithological description, control age points, density log, and magnetic susceptibility logs of sediment core LA-18-VC, characterizing seismic unit PTU 1. A) Massive fine sand of facies 1; B) Medium sand of Facies 2 with abundant fragmented bioclasts including *Pecten*; C) Erosional surface between fine sandy (Facies 1) and silty facies (Facies 2); D) Fine to medium sand of facies 1 showing some silt laminations; E) Massive fine sand of Facies 1 including some granule- to pebble-size shell fragments; F) Sandy gravels with bivalves and gastropods including a large shell; G) Massive fine sand of Facies 1.
- [66] **Figure 6.11:** Schematic block diagrams and cross sections showing the model of sedimentary evolution proposed for the formation of a generic transgressive deposit associated with the postglacial retreat of the Guadiana River mouth. Dashed lines and blue arrows show the position of sea level in the previous phases. A) Phase of clinoform body development (i.e., *sub-units a*), representing the establishment of a coastal regime, during which shallow-water, coarse-grained river-dominated deltas formed; B) Phase of delta-top distributary-channel formation following construction of transgressive delta; C) Phase of infilling of erosional channels (i.e., *sub-units b*) over the proximal areas of the clinoforms and fine-grained sediment export to construct distal sediment sheets (i.e., *sub-units c*); D) Final evolutionary phase of each transgressive deposit, characterized by shoreface reworking (i.e., *sub-units d*) of the previous fluvio-deltaic depositional system.
- [67] **Figure 6.12:** Proposed chronology of transgressive seismic units (including ages of PTU 5 after Lobo et al., 2015) and correlation with the postglacial sea-level pattern (rate of sea-level change above and amplitude of sea-level change below). The major climatic events include: Heinrich Event 1 (H1), the Bølling–Allerød warm period (B-A) and the Younger Dryas (YD) cold period, as well as the timing of Melt-Water Pulses (MWP) 1A and 1B and the 8.2 ka cooling event (in red). Plotted ages are named taking into account the coring site, the coring technique (VC stands for vibro coring), and the name of the seismic unit in which the samples were taken. The estimated water-depth locations of the Gulf of Cadiz transgressive clinoforms in relation to coeval sea levels are also indicated.



Scan this QR to access the images in high resolution

Tables:

- [1] **Table 1.1:** Sequence stratigraphic surfaces identified in high-resolution sequence stratigraphic studies (Catuneanu, 2006, 2019a; Zecchin and Catuneanu, 2013).
- [2] **Table 3.1:** Specific methodologies employed in each chapter of the PhD thesis. The boxes colored in yellow refer to the analysis and methodologies conducted by the PhD candidate, and the boxes colored in grey refer to the methods or analysis conducted by collaborators and coordinated or integrated by the PhD candidate.
- [3] **Table 3.2:** Summary table of studied sediment cores in this PhD thesis, including geographic location, length, and the water depths in which they were collected.
- [4] **Table 3.3:** AMS radiocarbon data obtained on benthic foraminifera and shells in the studied sediment cores. Ages written in italics point out the anomalous results that provide ages older than expected.
- [5] **Table 4.1:** Summary table of the seismic facies, including the seismic configurations, boundaries, interpretations and acronyms for each seismic unit characterized in the inner shelf paleovalley system identified in this chapter. IPs 1 and 2: Incised phases 1 and 2; UBI: Upper boundary of infilling; UBS: Upper boundary of sheet-like unit.
- [6] **Table 5.1:** Summary of the main morphometric characteristics of the two most recent incised valley incision phases characterized in the Guadiana Shelf study area.
- [7] **Table 5.2:** Summary table including the seismic facies, configuration, boundaries, geometry, interpretation, and acronyms for each seismic unit characterized in the studied incised valleys off the Guadiana River mouth.
- [8] **Table 6.1:** Summary table including the seismic facies, configuration, boundaries, and acronyms for each seismic sub-unit identified in this study.
- [9] **Table 6.2:** Summary table of the studied sediment vibro cores, including their coordinates, length, and the water depths in which they were obtained.
- [10] **Table 6.3:** AMS radiocarbon data obtained on benthic foraminifera and shells in the studied sediment cores. Ages written in italics point out the anomalous results that provide ages older than expected.



Scan this QR to access the tables in full page format

